

Alma Mater Studiorum - Università di Bologna

DOTTORATO DI RICERCA IN
CHIMICA

Ciclo 33

Settore Concorsuale: 03/C1 - CHIMICA ORGANICA

Settore Scientifico Disciplinare: CHIM/06 - CHIMICA ORGANICA

KINETIC AND MECHANISTIC STUDIES ON UNCONVENTIONAL
ANTIOXIDANT ACTIVITIES OF NATURAL COMPOUNDS

Presentata da: Yafang Guo

Coordinatore Dottorato

Domenica Tonelli

Supervisore

Luca Valgimigli

Co-supervisore

Marco Lucarini

Esame finale anno 2021

Abstract

Autoxidation of organic compounds is not only responsible for lipid degradation, but also for many age-related diseases, therefore the search for novel antioxidants remains an important area of research. In recent years interest has moved toward the investigation of the antioxidant properties of natural compounds, including essential oils, and other plant-derived molecules. Incidentally, the best established and most reliable method to test antioxidants is via inhibited autoxidation studies: i.e. monitoring their protection of a reference substrate under controlled conditions. Here, an oxygen uptake apparatus set in our lab is used to study antioxidant efficacies by measuring the kinetics of oxygen consumption during the inhibited autoxidation of a substrate.

Surprisingly, very few natural biomimetic substrates have been kinetically characterized for their autoxidation so far, limiting the quantitative testing of natural antioxidants under representative settings, i.e. close to those they experience in a natural environment, as well as the knowledge of a key feature concerning the antioxidant protection of food and agricultural materials. Thus, to fill this gap, we firstly report here the full kinetic characterization of four different substrates which are representative of the chemical diversity of natural oxidizable materials: stripped sunflower oil (SSO), stripped olive oil (OO), squalene (SQ), and p-cymene (p-C). Standard antioxidants such as PMHC (2,2,5,7,8-pentamethyl-6-chromanol) and DBHA (2,6-di-*tert*-butyl-4-methoxyphenol) were used to calibrate their autoxidation kinetics, and the calibration was validated by measuring the antioxidant activity of well-studied and structurally different antioxidants, like quercetin, magnolol, caffeic acid phenethyl ester, and 2,4,6-trimethylphenol, proving their usefulness as reference oxidizable substrates. Secondly, 18 essential oils (EO) samples, of different botanical species or different productions of same species, were studied for their antioxidant activity. Their antioxidant activities clearly depend on their composition in phenolic components although it was also reported that some non-phenolic EO components, such as γ -

terpinene, limonene, linalool and citral, show antioxidant activity by fast terminating chain-carrying peroxy radicals. The characterization of natural oxidizable substrates and the investigation of that antioxidant activity of essential oils is collected in Chapter 1.

Among the active essential oil components, the antioxidant mechanism of γ -terpinene was clarified, however, little was known on the interplay of its antioxidant activity with that of phenols. Thus, we set to investigate the possible interplay of γ -terpinene with reference antioxidants, where PMHC and DTBC (3,5-di-*tert*-butylcatechol) were chosen as prototype of mono- and poly-phenolic antioxidants respectively, with the aim of disclosing new unconventional synergistic combinations of antioxidants. Our studies on the inhibited autoxidation of styrene (reference) and of two of the natural substrates previously calibrated, squalene and SSO, showed that γ -terpinene only affords very modest protection unlike the phenolic antioxidants. However, combination of γ -terpinene with either monophenolic or polyphenolic antioxidants extended their inhibition duration without significantly changing the slope of the inhibited period, indicating a clear synergism proportional to the concentration of γ -terpinene, which acts as the co-antioxidant that regenerates the main (phenolic) antioxidants. It was found that regeneration depends on the release of HOO^\bullet by γ -terpinene upon being attacked by ROO^\bullet , thereby causing a chain-transfer with exchange of the chain-carrying species from ROO^\bullet to HOO^\bullet . Mechanistic experiments showed that γ -terpinene could only regenerate monophenols from their phenoxy radical, but a different, 2e- two-steps regeneration mechanism was demonstrated for polyphenols like catechols, which could be regenerated also from the oxidized quinone. Further, experiments on dietary lipids with biomimetic antioxidants showed the relevance of the synergic mechanism.

Among the relevant applications, the interplay of oxidizing ROO^\bullet and reducing/oxidizing HOO^\bullet as chain carrying species is well established in biological systems, and the reduction of quinones and hydroquinones by HOO^\bullet

was further investigated to better rationalize melanins's redox-mediated bioactivity. Melanins' structure was reported to be either reduced (catechol) or oxidized (*ortho*-quinone). Thus, the absolute kinetics of antioxidant interplay between HOO• and quinones was thoroughly investigated on model compounds. Then this knowledge was transferred to rationalize the mechanism of their antioxidant action of polydopamine (PDA), a well-established synthetic melanin. Inhibited autoxidation studies showed that PDA antioxidant activity decreased on increasing purification and can be attributed to unreacted catechol units adsorbed on polymer surface. Indeed, it has negligible activity to trap ROO• after accurate purification. However, in the presence of HOO• it turns into an effective antioxidant, which is due to regeneration of *ortho*-quinones to semiquinones and catechols by HOO•. This explains their redox-mediated bioactivity, given the abundance of O₂^{-•}/HOO• species in biological systems.

The antioxidant interplay of HOO• with phenols, polyphenols, quinones and quinone based melanins is presented in Chapter 2.

Regarding melanin, besides its reported role in many health-related functions, such as the antioxidant activity previously discussed, arguably its role in pigmentation of animal and vegetal tissues remains prevalent and its control is, consequently, most important. Food browning on storage and human skin hyperpigmentation (dyschromia) are two unwanted consequences of melanin's role, which can most efficiently be controlled through inhibition of tyrosinase, a copper containing oxidase widely distributed in nature. UV–Vis spectroscopy is routinely used in enzyme activity tests and remains as the most versatile method. However, the instability of the oxidation products L-dopa and dopaquinone forces to monitor tyrosinase kinetics only by monitoring the accumulation of late product dopachrome. Hence the reliability of kinetic measurements was challenged by setting a novel investigation method based on measuring oxygen consumption during reaction progress. Since the uptake of oxygen is stoichiometrically related to the generation of dopachrome, the two kinetic methods were matched to afford a robust combined investigation approach.

Glabridin from *Glycyrrhiza glabra*, is one of the most effective natural inhibitors, and there is major uncertainty on its actual activity on quantitative grounds, despite its central role as reference compound. On applying our kinetic approach to the discovery of tyrosinase inhibitors meant as unconventional antioxidants - where glabridin was used as reference - it occurred to us that both its mechanism and kinetic constants may require revision, which we set to undertake. Data in literature on the activity profile of this molecule indicate a non-competitive inhibitory activity, which implies that glabridin is capable of binding with the same affinity both the free enzyme (E) and the complex enzyme-substrate (ES). However, both the UV-Vis and combined oximetry kinetic analysis did not show pure non-competitive but preferring competitive inhibition. Accurate quantitative analysis indicated that the inhibition kinetics is of mixed type, where glabridin is able to interfere both with the E and the ES binding forms, with two distinct dissociation constants K_I and $K_{I'}$, which we were able to accurately quantify. Results allowed to solve a long-standing controversy on glabridin inhibiting mechanism, both for monophenolase and diphenolase activities, showing its prevailing competition with the respective substrates (l-tyrosine or l-DOPA). Our kinetic analysis afforded the competitive dissociation constants K_I as 13.95 nM and 61.22 nM, for monophenolase and diphenolase activities, respectively, supporting the role of glabridin as one of the most effective, reference natural inhibitors. Investigation on tyrosinase inhibition is presented in Chapter 3.

Acknowledgements

First of all, I want to thank the China Scholarship Council (CSC) for providing me with the necessary financial support, and my supervisor Luca Valgimigli for accepting me into his research group, which enabled me to be a PhD student at the University of Bologna.

I'd like to express my thanks to Luca Valgimigli, who has supported me throughout this research project. His guidance helped me in all the time of research, especially in writing this thesis. He has taught me the methodology to present the research work as clearly as possible.

I would also like to express my gratitude and appreciation for my co-supervisor Riccardo Amorati, whose guidance, especially his patient explanation to my research questions, and his encouragement has been invaluable throughout this study.

I also wish to thank Postdoctoral researcher Andrea Bascheri and Dr. Simone Gabbanini of BeC s.r.l. who have been a great source of support for this research. Furthermore, I would like to thank the other students who did their thesis in our research group, especially Fabio Mollica and Romeo Pizzol, for their dedicated research work and the constructive scientific exchanges. My sincere thanks also go to all my research colleagues, especially Alice Cariola and Cecila Poderi for their constant encouragement, and to my friends for being there for me in this journey. My thanks also go to all the people in the lab who created and provided a nice working environment to support me to complete the research work.

Last but not the least, I would like to thank my parents who are always there, giving me the most powerful support to move on.

Statement of Originality

I hereby certify that the work described in this thesis is the original work of the author, with exceptions for work performed by collaborators noted in the acknowledgement. The work in this thesis draws upon a great deal of published research. Any published (or unpublished) work by others is cited and fully acknowledged within the references.

Guo Yafang

Table of Contents

Abstract.....	I
Acknowledgements	V
Statement of Originality	VI
List of Schemes	XI
List of Figures	XIII
List of Tables	XIX
List of abbreviation	XXII

Chapter 1. Study of the antioxidant capability of essential oils and oxidizability calibration of natural lipids

1.1 Hydrocarbon Autoxidation	3
1.1.1 Initiation	4
1.1.2 propagation	6
1.1.3 Termination	8
1.2 Autoxidation inhibition and Antioxidants	10
1.2.1 Phenolic Antioxidants	11
1.2.2 Activity of phenolic antioxidants	12
1.3 Methods to test the antioxidant activity	15
1.3.1 Oximetry apparatus	16
1.3.2 Interpretation of kinetic data	19
1.4 Research objects	21
1.5 Calibration of natural substrates	22
1.5.1 Results and Discussion	24
1.5.2 Validation and specific advantages of the four oxidizable substrates in testing antioxidants	37

1.6 Antioxidant activities of essential oils	42
1.6.1 Phenolic composition of EOs	43
1.6.2 Antioxidant activity of EOs	44
1.6.3 Conclusion and Perspectives	50
1.7 Experimental sections	51
Appendix	54
Reference	63

Chapter 2. Regeneration of phenolic and polyphenolic antioxidants by γ -Terpinene and related hydroperoxide (HOO^\bullet) releasers. Implications in Melanins' antioxidant behavior.

2.1 Reactive Oxygen Species (ROS)	73
2.2 Oxidative Damage	74
2.2.1 Lipid peroxidation	74
2.2.2 Oxidative damage to proteins	75
2.2.3 Oxidative damage to DNA	76
2.3 The $\text{HOO}^\bullet/\text{O}_2^{\bullet-}$ System: a special case of ROS	76
2.3.1 Highlights on the generation of $\text{HOO}^\bullet/\text{O}_2^{\bullet-}$	77
2.3.2 Specificity and properties of $\text{HOO}^\bullet/\text{O}_2^{\bullet-}$ pair.....	86
2.4 Research objectives	87
2.5 Synergic Antioxidant Activity of γ-Terpinene with Phenols and Polyphenols.	88
2.5.1 Inhibition of the autoxidation of natural lipids by phenolic antioxidants with γ -terpinene	92
2.5.2. Exploration of the mechanism behind the synergy	95
2.5.3 Relevance of the interaction between quinones and γ -terpinene in food science and the application of the synergic antioxidant behavior in real food products	102

2.5.4 Conclusions on the synergic antioxidant activity of γ -terpinene with phenols in food preservation.	105
2.6 Hydrogen Atom Transfer from HOO• to ortho-Quinones Explains the Antioxidant Activity of Polydopamine	108
2.6.1 The reaction of ortho and para quinones with HOO•.....	108
2.6.2 The role of HOO• in the antioxidant activity of polydopamine (PDA).....	115
2.6.3 Conclusions on the role of HOO• on the antioxidant behavior of melanins....	117
2.7 Materials and Methods	118
Appendix	122
Reference	134

Chapter 3. kinetic study by combined UV-Vis spectroscopy and oximetry on monophenolase / diphenolase activities of tyrosinase inhibited by glabridin.

3.1 Pigmentation and tyrosinase	149
3.1.1 Pigmentation.....	149
3.1.2 Tyrosinase.....	151
3.2 The Fundamentals of Enzyme Inhibition Mechanism	153
3.2.1- Michaelis-Menten kinetics and Lineweaver–Burk plot.....	154
3.2.2 Types of reversible inhibition (plots interpretation)	157
3.2.3 Quantitative description of different reversible inhibitions	160
3.4 Research objects	161
3.5 Results and Discussion	164
3.5.1 Correlation of oxygen consumption to dopachrome generation.....	165
3.5.2 kinetic study on both monophenolase and diphenolase activities of tyrosinase inhibited by glabridin: UV–Vis spectroscopy and oximetric methods.	167
3.5.3 Inhibition kinetics by glabridin	169
3.5.4 Determination of IC ₅₀ (half-maximal inhibitory concentration)	174

3.5.5 Is Glabridin a substrate for tyrosinase?	175
3.6 Conclusions and perspective	176
3.7 Experimental sections	178
Appendix	182
Reference	184

List of Schemes

Scheme 1.1. Radical initiated Hydrocarbon autoxidation.....	3
Scheme 1.2. AIBN decomposition to nitrogen and two 2-cyanoprop-2-yl radicals.....	6
Scheme 1.3. The propagation steps of substrate: abstraction of an hydrogen atom by peroxy radical.....	6
Scheme 1.4. The possible combinations for termination.....	8
Scheme 1.5. The possible termination mechanism of primary and secondary alkyl radicals by forming a cyclic intermediate.....	9
Scheme 1.6. Mechanism of different types of antioxidants interfering with free radical autoxidation.....	10
Scheme 1.7. Phenolic radical-trapping antioxidants trap two peroxy radicals, as exemplified by BHT.....	13
Scheme 1.8. Solvent effects on the activity of phenolic antioxidants.....	14
Scheme 1.9. The proposed mechanism of acid-catalyzed reaction peroxy radicals with phenols.....	15
Scheme 1.10. Autoxidation of styrene initiated by AIBN.....	17
Scheme 1.11. Main reactions involved in the propagation of squalene autoxidation.....	33
Scheme 1.12. Autoxidation of p-cymene.....	34
Scheme 1.13. Chain-transfer in the propagation of p-cymene explaining the fast termination step.....	36
Scheme 1.14. Hydroperoxy radical (HOO•) reduce the semiquinone radical of CAPE.....	40
Scheme A.1.2 Autoxidation inhibited by chain-breaking antioxidants.....	54
Scheme 2.1. Elimination of O ₂ • ⁻ by peroxy radicals.....	78
Scheme 2.2. Thermal decomposition of di-(4-carboxybenzyl)hydronitrite to generate O ₂ • ⁻	79
Scheme 2.3. HOO• elimination mechanism of diethyl ether.....	79
Scheme 2.4. HOO• elimination from α-hydroxy alkylperoxy radicals.....	80
Scheme 2.5. HOO• generation during the oxidation of vitamin C.....	80
Scheme 2.6. O ₂ • ⁻ / HOO• propagated oxidation of pyrogallol or the propyl ester of gallic acid.....	81

Scheme 2.7. Oxidation of simple sugar	82
Scheme 2.8. Proposed mechanism of the chain oxidation of 1,4-dithiothreitol propagated by $O_2^{\bullet-}$	84
Scheme 2.9. Proposed mechanism for the formation of peroxy radicals and $O_2^{\bullet-}$ from beta-hydroxyalkyl and bis-allylic radicals produced by the one-electron oxidation of ArAc, respectively	84
Scheme 2.10. Mechanism of HOO^{\bullet} generation from cyclohexadiene (CHD).	85
Scheme 2.11. Oxidation of mechanism of 4a,4b-dihydrophenanthrenes or its derivatives like 9,10-cyclopentano-4a,4b-dihydrophenanthrene.	86
Scheme 2.12. Mechanisms of co-antioxidant activity of TEMPO or diarylamine phenoxazine with HOO^{\bullet}	87
Scheme 2.13. Mechanism of the antioxidant activity of (A) γ -terpinene alone (after Foti & Ingold, 2003) [90] and of the antioxidant synergy between (B) γ -terpinene and monophenolic antioxidants (using 1H as model compound) and (C) γ -terpinene and polyphenolic antioxidants (using 2H ₂ or 3H ₂ as model compound)	97
Scheme 2.14. (A) (Bio)synthetic pathway leading to the formation of melanins; (B, C) radical used to investigate the antioxidant activity of melanins	107
Scheme 2.15. Model compounds investigated in this study and semiquinones radicals transiently formed during the reactions	109
Scheme 2.16 Key reactions explaining the antioxidant activity of ortho and para-quinones, Q, in the presence of 1,4-cyclohexadiene, CHD	111
Scheme 2.17 Kinetic solvent effect for H-atom donation from HOO^{\bullet}	114
Scheme 2.18. Catechol and quinone units in the polydopamine polymer are non-reactive toward alkylperoxyl radicals (ROO^{\bullet}) but upon the reaction with HOO^{\bullet} the quinones are converted to semiquinone radicals with enhanced ability to trap both species, HOO^{\bullet} or ROO^{\bullet}	116
Scheme 3.1 key oxidation steps of phenols to melanin	150
Scheme 3.2. basic one substrate enzyme kinetic model.....	155
Scheme 3.3. Schematical kinetic model of competitive inhibition.....	158
Scheme 3.4. Schematically kinetic model of uncompetitive inhibition.....	158
Scheme 3.5. Schematically kinetic model of pure non-competitive inhibition	159
Scheme 3.6. Schematic kinetic model of mixed inhibition.....	160

List of Figures

Figure 1.1. Classification of phenolic antioxidants.....	11
Figure 1.2. Structures of the most putative and popular synthetic phenolic antioxidants	12
Figure 1.3 Differential oxygen uptake apparatus set in our lab for autoxidation kinetics.	18
Figure 1.4 Typical oxygen consumption plots obtained during autoxidation of styrene (A) in the absence of and antioxidant, (B) in the presence of a very good antioxidant, (C) in the presence of an average antioxidant, or D) in the presence of a modest antioxidant.....	19
Figure 1.5 Oxidizable substrates investigated in this study and reference antioxidants used to calibrate the substrates (1–4) and to validate their use (5–8).....	23
Figure 1.6 Uninhibited autoxidation of SSO measured in PhCl at 30°C. A) Plot of the oxygen consumption against R_i ($[SSO] = 0.517\text{ M}$); B) Plot of the oxygen consumption against SSO concentration, with $[AIBN] = 0.025\text{ M}$; C) Plot of the oxidizability of SSO against R_i ($[SSO] = 0.517\text{ M}$); D) Plot of the oxidizability of SSO against its concentration, with $[AIBN] = 0.025\text{ M}$	25
Figure 1.7 Oxygen consumption measured during the autoxidation of stripped sunflower oil (50 % v/v; 0.517M) initiated by AIBN (0.05 M) in chlorobenzene at 303K, without inhibitors (dashed line); or in the presence of: PMHC (1) 2.5 μM . Regression lines indicates the slopes of the inhibited and uninhibited periods, which can be processed with equations 8 and 7, respectively, to obtain the oxidizability ($k_p/\sqrt{2kt}$) and the value of k_p , respectively. The cross-point of the two regression lines indicates the inhibition time τ (1600 s in this experiment), which affords the measured rate of initiation R_i ($3.1 \times 10^{-9}\text{ Ms}^{-1}$, in this experiment) upon processing with equation 10	26
Figure 1.8. Infrared spectra in the O-H stretching region of PMHC 1 (A) and DBHA 2 (B) (0.01 M), dissolved in chlorobenzene (solid line) or in 1:1 SSO/chlorobenzene mixture (dashed line).....	28
Figure 1.9 Infrared spectra in the O–H stretching region of PMHC 1 (A) and DBHA 2 (B) (0.01 M), dissolved in chlorobenzene (solid line) or in a OO /chlorobenzene mixture (dashed line).....	31
Figure 1.10. Typical oxygen consumption plots during the autoxidation of p-cymene (3.2 M) initiated by AIBN (0.05 M) in PhCl at 30 °C without inhibitors or in the presence of antioxidants 1–4, each at a concentration of $5.0 \times 10^{-6}\text{ M}$	35

Figure 1.11 Oxygen consumption during the autoxidation of A-SSO(1.1M), B-OO(0.25M); C-Squalene (1.04);D-p-Cymene (3.2 M) initiated by AIBN (0.05 M) in PhCl at 30° C without inhibitors (dash) or in the presence of antioxidant (2.5×10 ⁻⁶ M): a (5), b (6), c (7), d (8) in all panels.	38
Figure 1.12. Oxygen consumption during the autoxidation of squalene (1.04 M) initiated by AIBN (0.05 M) in PhCl at 30° C without inhibitors (dotted) or in the presence of TEMPO 10×10 ⁻⁶ M (solid); the inserted scheme is the antioxidant behavior of TEMPO with HOO•.....	41
Figure 1.13 Phenolic compounds present in the studied essential oils.	44
Figure 1.14 Representative plots of oxygen consumption during cumene autooxidation (3.6M), initiated by AIBN (0.05M), in PhCl, at 30 ° C, uninhibited (grey line) or in the presence of essential oil (1 ppm) of: red thyme 2 (red), savory (pink), red thyme 3 (green), origan (black), Carnation (cyan), cinnamon (blue).	45
Figure 1.15 Representative plots of oxygen consumption during cumene autooxidation (3.6M), initiated by AIBN (0.025M), in PhCl, at 30 ° C, uninhibited (grey line) or in the presence of essential oil of: bay 2.4 ppm (red), savory 2.3 ppm (pink), birch 2.6 ppm (green), red thyme (sample 1) 2.3 ppm (dark red), spanish origan 2.6 ppm (cyan), cade 2.5 ppm (yellow).	45
Figure 1.16 Oxygen consumption during cumene (3.6M) autooxidation, initiated by AIBN (0.025M), in PhCl, at 30 ° C, uninhibited (grey line) or in the presence in the presence of essential oil (13 ppm) of clove 2 (black line).	46
Figure 1.17 oxygen consumption during cumene auto-oxidation (7.1M), initiated by AIBN (0.05M), in PhCl, at 30 ° C, uninhibited (grey line) or in the presence of essential oil (5.3 ppm) of clove 1 (black line).....	46
Figure 1.18 Representative plots of oxygen consumption during cumene autooxidation (3.6M), initiated by AIBN (0.025M), in PhCl, at 30 ° C, uninhibited (grey line) or in the presence of essential oil (13 ppm) of: carrots (red), marigold (pink), celery (blue), cedarwood (yellow).	47
Figure 2.1. Main exogenous and endogenous sources of ROS.....	73
Figure 2.2. Peroxyl radicals of D-glucose.....	83
Figure 2. 3. Oxidizable substrates and antioxidants investigated in this study.....	91
Figure 2. 4. Oxygen consumption during the autoxidation of SSO (A-B), and squalene (C-D). Each panel displays the curves recorded for the autoxidation of the substrates without inhibitors (dotted lines), and in in the presence of 15.65 mM γ -terpinene (dashed lines). In panels A and C grey plots represent the inhibition by PMHC 1H (2.5	

μM) alone, while black curves represent inhibition by the mixture of 1H (2.5 μM) with γ -terpinene (15.65 mM). In panels B and D grey plots represent inhibition by CAPE 2H2 (2.5 μM) alone, and black curves inhibition by the mixture of 2H2 (2.5 μM) with γ -terpinene (15.65 mM). Inserts: plots of the experimental inhibition periods τ vs the concentration γ -terpinene for different mixtures 1H or 2H2 (2.5 μM) / γ -terpinene.. 93

Figure 2.5. Oxygen consumption measured during the autoxidation of styrene initiated by 0.025 M AIBN at 30°C in the absence of antioxidant (dashed line in both panels), and inhibited by (A) PMHC 1H (2.5 μM) in the absence of γ -terpinene (green line), in the presence of γ -terpinene (7.83mM-yellow line; 15.7mM-blue line; 31.3mM -purple line), or by (B) CAPE 2H2 (2.5 μM) alone (green line) or in the presence of growing amounts of γ -terpinene (the same color coding as in panel A is used). 94

Figure 2.6. Oxygen consumption measured during the autoxidation of styrene initiated by 0.025 M AIBN at 30°C. (A) 1: uninhibited; 2: injection of 1H (2.5 μM); 3: injection of γ -terpinene (15.7 mM). (B) 1: uninhibited; 2: injection of 3H2 (7.5 μM); 3: injection of γ -terpinene (15.7 mM) 98

Figure 2.7. Oxygen consumption during the autoxidation of styrene initiated by 0.025 M AIBN at 30° without inhibitors and upon injection of antioxidants at the time points indicated by numbers: (A) 1 = injection of PMHC 1H (2.5 μM), 2 = subsequent injection of γ -terpinene (20 mM); (B) 1 = injection of γ -terpinene (15.7 mM), 2 = subsequent injection of PMHC 1H (2.5 μM), 3 = subsequent injection of γ -terpinene (15.7 mM). Note that inhibition period τ in panel B is larger than in panel A (where it corresponds to $n = 2.1$) despite the identical concentration of injected PMHC 99

Figure 2.8 (A) Growth of the UV signal at 400 nm due to quinone 3 during the autoxidation of styrene initiated by 0.025 M AIBN at 30°C, inhibited by 3H2 67 μM . (B) Oxygen consumption during the autoxidation of styrene initiated by 0.025 M AIBN at 30°C in the absence of antioxidant (1), and upon their addition: 2 = injection of DTBQ 3 (7.5 μM); 3 = injection of γ -terpinene (7.83 mM). (C) Oxygen consumption during the autoxidation of SSO initiated by 0.025 M AIBN at 30°C in the absence of antioxidant (1), and upon their addition: 2 = injection of DTBQ 3 (7.5 μM); 3 = injection of γ -terpinene (7.83 mM). (D) Oxygen consumption during the autoxidation of squalene initiated by 0.025 M AIBN at 30°C in the absence of antioxidant (1), or in the presence of a mixture of DTBQ 3 (7.5 μM) and γ -terpinene (7.83 mM). 100

Figure 2.9. Decay of the UV signal at 400 nm due to quinone 3 during the autoxidation of styrene initiated by 0.025 M AIBN at 30°C, inhibited by 3 (67 μM) and γ -terpinene (15.7 mM)..... 101

Figure 2.10. Oxygen consumption measured during the autoxidation of SSO initiated by 0.025 M AIBN at 30°C in the absence of antioxidants and (1) upon injection of DTBQ 3 (7.5 μM), (2) upon subsequent injection of γ -terpinene (15.7 mM). The blue

dashed line represents the autoxidation under identical settings inhibited by a mixture of DTBQ 3 (7.5 μM) and γ -terpinene (15.7 mM) injected together at the beginning of the autoxidation. Note that despite the identical concentration of the antioxidants their effectiveness is higher if they are added together, possibly meaning that some side reaction is consuming 3 in the absence of γ -terpinene..... 102

Figure 2.11 Oxygen consumption measured during the autoxidation of squalene initiated by 0.025 M AIBN at 30°C in the absence of antioxidant (black line), inhibited by 2.5 μM DTBQ 3 (red line), or inhibited by 2.5 μM DTBQ 3 and 15.7 mM γ -terpinene (green line)..... 103

Figure 2.12 Oxygen consumption measured during the autoxidation of sunflower oil initiated by 0.025 M AIBN at 30°C in the absence of antioxidants (dotted lines), inhibited by 15 mM γ -terpinene (dashed lines) or: (A) inhibited by 3 μM vitamin E (d- α -tocopherol, gray line) or by a mixture of 3 μM vitamin E + 15 mM γ -terpinene (black line); (B) inhibited by 6 μM hydroxytyrosol (gray line) or by a mixture of 6 μM hydroxytyrosol + 15 mM γ -terpinene (black line) 104

Figure 2.13 O₂ consumption during the autoxidation of styrene in chlorobenzene at 30 °C initiated with 25 mM AIBN in the absence of inhibitors (a), and in the presence of quinones: 4 (curve b), 3 (curve c), 4 + 0.023 M CHD (curve d), and 3 + 0.023 M CHD (curve e). The concentration of quinones was 5 μM . B) O₂ co-nsumption during the autoxidation of CHD (0.23 M) initiated by 25 mM AIBN at 30 °C in chlorobenzene with no antioxidants added (a), with 40 μM of 4 or 4H₂ (curves b and c, respectively), and with 5 μM 3H₂ or 3 (d and e, respectively) 110

Figure 2.14. O₂ consumption during the autoxidation of styrene in chlorobenzene at 30 °C initiated with 25 mM AIBN in the absence of inhibitors in the presence of 5 μM of quinone 3 (A) or 4 (B) and increasing amounts of CHD..... 111

Figure 2.15. (A) Numerical fitting of the O₂ consumption traces during the autoxidation of CHD initiated by AIBN in PhCl at 30 °C inhibited by 3. Experimental results for oxygen consumption (black, solid line) and the simulated results (red line), perfectly overlapping each other. The transient concentrations of the quinone or hydroquinone species obtained during the simulations are reported. (B-C) ESI-MS spectra showing 3H₂ formation during the reaction of 3 (0.1 mM) with CHD (0.23 M) and AIBN (50 mM) in MeCN at 30 °C; after 1 hour of reaction in positive (B) and negative (C) ion mode. 113

Figure 2.16. O₂ consumption measured during the autoxidation of CHD (0.13 M) in MeCN initiated by AIBN (0.5 mM) at 30 °C in the absence of antioxidants (a) or in the presence of 3 (a) 5 μM , (b) 25 μM 114

Figure 2.17. (A) dynamic light scattering of PDNPs water solution. (B) ATR-FTIR spectrum of dried PDNP. (C) O₂ consumption recorded during the styrene (2.1 M) autoxidation initiated by AIBN (25 mM) in MeCN without inhibitors (a) and in the presence of: (b) CHD; (c) PDA (25 g/mL); (d) PDA (25 μg/mL) + CHD. (D) Same conditions as C, without inhibitors (a) and in the presence of: (b) CHD; (c) 3 (5 μM); (d) 3H₂ (5 μM); (e) 3H₂ (5 μM) + CHD; (f) 3 (5 μM) + CHD. In all cases, [CHD] = 23 mM..... 115

Figure A. 2.1 A) Numerical fitting of the O₂ consumption traces during the autoxidation of CHD initiated by AIBN in PhCl at 30 °C inhibited by 3. Experimental results for oxygen consumption (black, solid line) and the simulated results (red line) perfectly overlap each other. The transient concentrations of the quinone or hydroquinone species obtained during the simulations are reported. B) Values of k₃ as a function of k₃ (logarithmic scale) obtained by numerical fitting of the rates of CHD autoxidations inhibited by 3 (□) or of styrene autoxidation inhibited by 3H₂ (○). 123

Figure A 2.2 Example of fitting of the autoxidation of styrene inhibited by 3H₂.... 126

Figure A. 2. 3 Total ion chromatograms (TIC) of derivatization products (A - 3HSiMe₃; B - 3(SiMe₃)₂) of 3H₂ formed during autoxidation of CHD (0.13 M) initiated by AIBN (0.05 M) in the presence of 3 (6×10⁻⁵ M) in MeCN at 30°C (brown line) and reference 3H₂ (2×10⁻⁵ M) in MeCN (green line)..... 128

Figure A. 2. 4 Mass pattern of compound 3HSiMe₃ (Mw = 294 Da)..... 129

Figure A. 2.5 Mass pattern of compound 3(SiMe₃)₂ (Mw = 366 Da). 129

Figure A. 2.6 Example of numerical fitting by Copasi of the O₂ consumption trace (b) reported in figure 2.16 130

Figure A. 2.7 Dynamic Light Scattering measurement of PDA nanoparticles; size distribution by intensity 131

Figure A. 2.8 TEM images of PDA nanoparticles. 132

Figure A. 2.9 ATR-FT-IR spectra of: (A) Dopamine HCl (solid); (B) non-purified polydopamine nanoparticles; (C) Purified polydopamine nanoparticles 133

Figure 3.1. Schematic representation of melanogenesis pathway (in the blue frame on the right) inside melanocytes, and melanosome transfer 149

Figure 3.2. Tyrosinase active site and its three forms..... 151

Figure 3.3. Monophenolase and diphenolase catalytic activities of tyrosinase enzyme 152

Figure 3.4. Change on the concentration of enzyme(E), substrate(S), enzyme-substrate complex (ES) and product (P) during the time course of reaction.	154
Figure 3.5. Hyperbolic plot of Michaelis-Menten kinetic model	156
Figure 3.6. Double reciprocal linear plot of Lineweaver-Burk kinetic model.....	157
Figure 3.7. The theoretical effect of a competitive inhibitor on the LB plots of substrate-initial rate relationship.....	158
Figure 3.8. The theoretical effect of uncompetitive inhibitor on the LB plots of substrate-initial rate relationship.	159
Figure 3.9. The theoretical effect of pure non-competitive inhibitor on the LB plots of substrate-initial rate relationship.	160
Figure 3.10. Non-enzymatic cyclization of dopaquinone to form dopachrome regenerating L-dopa.....	162
Figure 3.11. Structure of glabridin (from Glycyrrhiza glabra L.).....	164
Figure 3.12. Schematic set-up of the oxygen sensor.....	165
Figure 3.13. Representative time traces of O ₂ consumption (solid lines) and dopachrome formation (dashed lines) during the oxidation of L-dopa 1.6 mM (A: tyrosinase 3.85 U/ml; B: tyrosinase 5.78 U/ml) and L-tyrosine 1.6 mM (C: tyrosinase 7.70 U/ml; D: 11.55 U/ml) at 30°C, pH 6.8. The regression lines in plots C and D were drawn using the indicated (red) time range for the initial rate, and ratios (average 1.5±0.1) of their slopes was used to determine the stoichiometric ratio between oxygen consumption and dopachrome production for substrate L-tyrosine.....	166
Figure 3.14. Correlation of the stoichiometry of oxygen (O ₂) consumption to dopachrome (DC) production during oxidation of both L-tyrosine (A and B) and L-dopa (C and D), correlating initial rates of DC production and O ₂ consumption as a function of tyrosinase concentration at fixed concentration of substrate (A and C), and initial velocity of DC production and O ₂ consumption as a function of tyrosinase concentration at fixed concentration of tyrosinase (B and D).	167
Figure 3.15. Time-course of DC production and O ₂ consumption during the oxidation of L-dopa (A, B) and L-tyrosine (C, D) catalyzed by tyrosinase (3.85 U/ml for L-dopa and 7.70 U/ml for L-tyrosine). The inserts are the initial rates of oxygen consumption (B, D) and dopachrome formation (A, C) during oxidation of both L-dopa (A and B) and L-tyrosine (A and B) with the corresponding non-linear fitting of Michaelis-Menten kinetics (solid lines)	168
Figure 3.16. Plots A and B are the non-linear fittings based on Michaelis-Menten kinetics of glabridin inhibition of monophenolase and diphenolase tyrosinase activity.	

Data were obtained by UV-Vis spectrophotometry: (A) diphenolase activity on L-Dopa, glabridin concentrations: ● -0 nM, ■ - 90 nM, ▲ -180 nM, x-300 nM; (B) monophenolase activity on L-tyrosine, glabridin concentrations: x-0nM, ▲- 15 nM, ■ -37 nM, ●-50nM. (C) and (D) are the Lineweaver-Burk plots corresponding to A and B. (E) and (F) are the Lineweaver-Burk plots of glabridin inhibition on monophenolase and diphenolase activity studied by oximetry method: (E) diphenolase activity on L-Dopa, glabridin concentrations: ○ -0nM, □ -80nM, Δ-200nM; (F) monophenolase activity on L-tyrosine, glabridin concentrations: ○ -0nM, □ -20nM, Δ-40nM. Enzyme concentration for substrate L-dopa and L-tyrosine were 3.85 U/ml and 7.7U/ml respectively, all experiments were conducted at pH 6.5 and 30°C. Due to the higher rate of the diphenolase reaction, the V_{max} of this process was evaluated at the beginning of the process (between $t=0$ and $t=2$ min), the V_{max} of monophenolase activity was instead evaluated between 5 and 30 min..... 170

Figure 3.17. The time progresses of O₂ consumption during the oxidation of L-dopa at different initial concentration from 0.1 mM (purple line) to 1.2 mM (red line), inhibited by glabridin (80 nM). The black lines are the linear regression (V_0) for every L-dopa concentration, taken in the highlighted time range (40s to 160s) 180

Figure 3.18. Initial rates of oxygen consumption during tyrosinase catalyzed oxidation of L-dopa and the corresponding non-linear fitting to Michaelis-Menten kinetics 181

List of Tables

Table 1.1. Activation energy for thermal decomposition of common initiators.....	5
Table 1.2. C-H BDE and propagation rate constant (k_p) for hydrocarbon autoxidation at 30° C.....	7
Table 1.3. Rate constants for the autoxidation of selected of organic substrates in chlorobenzene at 303K. able 1.4. O-H BDE of some phenolic antioxidants.....	9
Table 1.4. O-H BDE of some phenolic antioxidants	13
Table 1.5 Kinetic parameters measured for the autoxidation of stripped sunflower oil (SSO) in chlorobenzene (50 %, v/v) at 30 °C, initiated by AIBN, in the presence of PMHC (1) or DBHA (2) as reference antioxidants.....	28
Table 1.6. Kinetic parameters measured for the autoxidation of OO in chlorobenzene at 30 °C, initiated by AIBN, in the presence of PMHC (1) or DBHA (2) as reference antioxidants.....	30

Table 1.7 Kinetic parameters measured for the autoxidation of Squalene in chlorobenzene at 30 °C, initiated by AIBN, in the presence of PMHC (1), DBHA (2), or 4-methoxyphenol (3) as reference antioxidants.....	32
Table 1.8 Kinetic parameters measured for the autoxidation of p-Cymene in chlorobenzene at 30 °C, initiated by AIBN, in the presence of PMHC (1), DBHA (2), 4-methoxyphenol (3) or BHT (4) as reference antioxidants.	36
Table 1.9 Oxidizability ($k_p / \sqrt{2k_t}$) and rate constants for chain propagation (k_p) and chain termination ($2k_t$) for the investigated natural oxidizable substrates, measured at 303 K in chlorobenzene (Mean \pm SD)	37
Table 1.10 Inhibition Rate Constant k_{inh} and Stoichiometric Factor n , for Trapping Peroxyl Radicals by Antioxidants 5-8 (figure 1.5) Measured in the Inhibited Autoxidation of Calibrated Substrates SQ, p-C and SSO at 303 K in Chlorobenzene (Mean \pm SD).....	39
Table 1.10 Phenolics' concentration in the samples of Essential Oils (EOs) and corresponding concentration of each component in the autoxidation mixture when the EOs were used as inhibitor or cumene autoxidation.	48
Table 1.11 Apparent values of k_{inh} of EO samples determined by inhibited autoxidations at 303K in PhCl, resulting sum of phenolic concentration and total phenolic concentration in the autoxidizing mixture from GC-MS analysis of the essential oil and the corresponding concentration of use (ppm).....	49
Table A.1.1. Table A. 1.1. GC-MS analysis of fatty acid composition in SSO, after trans-esterification to the corresponding methyl esters (FAME). For each FAME analysis was performed in Single Ion reconstructed chromatograms using the base peak (bp) in mass spectrum. Calibration was performed at 5 levels using Supelco and Aldrich standard FAME mixtures. % Amount was then calculated on the total fatty acid content found in the chromatogram.....	58
Table A 1.2 GC-MS analysis of fatty acid composition in OO, after trans-esterification to the corresponding methyl esters (FAME). For each FAME analysis was performed in Single Ion reconstructed chromatograms using the base peak (bp) in mass spectrum. Calibration was performed at 5 levels using Supelco and Aldrich standard FAME mixtures. % Amount was then calculated on the total fatty acid content found in the chromatogram.....	59
Table A. 1.3. The phenolic components of investigated EO samples, analyzed GC-MS (courtesy of Dr. Simone Gabbanini – BeC s.r.l.)	59
Table A 1.4 Phenolic compounds identified in the investigated essential oils (> 1.5% w/w) and corresponding k_{inh} values measured at 30°C in inhibited autoxidations.	61

Table 2.1. Main reactive oxygen species (ROS) of interest in oxidative stress.....	74
Table 2.2. The main O ₂ • ⁻ formation paths in biological processes	77
Table 2.3. Apparent stoichiometric factors (n) and inhibition rate constant (k _{inh}) of PMHC (1H) and CAPE (2H ₂) when mixed with different mounts of γ -terpinene during the autoxidation of styrene initiated by AIBN at 30°.....	95
Table A. 2.1. Species considered in numerical fitting of the autoxidation of 1,4-cyclohexadiene (CHD) initiated by AIBN at 30 °C.....	124
Table A. 2.2 Kinetic scheme considered in numerical fitting of the autoxidation of 1,4-cyclohexadiene (CHD) initiated by AIBN at 30 °C in chlorobenene.....	124
Table A. 2.3 Species considered in numerical fitting of the autoxidation of styrene initiated by AIBN at 30 °C in chlorobenzene.	125
Table A. 2.4. Kinetic scheme of the autoxidation of styrene initiated by AIBN at 30 °C in chlorobenzene.....	125
Table 3.1. ERelationships between apparent Km, Vmax and the inhibition constant for different reversible inhibition types	161
Table 3.2. Michaelis-Menten kinetics parameters measured both by UV-Vis spectrophotometry and by oximetry.....	169
Table 3.3. Kinetic parameters of tyrosinase diphenolase activity inhibition by glabridin. Kinetics data were obtained both by non-linear and linear regression fit (see experimental section) at different glabridin concentrations.....	172
Table 3.4. Kinetic parameters of tyrosinase monophenolase activity inhibition by glabridin. Kinetics data were obtained by non-linear and linear regression fit at different glabridin concentrations.	173
Table 3.5. IC ₅₀ values calculated according to Eq. 3.9 for tyrosinase inhibition by glabridin at different concentrations of L-tyrosine and L-dopa substrates.....	175
Table 3.6. Raw data of initial rates obtained from the linear fitting by Sigamplot software of initial rates of oxygen consumption for different L-dopa concentrations	180
Table 3.7. Non-linear fitting report by Sigmaplot of figure 3.18	181

List of abbreviation

AH: antioxidants

AIBN: 2,2' -Azobis(isobutyronitrile)

ArO•: phenoxyl radical

BDE: bond dissociation energy

BHA: butylated hydroxyanisole

BHT: butylated hydroxytoluene

CAPE: caffeic acid phenethyl ester

CHD: cyclohexadiene

DBHA: 2,6-Di-*tert*-butyl-4-methoxyphenol

DC: dopachrome

DTBC: 3,5-di-*tert*-butylcatechol

DTBQ: 3,5-di-*tert*-butyl-*o*-benzoquinone

DOPA: 1-3,4-dihydroxyphenylalanine

E: free enzyme

EOs: essential oils

EPR: electron paramagnetic resonance

ES: enzyme-substrate

FAME: fatty acid methyl esters

HO•: hydroxyl radicals

LB: Lineweaver-Burk

MM: Michaelis-Menten

MeCN: Acetonitrile

OO: stripped olive oil

OG: octyl gallate

P: product

p-C: p-cymene

PDA: polydopamine

PhCl: Chlorobenzene
PG: propyl gallate
PMHC: 2,2,5,7,8-pentamethyl-6-chromanol
pQ: para-benzoquinone
PUFA: polyunsaturated fatty acids
Q: *ortho*-benzoquinones
QH•: semiquinone radical
QH₂: hydroquinone/catechol
REqEPR: EPR radical equilibration
RH: Hydrocarbons
ROO•: Peroxyl radicals
RO•: alkoxy radicals
ROOH: Hydroperoxides
ROS: reactive oxygen species
S: substrate
SOD: Superoxide dismutase
SQ: squalene
SSO: stripped sunflower oil
TBHQ: *tert*-butylhydroquinone
TEMPO: (2,2,6,6-Tetramethylpiperidine-1-oxyl radical)
TMP: 2,4,6-trimethylphenol

Chapter 1

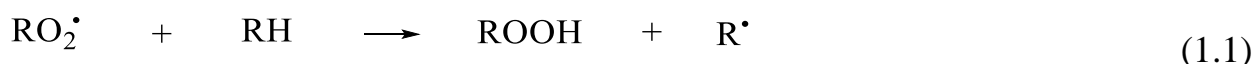
Study of the antioxidant capability of essential oils and oxidizability calibration of natural lipids

Summary

In this chapter, the characterization of natural oxidizable substrates and the investigation of that antioxidant activity of essential oils is collected. The basic mechanism of lipid oxidation and antioxidant capacity and their kinetic implication were introduced at the beginning of this chapter. Then the full kinetic characterization of four different substrates which are representative of the chemical diversity of natural oxidizable materials were reported, including stripped sunflower oil (SSO), stripped olive oil (OO), squalene (SQ), and p-cymene (p-C). Standard antioxidants such as 2,2,5,7,8-pentamethyl-6-chromanol (PMHC) and 2,6-di-*tert*-butyl-4-methoxyphenol or di-*tert*-butylhydroxyanisol (DBHA) were used to calibrate their autoxidation kinetics, and the calibration was validated by measuring the antioxidant activity of well-studied and structurally different antioxidants, like quercetin, magnolol, caffeic acid phenethyl ester, and 2,4,6-trimethylphenol, proving their usefulness as reference oxidizable substrates. Additionally, 18 essential oils (EO) samples, of different botanical species or different productions of same species, were studied for their antioxidant activity toward cumene autoxidation. Their antioxidant activities were clearly depending on their composition in phenolic components, which were analyzed by GC-MS. The relationship between the antioxidant behavior of individual components and the whole EOs is discussed.

1.1 Hydrocarbon Autoxidation

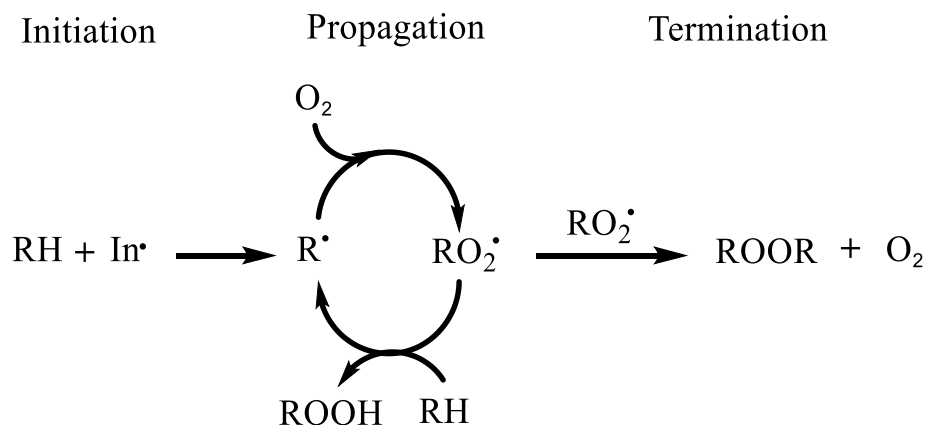
Hydrocarbons (RH), varying from plastics, lubricating oils, food lipids to biomolecules, generally undergo spontaneous oxidation in an oxygen-rich atmosphere, initiated by free radicals which have odd numbers of electrons (free valence) [1]. Peroxyl radicals (ROO•) thereby formed usually undergo two main kinds of reaction [2]: quench their own free valence by abstracting a hydrogen from the hydrocarbon substrate, releasing another radical:



or terminate with another peroxy radicals without conservation of the free valence:



Overall, hydrocarbons oxidation typically involves several steps, shown as in Scheme 1.1, which are classified as chain initiation, chain propagation, and chain termination [3,4].



Scheme 1.1. Radical initiated Hydrocarbon autoxidation.

Hydroperoxides (ROOH) generated during hydrocarbon autoxidation can undergo further oxidative deterioration, such as decomposing to alcohols, aldehydes, ketones, carboxylic acids or their esters, thus inducing damage to lipids, even producing toxicity [5]. In accordance to the importance of hydrocarbons in our life, efforts have been made to preserve hydrocarbons for decades and until now, which is also the main aim of our

study. Thus, consideration of hydrocarbon autoxidation mechanism would help analyze and bring about methods to prevent it.

1.1.1 Initiation

In lab study, a continuous generation of initiating radicals is usually applied to initiate hydrocarbon autoxidation, in order to carry out also kinetic studies under controlled conditions. Typically, radical initiators have weak bonds, capable of being broken photochemically, thermally or by metal catalysis. These bonds are, for example, the O-O bond in peroxides and peresters and the C-N bonds in azo-derivatives [6-8].



Generally, (hydro)peroxides undergo unimolecular decomposition with O-O bond splitting, generating alkoxy radicals (RO•) or hydroxyl radicals (HO•) [8].



Along with peroxides, synthetic azo-compounds are widely used as initiators of liquid-phase oxidation at mild temperatures, forming 2 equivalents of alkyl radicals (R•) and N₂ [9,10].



One of the most important characteristics of an initiator is their decomposition rate. Typically, the decomposition of the initiator gives rise to a pair of radicals trapped inside the cage made up of the solvent molecules (solvent cage). The fraction of radicals produced that comes out of the solvent cage constitutes a parameter called radical efficiency of the initiator (e). Considering aliphatic azo derivatives as initiators, they thermally decompose according to the equation [11,12]:



In which e represents the ability of the radicals to exit the solvent cage, and the value of e (0 < e < 1) depends on the temperature, the viscosity of the solvent and the intrinsic

characteristics of the initiator itself, while R_2 is the product of the recombination of the radicals within the cage. In the presence of a R-N=N-R azo-initiator, the rate of radical formation (R_i) linearly depends on its concentration (Eq.1.1).

$$R_i = 2eK_i[RN=NR] \quad (\text{Eq. 1.1})$$

Where K_i represents the decomposition rate constant of the azo derivative. In practice, the decomposition rate of initiator is usually expressed by the half-life ($t_{1/2}$), which is defined as the time required to consume half of their initial concentration at a given temperature. The correlation between (K_i) and half-life is derived according to Arrhenius equation:

$$K_i = A \cdot e^{-\frac{E_a}{RT}} \quad (\text{Eq. 1.2})$$

$$t_{1/2} = \frac{\ln 2}{K_i} \quad (\text{Eq. 1.3})$$

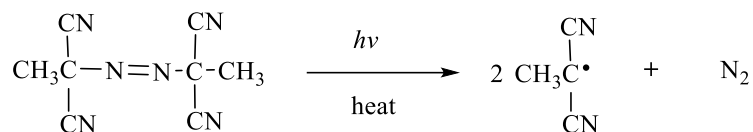
Where K_i is the rate constant for the initiator dissociation in s^{-1} , A is the Arrhenius frequency factor in s^{-1} , E_a is the activation energy for the initiator dissociation in J/mol; $R = 8.3142 \text{ J/mol}\cdot\text{K}$; T is the temperature in Kelvin degrees and $t_{1/2} =$ half-life in s. The activation energy of some common initiators is collected in table 1.1.

Table 1.1. Activation energy (E_a , J/mol) for thermal decomposition of common initiators [8].

Initiator	RN=NR			R ₁ O-OR ₂		
	MeO-AMVN	AAPH	AIBN	DCP	^t BuOO ^t Bu	CumylOOH
E_a	22.5	29.5	31.1	35.4	36.5	31.7

2,2'-Azobis(isobutyronitrile) (AIBN) is widely used as initiator, which has a half- life of around 2662 hours at 30°C, thus it can supply sufficient radicals at moderate

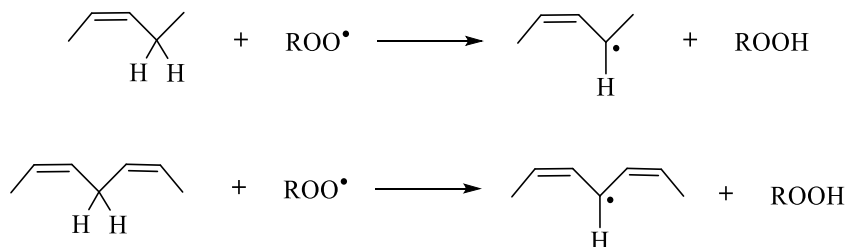
temperatures continuously, and it was used thoroughly in our autoxidation experiments which are set at 30°C [9].



Scheme 1.2. AIBN decomposition to nitrogen and two 2-cyanoprop-2-yl radicals

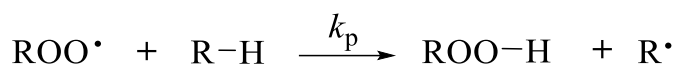
1.1.2 propagation

At this stage, alkyl radicals generated from the azo-initiator usually react rapidly ($\sim 10^9 \text{ M}^{-1}\text{s}^{-1}$) with oxygen, forming peroxy radicals ($\text{ROO}\cdot$), which react with the substrate, such as polyunsaturated fatty acids [13]. $\text{ROO}\cdot$ mainly abstracts an H-atom from the allylic and bis-allylic positions, releasing another alkyl radical which goes through the same pathway as the initiating alkyl radicals, and thus propagates the chain process, as depicted in scheme 1.3 [14].

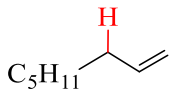
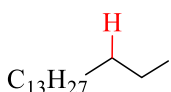
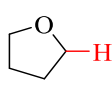
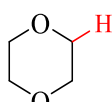
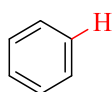
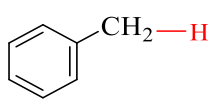
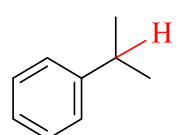


Scheme 1.3. The propagation steps of substrate: abstraction of an hydrogen atom by peroxy radical.

From the thermodynamic point of view, it is easy to predict whether a compound can undergo autoxidation or not, since the hydrogen transfer reaction takes place efficiently, in the propagation stage, if it is exothermic, *i.e.*, in the hydrogen transfer reaction, the breaking bond (C-H) should be weaker than the ROO-H bond of the hydroperoxide formed. And it is evident that only compounds with a (C-H) bond energy equal to or lower than 90 kcal/mol are promptly oxidizable [15].



(1.7)Table 1.2. C-H BDE, ΔH for the reaction with alkylperoxyl radicals and propagation rate constant (k_p) for hydrocarbon autoxidation at 30° C.

RH		BDE (R-H)	$\Delta H_{\text{react}}^a$	k_p
hydrocarbon		kcal/mole	kcal/mole	$\text{M}^{-1}\text{s}^{-1}$
methane	$\text{CH}_3\text{-H}$	104.0	14.0	--
1-octene		83.4	-6.6	1.0
<i>n</i> -hexadecane		98.0	8.0	0.01
tetrahydrofuran		92.0	2.0	4.3
1,4-dioxane		96.0	6.0	0.5
benzene		95.0	5.0	2.8×10^{-4}
methylbenzene		88.0	8.0	1.2×10^{-2}
cumene		84.5	4.5	0.18

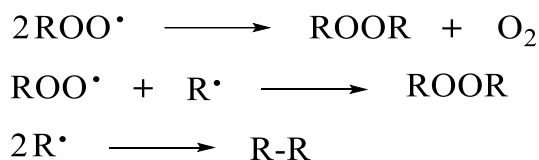
a) $\Delta H_{\text{react}} = \text{BDE (R-H)} - \text{BDE (ROO-H)}$, assuming that BDE (ROO-H) = 90 kcal/mol.

Based on the diverse structures of the substrates, the propagation rate constant, k_p , therefore, are unique to each oxidizable substrate. Specifically, the ease of oxidation

increases as the strength of the C-H bond decreases. And the propagation rate constant, k_p , for each oxidizable substrate will vary based on the structure of the substrate and the temperature of the autoxidation [16]. More specifically, the bond dissociation enthalpy of the C-H bond being broken (Table 1.2, in red) will influence the magnitude of k_p as the stronger the C-H bond, the lower the k_p will be, in general. Table 1.2 collects the C-H BDE and k_p of some common hydrocarbons [17].

1.1.3 Termination

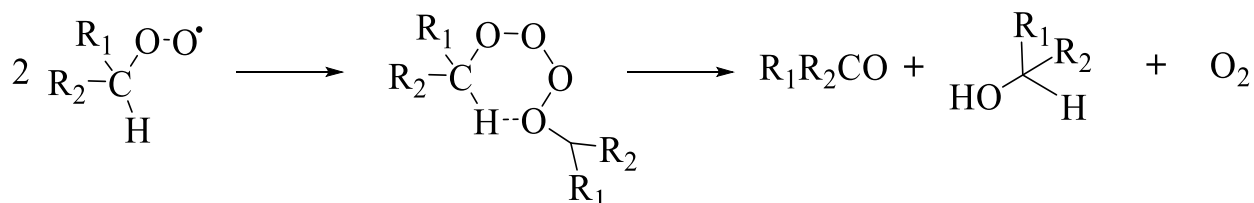
Apart from participating in H-atom abstraction, a combination of peroxy radicals can give rise to non-radical products that do not propagate further the chain, which thus is called termination. Termination can be done by combining peroxy radicals, also carbon-centered radicals, or by cross-combining of a peroxide with an alkyl (Scheme 1.4). Among these reactions, the predominant one is the combination of two peroxy radicals, as alkyl radicals react quickly with oxygen and do not live long enough to easily combine with each other or with a peroxide [18].



Scheme 1.4. The possible radical combinations for termination.

Generally, the more substituted the alkyl group the slower the termination rate constant ($2k_t$), due to increasing steric effects []. Tertiary peroxy radicals combine with a constant $2k_t$, approximately equal to $10^5 \text{ M}^{-1}\text{s}^{-1}$ to form a tetraoxide which rapidly decomposes giving molecular oxygen and a tertiary peroxide. The termination constants of the peroxy radicals derived from primary and secondary alkyl radicals vary in the interval between 10^6 and $10^9 \text{ M}^{-1}\text{s}^{-1}$, *i.e.* they are larger (up to 1000 times) than those characteristic for tertiary peroxy radicals [20]. Furthermore, the termination reaction between primary and secondary peroxy radicals differs from the combination reaction between tertiary peroxy radicals not only for the reaction rate, but also for the

mechanism. For example, Russell and Coote proposed that the peroxy radicals generated by the primary and secondary alkyl radicals form a cyclic intermediate (also in this case tetraoxide), which then fragments giving an equimolecular mixture of an alcohol, a carbonyl compound and oxygen [21,22].



Scheme 1.5. The possible termination mechanism of primary and secondary alkyl radicals by forming a cyclic intermediate.

Table 1.3. Rate constants for the autoxidation of selected of organic substrates in chlorobenzene at 303K.

Substrate	k_p ($\text{M}^{-1}\text{s}^{-1}$)	k_t ($\text{M}^{-1}\text{s}^{-1}$)	$k_p/(k_t)^{1/2}$
tetrahydrofuran	4.4	3.0×10^6	254.0
toluene	0.24	3.0×10^8	1.4
n-butylbenzene	0.57	5.0×10^7	8.1
styrene	41.0	4.2×10^7	890.0
methyl methacrylate ^a	2.96/1.0 ^b	2.0×10^6	209.0
acrylic acid ^a	2.77	1.4×10^7	75.8
1,4-cyclohexadiene	1400.0	1.3×10^9	3900.0
methyl oleate	0.89	1.0×10^6	89.0
methyl linoleate	62.0	8.8×10^6	2100.0

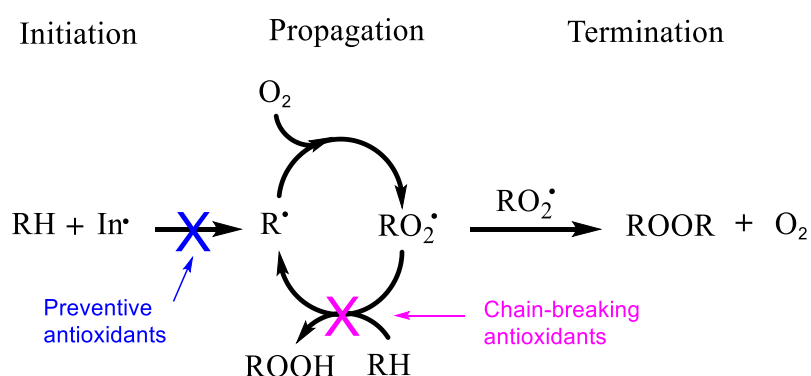
a) Value at 333K; b) value at 303K.

The terminating rates (k_t) are also important because the oxidizability of the hydrocarbon is defined as $k_p\sqrt{2kt}$, which influences the overall kinetics. Substrates with higher k_p and lower k_t are apparently easy to oxidize, due to the high peroxy radical concentration at the steady-state. Oxidizability of numerous substrates were

reported in the literature, the k_p and k_t values of some such substrates are listed in table 1.3 [23]. It is clear from the table that oxidizability of hydrocarbons can vary considerably, 1000-fold's difference can be seen from some saturated to polyunsaturated hydrocarbons [13].

1.2 Autoxidation inhibition and Antioxidants

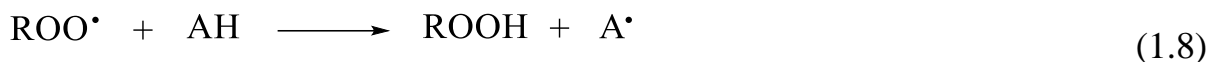
In order to understand how to inhibit the autoxidation process, a lot of researches have been carried out. In the past 60 years, research of antioxidants (AH) has expanded to a variety of multidisciplinary fields to understand their behavior. Compounds capable of directly suppressing free radical formation and chain reaction of autoxidation are called *direct antioxidants* and have been widely studied, ranging from natural compounds to the synthetic ones [24]. They are usually divided into two main groups, *preventive antioxidants* and *chain-breaking antioxidants* (also called radical-trapping antioxidants), as they interfere with the initiation and propagation reactions, respectively [4,23]. Preventive antioxidants include UV filters, preventing the photochemical decomposition of biomolecules, such as melanin in mammal's skin, metal (copper and iron) chelators, preventing generation of HO• and RO• radicals by Fenton reactions, and some ROS decomposers like SOD enzymes [25].



Scheme 1.6. Mechanism of different types of antioxidants interfering with free radical autoxidation.

Chain-breaking antioxidants including α -tocopherol (vit. E), flavonoids and ubiquinol (CoQH₂), perhaps the most important and effective small molecule antioxidants, which

react with peroxy radicals rapidly, faster than oxidative chain propagation, forming new inactive radicals which do not propagate the autoxidation chain [26].



1.2.1 Phenolic Antioxidants

Researches on antioxidants has been expanded in a wide variety of fields, such as food and pharmaceutical products, owing to their protective roles toward oxidative damage, as well as reducing oxidative stress associated with pathological processes [27,28]. Specifically, a growing number of studies are devoted to addressing the roles of antioxidants in oxidative stress, apoptosis and neurological diseases, cancers and cardiovascular health problems [29], etc.

Humans could get antioxidants from supplements or directly from dietary food such as fruits and vegetables, where the most abundant ones are phenolics, also including polyphenolics and flavonoids. Of course, there are also nonphenolic antioxidants such as the well-known ascorbic acid [30] and sulfenic acids [31,32]. Comprehensive reviews on the types, activity and mechanism of antioxidants have been published, here only the general classification of antioxidants is given in Figure 1.1 [33].

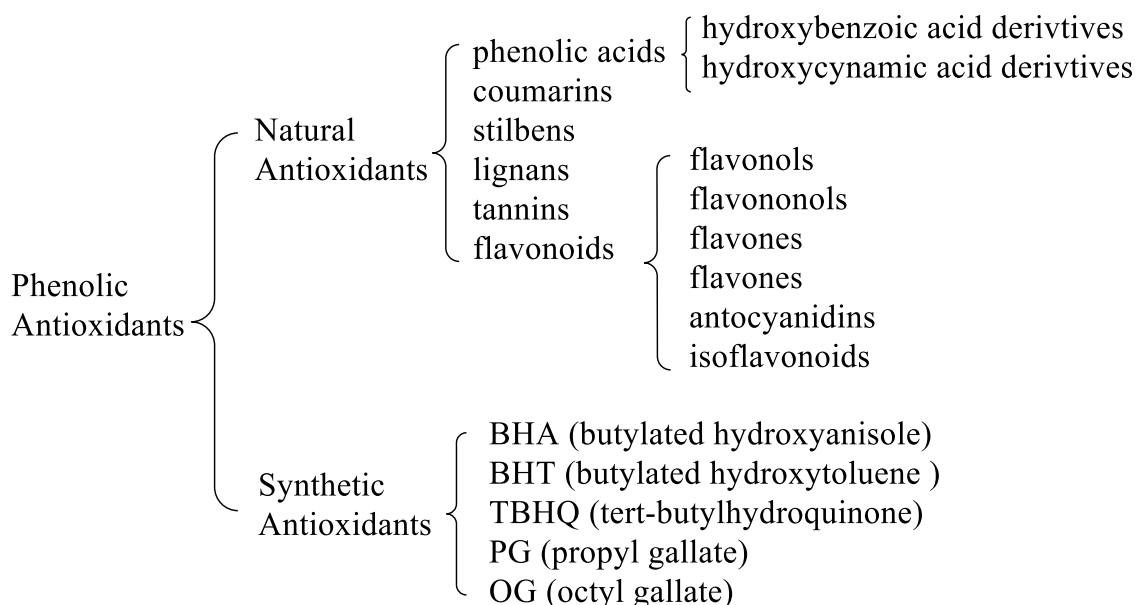


Figure 1.1. Classification of phenolic antioxidants

Phenolic antioxidants are also widely used antioxidants in industry, especially in the food industry, where they are added to maintain food flavors, colors and textures, thus prolong shelf life [32].

Among synthetic phenolic antioxidants, which are effective and cheap, the most popular are butylated hydroxyanisole (BHA), butylated hydroxytoluene (BHT), *tert*-butylhydroquinone (TBHQ), propyl gallate (PG) and octyl gallate (OG), shown in Figure 1.2 [34]. These synthetic phenolic antioxidants are also used as a standard to compare and test activity of other antioxidants.

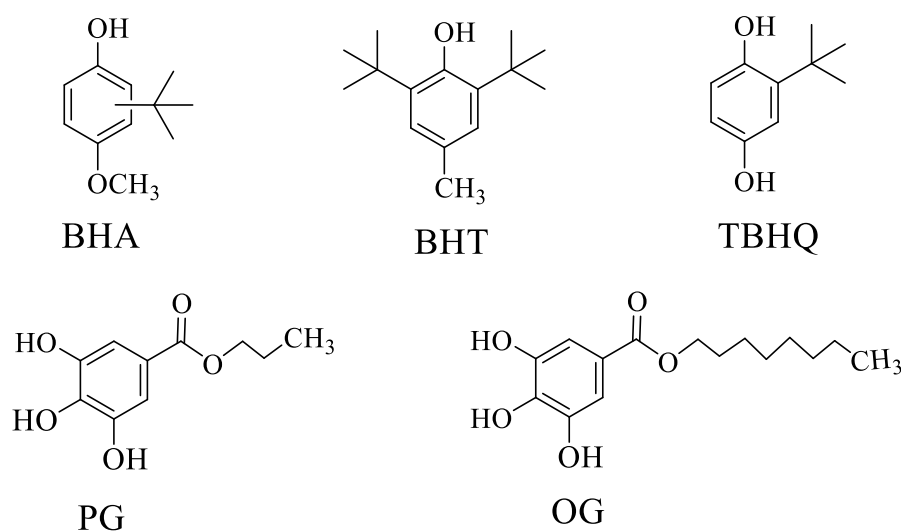
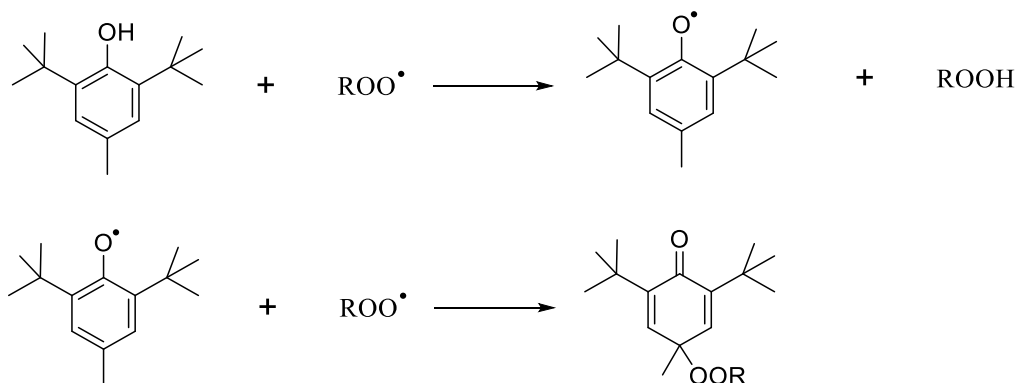


Figure 1.2. Structures of the most putative and popular synthetic phenolic antioxidants

1.2.2 Activity of phenolic antioxidants

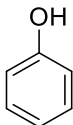
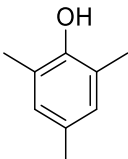
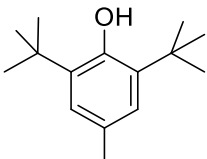
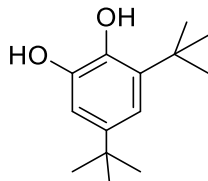
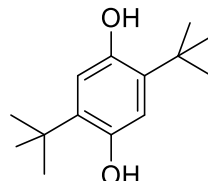
The activity of phenolic antioxidants depends on their hydroxyl groups which transfer an H-atom to peroxy radicals, yielding a stable phenoxyl radical ($\text{ArO}\cdot$) that is unreactive to carry on the autoxidation chain [35]. In fact, $\text{ArO}\cdot$ are persistent until they combine with another radical to quench their free valence, yielding a variety of non-radical products (e.g. Scheme 1.7). That's why mono-phenolic antioxidant are reported to have a stoichiometric $n = 2$, such as BHT, whose mechanism is presented below as an example [26].



Scheme 1.7. Phenolic radical-trapping antioxidants trap two peroxy radicals, as exemplified by BHT.

When talking about the antioxidant activity, not only n , but also their rate constants of reaction with peroxy radicals (k_{inh}) need to be considered to describe their autoxidation inhibition efficiency. Generally, higher k_{inh} and n means better effect, where k_{inh} is considered as the most important parameter. The performance of phenolic antioxidants is influenced mainly by their own structure-determined properties, such as their O-H BDEs, the steric hinderance around the OH group, and their interactions with solvent and the oxidized substrates [36].

Table 1.4. O-H BDE of some phenolic antioxidants [39,40].

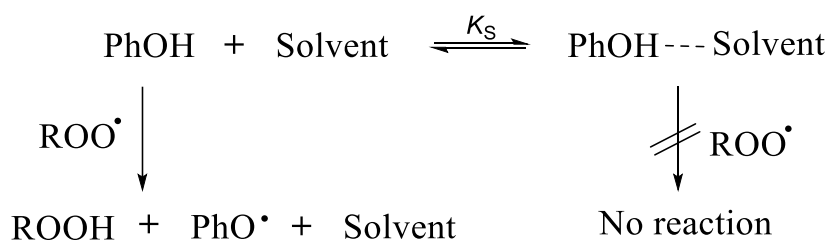
Phenolic Antioxidants					
O-H BDE (kcal/mol)	88.3	82.7	81.0	79.3	80.8

O-H BDE of phenolic antioxidants is a major contributor to their antioxidant potentials, and lower O-H BDE usually means higher activity. As shown in Table 1.4, the O-H BDE of phenols is directly influenced by the substituents on the aromatic ring. Generally, electron donating substituents (e.g. 4-OMe) lower the O-H BDE, inversely,

electron withdrawing substituents (e.g. 4-NO₂) increase the O–H BDE. Moreover, as shown in Table 1.4, alkyls (e.g. methyl or *tert*-butyl) give similar contribution to the O-H BDE [37]. In addition, introduction of a second OH group in the *ortho* or *para* positions of the aromatic ring could decrease the O–H BDE in phenols significantly [38].

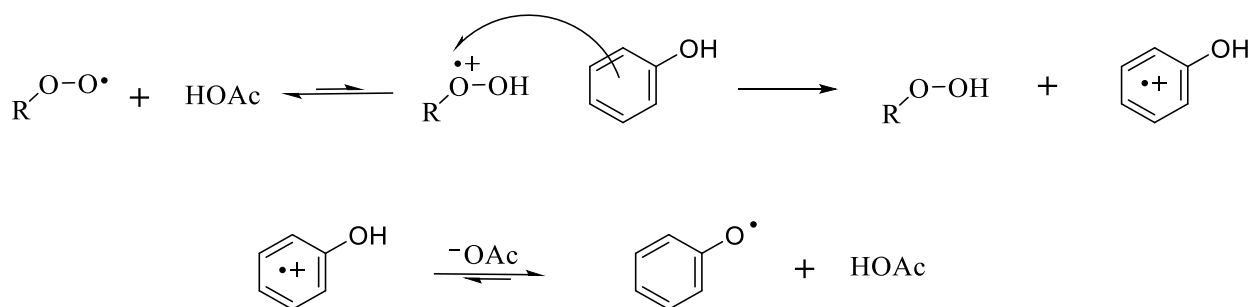
Steric hindrance largely and obviously influences the reactivity of phenols, which also depends on the identity and position of substituents. More hindered OH groups usually indicate less effective antioxidants because they react slower with peroxy radicals.

Hindered phenoxyl radicals have generally longer life-time, but this is not related to the antioxidant activity. More hindered phenols are also more stable and convenient to manufacture, which is why they are so widely represented in commercial synthetic antioxidants. They are also more convenient to study with EPR radical equilibration (REqEPR) technique (see below) and so they are useful to measure the O-H BDE of substituted phenols, knowing that, as said, any alkyl substituent will give similar contribution to the O-H BDE. The O–H BDEs of representative phenols in Table 1.4 were all measured by REqEPR technique, based on measuring by EPR spectroscopy the equilibrium of H-atom exchange between two couples of phenol/phenoxyl radicals generated together in the same sample. Measurement of the equilibrium constant affords the O-H BDE of an unknown phenol, provided the value is known for the other (reference) phenol, e.g. from previous studies or from high precision calorimetry [41]. Beside structure, also the reaction medium affects the antioxidant activity of phenols. In general, kinetic solvent effects influence the efficacy of phenolic antioxidants due to the hydrogen bond formed between the hydrogen accepting solvent (e.g. acetonitrile) and acidic phenolic O-H group, as depicted in scheme 1.8, thus decreasing k_{inh} [42].



Scheme 1.8. Solvent effects on the activity of phenolic antioxidants.

Moreover, acids, such as acetic acid, have recently been demonstrated to dramatically enhance the reactivity of phenols in relatively polar H-bonding organic solvent such as acetonitrile [43]. The rate acceleration increases positively with the increase of acid concentration, but not with their strength, and proposed mechanism [43] is shown in Scheme 1.9.



Scheme 1.9. The proposed mechanism of acid-catalyzed reaction peroxy radicals with phenols.

In practical terms, discussions on the antioxidant performance should also take into account the specific substrates that need to be protected. Since the experimental k_{inh} in principle is not dependent of the oxidizable substrate, it can be used to compare with the propagation rate constant of the substrate (k_p) to judge the possible protection [23]. Take BHT ($k_{inh} = 1.1 \times 10^4 \text{ M}^{-1} \text{ s}^{-1}$) as an example: used at 0.1% compared to the substrate to protect, it provides excellent protection of cumene ($k_p = 0.34 \text{ M}^{-1} \text{ s}^{-1}$) and fairly good protection of tetrahydrofuran ($k_p = 4.4 \text{ M}^{-1} \text{ s}^{-1}$); however, it hardly competes with the propagation of styrene, offering humble protection of styrene ($k_p = 41 \text{ M}^{-1} \text{ s}^{-1}$) [35,44].

1.3 Methods to test the antioxidant activity

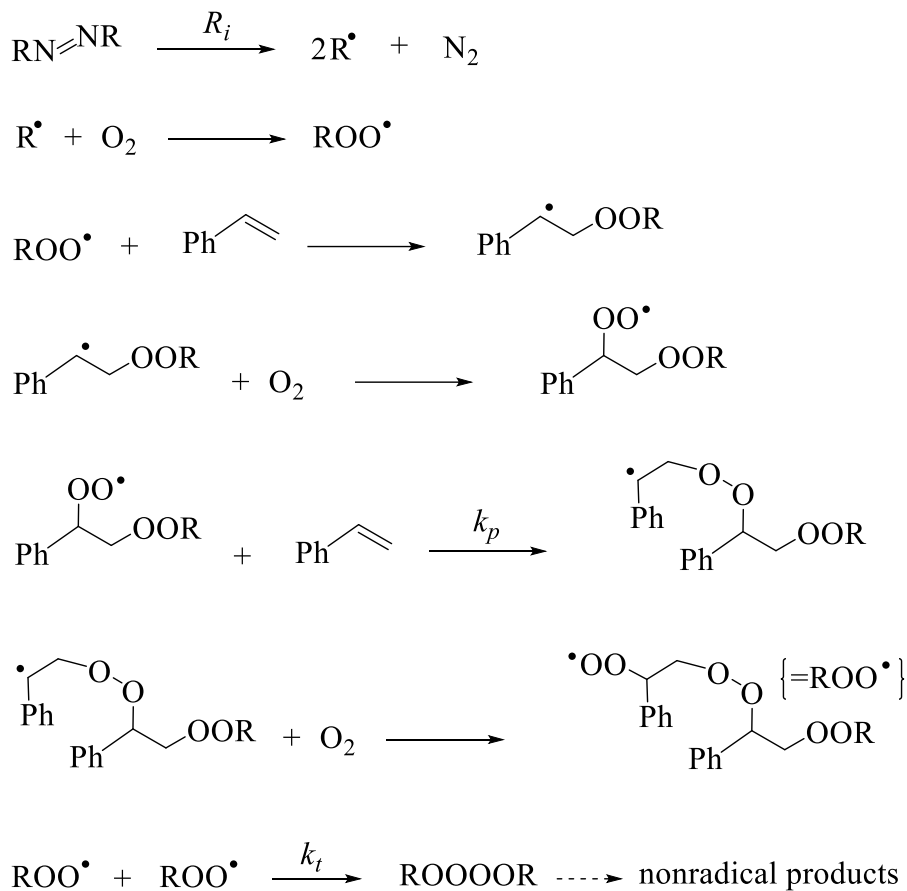
Screening and comparing antioxidant properties require appropriate methods. Plenty different methods were developed to evaluate antioxidant activity of various samples of different research interests. Methods exist to measure reactivity of antioxidants, and their limits and advantages have been recently reviewed [45,46], including direct methods like peroxy radical clocks and inhibited autoxidation studies, where the

formation of products like hydroperoxides or the disappearance of reactants like oxygen is monitored and kinetically analyzed. Other indirect methods include DPPH (1,1-diphenyl-2-picrylhydrazyl radical scavenging), ABTS⁺ (2,2'-azinobis-(3-ethylbenzothiazoline-6-sulphonate) radical scavenging, FRAP (ferric reducing antioxidant power assay), CUPRAC (cupric ions, Cu²⁺ reducing power assay), which are based on the reduction of persistent radicals or of inorganic oxidizing species. There are also some direct methods that do not involve the oxidation of substrates, such as laser flash photolysis [47] and electron paramagnetic resonance (EPR) [43].

1.3.1 Oximetry apparatus

The meaningful measurement of antioxidant properties requires proper methods, wherein, the best-established quantitative method for chain-breaking termination-enhancing antioxidants is arguably the one based on inhibited autoxidation [48]. This method bases on measuring the autoxidation kinetics of a reference substrate, such as styrene and cumene, both in the presence and absence of the investigated antioxidants [48]. Usually, disappearance of reactants (*e.g.* O₂) or the formation of products (*e.g.* hydroperoxides) is monitored to determine the autoxidation kinetics. It's well known that autoxidation occurs spontaneously under air atmosphere; however, in order to control the kinetics of autoxidation, radical initiators such as (AIBN) are usually added at a given temperature to ensure a constant and well-defined rate of initiation (R_i) [49]. The controlled autoxidation of styrene is depicted in Scheme 1.10 [50]. Although the propagation of styrene autoxidation proceeds by addition of the peroxy radical to its C=C double bond, at variance with the propagation mechanism of alkylarenes (*e.g.* cumene) and polyunsaturated fatty acids/esters (*e.g.* methyl linoleate), the kinetics are identical to those of non-polymerizable hydrocarbons and can be subjected to the same kinetic analysis. Styrene is an ideal candidate as the oxidizable substrate to be used in our studies, as it is a highly stable molecule, easy to purify, easy to obtain at modest cost, and with a well established oxidation mechanism. Besides, it has a relatively high

propagation constant ($k_p = 41 \text{ M}^{-1}\text{s}^{-1}$) and consequent oxidizability, which makes it ideal to use with good to very good antioxidants [23].



Scheme 1.10. Autoxidation of styrene initiated by AIBN.

Oxygen consumption is a simple, cost-effective, reliable and predictive method to evaluate the performance of antioxidants, and the interpretation of kinetic data is well-established, thus it is widely used throughout our studies on antioxidants. In our lab, the autoxidation is conducted in a closed system and the consumption of oxygen is monitored by a differential pressure transducer (Figure 1.3) [35,51].

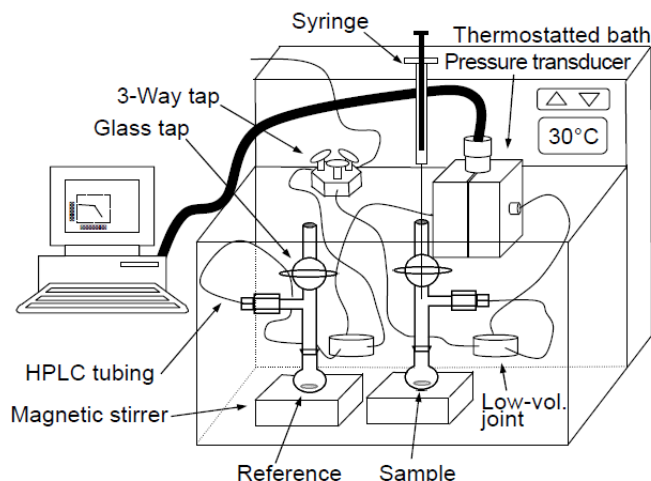


Figure 1.3 Differential oxygen uptake apparatus set in our lab for autoxidation kinetics.

In this apparatus, built in our lab, there are two identical reaction vessels placed in a thermostatic bath which is set at 30°, both the sample and reference flasks are attached to the opposite sides of a differential pressure sensor (based on a variable reluctance membrane) through PEEK™ (or stainless steel) high performance liquid chromatography (HPLC) tubes. The equilibration and isolation of the two channels could be achieved through a three-way valve, which is connected to air and the two channels, and the continuous stirring by magnetic stirrers is used to ensure oxygen equilibration between the air and solutions. In the reference vessel, autoxidation of the substrate is totally inhibited by an excessive amount of a good antioxidant such as (α -tocopherol (α -TOH), $k_{\text{inh}} = 3.2 \times 10^6 \text{M}^{-1} \text{s}^{-1}$), guaranteeing that no oxygen is consumed [52]. However, the substrate in the sample is set to oxidize freely at the beginning in order to get the autoxidation kinetics of the substrate, later on the antioxidant can be injected into the sample flask by a micro syringe through its openable tap, resulting in retarded oxygen consumption until the antioxidant is consumed.

Oxygen uptake plots are recorded as a function of time, as shown in Figure 1.4, where the first line is the autoxidation of substrate without any inhibitor, and the other lines are the inhibited tracts obtained after the addition of antioxidants with different activities.

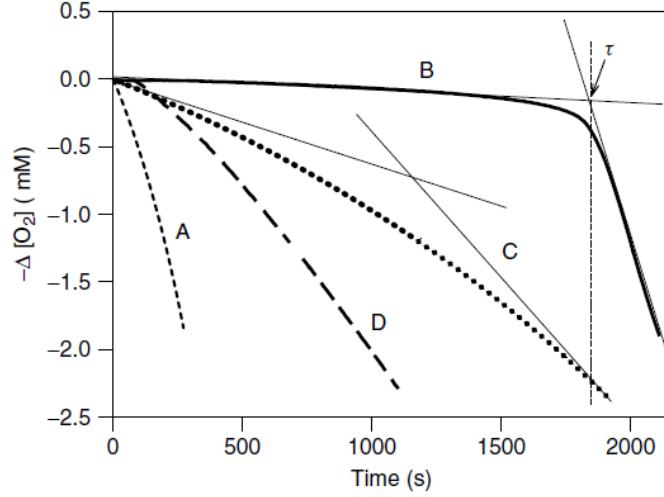


Figure 1.4 Typical oxygen consumption plots obtained during autoxidation of styrene (A) in the absence of and antioxidant, (B) in the presence of a very good antioxidant, (C) in the presence of an average antioxidant, or D) in the presence of a modest antioxidant.

1.3.2 Interpretation of kinetic data

(Derivation of the equations below are shown in Appendix 1.1 and 1.2)

The oxygen consumption in the sample chamber, in fact, reflects the extent of propagation of substrate oxidation. At the initial stages of autoxidation without any antioxidants, the use of azo initiator eliminates the kinetic complications yielding a linear plot of oxygen consumption (plot A in figure 1.4). Steady-state approximation is applied for transient radical species such as $R\cdot$ and $ROO\cdot$.

$$d[R\cdot]/dt = 0 \quad (\text{Eq. 1.4})$$

$$d[ROO\cdot]/dt = 0 \quad (\text{Eq. 1.5})$$

Given that the evolution of reactants (O_2 and RH) and products ($ROOH$) with time are numerically equal, the autoxidation kinetics of substrate could be obtained as follows (Eq.1.6) when the autoxidation chain is sufficiently long [53].

$$\frac{-d[O_2]}{dt} = \frac{-d[RH]}{dt} = \frac{d[ROOH]}{dt} = \frac{k_p}{\sqrt{2k_t}} \sqrt{R_i} [RH]_0 + R_i \quad (\text{Eq. 1.6})$$

Where $[RH]_0$ is the initial concentration of oxidizable substrate (the substrate consumption at the initial stages of autoxidation was taken as negligible), R_i is the initiation rate; $k_p/(2k_t)^{1/2}$ is the oxidizability of substrates.

As shown in the plot B of Figure 1.4, an effective antioxidant could inhibit the oxygen consumption almost completely until the antioxidant is consumed totally, then an

uninhibited autoxidation, similar to the one obtained without antioxidant, will show up again.

During the inhibited period, antioxidant competes with the propagation by quenching the peroxy radicals produced by the initiators (or from substrate oxidation), thus the length of the inhibition periods τ (Figure 1.4) could provide an equation as follow (equation 1.7) to determine the stoichiometric factors n [23].

$$R_i = \frac{n[AH]}{\tau} \quad (\text{Eq. 1.7})$$

$[ArOH]_0$ is the initial concentration of the antioxidant, and τ is the length of the inhibition periods. Alternatively, this equation could also be used to determine the initiation rate (R_i) based on an autoxidation inhibited by a known amount of effective antioxidant, such as α -TOH, whose stoichiometric coefficient is well established [23].

The initial slope of oxygen consumption during the inhibited period provides equation 1.8 to determine the inhibition rate constant k_{inh} by assuming that every ROO• radical is trapped by the antioxidant and its corresponding radical [54,55].

$$-\frac{d[O_2]}{dt} = \frac{k_p}{nk_{inh}} \frac{[RH]R_i}{[AH]} + R_i \quad (\text{Eq. 1.8})$$

If the inhibited period in Figure 1.4 is not so clearly identified as in plot B, or the initial portion of the plot is not usable to get oxygen consumption rate (plot C), equation 1.9 can be used [54,55].

$$\Delta[O_2]t = \frac{k_p[RH]R_i}{k_{inh}} \ln\left(1 - \frac{t}{\tau}\right) \quad (\text{Eq. 1.9})$$

There are also some cases like in plot D, where the efficiency of the antioxidant is so small that inhibition period cannot be observed clearly: equation 1.10 was derived by Denisov and Khudyakov to determined k_{inh} in such cases [56].

$$\frac{R_{ox,0}}{R_{ox}} - \frac{R_{ox}}{R_{ox,0}} = \frac{nk_{inh}[AH]_0}{\sqrt{R_i 2k_t}} \quad (\text{Eq. 1.10})$$

where R_{ox} and $R_{ox,0}$ are the rates of oxygen consumption ($-d[O_2]/dt$) measured from the plots, under identical experimental settings, in the presence and absence of the antioxidant, respectively. Besides, kinetic data and the changes in reactants and

products could also be obtained by computational simulation (e.g. with Copasi software) of the oxygen-uptake trace [50].

In a summary, hydrocarbon autoxidation follows a free radical chain mechanism in the absence of inhibitors, leading to a constant rate of oxygen consumption when it is initiated with a constant rate R_i . Antioxidants (AH) can break the radical chain and compete with propagation, resulting in oxygen consumption that is slowed down and/or delayed by an inhibition time τ . From the plot of oxygen consumption obtained with a substrate whose rate constants for oxidative chain propagation k_p and termination $2k_t$ are already known, it is possible to calculate the inhibition rate constant (k_{inh}) and the stoichiometric factor (n) for the trapping of chain-carrying peroxyl radicals by the antioxidant from (Eq.1.7 and Eq.1.8-1.10) [48]. Vice versa, Eq. 1.6 and Eq. 1.8-1.10 allow to determine k_p and $2k_t$ of an unknown substrate by performing autoxidations in the presence of an inhibitor whose values of k_{inh} and n are known. The relative rate constants can be used to compare the antioxidant activity of compounds or the oxidizability of substrates [57]. Thus, the autoxidation kinetics of relevant substrates like stripped sunflower oil (SSO), olive oil (OO), squalene (SQ), and p-cymene (p-C) were calibrated by using the same oximetry method, as described in the following section.

1.4 Research objects

Despite the very extensive research on antioxidants in different fields of science, which has brought to an enormous number of publications on the topic in recent and less recent years, still very few investigations have addressed the discovery and characterization of new antioxidants on a truly quantitative basis, focusing on the kinetics and mechanism of the antioxidant action. This is particularly true in the vast field of natural antioxidants. Among them, plant essential oils have received enormous interest in recent years, both for their purported beneficial properties to human health and for the possibility to use them as natural preservatives for food products, where

most of them can also contribute antimicrobial preservative action, thereby allowing to replace synthetic preservatives of all kinds with natural alternatives, which are better perceived by the consumer. Despite this interest, extremely limited data are available of the kinetic behavior of essential oils or their components, and k_{inh} , n values for such compounds are virtually absent from the literature, most investigation being based on rapid tests affording misleading or contradicting results [46]. At the same time, to obtain quantitative measurements of the antioxidant activity, the best-established method is that of controlled inhibited autoxidation of a reference substrate (see previous section). This, in turn, requires well characterized substrates. Surprisingly very few natural materials have been kinetically characterized in this respect, so far, limiting the investigation of new natural antioxidants in food-born or biomimetic settings. To overcome this lack of knowledge, we have worked in two parallel directions in two studies that will be presented in the following of this chapter. First, we have duly investigated and accurately calibrated natural oxidizable substrates, which could be used for future investigation on new antioxidants. Second, we have undertaken a systematic study on the antioxidant activity of common essential oils and their representative components.

1.5 Calibration of natural substrates

(published as *J. Agric. Food Chem.* 2019, 67, 6902–6910. DOI: 10.1021/acs.jafc.9b01400)

The protection from autoxidation of food products or other agricultural materials used in manufactured goods such as cosmetics and pharmaceuticals, is of the utmost importance to guarantee their safety. Therefore, the search for novel antioxidants remains an important area of research. [46]. The rational strategies to guarantee the protection of different natural materials would require knowledge of their kinetics of autoxidation, since the inhibition of autoxidation is always a process regulated on kinetic bases [23].

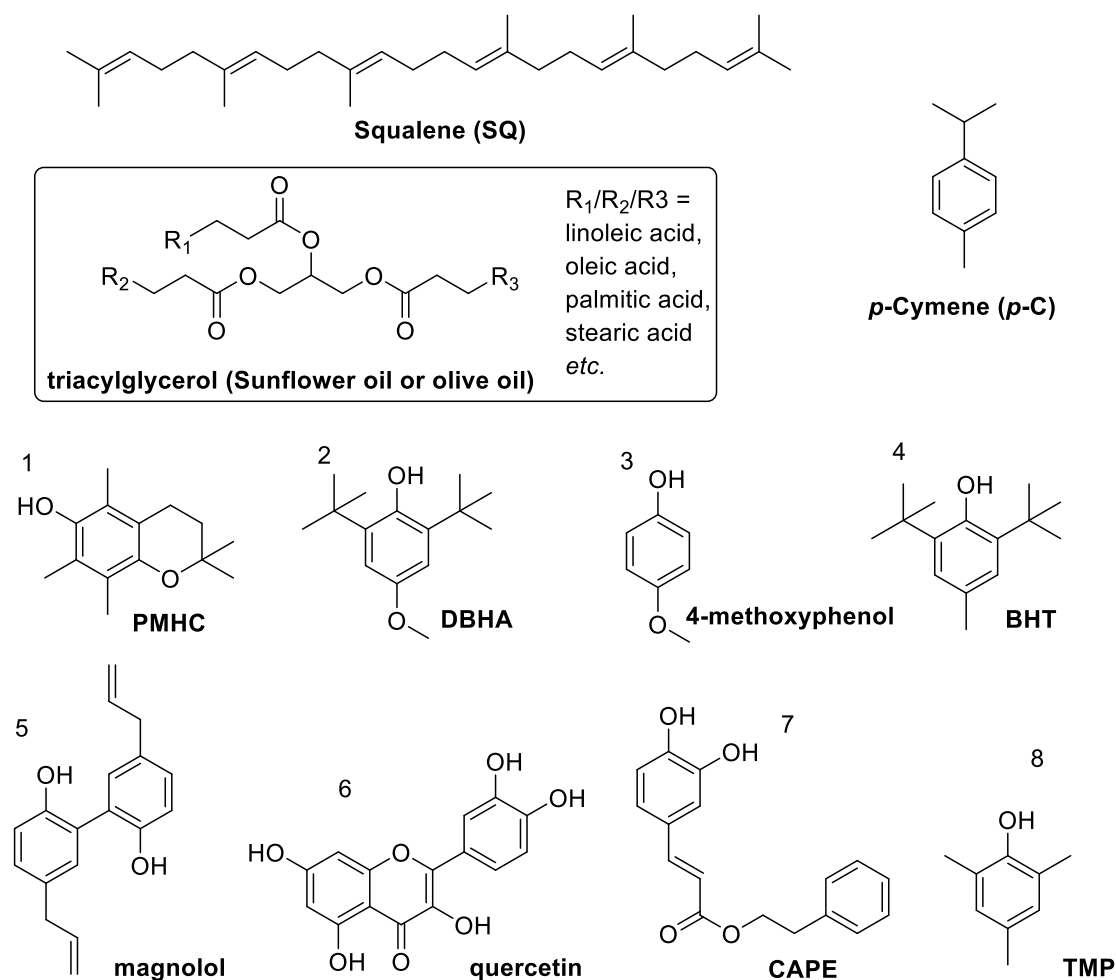


Figure 1.5 Oxidizable substrates investigated in this study and reference antioxidants used to calibrate the substrates (1–4) and to validate their use (5–8).

Surprisingly, very few natural biomimetic substrates have been kinetically characterized so far, limiting the quantitative testing of phytochemicals under representative settings, as well as the knowledge of a key feature concerning the antioxidant protection of food and agricultural materials. The choice is restricted to (scarcely available) purified methyl esters of oleic, linoleic, and linolenic acids [58], while more recently the rate constants for chain propagation (k_p) for other unsaturated fatty acids and their methyl esters (arachidonic, eicosapentenoic, docosapentenoic), cholesterol, 7-dehydrocholesterol [59], and other cholestadienols [60,61] have been reported, and their mechanism of autoxidation has been discussed [60,62]. None of the many triglyceride-based natural oils have been kinetically characterized to date.

Similarly, knowledge of the behavior of other representative natural materials is missing. To fill this gap, we report here the full kinetic characterization of four different substrates which are representative of the chemical diversity of natural oxidizable materials: namely, stripped sunflower oil (SSO), and stripped olive oil (OO), two triglyceride, squalene (SQ), an unsaturated hydrocarbon that is the main component of olive oil unsaponifiable fraction, and p-cymene (p-C), a monoterpene ubiquitous in essential oils and olive oil (Figure 1.5). Phenols 1–4 were used as reference antioxidants. Further, we show the usefulness of such commonly available substrates in studying representative chain-breaking antioxidants: magnolol (5), quercetin (6), caffeic acid phenethyl ester (CAPE, 7), and 2,4,6-trimethylphenol (TMP, 8), chosen to comprise the structural variability encountered in phenolic antioxidants.

1.5.1 Results and Discussion

1.5.1.1 Autoxidation kinetics of SSO

Stripped sunflower oil (SSO) is obtained from sunflower oil upon removing naturally occurring phenolic components and carotenoids, which would protect the oil from oxidation, by treatment with alumina and vegetal carbon. It was chosen as a reference substrate due to its modest cost, high availability, facile oxidation and because it had been used before for (qualitative) antioxidant tests [63]. The ease with which organic substrates undergo autoxidation is quantified by a kinetic parameter named oxidizability, which is given by the ratio of the rate constant for radical chain-propagation k_p and the square root of the constant for chain-termination $2k_t$ (Eq.1.11) [23,64]. Under constant rate of radical initiation R_i , this quantity determines the rate of autoxidation as detailed in reaction 1.3 [35].

$$\text{Oxidizability} = \frac{k_p}{\sqrt{2k_t}} \quad (\text{E.q. 1.11})$$

Regular sunflower seed oil (*i.e.* not considering “high oleic” and “mid oleic” varieties) is composed mainly of triacylglycerols where about 60% of fatty acids residues is

represented by highly oxidizable linoleic acid (C18:2), with negligible content of linolenic acid (C18:3) or other PUFA, while the remaining residues are typically represented by less oxidizable oleic acid (C18:1) and saturated fatty acids (C18:0 and C16:0) [65].

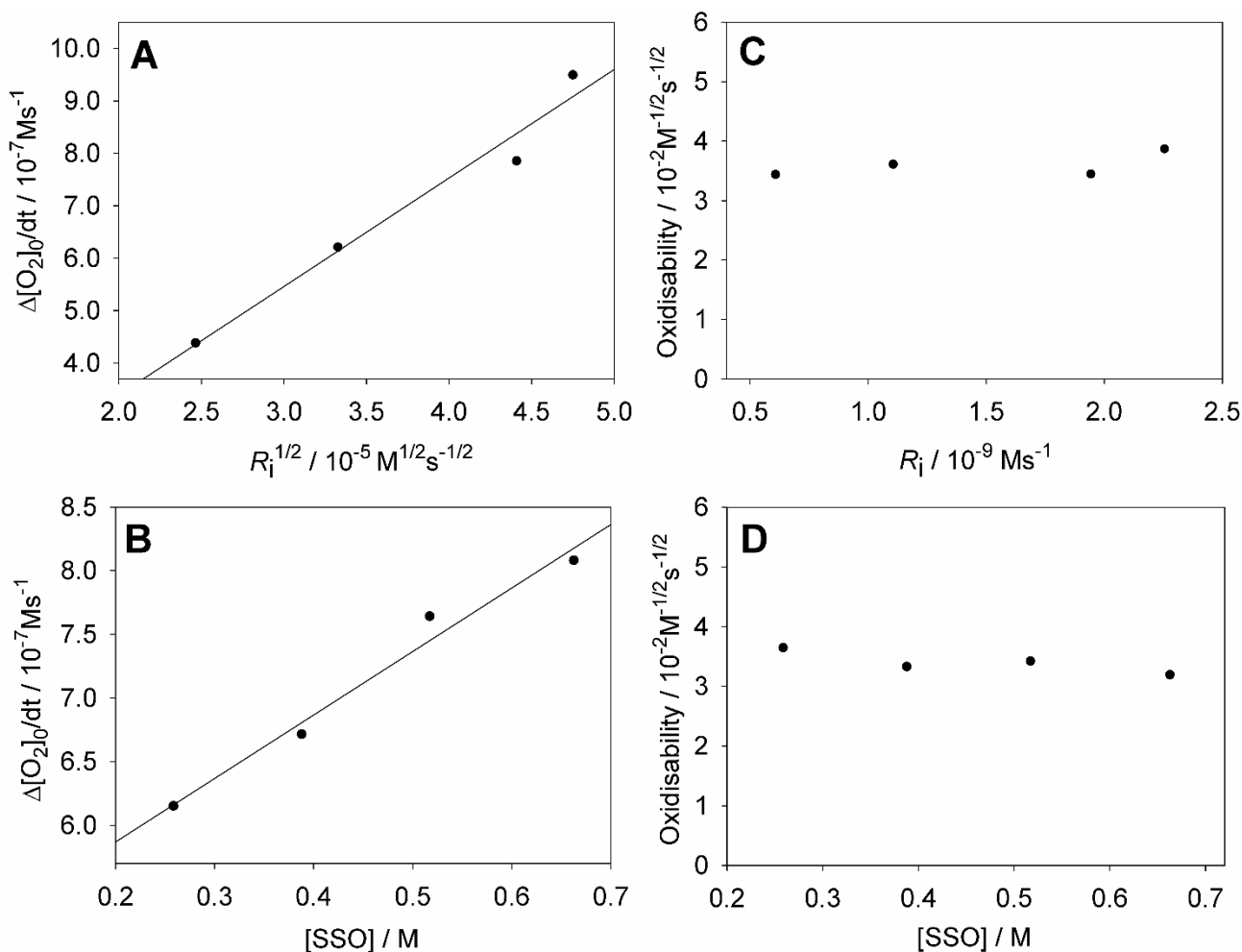


Figure 1.6 Uninhibited autoxidation of SSO measured in PhCl at 30°C. A) Plot of the oxygen consumption against R_i ($[\text{SSO}] = 0.517 \text{ M}$); B) Plot of the oxygen consumption against SSO concentration, with $[\text{AIBN}] = 0.025 \text{ M}$; C) Plot of the oxidizability of SSO against R_i ($[\text{SSO}] = 0.517 \text{ M}$); D) Plot of the oxidizability of SSO against its concentration, with $[\text{AIBN}] = 0.025 \text{ M}$.

Since linoleic acid has oxidizability 24-fold higher than oleic acid and thousands-fold higher than saturated fatty acid [23]. One can expect that the oxidizability of sunflower oil is dictated by its content in linoleic acid. This is due to the much higher reactivity of peroxy radical in abstracting H-atoms from of the $>\text{CH}_2$ function in bis-allylic position (C11) in linoleic residues ($k_p = 62 \text{ M}^{-1}\text{s}^{-1}$ at 303 K) [23] as compared to the

allylic position ($k_p = 0.89 \text{ M}^{-1}\text{s}^{-1}$ for 2 methylene groups in oleic acid at C8 and C11) or to saturated chains ($k_p \sim 0.01 \text{ M}^{-1}\text{s}^{-1}$ for a C18:0) [23]. Therefore, the average molar concentration of triglycerides in neat SSO ($d = 0.907 \text{ g/mL}$) was estimated as 1.034 mol/L, based on the average molecular weight of SSO triglycerides determined from fatty acid composition (MW = 877.4 g/mol), which was analyzed by GC-MS (table A.1.1)

Autoxidation kinetic measurements revealed that SSO is a “well behaved” oxidizable substrate, with the rate of oxygen consumption being linearly dependent on the concentration of the substrate in the tested concentration range, and the oxidizability being a true constant: $k_p / \sqrt{2k_t} = 0.036 \text{ M}^{-1/2}\text{s}^{-1/2}$ at 303K in chlorobenzene, independent of the concentration of substrate and of the rate of radical initiation (Figure 1.6). In order to measure the absolute value of k_p , we performed a series of autoxidation kinetic measurements in the presence of different amounts of PMHC (1) or DBHA (2), as reference antioxidants, the typical and representative plot was shown in figure 1.7.

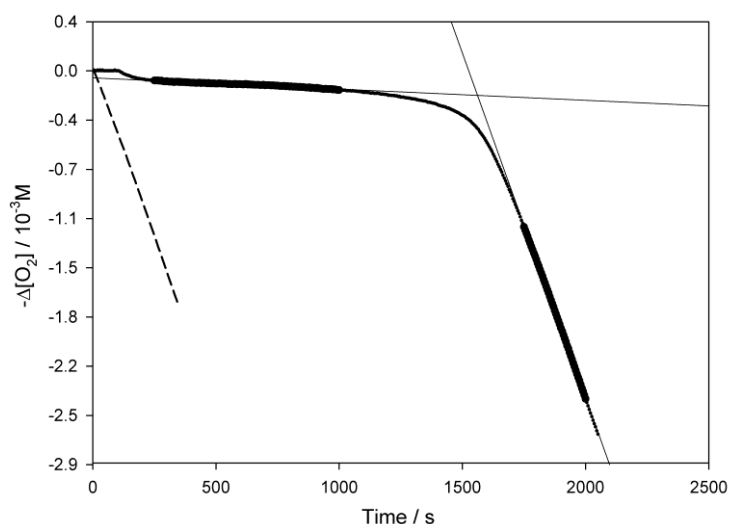


Figure 1.7 Oxygen consumption measured during the autoxidation of stripped sunflower oil (50 % v/v; 0.517M) initiated by AIBN (0.05 M) in chlorobenzene at 303K, without inhibitors (dashed line); or in the presence of: PMHC (1) 2.5 \square M. Regression lines indicates the slopes of the inhibited and uninhibited periods, which can be processed with equations 8 and 7, respectively, to obtain the oxidizability ($k_p / \sqrt{2k_t}$) and the value of k_p , respectively. The cross-point of the two regression lines indicates the inhibition time τ (1600 s in this experiment), which affords the measured rate of initiation R_i ($3.1 \times 10^{-9} \text{ Ms}^{-1}$, in this experiment) upon processing with equation 10.

Under these conditions (in the presence of a chain-breaking antioxidant) chain termination is given mainly by reaction of the antioxidant with peroxy radicals, and self-termination of the radical chain becomes negligible[23,64]. Therefore, the rate of oxygen consumption can be analyzed by eqs 1.8-1.10, using the known inhibition constants (k_{inh}) of the two antioxidants to obtain the rate constant k_p with high accuracy [64].

Although k_{inh} for both PMHC and DBHA are known with high accuracy in chlorobenzene (the solvent used for autoxidations), upon using such k_{inh} values (3.2×10^6 and $1.1 \times 10^5 \text{ M}^{-1}\text{s}^{-1}$, respectively [23,66]) to calculate the k_p of SSO, results obtained from the autoxidations inhibited by PMHC or DBHA were in clear disagreement. This behavior was attributed to the presence in SSO of ester groups, able to accept H-bonds from the reference phenols, thus lowering their ability to react with radicals and their k_{inh} [42,26]. This well-known effect is expected to be different in magnitude for the two phenols because the steric crowding of the *tert*-butyl groups in DBHA (2) protects the phenolic OH from forming H-bonds with SSO [26]. To quantitatively ascertain the degree of H-bond formation, the infrared spectrum of the reference phenols in chlorobenzene in the presence or in the absence of SSO was measured (Figure 1.8) [66]. In the weak H-bonding solvent chlorobenzene, the stretching of the “free” phenolic OH gives a sharp peak at about 3610 cm^{-1} . In the presence of SSO, this peak decreases in intensity, and is replaced by a broader peak at lower frequency corresponding to the H-bonded OH group. As it is clearly visible in Figure 1.8, H-bond formation is more important for of PMHC than for DBHA, due to the different steric crowding.

From IR spectra the amount of PMHC not H-bonded to SSO was calculated as 48%, while that of DBHA as 88%. Therefore, considering that phenols H-bonded to substrate molecules (here acting as a co-solvent) are not reactive toward peroxy radicals [42] the “effective” k_{inh} of the two antioxidants in the presence of SSO needs to be downscaled to 1.5×10^6 and $9.8 \times 10^4 \text{ M}^{-1}\text{s}^{-1}$ respectively for PMHC and DBHA [26]. By

applying this correction, the k_p of SSO obtained with the two reference phenols converged, affording $k_p = 66.9 \pm 5.8 \text{ M}^{-1} \text{ s}^{-1}$ for SSO at 30°C, (see table 1.5).

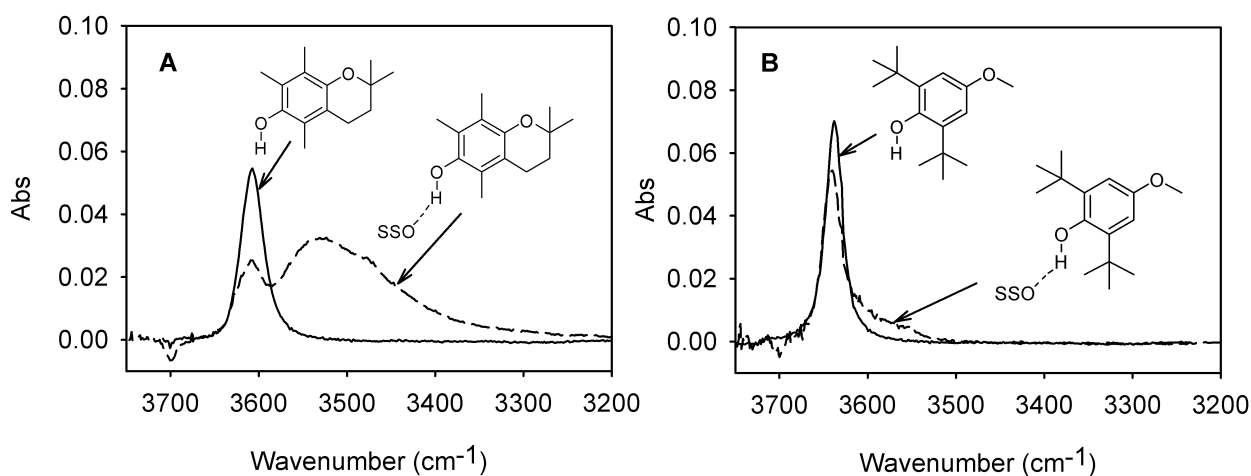


Figure 1.8. Infrared spectra in the O-H stretching region of PMHC **1** (A) and DBHA **2** (B) (0.01 M), dissolved in chlorobenzene (solid line) or in 1:1 SSO/chlorobenzene mixture (dashed line).

Table 1.5 Kinetic parameters measured for the autoxidation of stripped sunflower oil (SSO) in chlorobenzene (50 %, v/v) at 30 °C, initiated by AIBN, in the presence of PMHC (**1**) or DBHA (**2**) as reference antioxidants.

entry	[antiox.] (μM)	R_i (M s^{-1})	$d[\text{O}_2]_0/dt$ (M s^{-1})	$d[\text{O}_2]_{in}/dt$ (M s^{-1})	$k_p/\sqrt{2k_t}$ ($\text{M}^{-1/2} \text{ s}^{-1/2}$)	k_p ($\text{M}^{-1} \text{ s}^{-1}$)
PMHC						
1	5.0	3.5×10^{-9}	1.24×10^{-6}	1.30×10^{-8}	0.038	58.8
2	2.5	1.4×10^{-9}	6.93×10^{-7}	1.05×10^{-8}	0.033	66.1
3	1.3	1.3×10^{-9}	7.18×10^{-7}	2.87×10^{-8}	0.036	76.1
DBHA						
4	11	3.7×10^{-9}	1.22×10^{-6}	1.83×10^{-7}	0.038	71.2
5	11	3.5×10^{-9}	1.05×10^{-6}	8.41×10^{-8}	0.033	67.8
6	14	1.4×10^{-9}	7.54×10^{-7}	7.50×10^{-7}	0.037	61.2
7	5.5	1.6×10^{-9}	7.57×10^{-7}	7.20×10^{-8}	0.038	66.9
mean \pm SD					0.036 \pm 0.002 ^a	66.9 \pm 5.8 ^a

Finally, upon combining it with the oxidizability ($k_p/\sqrt{2k_t}$) value, the value of $2k_t$ for

SSO was determined as $3.45 \times 10^6 \text{ M}^{-1}\text{s}^{-1}$ (Table 1.9). It is interesting to compare the oxidizability measured for SSO to that of the monoester methyl linoleate, as it is proportional to the number of linoleic acid residues in the molecule. Each triacylglycerol unit contains an average of 1.7 molecules of linoleic acid and has $k_p / \sqrt{2k_t}$ 1.7-fold that of methyl linoleate ($0.021 \text{ M}^{-1/2}\text{s}^{-1/2}$ at 30° [67]). This observation is in agreement with the pioneering work of Pryor and coworkers who found that the oxidizability of synthetic linoleyl mono- di- and tri-glycerides was proportional to the total number of “activated” $>\text{CH}_2$ groups in bis-allylic position in the molecule, *i.e.* to the number of linoleyl residues [68].

Counterintuitively, our data show for the first time that this relationship does not hold for the (most important) propagation rate constant, as k_p of SSO is close to that of methyl linoleate, and much lower than the value ($62 \times 1.7 = 105 \text{ M}^{-1}\text{s}^{-1}$) that would be expected in case the same proportionality was maintained. Therefore, the higher oxidizability of the triacylglycerol is (almost) entirely due to the lower rate of chain termination (*viz.* $3.5 \times 10^6 \text{ M}^{-1}\text{s}^{-1}$ vs. $8.8 \times 10^6 \text{ M}^{-1}\text{s}^{-1}$ at 30°C in chlorobenzene [23]).

1.5.1.2 Autoxidation kinetics of olive oil

Olive oil is among the most common vegetable oils, which is usually used in cooking like SSO, salad seasoning, as well as in cosmetic and pharmaceutical manufacturing. It is mainly composed of oleic acid, with a small amount of other fatty acids, such as linoleic acid and palmitic acid. Olive oil, being a complex mixture of triglycerides, is hard to characterize as a substrate due to its high variability depending on its geographic origin, type of olive and multiple other variables. In this study, the olive oil was purchased from the local market, the average molar concentration of triglycerides in neat OO ($d = 0.911 \text{ g/mL}$) was estimated as 1.012 mol/L , based on the average molecular weight of OO triglycerides according to its fatty acid composition (MW = 900 g/mol) determined by GC-MS (table A.1.2.). When OO was subjected to controlled

autoxidation, the rate of oxygen consumption, was related to $\sqrt{R_i}$ and its oxidizability $k_p/\sqrt{2k_t}$ remained constant as previously observed for SSO (Table 1.6).

Table 1.6. Kinetic parameters measured for the autoxidation of OO in chlorobenzene at 30 °C, initiated by AIBN, in the presence of PMHC (1) or DBHA (2) as reference antioxidants.

entry	OO (M)	R_i (M s ⁻¹)	$d[O_2]_0/dt$ (M s ⁻¹)	$k_p/\sqrt{2k_t}$ (M ^{-1/2} s ^{-1/2})	antiox. (M)	$d[O_2]_{in}/dt$ (Ms ⁻¹)	k_p (M ⁻¹ s ⁻¹)
2	0.506	49×10^{-9}	-3.02×10^{-7}	9.44×10^{-3}	PMHC2.5	1.41×10^{-8}	32.4
3	0.38	3.69×10^{-9}	-1.98×10^{-7}	8.57×10^{-3}	PMHC2.5	1.16×10^{-8}	36.7
4	0.25	4.4×10^{-9}	-1.54×10^{-7}	9.06×10^{-3}	PMHC2.5	1.07×10^{-8}	37.2
6	0.506	3.8×10^{-9}	-2.86×10^{-7}	9.17×10^{-3}	DBHA 5	7.47×10^{-8}	33.6
7	0.38	3.27×10^{-9}	-2.00×10^{-7}	9.22×10^{-3}	DBHA 5	5.38×10^{-8}	37.0
8	0.25	4.13×10^{-9}	-1.45×10^{-7}	9.02×10^{-3}	DBHA 5	4.37×10^{-8}	34.9
9	0.506	3.08×10^{-9}	-2.29×10^{-7}	8.86×10^{-3}	DBHA 5	5.65×10^{-8}	31.2
mean \pm SD				$(9.0 \pm 0.8) \times 10^{-3}$	mean \pm SD		34.7 ± 1.6

Similarly, to SSO, we measured the k_p value by performing inhibited autoxidation using reference PMHC and DBHA as antioxidants.

Being a triglyceride, its ester groups were also confirmed by the IR spectrum (Figure 1.9) to be able to accept H-bonds from the reference phenols, thus lowering their ability to react with radicals and their k_{inh} , as previously observed for SSO, and the amount of PMHC not H-bonded to OO was calculated as 42%, while that of DBHA as 74%. Thus, the “effective” k_{inh} of the two antioxidants in the presence of OO needs to be downscaled to 1.3×10^6 and 9.1×10^4 M⁻¹s⁻¹ respectively for PMHC and DBHA. **(95)** By applying this correction, the k_p of OO obtained with the two reference phenols was $k_p = 34.7 \pm 5.8$ M⁻¹s⁻¹ at 30°C, affording $2k_t = 1.5 \times 10^7$ M⁻¹s⁻¹ (Table 1.9).

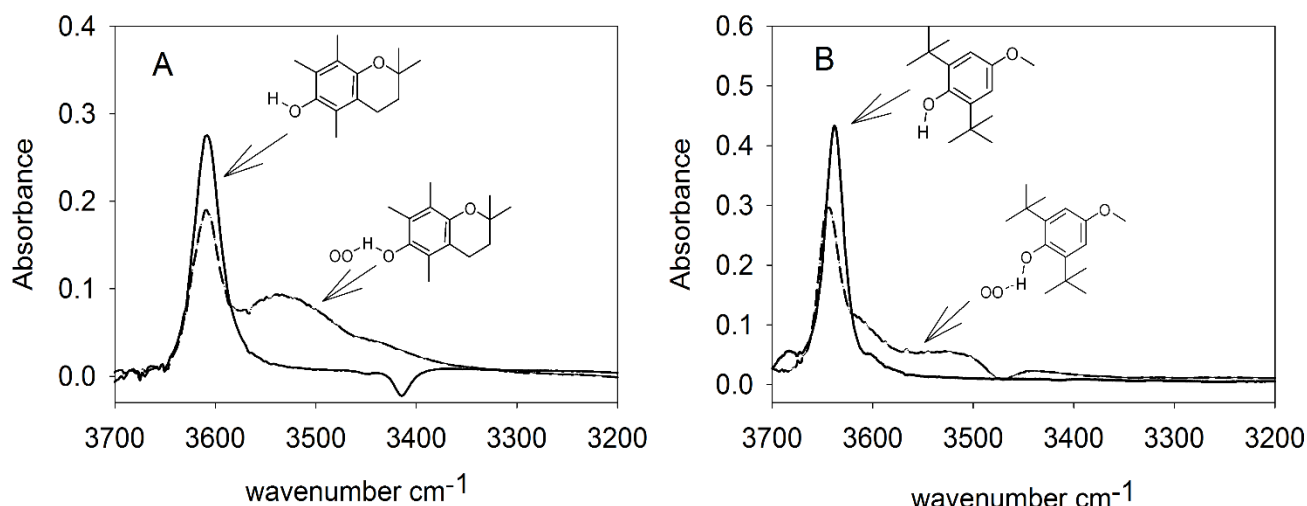


Figure 1.9 Infrared spectra in the O–H stretching region of PMHC 1 (A) and DBHA 2 (B) (0.01 M), dissolved in chlorobenzene (solid line) or in a OO /chlorobenzene mixture (dashed line).

1.5.1.3 Autoxidation kinetics of Squalene

Squalene is a triterpenic polyunsaturated hydrocarbon that represents the main component of olive oil unsaponifiable fraction. In this form it is widely used in cosmetics and dermatologic products as skin emollient and to treat disorders like acne, psoriasis, and atopic dermatitis [69]. It is ubiquitous in plants and abundant in vegetable oils such as amaranth, rice and wheat [69,70]. It is found in all animals and in humans, being the precursor of sterols, including cholesterol, along the mevalonic acid pathway [71]. It is most abundant in shark (*Squalus* genus) liver, which remains the main source for its pharmaceutical use as immunologic stimulant [71,72], although more sustainable sources are being investigated [73]. Squalene has long been used as adjuvant in vaccines (*e.g.* for influenza) [72], and it has controversially been implicated in Gulf War Syndrome [84]. Squalene is also used as diet supplement and functional food for a variety of claimed beneficial properties [71,75,76]. By contrast, squalene is also considered the primary target of human skin lipid peroxidation [76,77] and its hydroperoxide oxidation products have been attributed a role in the development of skin affections [76,77].

When we subjected it to controlled autoxidation, it followed the typical kinetic behavior of a free radical chain reaction. It undergoes rapid autoxidation with a rate of

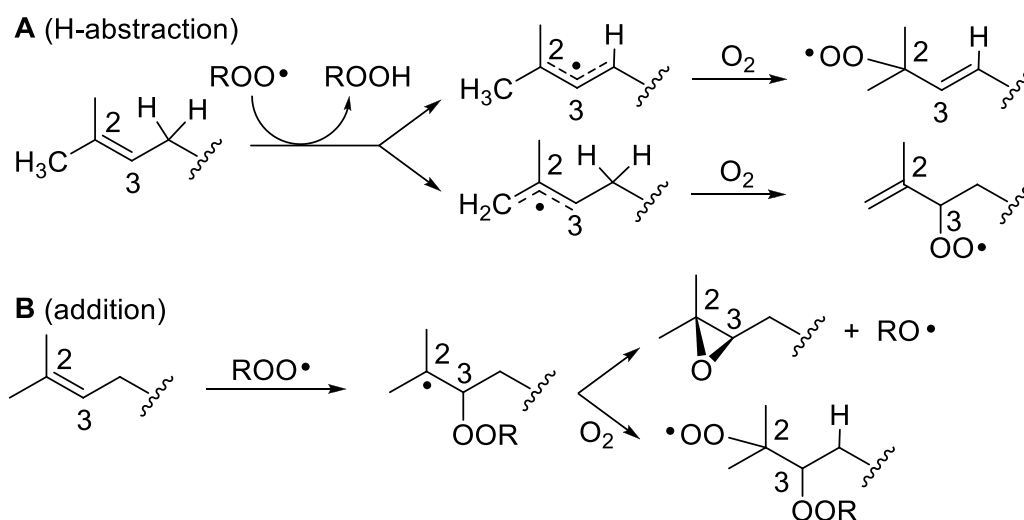
oxygen consumption proportional both to its concentration and to the square root of the rate of initiation as dictated by eq. 1.6, while its oxidizability remains constant. Measured value was $k_p/\sqrt{2k_t} = 0.025 \text{ M}^{-1/2}\text{s}^{-1/2}$ at 303K in chlorobenzene, slightly lower than that of SSO (Table 1.7).

Table 1.7 Kinetic parameters measured for the autoxidation of Squalene in chlorobenzene at 30 °C, initiated by AIBN, in the presence of PMHC (1), DBHA (2), or 4-methoxyphenol (3) as reference antioxidants.

entry	squalene (M)	R_i (M s ⁻¹)	$d[\text{O}_2]_0/dt$ (M s ⁻¹)	$k_p/\sqrt{2k_t}$ (M ^{-1/2} s ^{-1/2})	antiox. (μM)	$d[\text{O}_2]_{in}/dt$ (Ms ⁻¹)	k_p (M ⁻¹ s ⁻¹)
1	1.04	1.12×10 ⁻⁹	8.73×10 ⁻⁷	0.025	PMHC (1.2)	2.26×10 ⁻⁸	63.9
2	1.04	1.95×10 ⁻⁹	1.06×10 ⁻⁶	0.023	PMHC (2.5)	2.52×10 ⁻⁸	69.7
3	1.04	3.43×10 ⁻⁹	1.56×10 ⁻⁶	0.026	PMHC (5.0)	1.73×10 ⁻⁸	66.8
					PMHC (6.2)	1.43×10 ⁻⁸	69.4
					DBHA (7.0)	2.07×10 ⁻⁷	60.8
					DBHA (7.5)	2.65×10 ⁻⁷	68.9
					DBHA (7.5)	2.44×10 ⁻⁷	72.0
					MeOPhOH(6.2)	1.75×10 ⁻⁷	72.3
					MeOPhOH(7.5)	1.90×10 ⁻⁷	72.0
4	1.04	5.03×10 ⁻⁹	1.79×10 ⁻⁶	0.024	PMHC (5.0)	3.21×10 ⁻⁸	66.1
					PMHC (6.2)	2.42×10 ⁻⁸	65.7
5	0.78	3.94×10 ⁻⁹	1.32×10 ⁻⁶	0.027			
6	0.52	4.40×10 ⁻⁹	8.25×10 ⁻⁷	0.024			
7	0.26	4.38×10 ⁻⁹	4.26×10 ⁻⁷	0.025			
mean ± SD				0.025±0.002	mean ± SD		68.0±3.7

As illustrated for SSO and OO, to determine the absolute value of k_p , we performed two series of standard inhibited autoxidations in the presence of PMHC (1) and DBHA (2) as reference antioxidants. Unlike SSO and OO, experiments with the two reference antioxidants processed via eq. 1.18 afforded identical k_p values, without any correction, *i.e.* 66.9±2.2 M⁻¹s⁻¹ and 67.2±5.8 M⁻¹s⁻¹, respectively. This indicates that, as expected, no significant H-bonding interaction between the substrate and the antioxidant is occurring. To confirm this finding, calibration was repeated using 4-methoxyphenol

($k_{inh} = 2.2 \times 10^5 \text{ M}^{-1}\text{s}^{-1}$) as standard antioxidant, as it has lower steric hindrance and higher H-bond donating ability than both PMHC and DBHA [26]. Results were coincident within experimental error (see table 1.7). Averaged $k_p = 68.0 \pm 3.7 \text{ M}^{-1}\text{s}^{-1}$ is very close to that of SSO and implies a two-fold larger rate of chain-termination ($2k_t = 7.40 \times 10^6 \text{ M}^{-1}\text{s}^{-1}$ at 303 K, see Table 1.9). Concerning the mechanism of chain-propagation, it is expected to occur mainly via H-abstraction from the methylene ($>\text{CH}_2$) and (to lesser extent) from the methyl ($-\text{CH}_3$) groups in allylic position (scheme 1.11A), as witnessed by the very recent identification of hydroperoxides in position 2 and 3, respectively, as the main and second main products of squalene free-radical autoxidation at 50 °C (hydroperoxides in position 6, 7, 10 and 11 were also identified). [76] However, addition of alkylperoxyl radicals to the double bonds to yield a tertiary carbon-centered radical (scheme 1.11B) is expected to play a comparatively larger role than in unsaturated fatty acids where a less stable secondary carbon-centered radical is formed, somewhat resembling the known reactivity of cholesterol[62]. The identification of epoxides among the products of squalene spontaneous oxidation at 62 °C supports the contribution of C=C addition [77].

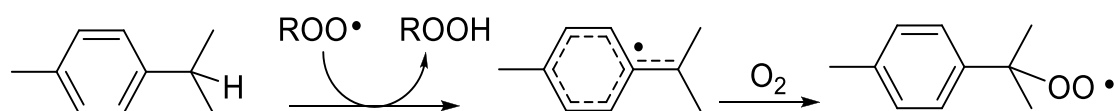


Scheme 1.11. Main reactions involved in the propagation of squalene autoxidation

1.5.1.4 Autoxidation kinetics of *p*-Cymene

p-Cymene is a common aromatic monoterpene component of plant essential oils, particularly abundant in turpentine, thyme, oregano [78], cumin, santureja [79] and

citrus. It has antibacterial activity [78] based on uncoupling mitochondrial respiration, which boosts its interest as potential food preservative, besides its aroma [80]. *p*-Cymene undergoes radical-mediated oxidation mainly by H-abstraction from the isopropyl group to form a tertiary carbon-centered radical in benzyl position with spin delocalization onto the aromatic ring, which propagates the chain via the formation of the tertiary alkylperoxyl radical (scheme 1.12), as established by the formation of the tertiary hydroperoxide as main oxidation product [81].



Scheme 1.12. Autoxidation of *p*-cymene

When the autoxidation of *p*-cymene was monitored under controlled conditions, it followed the typical kinetic behavior predicted by eq. 1.6 and, under our experimental settings, oxidizability did not change on changing the concentration of the substrate or the rate of chain-initiation. Measured $k_p/\sqrt{2k_t} = (4.9 \times 10^{-4} \text{ M}^{-1/2}\text{s}^{-1/2})$ (Table 1.8) was found at 303K in chlorobenzene, which, surprisingly, was significantly lower than the corresponding value ($1.6 \times 10^{-3} \text{ M}^{-1/2}\text{s}^{-1/2}$ in 50% PhCl at 303 K) for structurally related cumene (*iso*-propylbenzene), a well-established synthetic oxidizable substrate used in antioxidant testing [23,82]. As previously described for SSO and squalene, deconvolution of k_p and $2k_t$ was achieved by performing sets of standard autoxidations in the presence of reference antioxidants (having known value of k_{inh}) and processing the rate oxygen consumption with eq. 1.8. When PMHC (**1**) was used as reference antioxidant inhibition was complete, preventing the reliable measurement of k_p . Therefore, beside DBHA (**2**), more effective 4-methoxyphenol (**3**) [67] and less effective BHT (**4**) [23] - a well-known synthetic antioxidant - were used as reference (Figure 1.10).

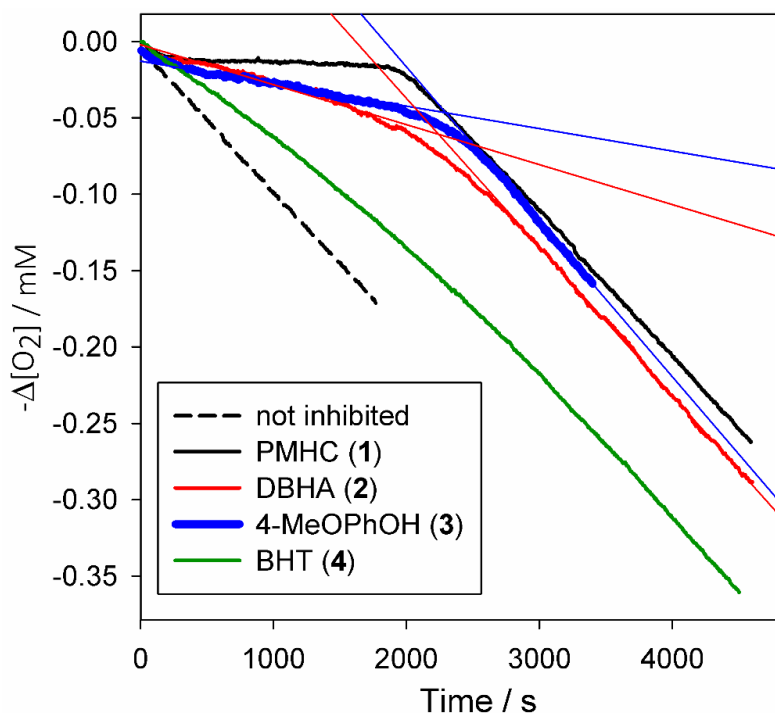
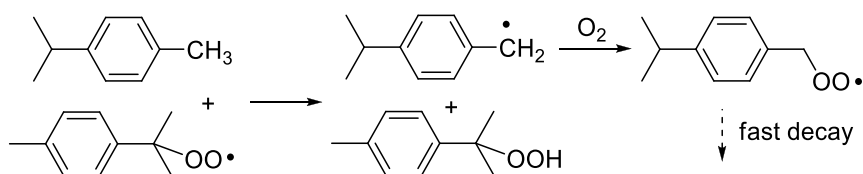


Figure 1.10. Typical oxygen consumption plots during the autoxidation of *p*-cymene (3.2 M) initiated by AIBN (0.05 M) in PhCl at 30 °C without inhibitors or in the presence of antioxidants **1–4**, each at a concentration of 5.0×10^{-6} M.

Results from the three calibrations converged (see Supporting Information) yielding $k_p = 0.8 \text{ M}^{-1}\text{s}^{-1}$ (Table 1.8), which was used in eq. 5 to afford $2k_t = 2.87 \times 10^6 \text{ M}^{-1}\text{s}^{-1}$ (table 1.9). Interestingly, k_p is 2.5-fold larger for *p*-cymene compared to cumene, which is perfectly justified by the lower bond dissociation enthalpy in the tertiary C-H due to the electron-donating effect of the *p*-methyl group on the aromatic ring. On the other hand, chain-termination is 64-fold faster for *p*-cymene, likely due to reaction of the tertiary peroxy radical with the *p*-methyl group of *p*-cymene to afford faster decaying primary peroxy radicals (scheme 1.13). Isolation of 16% primary hydroperoxides in *p*-cymene oxidation at 72 °C [83] supports this explanation.

Table 1.8 Kinetic parameters measured for the autoxidation of *p*-Cymene in chlorobenzene at 30 °C, initiated by AIBN, in the presence of PMHC (1), DBHA (2), 4-methoxyphenol (3) or BHT (4) as reference antioxidants.

entry	<i>p</i> -cumene (M)	R_i (M s ⁻¹)	$d[O_2]_0/dt$ (M s ⁻¹)	$k_p/\sqrt{2k_t}$ (M ^{-1/2} s ^{-1/2})	antioxidant. (□M)	$d[O_2]_{in}/dt$ (Ms ⁻¹)	k_p (M ⁻¹ s ⁻¹)
1	3.2	1.1×10 ⁻⁹	4.49 × 10 ⁻⁸	0.000422	DBHA (1.25)	1.66 × 10 ⁻⁸	0.7981
2	3.2	2.4×10 ⁻⁹	6.96 × 10 ⁻⁸	0.000444	DBHA (2.5)	2.05 × 10 ⁻⁸	0.7569
			7.16 × 10 ⁻⁸	0.000457	DBHA (1.25)	2.41 × 10 ⁻⁸	0.7741
3	3.2	5.1×10 ⁻⁹	1.04 × 10 ⁻⁷	0.000454	PMHC (2.5)	/	/
			1.11 × 10 ⁻⁷	0.000487	DBHA (2.5)	3.86 × 10 ⁻⁸	0.8497
					DBHA (5.0)	1.80 × 10 ⁻⁸	0.8750
			1.10 × 10 ⁻⁷	0.000481	MeOPhOH (2.5)	2.23 × 10 ⁻⁸	0.8360
					MeOPhOH (5.0)	1.36 × 10 ⁻⁸	0.8525
			1.01 × 10 ⁻⁷	0.000443	BHT (2.5)	8.06 × 10 ⁻⁸	0.9451
			1.04 × 10 ⁻⁷	0.000454	BHT (5.0)	5.69 × 10 ⁻⁸	0.7147
					BHT (12.5)	3.65 × 10 ⁻⁸	0.9007
					BHT (2.5)	7.94 × 10 ⁻⁸	0.8229
					BHT (5.0)	6.35 × 10 ⁻⁸	0.8696
4	3.2	6.5×10 ⁻⁹	1.34 × 10 ⁻⁷	0.000521	DBHA (2.5)	7.18 × 10 ⁻⁸	0.8198
			1.39 × 10 ⁻⁷	0.000539	DBHA (5.0)	2.58 × 10 ⁻⁸	0.8174
5	2.4	4.9×10 ⁻⁹	8.14 × 10 ⁻⁸	0.000484			
6	1.6	4.7×10 ⁻⁹	5.73 × 10 ⁻⁸	0.000523			
7	0.9	5.1×10 ⁻⁹	3.64 × 10 ⁻⁸	0.000566			
mean ± SD				(4.9±0.7) × 10 ⁻⁴	mean ± SD		0.83±0.06



Scheme 1.13. Chain-transfer in the propagation of *p*-cymene explaining the fast termination step.

Table 1.9 Oxidizability ($k_p/\sqrt{2k_t}$) and rate constants for chain propagation (k_p) and chain termination ($2k_t$) for the investigated natural oxidizable substrates, measured at 303 K in chlorobenzene (Mean \pm SD).

Substrates	$k_p/\sqrt{2k_t}$	k_p	$2k_t$
SSO	$(3.6\pm 0.2) \times 10^{-2}$	66.9 ± 5.8	3.45×10^6
OO	$(9.0\pm 0.8) \times 10^{-3}$	34.7 ± 1.6	1.50×10^7
SQ	$(2.5\pm 0.2) \times 10^{-2}$	68.0 ± 3.7	7.40×10^6
p -C	$(4.9\pm 0.2) \times 10^{-4}$	0.83 ± 0.06	2.87×10^6

1.5.2 Validation and specific advantages of the four oxidizable substrates in testing antioxidants

In order to validate the calibrated substrates and to highlight their distinctive usefulness in testing antioxidants, controlled autoxidation studies were performed using each oxidizable substrate inhibited by a different set of phenolic antioxidants, not previously employed for calibration. Antioxidants were natural polyphenolic magnolol (**5**, from *Magnolia officinalis*), quercetin (**6**), and caffeic acid phenethyl ester (**7**, CAPE) along with synthetic monophenolic 2,4,6-trimethylphenol (**8**). They were chosen so to comprise the structural variability encountered in typical phenolic antioxidants, and because their antioxidant chemistry is known with great accuracy from previous studies [23, 83-85].

Magnolol **5** is a moderately effective antioxidant able to trap two peroxy radicals with greater efficiency (higher k_{inh} of $6 \times 10^4 \text{ M}^{-1}\text{s}^{-1}$, see Table 1.10) and about two more peroxy radicals in the second phenolic ring with lower efficiency [83]. This behavior was visible when it was tested in the inhibition of p -cymene and OO (see figure 1,11B, D), affording stoichiometric factors in very good agreement with literature (Table 1.10). The rate constants afforded by the substrate p -cymene was in good agreement with literature, however, the rate constant afforded by substrate OO was smaller, which

might be due to H-bonding of the antioxidant to the ester groups of the OO mentioned above. Magnolol **5** also acted as antioxidant toward squalene and SSO, however with both substrates it was not efficient enough to produce a neat inhibition period, so only a reduced rate of autoxidation was observed. This is due to the much higher rate of chain propagation (k_p) of the latter

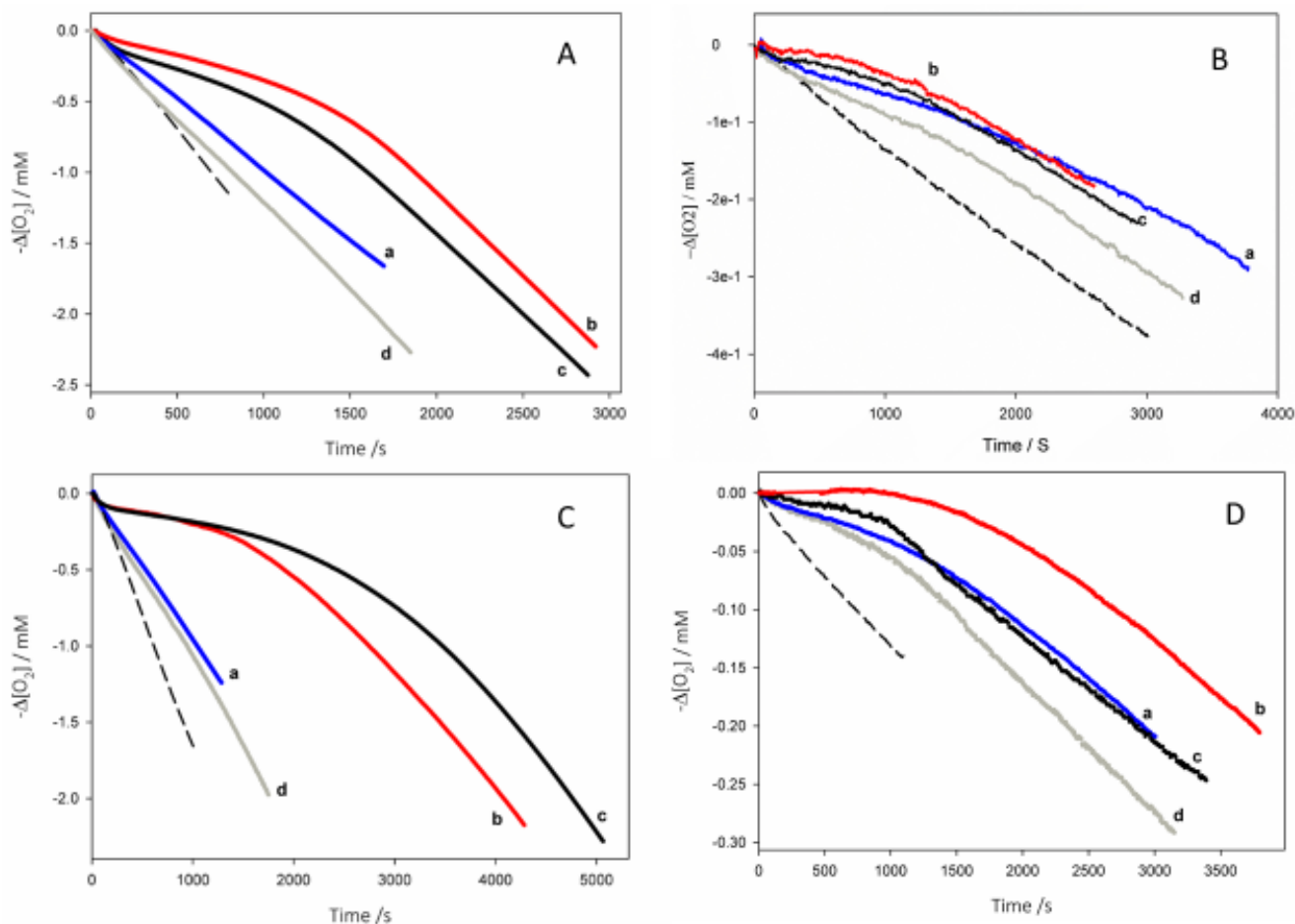


Figure 1.11 Oxygen consumption during the autoxidation of A-SSO(1.1M), B-OO(0.25M); C-Squalene (1.04);D-*p*-Cymene (3.2 M) initiated by AIBN (0.05 M) in PhCl at 30° C without inhibitors (dash) or in the presence of antioxidant (2.5×10^{-6} M): **a** (**5**), **b** (**6**), **c** (**7**), **d** (**8**) in all panels.

substrates compared to *p*-cymene and OO, a feature that is more suited to test faster chain-breaking antioxidants. Consequently, kinetic analysis could not provide the stoichiometric factor and only the fastest kinetic constant for trapping (the first two) peroxy radicals was visible. Inhibition rate constant measured with squalene was, again, in good agreement with literature, while the inhibition of SSO occurred with

lower rate constant, due to H-bonding of the antioxidant to the ester groups of the substrate [42,26], as previously discussed (see 3.1). Clearly, less oxidizable and non H-bonding *p*-cymene is most suited to test the performance of magnolol. An opposite behavior occurred when we used more effective quercetin (**6**) as antioxidant. Inhibition of squalene autoxidation afforded results in very good agreement with previous knowledge: the trapping of two peroxy radicals with very high efficiency ($k_{\text{inh}} \sim 10^6 \text{ M}^{-1}\text{s}^{-1}$) and two more radicals with lower k_{inh} which differed less than a factor of two from literature value (Table 1.10) [84]. On the other hand, inhibition of less oxidizable *p*-cymene was too complete to be measurable and only information on the overall number of trapped radicals ($n = 3.8 \pm 0.2$) was obtained, in excellent agreement with literature. Once again, inhibition of SSO was less efficient than that of squalene, despite the similar k_p value, due to H-bonding of the antioxidant to the substrate [26], allowing to observe only the fastest trapping of the first two peroxy radicals (table 1.10).

Table 1.10 Inhibition Rate Constant k_{inh} and Stoichiometric Factor n , for Trapping Peroxy Radicals by Antioxidants **5-8** (figure 1.5) Measured in the Inhibited Autoxidation of Calibrated Substrates SQ, *p*-C and SSO at 303 K in Chlorobenzene (Mean \pm SD).

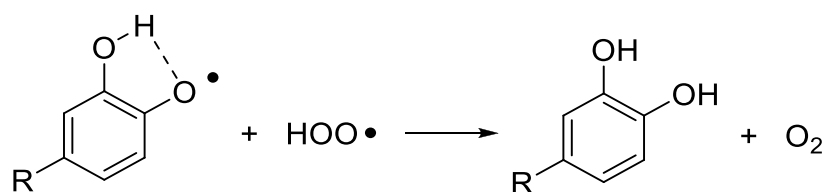
Antiox.	Squalene (SQ)		<i>p</i> -Cymene (<i>p</i> -C)		Sunflower oil (SSO)		Olive oil (OO)		Reference (lit.)	
	$k_{\text{inh}} (\text{M}^{-1}\text{s}^{-1})$	n	$k_{\text{inh}} (\text{M}^{-1}\text{s}^{-1})$	n	$k_{\text{inh}} (\text{M}^{-1}\text{s}^{-1})$	n	$k_{\text{inh}} (\text{M}^{-1}\text{s}^{-1})$	n	$k_{\text{inh}} (\text{M}^{-1}\text{s}^{-1})$	n
5	$(5.0 \pm 0.1) \times 10^4$	/	$(7.7 \pm 0.2) \times 10^4$	1.9 ± 0.2	$(1.4 \pm 0.1) \times 10^4$	/	$(1.6 \pm 0.3) \times 10^4$	2.4 ± 0.3	6.1×10^4 ⁴⁶	2.0 ⁴⁶
			$(9.0 \pm 0.3) \times 10^3$	1.6 ± 0.2					4.3×10^3 ⁴⁶	1.7 ⁴⁶
6	$(9.3 \pm 0.5) \times 10^5$ ^a	2.0 ± 0.2	/	3.8 ± 0.2	$(1.2 \pm 0.2) \times 10^5$	2.1 ± 0.2	$(3.7 \pm 0.4) \times 10^5$	1.8 ± 0.2	1.0×10^6 ⁴⁷	1.9 ⁴⁷
	$(1.0 \pm 0.1) \times 10^5$	1.9 ± 0.2							5.2×10^4 ⁴⁷	1.6 ⁴⁷
7	$(6.2 \pm 0.3) \times 10^5$ ^b	2.3 ± 0.2	$(5.4 \pm 0.3) \times 10^5$	2.2 ± 0.2	$(1.1 \pm 0.1) \times 10^5$	2.0 ± 0.1	$(2.1 \pm 0.2) \times 10^5$	2.1 ± 0.1	6.8×10^5 ⁴⁸	1.5 ⁴⁸
8	$(6.2 \pm 0.5) \times 10^4$	2.5 ± 0.2	$(6.5 \pm 0.3) \times 10^4$	2.2 ± 0.2	$(2.5 \pm 0.1) \times 10^3$	/	$(1.3 \pm 0.1) \times 10^4$	2.3 ± 0.2	8.5×10^4 ⁴	/

a) Experiment performed with 0.03% MeOH to aid dissolution of the antioxidant. b) Following the main inhibition period, additional inhibition corresponding to apparent $k_{\text{inh}} = (1.8 \pm 0.2) \times 10^5 \text{ M}^{-1}\text{s}^{-1}$ and $n = 2.1 \pm 0.2$ was observed (see Supporting Information).

Consistent with the above, CAPE (**7**) and TMP (**8**), having intermediate reactivity compared to magnolol and quercetin, gave good inhibition of all the tested substrates with consistent k_{inh} values measured in the inhibition of squalene or *p*-cymene, which

were in excellent agreement with literature (Table 1.10). Both antioxidants afforded lower k_{inh} values in the inhibition of SSO due to H-bonding.

Of interest, when tested in the inhibition of squalene CAPE (7) showed protection of extended duration with respect to expectations based on the trapping of two peroxy radicals (see footnotes in Table 1.10). We tentatively explain this behavior suggesting that, during autoxidation, squalene may release hydroperoxyl radicals ($\text{HOO}\cdot$), as a side reaction along propagation path B (scheme 1.11), *e.g.* via the mechanism recently disclosed by Pratt and coworkers for other unsaturated hydrocarbons [86]. Hydroperoxyl radical could partly reduce the semiquinone radical of CAPE back to the starting catechol (scheme 1.14), making it available for further antioxidant activity, as recently shown for other antioxidants during the autoxidation of cyclohexadiene [87].



Scheme 1.14. Hydroperoxyl radical ($\text{HOO}\cdot$) reduce the semiquinone radical of CAPE.

The hypothesis of such side chemistry of squalene, consisting in the release of $\text{HOO}\cdot$ during autoxidation, was investigated by studying the inhibition of squalene autoxidation, by TEMPO (2,2,6,6-Tetramethylpiperidine-1-oxyl radical).

As shown in figure 1.12, the oxidation of squalene was retarded by TEMPO. This is a radical without significant antioxidant property; however, it works as an antioxidant catalyst in the presence of a source of hydrogen atoms, *e.g.* when the oxidizing substrates releases $\text{HOO}\cdot$ during its autoxidation [88]. Overall, results collected in table 1.10 validate the quality of our calibrations, as the rate constants measured using squalene and *p*-cymene were in good reciprocal agreement and were fully consistent with the known chemistry of those antioxidants, differing in all cases by less than a

factor of two with respect of literature values. Results also highlight the different usefulness of the substrates.

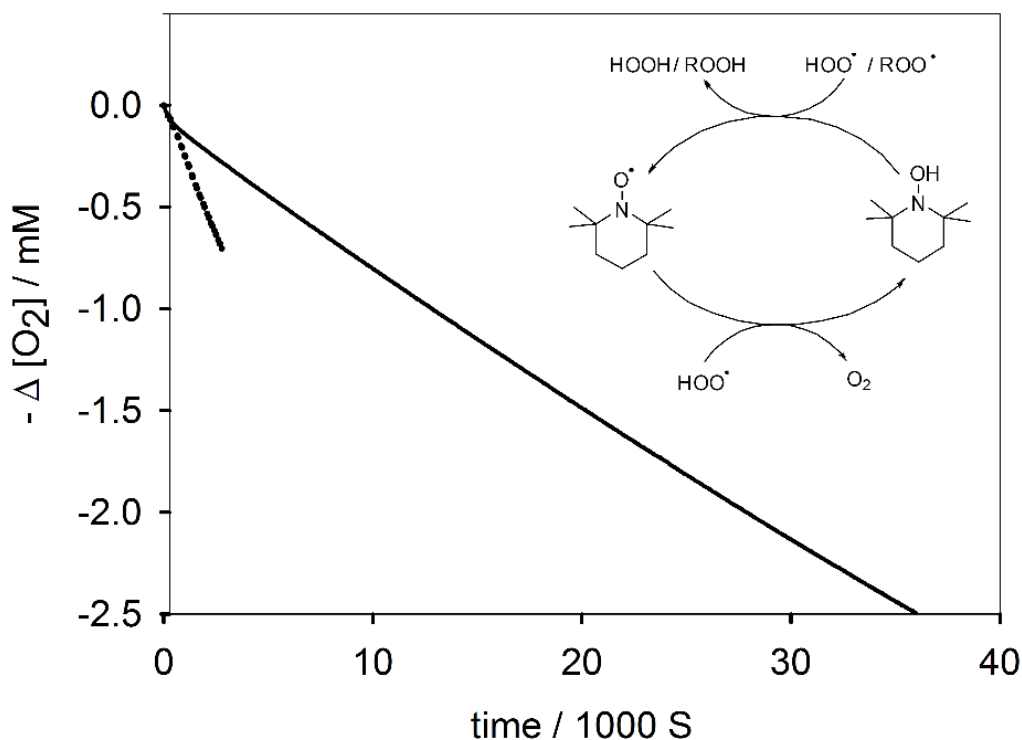


Figure 1.12. Oxygen consumption during the autoxidation of squalene (1.04 M) initiated by AIBN (0.05 M) in PhCl at 30° C without inhibitors (dotted) or in the presence of TEMPO 10×10^{-6} M (solid); the inserted scheme is the antioxidant behavior of TEMPO with $\text{HOO}\cdot$.

Indeed, highly oxidizable substrates like SSO and squalene are more suited to test fast chain-breaking antioxidants, while less oxidizable *p*-cymene is better suited to less effective antioxidants or to accurately measure stoichiometric factors (n) for any antioxidant. Although SSO and squalene have similar k_p values and oxidizability, their difference in antioxidant testing is clearly visible: due to H-bonding, for any acidic antioxidant the performance in protecting SSO will always be lower than recorded with squalene. Therefore, on comparing the performance with the two substrates one can gather important information of the role of H-bonding on the protection of specific substrates and account for the different performance of antioxidants in real-life protection of food, or of relevant biomolecules.

We wish to remark that the method described here is a powerful tool to investigate the oxidation chemistry of relevant substrates at near room temperature, as well as the antioxidant behavior of phytochemicals on quantitative grounds.

1.6 Antioxidant activities of essential oils

In various strategies aimed at improving food preservation, antioxidants play an important role because they can slow down the oxidation of unsaturated fats and prevent the development of rancidity in foods. In recent years, consumers' choice has pushed food technologists toward finding more natural and safer alternatives to synthetic food antioxidants, especially focusing on plant-derived antioxidants [89]. Since ancient times, plants have provided effective ingredients for medicines and have been the subject of research. They have attracted people's attention due to their distinctive colors, shapes, flavors, smells and aromas. Medicinal and aromatic plants have been the center of research and are regarded as valuable resources in the fields of pharmacy, medicine, cosmetics and food [90]. Today, more than 80% of the world's population still relies on drugs that use their active ingredients. Over the centuries, essential oils (EOs) have been used with variable frequency. These are natural compounds, most of which are volatile and have a distinctive scent [91]. They are extracted from different plant organs (flowers, seeds, wood, leaves, bark, etc.), through various extraction methods including fermentation processes, solvent extraction, supercritical CO₂ extraction, microwave-assisted extraction, steam distillation, dry distillation, and mechanical pressing [92].

EOs have a wide range of properties, such as antibacterial, antiviral, antifungal, antioxidant and many others [93]. This wealth makes them important resources in the fields of medicine and pharmaceuticals, food flavoring, cosmetics, cultural heritage protection, agriculture and animal production, etc [94]. Various types of essential oils have also been proposed as active antioxidants to replace the synthetic ones. For example, the essential oils of thyme and oregano have been proposed to protect food, especially meat and fish, from various forms of oxidative deterioration [95]. However,

the research conducted is rarely based on sound scientific methods able to afford reliable quantitative data, limiting to a rough evaluation of the antibacterial or antioxidant properties of oils, which are sometimes mixed – *e.g.* tests of food spoilage often do not distinguish what is caused by microorganisms and what is caused by air oxidation. For this reason, we believe that the following data will help clarify the antioxidant potential of essential oils on quantitative grounds.

1.6.1 Phenolic composition of EOs

EOs are complex mixtures (usually 10 to 60 different active ingredients are observed), where some of the main ingredients might be present in high concentrations (20-70%), such as limonene in citrus oils. These mixtures have different components for different plants and even for different varieties of the same plant, and are affected by factors such as climate, environment and plant growth location, as well as their extraction method [96]. Therefore, there may be different chemical types (called chemotypes) in a species, such as the *red thyme* in our study. Furthermore, their properties are attributed to their chemical components thus it is important to fully understand the composition of each oil to relate their properties, including the antioxidant to the identity and concentration of the main components in the mixture. Our research interest is focused on their antioxidant activities which mainly depends on their phenolic components. Thus, the phenolic pattern in 18 essential oil samples was analyzed, in the frame of a collaborative project by Dr. Simone Gabbanini at BeC s.r.l a company, who also provided the 18 EOs samples used in this study. The phenolic components and their concentration in all the 18 essential oils are listed in Appendix Table A1.3.

Here, the structure of the main phenolic components is displayed in Figure 1.13. As anticipated, essential oils obtained for the same botanical species might differ in composition, hence in antioxidant properties. For this reason we included in our 18 samples different specimens of oils from the same botanical sources that are especially renowned for their antioxidant properties, namely: red thyme (3 different specimens), savory (2 different specimens), clove (3 different specimens).

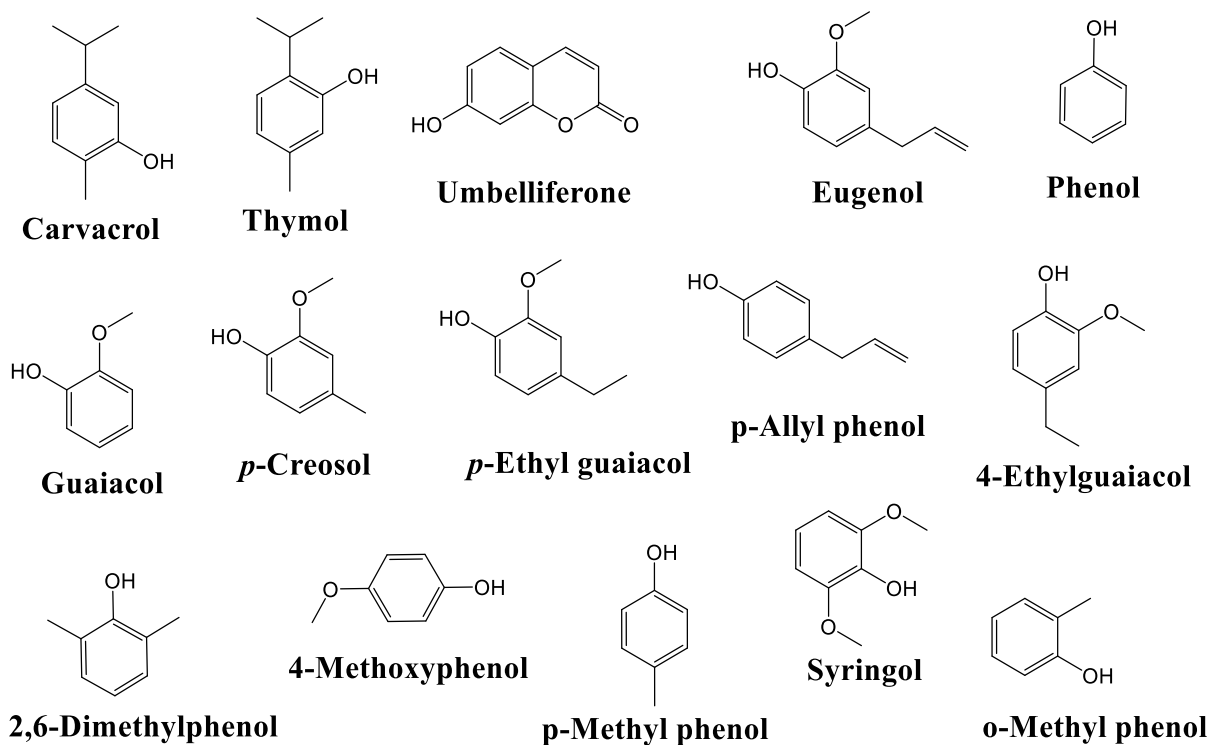


Figure 1.13 Phenolic compounds present in the studied essential oils.

1.6.2 Antioxidant activity of EOs

Measurements were performed by conducting cumene autoxidations inhibited by each of the 18 essential oils. It should be pointed out that, in order to properly determine the antioxidant properties and rate constants of the essential oils, the use of a well-known oxidizable substrate was needed. The use of cumene was prioritized over styrene and the substrates characterized in section 1.5, as the antioxidant power of the essential oils was predicted to be substantially lower than that of PMHC, therefore a substrate with low oxidizability would be more suited to the study and provide better inhibited autoxidation plots, facilitating the analysis of results [83].

The following figures (Figures 1.14-1.18) show the typical autoxidation inhibition resulting from the application of various essential oils. Inspection of autoxidation plots reveals that 14 of the 18 tested EOs gave moderate to good, antioxidant protection of cumene at the used concentration range of 1-5 $\mu\text{L/L}$ (ppm) (Figures 1.14 to 1.17), while the remaining 4 (carrot, marigold, cedarwood and celery) did not show any appreciable antioxidant behavior. This is not entirely surprising if we match this behaviour with the

composition of the EOs reported in Appendix (Table A1.3), which reveals that those 4 oils are the only in our selection with no significant content in phenolic components. Therefore, as a first glance, it is apparent that the observed antioxidant behavior should depend exclusively or mostly from the phenolic components.

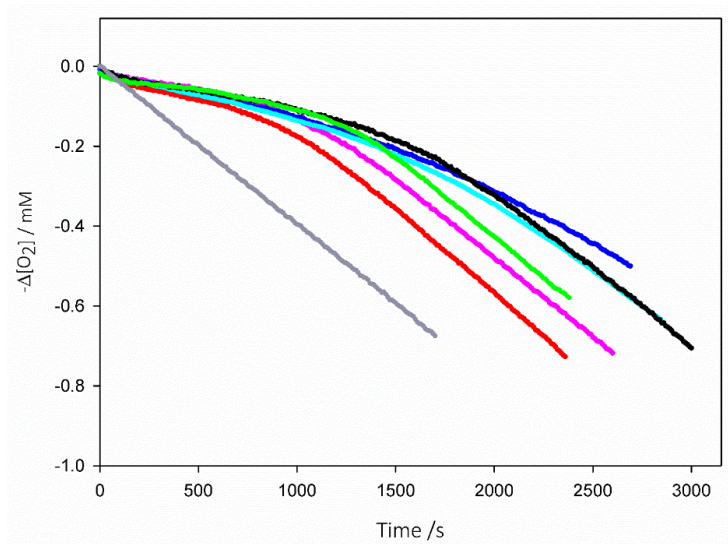


Figure 1.14 Representative plots of oxygen consumption during cumene autooxidation (3.6M), initiated by AIBN (0.05M), in PhCl, at 30 ° C, uninhibited (grey line) or in the presence of essential oil (1 ppm) of: red thyme 2 (red), savory (pink), red thyme 3 (green), origan (black), Carnation (cyan), cinnamon (blue).

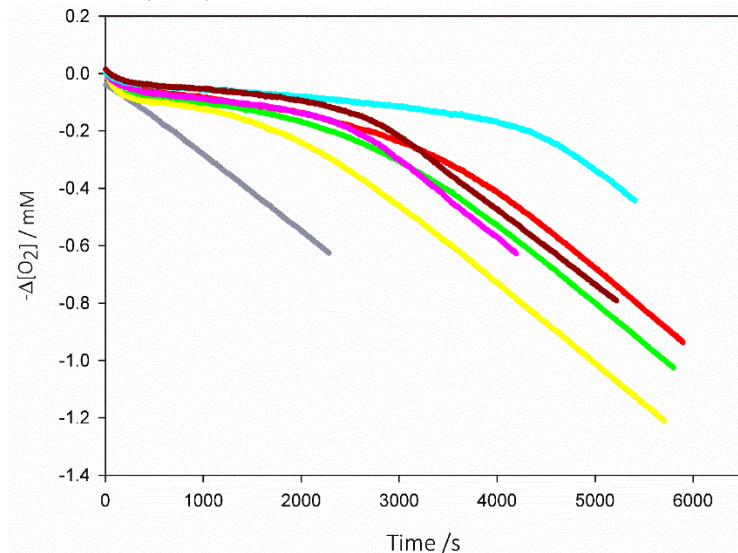


Figure 1.15 Representative plots of oxygen consumption during cumene autooxidation (3.6M), initiated by AIBN (0.025M), in PhCl, at 30 ° C, uninhibited (grey line) or in the presence of essential oil of: bay 2.4 ppm (red), savory 2.3 ppm (pink), birch 2.6 ppm (green), red thyme (sample 1) 2.3 ppm (dark red), spanish origan 2.6 ppm (cyan), cade 2.5 ppm (yellow).

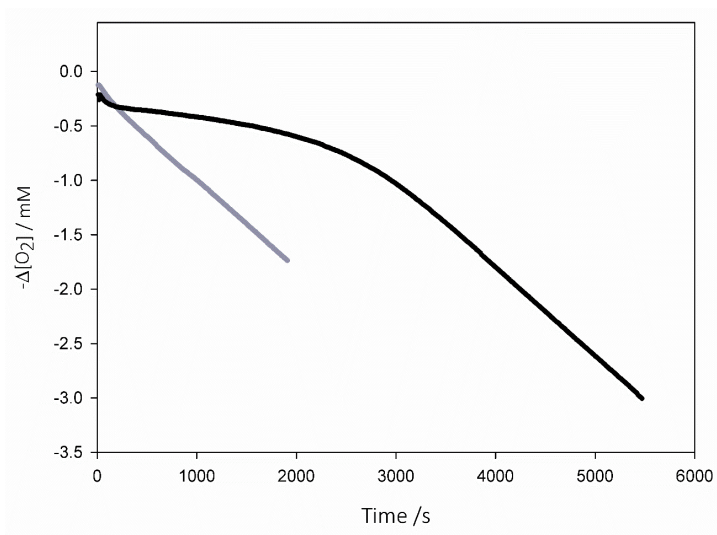


Figure 1.16 Oxygen consumption during cumene (3.6M) autooxidation, initiated by AIBN (0.025M), in PhCl, at 30 ° C, uninhibited (grey line) or in the presence in the presence of essential oil (13 ppm) of clove 2 (black line).

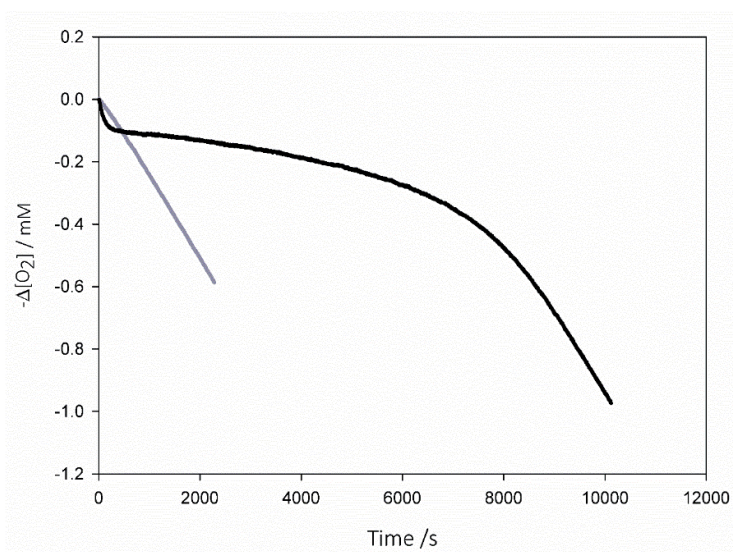


Figure 1.17 oxygen consumption during cumene auto-oxidation (7.1M), initiated by AIBN (0.05M), in PhCl, at 30 ° C, uninhibited (grey line) or in the presence of essential oil (5.3 ppm) of clove 1 (black line).

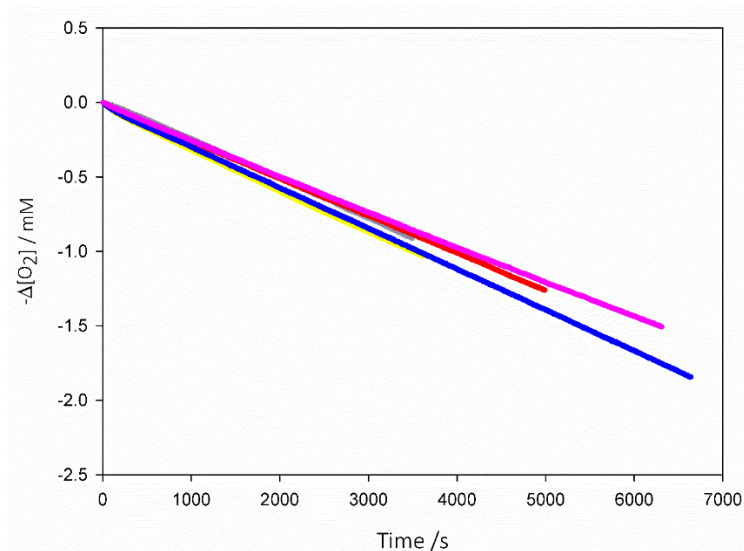


Figure 1.18 Representative plots of oxygen consumption during cumene autooxidation (3.6M), initiated by AIBN (0.025M), in PhCl, at 30 ° C, uninhibited (grey line) or in the presence of essential oil (13 ppm) of: carrots (red), marigold (pink), celery (blue), cedarwood (yellow).

Observation that the four oils not containing phenolic components did not show significant inhibition of cumene, does not necessarily mean that they don't possess any kind of antioxidant properties, as it has been shown that some non-phenolic elements of essential oils can also help to stop or delay autoxidation [82]. However, this occurs with a termination-enhancing mechanism that requires much higher concentration of the antioxidant for appreciable results. Such higher concentrations were not the point of study in this work, and this will certainly deserve attention in further investigation.

Each essential oil which gave good inhibition contains multiple phenolic components each endowed with its antioxidant activity, and a list of k_{inh} values determined by inhibited autoxidation studies by our group is collected in Appendix (Table A. 1.3). For those components identified in our EOs whose k_{inh} values were unknown, these were determined by other students in the group in parallel projects and were added to Table A. 1.3 for reference.

Since, as previously noted, the antioxidant activity of EOs is related to the phenolic components, in order to analyze the inhibition kinetics, we considered the weighted sum of such components for each essential oil as the active inhibitor. This was

calculated from data in Table 1.10, upon taking into account the concentration of each essential oil used in autoxidation (in ppm = mg/Kg), the density of the essential oil and the molecular weight of each phenolic component.

Table 1.10 Phenolics' concentration in the samples of Essential Oils (EOs) and corresponding concentration of each component in the autoxidation mixture when the EOs were used as inhibitor or cumene autoxidation.

<i>Essential Oil</i>	Conc /ppm ^a	Antioxidant components % [10 ⁻⁶ M] ^b							
		Carva-crol	<i>Thymol</i>	<i>Eugenol</i>	<i>4-Allyl phenol</i>	Guaia-col	4-Ethyl guaiacol	p-Creosol	Other ^c
Red Thyme 1	2.25	36.39 [5.5]	3.44 [0.52]	/	/	/	/	/	/
Spanish Origan	2.25	69.43 [10]	/	/	/	/	/	/	/
Clove 1	5.25	/	/	73.9 [24]	/	/	/	/	/
Cade	2.45	/	/	0.59 [0.09]	/	2.7 [0.53]	3.68 [0.59]	5.04 [0.89]	10.33 [2.2]
Birch	2.61	/	/	1.22 [0.19]	/	8.93 [1.9]	7.92 [1.4]	14.73 [2.8]	18.85 [4.1]
Bay St. Thomas	2.4	/	/	51.3 [7.6]	8.7 [1.6]	/	/	/	/
Savory 1	2.3	23.5 [3.6]	18.7 [2.9]	1.23 [0.18]	/	/	/	/	/
Red Thyme 2	1.0	33.9 [2.3]	4 [2.7]	/	/	/	/	/	/
Red Thyme 3	1.0	3.1 [0.21]	53.1 [3.5]	/	/	/	/	/	/
Savory 2	1.0	46.6 [3.1]	1.7 [0.11]	/	/	/	/	/	/
Origan	1.0	69.2 [4.6]	0.4 [0.03]	/	/	/	/	/	/
Cinnamon	1.0	/	/	81.5 [5.0]	/	/	/	/	/
Clove 2	1.0	/	/	84.6 [5.2]	/	/	/	/	/
Clove 3	1.0	/	/	80.8 [4.9]	/	/	/	/	/

a) Concentration of the EO used in inhibited autoxidation in $\mu\text{L/L}$. b) % content of each phenolic components in the EO and corresponding micromolar concentration in the autoxidation experiments when the EO was used as inhibitor. c) See appendix Table A. 1.3.

Analysis of autoxidation plots by means of Eq.1.7 (assuming $n = 2$ for the mixture of phenols, since it is $n = 2$ for each component) and of Eq.1.8, afforded the apparent k_{inh} values for each EO from the slope of the inhibition period, and the total concentration

of active antioxidant components ($\Sigma[M]_{\text{exp}}$) from its duration. Results are collected in Table 1.11.

Table 1.11 Apparent values of k_{inh} of EO samples determined by inhibited autoxidations at 303K in PhCl, resulting sum of phenolic concentration and total phenolic concentration in the autoxidizing mixture from GC-MS analysis of the essential oil and the corresponding concentration of use (ppm = mg/Kg).

<i>Essential Oil</i>	Conc. (ppm)	$\Sigma[M]_{\text{WSM}}^{\text{a}}$	$\Sigma[M]_{\text{exp}}^{\text{b}}$	$k_{\text{inh}} / \text{M}^{-1}\text{s}^{-1} \text{ }^{\text{c}}$
Red Thyme 1	2.25	6.0×10^{-6}	$(6.9 \pm 0.1) \times 10^{-6}$	$(1.5 \pm 0.3) \times 10^4$
Spanish Origan	2.25	1.0×10^{-5}	$(1.1 \pm 0.1) \times 10^{-5}$	$(1.1 \pm 0.1) \times 10^4$
Clove 1	5.25	2.4×10^{-5}	$(2.2 \pm 0.2) \times 10^{-5}$	$(5.0 \pm 0.1) \times 10^3$
Cade	2.45	4.3×10^{-6}	$(5.7 \pm 0.3) \times 10^{-6}$	$(1.9 \pm 0.2) \times 10^4$
Birch	2.61	1.0×10^{-5}	$(9.8 \pm 0.1) \times 10^{-6}$	$(7.9 \pm 0.1) \times 10^3$
Bay St. Thomas	2.4	9.2×10^{-6}	$(9.2 \pm 0.3) \times 10^{-6}$	$(5.6 \pm 0.1) \times 10^3$
Savory 1	2.3	6.7×10^{-6}	$(6.4 \pm 0.2) \times 10^{-6}$	$(1.1 \pm 0.1) \times 10^4$
Red Thyme 2	1.0	5.0×10^{-6}	$(2.5 \pm 0.1) \times 10^{-6}$	$(1.5 \pm 0.1) \times 10^4$
Red Thyme 3	1.0	3.7×10^{-6}	$(4.0 \pm 0.1) \times 10^{-6}$	$(1.4 \pm 0.1) \times 10^4$
Savory 2	1.0	3.2×10^{-6}	$(2.9 \pm 0.1) \times 10^{-6}$	$(1.3 \pm 0.1) \times 10^4$
Origan	1.0	4.6×10^{-6}	$(4.8 \pm 0.1) \times 10^{-6}$	$(1.3 \pm 0.1) \times 10^4$
Cinnamon	1.0	5.0×10^{-6}	$(4.4 \pm 0.3) \times 10^{-6}$	$(4.9 \pm 0.3) \times 10^3$
Clove 2	1.0	5.2×10^{-6}	$(6.3 \pm 0.2) \times 10^{-6}$	$(1.1 \pm 0.1) \times 10^4$
Clove 3	1.0	4.9×10^{-6}	$(4.6 \pm 0.2) \times 10^{-6}$	$(5.5 \pm 0.2) \times 10^3$

a) Calculated as the weighted sum of all phenolic components from GC-MS analysis (data from Table 1.10). b) Determined from the length of inhibited period in autoxidation experiments assuming that $n = 2$. c) Apparent inhibition rate constant from cumene (3.6M) autoxidation experiments in chlorobenzene, with [AIBN] 50 mM, T = 30°C.

Although this is a simplified analysis that assumes similar contribution to the overall antioxidant behavior by all active components, it is interesting to compare this autoxidation-derived total concentration of antioxidant components ($\Sigma[M]_{\text{exp}}$) with the weighted sum of phenolic components ($\Sigma[M]_{\text{WSM}}$) obtained from GC-MS analysis as previously detailed. Analysis of Table 1.11 reveals a reasonably good matching of

$\Sigma[M]_{\text{exp}}$ with $\Sigma[M]_{\text{WSM}}$, indicating that our initial assumption was correct and the presence of phenolic components explains almost entirely the antioxidant behaviour of the investigated essential oils.

On the other hand, the magnitude of k_{inh} for most essential oils is in line with that of common synthetic antioxidants used to protect food products, *e.g.* BHT ($k_{\text{inh}} = 1.1 \times 10^4 \text{ M}^{-1}\text{s}^{-1}$), fully supporting their potential application as natural food preservatives, or to protect other manufactured goods, such as cosmetic products, where natural additives might represent a higher perceived value by the customer.

1.6.3 Conclusion and Perspectives

Several investigations accumulated so far indicate that plants with antioxidant and pharmacological properties own their properties to the presence of phenolic compounds (especially phenolic acids). Effective research on the sources of natural antioxidant compounds requires reliable evaluation methods for the antioxidant activity. There is currently a large number of analysis methods that can be used to determine the antioxidant capacity of target substances; however, the variety of experimental setting and the difficulty to obtain comparable results, often limits their usefulness and value.

In this study, although more detailed experiments are needed, it has been proved that the method of inhibited autoxidation of a reference substrate can be used to quantitatively analyze the antioxidant activity of essential oils so to establish clear correlations with their active components. Nonetheless, the total antioxidant capacities of target species depend on a number of factors, for example some non-phenolic compounds from essential oils have been found to have antioxidant properties [82] and they may also interact with phenolic antioxidants. Clearly further studies will be needed in this regard, but the approach described in this chapter will certainly provide a valuable tool for such studies.

1.7 Experimental section

1.7.1 Materials

All chemicals and solvents were commercially available (Aldrich-Fluka-Sigma, Milan, Italy). 2,2'-Azobis(isobutyronitrile) (AIBN) was recrystallized from methanol. 2,6-Di-tert-butyl-4-methoxyphenol (DBHA), 2,2,5,7,8-pentamethyl-6-chromanol (PMHC), and 2,4,6-trimethylphenol (TMP) were recrystallized from hexane. 4-Methoxyphenol was recrystallized twice from hexane/ethyl acetate. Magnolol, quercetin, and caffeic acid phenethyl ester (CAPE) were used as received. and cumene (99%) were percolated twice through activated alumina to remove impurities and traces of hydroperoxides.

1.7.2 Purification of substrates

It was necessary to carry out a preventive purification of the oxidizable substrates (squalene and p-cymene), by eliminating antioxidant components present in the matrix that prevented oxidation, as noted by some preliminary tests. The purification was carried out by elution on a chromatographic column with a stationary phase consisting of a third of alumina, a third of silica and, of another third, alumina. Silica is able to retain polar impurities, such as any peroxides that can favor the oxidative phenomenon, while alumina retains compounds stabilizers, which can hinder it.

1.7.3 Autoxidation Experiments.

Autoxidation experiments were performed in a two-channel oxygen uptake apparatus, based on a Validyne DP 15 differential pressure transducer built in our laboratory [35, 97-101]. In a typical experiment, an air-saturated solution of the oxidizable substrate containing AIBN (0.005–0.05 M) was equilibrated at 30 °C with an identical reference solution containing excess 2,2,5,7,8-pentamethyl-6-hydroxychromane (PMHC, 25 mM). After the mixture was equilibrated and when a constant O₂ consumption was reached, a stock solution of the antioxidant (typically 1.0 mM in PhCl) was injected in

the sample flask, in order to reach the desired concentration in the range 1–20 μM in the sample flask. The oxygen consumption in the sample was measured after calibration of the apparatus from the differential pressure recorded with time between the two channels.

1.7.4 Infrared Spectroscopy

The liquid-phase FT-IR spectra were recorded at 298 K under a nitrogen atmosphere in a sealed KBr cell with a 0.5 mm optical path. Solutions of PMHC (1) and DBHA (2) were prepared in chlorobenzene or in 1/1 chlorobenzene/SSO in the concentration range of 5–10 mM to avoid self-association of the phenols [35]. Spectra were recorded in absorbance mode, and the signal in the “free” O–H stretching region at ca. 3610–3630 cm^{-1} was manually integrated after manual baseline correction

1.7.5 GC-MS analysis of fatty acid composition

Fatty acid composition of SSO and OO. Analysis was performed by GC-MS upon conversion of the triglyceride into fatty acid methyl esters (FAME). This was obtained according to previous work [102] by saponification of the oil with 0.01 N NaOH at r.t. for 1 h, followed by acidification with HCl 6 N and extraction in diethyl ether. Methylation of the isolated fatty acid mixture was obtained by reacting with 10% methanolic solution of boron trifluoride at 80 $^{\circ}\text{C}$ for 2 min. GC–MS analysis for SSO was performed on ZB-5 column, eluting with helium at 1.0 ml/min with temperature programming: 45 $^{\circ}\text{C}$ for 3 min, ramp to 150 $^{\circ}\text{C}$ at 5 $^{\circ}\text{C}/\text{min}$, then to 260 $^{\circ}\text{C}$ at 2 $^{\circ}\text{C}/\text{min}$, hold for 1 min. GC–MS analysis for OO was performed on ZB-5 column, eluting with helium at 1.2 ml/min with temperature programming: 100 $^{\circ}\text{C}$ for 2 min, ramp to 200 $^{\circ}\text{C}$ at 5 $^{\circ}\text{C}/\text{min}$, hold for 4 min. MS analysis was obtained in electron impact (EI+) positive mode at 70 eV in the range m/z 40 to 400. For quantitative analysis SIM chromatograms were reconstructed at the base peak for each standard FAME (see Supporting Information). Calibration of the spectrometer response (5 levels) was

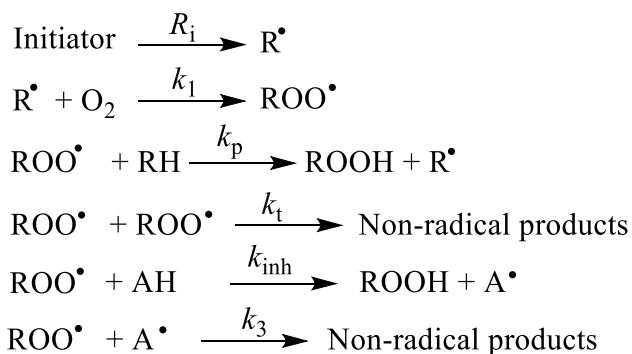
performed by injecting commercial standard organic solutions of mixed target methylated fatty acids as previously described.

1.7.5 Statistical Analysis

All the reported rate constants are expressed as average \pm standard deviation from at least three independent measurements.

Appendix

A.1.2 Derivation of basic equations to calculate antioxidant activity.



Scheme A.1.2 Autoxidation inhibited by chain-breaking antioxidants

Applying the law of mass action, there are

$$-\frac{d[O_2]}{dt} = k_1[R^\bullet][O_2]$$

(A.1.13)

$$\frac{d[R^\bullet]}{dt} = R_i + k_p[ROO^\bullet][RH] - k_1[R^\bullet][O_2]$$

(A.1.14)

$$\begin{aligned} \frac{d[ROO^\bullet]}{dt} &= k_1[R^\bullet][O_2] - 2k_t[ROO^\bullet]^2 - k_p[ROO^\bullet][RH] - k_{inh}[ROO^\bullet][AH] - \\ &k_3[ROO^\bullet][A^\bullet] \end{aligned}$$

(A.1.15)

$$\frac{d[A^\bullet]}{dt} = k_{inh}[ROO^\bullet][AH] - k_3[ROO^\bullet][A^\bullet]$$

(A.1.16)

In the context of the steady-state approximation the expressions (A.1.14) and (A.1.16) can be set equal to zero, therefore

$$k_1[R^\bullet][O_2] = R_i + k_p[ROO^\bullet][RH]$$

(A.1.17)

$$k_{inh}[\text{ROO}\cdot][\text{AH}] = k_3[\text{ROO}\cdot][\text{A}\cdot]$$

(A.1.18)

Substituting these last two expressions in equation (A.1.15) and taking into account the approximation of the steady state for the species $\text{ROO}\cdot$ will have:

$$2k_t[\text{ROO}\cdot]^2 + 2k_{inh}[\text{ROO}\cdot][\text{AH}] - R_i = 0$$

(A.1.19)

Solving the equation (A.1.19) with respect to $[\text{ROO}\cdot]$ and ignoring the negative solution will have:

$$[\text{ROO}\cdot] = \frac{1}{2k_t} \left\{ -k_{inh}[\text{AH}] + \sqrt{k_{inh}^2[\text{AH}]^2 + 2k_t R_i} \right\}$$

(A.1.20)

Substituting equation (A.1.17) into (A.1.13) will find:

$$-\frac{d[\text{O}_2]}{dt} = k_p[\text{ROO}\cdot][\text{RH}] + R_i$$

(A.1.21)

Substituting the expression (A.1.20) for $[\text{ROO}\cdot]$ will have:

$$-\frac{d[\text{O}_2]}{dt} = \frac{k_p[\text{RH}]}{2k_t} \left\{ -k_{inh}[\text{AH}] + \sqrt{k_{inh}^2[\text{AH}]^2 + 2k_t R_i} \right\} + R_i$$

(A.1.22)

The expression (A.1.22) is of a general nature and represents the consumption of oxygen both in the absence and in the presence of an induction period. In the latter case it is possible to derive a simpler equation if we consider that, in the presence of a good antioxidant, it is possible to neglect the recombination reaction between two peroxy radicals ($2 \text{ROO}\cdot \rightarrow \text{Products}$), as the termination reactions with the antioxidant ($\text{ROO}\cdot + \text{AH}$) and with the corresponding radical ($\text{ROO}\cdot + \text{A}\cdot$) are by far more important. Based on these considerations the equation (A.1.15) becomes

$$\frac{d[\text{ROO}\cdot]}{dt} = k_1[\text{R}\cdot][\text{O}_2] - k_p[\text{ROO}\cdot][\text{RH}] - k_{inh}[\text{ROO}\cdot][\text{AH}] - k_3[\text{ROO}\cdot][\text{A}\cdot]$$

(A.1.23)

while equation (A.1.19) can be rewritten as:

$$2k_{inh}[\text{ROO}\cdot][\text{AH}] - R_i = 0$$

(A.1.24)

Since in this case

$$[\text{ROO}\cdot] = \frac{R_i}{2k_{inh}[\text{AH}]}$$

(A.1.25)

substituting equation (A.1.25) in (A.1.21), the oxygen consumption in the inhibited tract will be first we will have:

$$-\frac{d[\text{O}_2]}{dt} = \frac{k_p[\text{RH}]R_i}{2k_{inh}[\text{AH}]} + R_i$$

(A.1.26)

If the chain is long enough, the term R_i can be neglected with respect to the

$$-\frac{d[\text{O}_2]}{dt} = \frac{k_p[\text{RH}]R_i}{2k_{inh}[\text{AH}]}$$

(A.1.27)

Now considering the equation that describes the decay of the inhibitor

$$-\frac{d[\text{AH}]}{dt} = k_{inib}[\text{AH}][\text{ROO}\cdot]$$

(A.1.28)

Substituting in equation (A.1.28) the equation (A.1.25) will have:

$$-\frac{d[\text{AH}]}{dt} = \frac{R_i}{2}$$

(A.1.29)

Integrating the differential equation will have:

$$-\int_0^t d[\text{AH}] = \frac{R_i}{2} \int_0^t dt$$

(A.1.30)

$$[\text{AH}]_0 - [\text{AH}]_t = \frac{R_i}{2} t$$

(A.1.31)

By choosing $t = \tau$, that is the time at which all the inhibitor has been consumed will obtain

$$[\text{AH}]_0 = \frac{R_i}{2} \tau$$

(A.1.32)

$$R_i = \frac{2[\text{AH}]_0}{\tau}$$

(A.1.33)

The term 2 that appears in the numerator is the stoichiometric coefficient which in general can assume values between 1 and 2. (A.1.32) it is therefore possible, given the initiation speed R_i , and the induction time τ , determine the stoichiometric of the inhibitor, or vice versa ^c.

^c) If the inhibition time τ is not known, the stoichiometric coefficient or the rate of initiation can be calculated using equation (A.1.30).

Table A. 1.1. GC-MS analysis of fatty acid composition in SSO, after transesterification to the corresponding methyl esters (FAME). For each FAME analysis was performed in Single Ion reconstructed chromatograms using the base peak (bp) in mass spectrum. Calibration was performed at 5 levels using Supelco and Aldrich standard FAME mixtures. % Amount was then calculated on the total fatty acid content found in the chromatogram.

Entry	R.t. (min)	Compound (FAME)	Characteristic Ms Ions	Fatty acid content (w/w) ^a
1	25.40	Lauric acid methyl ester	74 (bp), 55, 87, 214	Trace ^b
2	31.94	Myristic acid methyl ester	74 (bp), 87, 143, 242	0.01
3	39.94	Palmitic acid methyl ester	74 (bp), 87, 143, 270	7.29
4	47.00	Linoleic acid methyl ester	67 (bp), 81, 95, 294	57.02
5	47.31	Oleic acid methyl ester	55 (bp), 69, 97, 296	29.81
6	47.69	Linolenic acid methyl ester	81 (bp), 67, 95, 292	0.12
7	48.47	Stearic acid methyl ester	74 (bp), 87, 143, 298	4.98
8	55.39	Eicosadienoic acid methyl ester	67 (bp), 81, 95, 322	Trace ^b
9	55.75	Eicosenoic acid methyl ester	55 (bp), 97, 292, 324	Trace ^b
10	56.91	Arachidic acid methyl ester	74 (bp), 87, 143, 326	0.61
11	64.93	Behenic acid methyl ester	74 (bp), 87, 143, 354	0.09

a) % Amount calculated on the total fatty acid fraction from the measured molar concentration of FAME. b) Content lower than 0.01% w/w; not considered in calculating %.

Table A. 1.2. GC-MS analysis of fatty acid composition in OO, after transesterification to the corresponding methyl esters (FAME). For each FAME analysis was performed in Single Ion reconstructed chromatograms using the base peak (bp) in mass spectrum. Calibration was performed at 5 levels using Supelco and Aldrich standard FAME mixtures. % Amount was then calculated on the total fatty acid content found in the chromatogram.

Entry	R.t. (min)	Compound (FAME)	Characteristic Ms Ions	Fatty acid content (w/w) ^a
1	20.51	Palmitoleic acid methyl ester	74(bp), 69, 84, 87, 55	0.21
2	20.94	Palmitic acid methyl ester	74(bp), 87, 43, 55, 41	7.70
3	24.14	Linolelaidic acid methyl ester	67(bp), 81, 55, 41, 79	1.64
4	24.25	Oleic acid methyl ester	55(bp), 41, 69, 74, 43	82.16
5	24.35	Elaidic acid methyl ester	55(bp), 41, 69, 43, 74	4.84
6	24.73	Stearic acid methyl ester	74(bp), 87, 43, 55, 41	2.83

a) % Amount calculated on the total fatty acid fraction from the measured molar concentration of FAME.

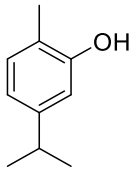
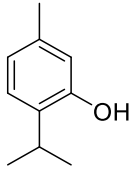
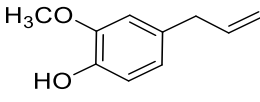
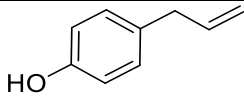
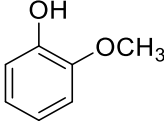
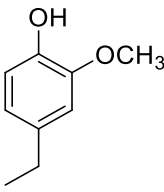
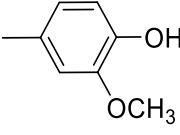
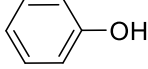
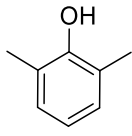
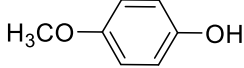
Table A. 1.3. The phenolic components of investigated EO samples, analyzed GC-MS (courtesy of Dr. Simone Gabbanini – BeC s.r.l.)

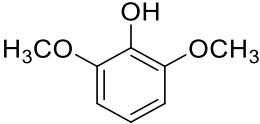
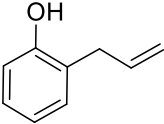
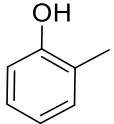
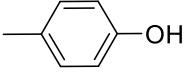
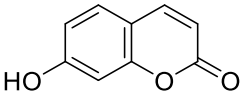
	Essential oils (Italian / English)	Aromatic plant	Phenolic components	Content % (w/w)
1	Cade / Cade	<i>Juniperus oxycedrus</i>	Phenol	1.10
			o-Cresol	1.00
			m-Cresol	2.34
			Guaiacol	2.70
			2,4-Dimethylphenol	0.78
			2,3-Dimethylphenol	0.55
			4-Methylguaiacol	5.04
			4-Ethylguaiacol	3.67
2	Betulla / Birch	<i>Betula alba</i>	4-Propylguaiacol	1.32
			Phenol	1.90
			o-Cresol	2.03
			m-Cresol	4.33
			Guaiacol	8.91
			2,4-Dimethylphenol	1.35
			2,3-Dimethylphenol	0.86
			4-Methylguaiacol	14.68
			4-Ethylguaiacol	7.89
Syringol	2.01			
Eugenol	1.22			

			4-Propylguaiacol	2.06
			Syringol	2.64
3	Bay st Thomas / Bay rum tree	<i>Pimenta racemose</i>	4-Allylphenol	8.47
			Eugenol	50.97
4 ^a	Carota semi / Carrot seeds	<i>Daucus carota</i>	(beta-Myrcene)	2.70
			(β –Terpinene)	11.11
			(γ-Terpinene)	4.39
5	Santoreggia (esperis) 1 / Savory (esperis) 1	<i>Satureja ortensis</i>	Thymol	18.7
			Carvacrol	23.5
			Eugenol	1.23
6	Timo Capitato / Spanish Origan	<i>Thymbra capitata</i>	Carvacrol	69.70
7	Garofano Chiodi 1 / Clove 1	<i>Eugenia caryophyllus</i> or <i>Syzygium aromaticum</i>	Eugenol	73.90
8	Timo Rosso 1 / Red Thyme 1	<i>Thymus vulgaris</i>	carvacrol	33.51
				48.72
9 ^a	Sedano / Celery	<i>Apium graveolens</i>	(Sedanolide)	2.19
10 ^a	Calendula / Marigold	<i>Calendula officinalis</i>	(Ocimene)	14.53
11 ^a	Cedro Atlas / Atlas Cedarwood	<i>Cedrus atlantica</i>	(β-Himachalene)	49.02
12	Timo Rosso 2 / Red thyme 2	<i>Thymus vulgaris</i>	Carvacrol	33.90
			Thymol	4.01
13	Timo Rosso 3 / Red thyme 3	<i>Thymus vulgaris</i>	Carvacrol	3.1
			Thymol	53.10
14	Santoreggia 2 / Savory 2	<i>Satureja ortensis</i>	Carvacrol	46.60
			Thymol	1.70
15	Origano / Origan	<i>Origanum vulgare</i>	Carvacrol	69.20
			Thymol	0.41
16	Cannella / Cinnamon	<i>Cinnamomum verum</i>	Eugenol	81.51
17	Chiodi di Garofano 2 / Clove 2	<i>Eugenia caryophyllus</i> or <i>Syzygium aromaticum</i>	Eugenol	84.62
18	Chiodi di Garofano 3 / Clove 3	<i>Eugenia caryophyllus</i> or <i>Syzygium aromaticum</i>	Eugenol	80.81

a) These essential oils contained no phenolic component at concentration > 1% (w/w). The components reported in brackets are just characteristic marker components, with no known antioxidant activity

Table A 1.4. Phenolic compounds identified in the investigated essential oils (> 1.5% w/w) and corresponding k_{inh} values measured at 30°C in inhibited autoxidations.

Phenolic compound	Structure	k_{inh} ($M^{-1}s^{-1}$) ^a (140)	Reference
Carvacrol ^b		$(1.3 \pm 0.1) \times 10^4$	unpublished
Thymol ^b		$(1.3 \pm 0.2) \times 10^4$	unpublished
Eugenol		$(4.8 \pm 0.2) \times 10^3$	[103]
4-Allylphenol ^b		$(1.2 \pm 0.1) \times 10^5$	unpublished
Guaiacol		0.47×10^4	[104]
4-Ethylguaiacol ^c		1.2×10^4	[104,105]
<i>p</i> -Creosol		7.5×10^3	[103]
Phenol		6.0×10^3	[104]
2,6-Dimethylphenol		1.5×10^4	[104]
4-Methoxyphenol		2.7×10^5	[104]

Syringol		1.8×10^4	[104]
2-Allylphenol		2.4×10^4	[83]
<i>o</i> -Methylphenol		1.6×10^4	[83]
<i>p</i> -Methylphenol		2.3×10^4	[83]
Umbelliferone ^b		$(1.9 \pm 0.3) \times 10^3$	unpublished

a) the k_{inh} values from reference were analyzed by inhibited autoxidation of styrene (or Cumene) in PhCl at 30°C. b) These unpublished inhibition constants of these phenolic compounds were analyzed by conducting the inhibited autoxidation of cumene in PhCl at 30°C, initiated by AIBN (0.05M), which were conducted by other students in our lab. c) k_{inh} of 4-Ethylguaiacol was estimated base on the of k_{inh} since 4-methylguaiacol, and 4-ethylguaiacol were reported exerting similar antioxidant activities in a dose-dependent manner [104,105].

References:

- [1] L. Bergendi, L. Beneš. Z. Ďuračková, M. Ferenčík. Chemistry, physiology and pathology of free radicals. *Life Sciences*. 1999, 65(18–19), 1865–1874.
- [2] K. U. Ingold. Peroxy radicals. *Accounts of Chemical Research*. 2(1), 1969, 1–9.
- [3] K. U. Ingold. Inhibition of the Autoxidation of Organic Substances in the Liquid Phase. *Chem. Rev.* 1961, 61, 563–589.
- [4] K. U. Ingold, D. A. Pratt. Advances in radical-trapping antioxidant chemistry in the 21st century: a kinetics and mechanisms perspective. *Chem. Rev.* 2014, 114, 9022–9046.
- [5] E. N. Frankel. Lipid oxidation. *Progress in Lipid Research*. 1980, 19(1–2), 1–22.
- [6] E. T. Denisov. Liquid-phase reaction rate constants. New York: IFI/Plenum, 1974.
- [7] T. Koenig. In: JK Kochi ed. Free Radicals, New York: Wiley, 1973, 1, 113–155.
- [8] E. T. Denisov, T. G Denisova, T. S. Pokidova. Handbook of radical initiators. New York: Wiley, 2003.
- [9] P. S. Engel. Mechanism of the thermal and photochemical decomposition of azoalkanes. *Chem. Rev.* 1980, 80, 99–150.
- [10] K. Chakravorty, J. M. Pearson, M. Szwarc. Photolysis of 1, 1, 1-trifluoromethylazocyclopropane. Fate of the NN-C-C₃H₅ radical. *J. Phys. Chem.* 1969, 73, 746–748.
- [11] E.T. Denisov, O. M. Sarkisov, G. I. Likhtenstein. Chemical kinetics. Amsterdam: Elsevier, 2003.
- [12] A. M. North. The collision theory of chemical reactions in liquids. London: Methuen, 1964.
- [13] B. Maillard, K. U. Ingold, J. C. Scaiano. Rate constants for the reactions of free radicals with oxygen in solution. *J. Am. Chem. Soc.* 1983, 105, 5095–5099.
- [14] L. Gómez-Hortigüela, F. Corà, and C. R. A. Catlow. Aerobic oxidation of hydrocarbons catalyzed by Mn-doped nanoporous aluminophosphates(I): Preactivation of the Mn sites. *ACS Catal.* 2011, 1, 1, 18–28
- [15] D. D. M. Wayner, E. Lusztyk, D. Pagé, K. U. Ingold, P. Mulder, L. J. J. Laarhoven, and H. S. Aldrich. Effects of solvation on the enthalpies of reaction of *tert*-butoxyl radicals with phenol and on the calculated O—H bond strength in phenol. *J. Am. Chem. Soc.* 1995, 117, 8737–8744.
- [16] S. Korcek, J. H. B. Chenier, J. A. Howard, and K. U. Ingold. Absolute rate constants for hydrocarbon autoxidation. XXI. activation energies for propagation and the correlation of propagation rate constants with carbon hydrogen bond strengths. *Canadian Journal of Chemistry* 1972, 50, 2285—2297.
- [17] E. T. Denisov, I. B. Afanas'ev. Oxidation and antioxidants in organic chemistry and biology. CRC Press Taylor & Francis Group, New York, 2005
- [18] R. E. Pliss, V.A. Machtin, E. M Pliss. In: Abstracts of conference regulation of biological processes by free radicals: Role of antioxidants, free radical scavengers, and chelators. Moscow, Yaroslavl, Yaroslavl State Technical University, 1998, p 17.
- [19] P. D. Bartlett, R. R. Hiatt. A series of tertiary butyl peresters showing concerted decomposition. *J. Am. Chem. Soc.* 1958, 80, 1398–1405.

- [20] P. Neta, R. E. Huie, A. B. Ross. Rate constants for reactions of peroxy radicals in fluid solutions. *J. Phys. Chem. Ref.* 1990, 19, 413–513.
- [21] G. A. Russell. Deuterium-isotope effects in the autoxidation of aralkyl hydrocarbons. Mechanism of the interaction of peroxy radicals. *J. Am. Chem. Soc.* 1957, 79, 3871–3877.
- [22] R. Lee, G. Gryn'ova, K. U. Ingold, M. L. Coote. Why are *sec*-alkylperoxy bimolecular self-reactions orders of magnitude faster than the analogous reactions of *tert*-alkylperoxyls? The unanticipated role of CH hydrogen bond donation. *Phys. Chem. Chem. Phys.* 2016, 18, 23673–23679.
- [23] L. Valgimigli, D. A. Pratt. Antioxidants in chemistry and biology. In: Chatgililoglu C, Studer A, (Editors). Encyclopedia of radicals in chemistry, biology and materials. Chirchester, UK: Wiley, 2012. 3, 1623–1677.
- [24] I. S. Young, J. V. Woodside. Antioxidants in health and disease. *J Clin Pathol.* 2001,54(3),176–186.
- [25] R. J. Ruch, S. Cheng, J. E. Klaunig. Prevention of cytotoxicity and inhibition of intercellular communication by antioxidant catechins isolated from Chinese green tea, *Carcinogenesis*, 1989, 10(6) , 1003–1008,
- [26] R. Amorati, L. Valgimigli. Modulation of the antioxidant activity of phenols by non-covalent interactions. *Org Biomol Chem.* 2012,10,4147-4158
- [27] S. Cakmakci, E. F. Topdaş, P. Kalın, H. Han, P. Şekerci, K. L. Polat, I. Gulcin. Antioxidant capacity and functionality of oleaster (*Elaeagnus angustifolia* L.) flour and crust in a new kind of fruity ice cream. *Int J Food Sci Technol* 2015, 50(2), 472–481
- [28] H. Gocer, A. Akıncioğlu, N. Oztaşkın, S. Göksu, I. Gulcin. Synthesis, antioxidant and antiacetylcholinesterase activities of sulfonamide derivatives of dopamine related compounds. *Arch Pharm* 2013, 346(11),783–792
- [29] V. Sindhi, V. Gupta, K. Sharma, S. Bhatnagar, R. Kumari, N. Dhaka. Potential applications of antioxidants—a review. *J Pharm Res* 2013, 7, 828–835
- [30] L. Valgimigli, R. Iori. Antioxidant and pro-oxidant capacities of ITCs. *Environmental and Molecular Mutagenesis.* 2009, 50, 222–237.
- [31] A.J. McGrath, G.E. Garrett, L. Valgimigli, D.A. Pratt. The redox chemistry of sulfenic acids. *Journal of the American Chemical Society* 132, 2010, 16759–16761.
- [32] E. Bursal, E. Köksal, İ. Gülçin, G. Bilsel, A. C. Gören. Antioxidant activity and polyphenol content of cherry stem (*Cerasus avium* L.) determined by LC-MS/MS. *Food Res Int* 2013, 51, 66–74
- [33] A. A. Hamid, O. O. Aiyelaagbe, L. A. Usman, O. M. Ameen, A. Lawal. Antioxidants: Its medicinal and pharmacological applications. *Afr. J. Pure Appl. Chem.* 2010,4(8),142-151.
- [34] I. Gulcin. Antioxidant activity of food constituents: an overview. *Arch Toxicol.* 2012, 86(3), 345–391.
- [35] G. W. Burton, T. Doba, E. Gabe, L. Hughes, F. L. Lee, L. Prasad, K. U. Ingold. Autoxidation of biological molecules. 4. Maximizing the antioxidant activity of phenols. *J. Am. Chem. Soc.* 1985, 107(24), 7053–7065

- [36] F. Shahidi, P. K. Janitha, P. D. Wanasundara. Phenolic antioxidants. *Critical reviews in food science and nutrition*. 1992, 32(1),67-103
- [37] D. A. Pratt, G. A. DiLabio, P. Mulder, K. U. Ingold. Bond strengths of toluenes, anilines, and phenols: to Hammett or not. *Acc. Chem. Res.* 2004, 37, 334–340.
- [38] L. R. C. Barclay. C. E. Edwards, M. R. Vinqvist. Media effects on antioxidant activities of phenols and catechols. *J. Am. Chem. Soc.* 1999, 121, 26, 6226–6231
- [39] G. Brigati, M. Lucarini, V. Mugnaini, G. F. Pedulli. Determination of the substituent effect on the O–H bond dissociation enthalpies of phenolic antioxidants by the EPR radical equilibration technique. *J. Org. Chem.* 2002, 67, 14, 4828–4832.
- [40] J. S. Wright, E. R. Johnson, G. A. DiLabio. Predicting the activity of phenolic antioxidants: Theoretical method, analysis of substituent effects, and application to major families of antioxidants. *J. Am. Chem. Soc.* 2001, 123, 6, 1173–1183.
- [41] P. Mulder, H.-G. Korth, D. A. Pratt, G. A. DiLabio, L. Valgimigli, G. F. Pedulli, K. U. Ingold. Critical re-evaluation of the O–H bond dissociation enthalpy in phenol. *J. Phys. Chem. A* 2005, 109(11), 2647–2655
- [42] D. W. Snelgrove, J. Lusztyk, J. T. Banks, P. Mulder, K. U. Ingold. Kinetic solvent effects on hydrogen-atom abstractions: reliable, quantitative predictions via a single empirical equation. *J. Am. Chem. Soc.* 2001, 123, 469–477.
- [43] L. Valgimigli, R. Amorati, S. Petrucci, G. F. Pedulli, D. Hu, J. J. Hanthorn, D. A. Pratt. Unexpected acid catalysis in reactions of peroxy radicals with phenols. *Angew. Chem. Int. Ed.*, 2009, 48, 8348–8351.
- [44] R. F. Enes, A. C. Tome, J. A. S. Cavaleiro, R. Amorati, M. G. Fumo, G. F. Pedulli, L. Valgimigli. Synthesis and antioxidant activity of [60] fullerene–BHT conjugates. *Chem.—Eur. J.*, 2006, 12, 4646–4653.
- [45] B. Li, D. A. Pratt. Methods for determining the efficacy of radical-trapping antioxidants. *Free Radic. Biol. Med.* 2015, 82, 187–202.
- [46] R. Amorati, L. Valgimigli. Methods to measure the antioxidant activity of phytochemicals and plant extracts. *J. Agric. Food Chem.* 2018, 66(13), 3324–3329
- [47] J. Lalevée, X. Allonas, J. P. Fouassier. New access to the peroxy radicals reactivity? *Chem. Phys. Lett.* 2007, 445, 62–67.
- [48] R. Amorati, L. Valgimigli. Advantages and limitations of common testing methods for antioxidants. *Free Radical Research* 2015 49(5). 1-12.
- [49] L. Valgimigli, M. Lucarini, G. F. Pedulli, K. U. Ingold. Does beta-carotene really protect vitamin E from oxidation? *J. Am. Chem. Soc.* 1997, 119:8095-8096
- [50] R. Amorati, A. Baschieri, L. Valgimigli. Measuring antioxidant activity in bioorganic samples by the differential oxygen uptake apparatus: Recent advances, *Hindawi Journal of Chemistry*, 2017
- [51] L. R. C. Barclay, K. A. Baskin, S. J. Locke, T. D. Schaefer, Benzophenone-photosensitized autoxidation of linoleate in solution and sodium dodecyl sulfate micelles. *Can. J. Chem.*, 1987, 65, 2529–2540.
- [52] R. Amorati, F. Ferroni, M. Lucarini, G. F. Pedulli, L. Valgimigli. A Quantitative approach to the recycling of α -tocopherol by coantioxidants. *J. Org. Chem.* 2002, 67(26), 9295–9303

- [53] G. Mugesh, W.-W. du Mont, H. Sies. Chemistry of biologically important synthetic organoselenium compounds. *Chem. Rev.*, 2001, 101, 2125–2179.
- [54] J. A. Howard, Homogeneous liquid phase autoxidations. In *Free Radicals*, eds J. K. Kochi, John Wiley & Sons, Inc., New York, 1973.
- [55] W. A. Pryor, T. Strickland, D. F. Church, Comparison of the efficiencies of several natural and synthetic antioxidants in aqueous SDS [sodium dodecyl sulfate] micelle solutions. *J. Am. Chem. Soc.*, 1988, 110, 2224–2229.
- [56] E. T. Denisov, I. V. Khudyakov, Mechanisms of action and reactivities of the free radicals of inhibitors. *Chem. Rev.*, 1987, 87, 1313–1357.
- [57] EFSA Panel on Food Additives and Nutrient Sources Added to Food (ANS). Scientific Opinion on the reevaluation of butylated hydroxytoluene BHT (E 321) as a food additive. *EFSA J.* 2012, 10, 2588 – 2630.
- [58] J. A. Howard, K. U. Ingold. Absolute rate constants for hydrocarbon autoxidation. VI. Alkyl aromatic and olefinic hydrocarbons. *Can. J. Chem.* 1967, 45, 973–802.
- [59] L. Xu, T. A. Davis, N. A. Porter. Rate constants for peroxidation of polyunsaturated fatty acids and sterols in solution and in liposomes. *J. Am. Chem. Soc.* 2009, 131, 13037-13044.
- [60] H. Yin, L. Xu, N. A. Porter. Free radical lipid peroxidation: mechanisms and analysis. *Chem. Rev.* 2011, 111, 5944–5972.
- [61] L. Xu, N. A. Porter. Reactivities and products of free radical oxidation of cholestadienols. *J. Am. Chem. Soc.* 2014, 136, 5443–5450.
- [62] Z. A. M. Zielinski, D. A. Pratt. Lipid peroxidation: Kinetics, mechanisms, and products. *J. Org. Chem.* 2017, 82, 2817–2825.
- [63] K. Warner. Effects on the flavor and oxidative stability of stripped soybean and sunflower oils with added pure tocopherols. *J. Agric. Food Chem.* 2005, 53, 9906–9910.
- [64] R. Amorati, A. Baschieri, G. Morroni, R. Gambino, L. Valgimigli. peroxy radical reactions in water solution: A gym for proton-coupled electron-transfer theories. *Chem. Eur. J.* 2016, 22, 7924 – 7934.
- [65] Codex Alimentarius CODEX STAN 210-1999. Standard for named vegetable oils. 2017 (<http://www.fao.org/fao-who-codexalimentarius/codex-texts/all-standards/en/>). (Accessed on Dec. 2018).
- [66] L. Valgimigli, D. Bartolomei, R. Amorati, E. Haidasz, J. J. Hanthorn, S. J. Nara, J. Brinkhorst, D. A. Pratt. 3-Pyridinols and 5-pyrimidinols: tailor-made for use in synergistic radical-trapping co-antioxidant systems. *Beilstein J. Org. Chem.* 2013, 9, 2781–2792.
- [67] E. Niki. Assessment of antioxidant capacity in vitro and in vivo. *Free Radic. Biol. Med.* 2010, 49, 503–51.
- [68] J. P. Cosgrove, D. F. Church, W. A. Pryor. The kinetics of the autoxidation of polyunsaturated fatty acids. *Lipids* 1987, 22, 299-304.
- [69] K. Wołosik, M. Knaś, A. Zalewska, M. Niczyporuk, A. W. Przystupa. The importance and perspective of plant-based squalene in cosmetology. *J. Cosmet. Sci.* 2013, 64, 59-66.

- [70] X. Li, Y. Shen, G. Wu, X. Qi, H. Zhang, L. Wang, H. Qian. Determination of key active components in different edible oils affecting lipid accumulation and reactive oxygen species production in HepG2 Cells. *J. Agric. Food Chem.* 2018, *66*, 11943–11956.
- [71] L. H. Reddy, P. Couvreur. Squalene: A natural triterpene for use in disease management and therapy. *Adv. Drug Deliv. Rev.* 2009, *61*, 1412–1426.
- [72] A. Di Pasquale, S. Preiss, F. Tavares Da Silva, N. Garçon. Vaccine adjuvants: from 1920 to 2015 and beyond. *Vaccines* 2015, *3*, 320-343.
- [73] J. Park, B. J. Yu, J. Choi, H. M. Woo. heterologous production of squalene from glucose in engineered corynebacterium glutamicum using multiplex CRISPR interference and high-throughput fermentation. *J. Agric. Food Chem.* 2019, Articles ASAP.
- [74] C. J. Phillips, G. R. Matyas, C. J. Hansen, C.R. Alving, T. C. Smith, M.A. Ryan. Antibodies to squalene in US Navy Persian Gulf War veterans with chronic multisymptom illness. *Vaccines* 2009, *27*, 3921-6.
- [75] H. Chen, R. H. Liu. Potential Mechanisms of Action of Dietary Phytochemicals for Cancer Prevention by Targeting Cellular Signaling Transduction Pathways. *J. Agric. Food Chem.* 2018, *66*, 3260–3276.
- [76] N. Shimizu, J. Ito, S. Kato, Y. Otoki, M. Goto, T. Eitsuka, T. Miyazawa, K. Nakagawa. Oxidation of squalene by singlet oxygen and free radicals results in different compositions of squalene monohydroperoxide isomers. *Sci. Rep.* 2018, *8*, 9116.
- [77] E. Naziri, R. Consonni, M. Z. Tsimidou. Squalene oxidation products: Monitoring the formation, characterisation and pro-oxidant activity. *Eur. J. Lipid Sci. Technol.* 2014, *116*, 1400–1411.
- [78] M. Cristani, M. D'Arrigo, G. Mandalari, F. Castelli, M. G. Sarpietro, D. Micieli, V. Venuti, G. Bisignano, A. Saija, D. Trombetta. Interaction of four monoterpenes contained in essential oils with model membranes: implications for their antibacterial activity. *J. Agric. Food Chem.* 2007, *55*, 6300–6308.
- [79] M. Koşar, B. Demi'rci', F. Demi'rci', K. H. Can Başer. Effect of maturation on the composition and biological activity of the essential oil of a commercially important satureja species from turkey: *Satureja cuneifolia* Ten. (Lamiaceae). *J. Agric. Food Chem.* 2008, *56*, 2260–2265.
- [80] E. Block. Molecular basis of mammalian odor discrimination: A status report. *J. Agric. Food Chem.* 2018, *66*, 13346–13366,
- [88--81] H. Boardman. The mechanism of oxidation of p-cymene. *J. Am. Chem. Soc.* 1962, *84*, 1376-1382.
- [82] A. Baschieri, M. D. Ajvazi, J. L. F. Tonfack, L. Valgimigli, R. Amorati. Explaining the antioxidant activity of some common nonphenolic components of essential oils. *Food Chem.* 2017, *232*, 656–663.
- [83] R. Amorati, J. Zotova, A. Baschieri, L. Valgimigli. Antioxidant activity of magnolol and honokiol: kinetic and mechanistic investigations of their reaction with peroxy radicals. *J. Org. Chem.* 2015, *80*, 10651–10659.

- [84] M. Massaro, S. Riela, S. Guernelli, F. Parisi, G. Lazzara, A. Baschieri, L. Valgimigli, R. Amorati. A synergic nanoantioxidant based on covalently modified halloysite–trolox nanotubes with intra-lumen loaded quercetin. *J. Mater. Chem. B* 2016, 4, 2229–2241.
- [85] C. Spatafora, C. Daquino, C. Tringali, R. Amorati. Reaction of benzoxanthene lignans with peroxy radicals in polar and non-polar media: cooperative behaviour of OH groups. *Org. Biomol. Chem.* 2013, 11, 4291–4294.
- [86] K. A. Harrison, E. A. Haidasz, M. Griesser, D. A. Pratt. Inhibition of hydrocarbon autoxidation by nitroxide-catalyzed cross-dismutation of hydroperoxyl and alkylperoxyl radicals. *Chem. Sci.* 2018, 9, 6068-6079.
- [87] J. Cedrowski, G. Litwinienko, A. Baschieri, R. Amorati. Hydroperoxyl radicals (HOO·): Vitamin E regeneration and H - bond effects on the hydrogen atom transfer. *Chemistry – A European Journal* 2016,22(46), 16441-16445.
- [88] A. Baschieri, L. Valgimigli, S. Gabbanini, G A. DiLabio, E. Romero-Montalvo, R. Amorati. Extremely Fast Hydrogen Atom Transfer between Nitroxides and HOO· Radicals and Implication for Catalytic Coantioxidant Systems. *J. Am. Chem. Soc.* 2018, 140, 32, 10354–10362. DOI: 10.1021/jacs.8b06336.
- [89] M. A. Saleh, S. Clark, B. Woodard, S. A. Deolu-Sobogun. Antioxidant and free radical scavenging activities of essential oils. *Ethnicity & Disease*, 2010, 20, 78-82
- [90] W. Zheng, S. Y. Wang. Antioxidant activity and phenolic compounds in selected herbs. *J. Agric. Food Chem.* 2001, 49(11), 5165–5170
- [91] I. Bettaieb, S. Bourgou, W. A. Wannes, I. Hamrouni, F. Limam, B. Marzouk. Essential Oils, Phenolics, and antioxidant activities of different parts of cumin (*Cuminum cyminum* L.). *J. Agric. Food Chem.* 2010, 58(19), 10410–10418
- [92] F. Bakkali, S. Averbeck, D. Averbeck, M. Idaomar. Biological effects of essential oils – A review. *Food and Chemical Toxicology.* 2008, 46(2), 446-475
- [93] D. Kalemba, A. Kunicka. Antibacterial and antifungal properties of essential oils. *Current Medicinal Chemistry.* 2003, 10(10), 813-829
- [94] J. S. Raut, S. M. Karuppayil. A status review on the medicinal properties of essential oils. *Industrial Crops and Products.* 2014, 62, 250-264.
- [95] S. Harpaz, L. Glatman, V. Drabkin, A. Gelman. Effects of herbal essential oils used to extend the shelf life of freshwater-reared asian sea bass fish (*Lates calcarifer*). *J Food Prot.* 2003, 66 (3), 410–417.
- [96] B. Sampaio, R. Edrada-Ebel, F. Da Costa, Effect of the environment on the secondary metabolic profile of *Tithonia diversifolia*: a model for environmental metabolomics of plants. *Sci Rep.* 2016, 6, 29265.
- [97] R. Amorati, P. T. Lynett, L. Valgimigli, D. A. Pratt. The reaction of sulfenic acids with peroxy radicals: insights into the radical trapping antioxidant activity of plant-derived thiosulfinates. *Chem. Eur. J.* 2012, 18, 6370-6379.
- [98] R. Amorati, G. F. Pedulli, L. Valgimigli. Kinetic and thermodynamic aspects of the chain-breaking antioxidant activity of ascorbic acid derivatives in non-aqueous media. *Org. Biomol. Chem.* 2011, 9, 3792–3800.

- [99] R. Amorati, G. F. Pedulli, D. A. Pratt, L. Valgimigli. TEMPO reacts with oxygen-centered radicals under acidic conditions. *Chem. Commun.* 2010, *46*, 5139–5141.
- [100] M. Lucarini, G. F. Pedulli, L. Valgimigli, R. Amorati, F. Minisci. Thermochemical and Kinetic Studies of a Bisphenol Antioxidant. *J. Org. Chem.* 2001, *66*, 5456-5462
- [101] R. Amorati, L. Valgimigli, P. Dinér, K. Bakhtiari, M. Saeedi, L. Engman. Multifaceted reactivity of alkyltellurophenols towards peroxy radicals: catalytic antioxidant versus thiol-depletion effect. *Chem. Eur. J.* 2013, *19*, 7510 – 7522.
- [102] M. Khoobchandani, B. K. Ojeswi, N. Ganesh, M. M Srivastava, S. Gabbanini, R. Matera, R. Iori, L Valgimigli. Antimicrobial properties and analytical profile of traditional *Eruca sativa* seed oil: Comparison with various aerial and root plant extracts. *Food Chem.* **2010**, *120*, 217–224.
- [103] A. Baschieri, L. Pulvirenti, V. Muccilli, R. Amorati, C. Tringali. Chain-breaking antioxidant activity of hydroxylated and methoxylated magnolol derivatives: the role of H-bonds. *Org. Biomol. Chem.* 2017, *15*, 6177-6184.
- [104] R. Amorati, S. Menichetti, E. Mileo, G. F Pedulli, C. Viglianisi. Hydrogen - Atom Transfer Reactions from ortho - Alkoxy - Substituted Phenols: An Experimental Approach. *Chem. Eur. J.* 2009, *15*, 4402 – 4410.
- [105] D. Zhao, J. Sun, B. Sun, M. Zhao, F. Zheng, M. Huang. Intracellular antioxidant effect of vanillin, 4-methylguaiacol and 4-ethylguaiacol: three components in Chinese Baijiu. *Rsc Advances.* 2017, *7*(73), 46395-46405

Chapter 2

Regeneration of phenolic and polyphenolic antioxidants by γ -Terpinene and related hydroperoxide (HOO•) releasers.
Implications in Melanins' antioxidant behavior.

Summary

In this chapter, we set to investigate the possible interplay of γ -terpinene with reference antioxidants, where PMHC and DTBC were chosen as prototype of mono- and polyphenolic antioxidants respectively, with the aim of disclosing new unconventional synergistic combinations of antioxidants. Our studies show a clear synergism between γ -terpinene with either monophenolic or polyphenolic antioxidants, where γ -terpinene acts as the co-antioxidant that regenerates the main (phenolic) antioxidants. It was found that regeneration depends on the release of HOO^\bullet by γ -terpinene upon being attacked by ROO^\bullet , thereby causing a chain-transfer with exchange of the chain-carrying species from ROO^\bullet to HOO^\bullet . In this system HOO^\bullet carries on a dual function: it is the oxidative-chain carrier and it also acts as reducing species for phenoxy radicals, which regenerates the inhibitor. Mechanistic experiments showed that γ -terpinene could only regenerate monophenols from their phenoxy radical, but a different, 2e-two-steps regeneration mechanisms was demonstrated for polyphenols like catechols, which could be regenerated also from the oxidized quinone. Since quinones and hydroquinones/catechols are the redox-active structural motif of melanins, this chemistry was judged key to understanding their previously unexplained antioxidant behavior. Therefore, the reduction of quinones by HOO^\bullet , along with the oxidation of catechols/hydroquinones and reduction of the parent semiquinone radicals by the same species (HOO^\bullet) was investigated on quantitative grounds and the resulting knowledge was used to better rationalize melanins's redox-mediated bioactivity. To this goal studies were extended on polydopamine (PDA) as a representative member of melanins's family. PDA was found to have modest activity in trapping ROO^\bullet radicals, after accurate purification. However, in the presence of HOO^\bullet , it turns into an effective antioxidant, which is due to reduction of *ortho*-quinones to semiquinones and catechols by HOO^\bullet . This explains their redox-mediated bioactivity, given the abundance of $\text{O}_2^{\bullet-}/\text{HOO}^\bullet$ species in biological systems. This chapter addresses this chemistry stepping from a short review of current knowledge concerning the generation of $\text{O}_2^{\bullet-}/\text{HOO}^\bullet$ in biological systems.

2.1 Reactive Oxygen Species (ROS)

Life is sustained by oxygen (dioxygen or triplet O_2), which is necessary for our energetic metabolism due to its oxidizing activity that allows producing adenosine triphosphate (ATP) during oxidative phosphorylation [1,2]. However, the respiration and metabolism processes in organisms also generate reactive oxygen species (ROS), which can lead to biological toxicity when they are not balanced or formed in excessive quantities [3,4]. Besides, a variety of exogenous agents, such as radiation, pollutants and toxins (Figure 2.1) [5,6], can also stimulate their generation.

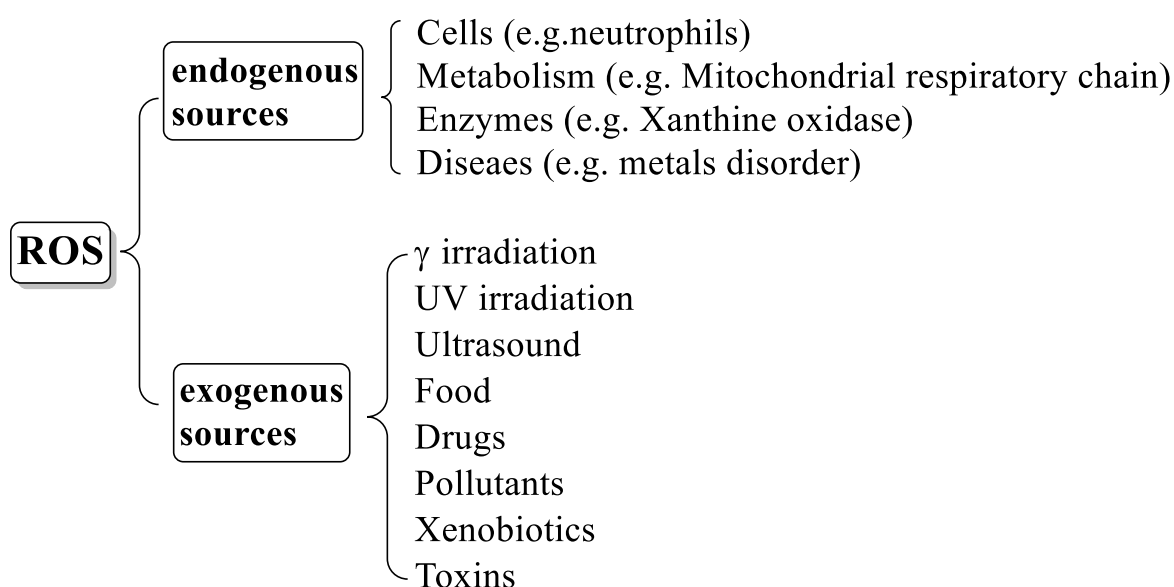


Figure 2.1. Main exogenous and endogenous sources of ROS.

Biologically significant reactive oxygen species are listed in Table 2.1 [7,8], and mainly include highly reactive free radicals, such as superoxide anion ($O_2^{\cdot-}$) in the electron-transport chain, its protonated (neutral) form, the hydroperoxyl radical ($HOO\cdot$), highly reactive hydroxyl / alkoxy radicals ($HO\cdot / RO\cdot$) formed from decomposition of peroxides (e.g. Fenton reaction), more lipid soluble peroxy radicals ($HOO\cdot / ROO\cdot$), and some non-radicals, such as peroxides ($H_2O_2 / ROOH$) and ozone (O_3). There are also reactive nitrogen species (RNS), such as nitric oxide, nitrous oxide (N_2O), peroxyxynitrite ($ONOO^-$), peroxyxynitrous acid ($ONOOH$), etc. These species overall contribute to the oxidative stress in biological systems, if not balanced by antioxidant defences [9,10].

Table 2.1. Main reactive oxygen species (ROS) of interest in oxidative stress

Free Radical Species		Non-Radical Species	
hydroxyl radical	HO•	hydrogen peroxide	H ₂ O ₂
superoxide radical	O ₂ ^{•-}	singlet oxygen	¹ O ₂
hydroperoxyl radical	HOO•	ozone	O ₃
aloxyl radical	RO•	peroxide	ROOH
peroxyl radical	ROO•	hypochlorite	HOCl
nitrogen oxide/dioxide radical	NO•/ NO ₂ •	peroxy nitrite/peroxynitrous acid	ONOO ⁻ / ONOOH
thiyl radical	RS•	nitrous oxide and nitroxyl anion/ cation	NO/NO ⁻ / NO ⁺

2.2 Oxidative Damage

ROS, especially free radicals, i.e. molecular fragments with an unpaired electron, display high reactivity toward their surrounding molecules, such as lipids, proteins and DNA, resulting in biological damage [11]. And oxidative stress is thought to be involved in the development of several human diseases such as cancer, Parkinson's disease, Alzheimer's disease, atherosclerosis, heart failure, infection, and chronic fatigue etc. [12-14]

2.2.1 Lipid peroxidation

Among the oxidative damaging biomolecular targets, damage to lipids, especially polyunsaturated fatty acids (PUFA) and the derived triglycerides and phospholipids, are primary due to the radical chain propagated peroxidation [15]. Radicals species, such as HO•, HOO•, RO•, and ROO•, could abstract an hydrogen atom from the allylic (or bis-allylic) position of PUFA, yielding the corresponding alkyl (C-centered) radical to initiate the lipid peroxidation process [16]. The alkyl radical reacts extremely quickly (diffusion controlled) with molecular oxygen [17], forming a related peroxy

radical, which is able to abstract another hydrogen from the lipid molecule, thus propagating the oxidation chain and leading to the progressive lipid oxidation, unless external antioxidants terminate such radical chain [18].

2.2.2 Oxidative damage to proteins

Proteins, as major constituents of cellular membrane, are also vulnerable to ROS attack, which might lead to damage of the protein's structure and function, particularly to enzyme [19]. These protein oxidative damages include various pathways: radicals can attack amino acids, peptides and proteins, forming various modifications, such as protein backbone cleavage or crosslink, formation of protein carbonyls, etc [20].

Protein backbone oxidation is induced by hydroxyl radicals, which abstract alpha-hydrogens, forming the corresponding carbon-centred radical [21]. In the absence of oxygen, such carbon-central radicals could react with each other, forming (-C-C-) crosslink. Additionally, other (-S-S-) or (-S-N-) crosslinks have been reported to be formed by oxidation of amino acids with specific residues, for example, cysteine, lysine and arginine [22]. In fact, oxygen can rapidly add to carbon-centered radicals, inducing the cleavage of peptides by diamide or α -amidation pathways. Moreover, radicals might attack at the β -(C3)-position of protein, releasing a carbonyl compound and α -carbon-central radical, which could proceed with backbone fragmentation through mechanisms similar to diamide or α -amidation pathways. Additionally, oxidation of side chains such as glutamyl, aspartyl, and prolyl can also form protein fragmentation via single backbone cleavage [23]. Protein carbonyls are the most common damage for proteins: they form not only from the backbone fragmentation mentioned above, but also can be introduced by side-chain oxidation including proline, arginine, lysine, and threonine. Alternatively, they can also generate through addition with reactive aldehyde or ketone derivatives from oxidation of lipids and sugars [24].

2.2.3 Oxidative damage to DNA

Although DNA is a quite stable and resistant molecule, oxidative damage still possibly happens upon interaction with ROS, especially hydroxyl radicals [25]. HO[•] radicals

predominantly add to 4, 5, or 8 position in the purine ring, and in 5 or 6 position in the pyrimidine ring, yielding chemically modified bases [26]. ROS can also damage deoxyribose sugar, producing sugar peroxy radicals, which can undergo further reactions yielding carbonyl products [27]. Ultimately, those reactions under ROS attacks lead to DNA damages, even cell death and cancer.

2.3 The $\text{HOO}^\bullet/\text{O}_2^{\bullet-}$ System: a special case of ROS

$\text{O}_2^{\bullet-}$ generated by the reduction of molecular oxygen, $\text{O}_2 + e^- \rightarrow \text{O}_2^{\bullet-}$ is the predominant form of superoxide in neutral water [28,29]; however, its protonated form, HOO^\bullet radical is an acid, the only species present under strongly acid condition [30,31]. They work as the precursor of most other reactive oxygen species, for example, the disproportionation of $\text{HOO}^\bullet/\text{O}_2^{\bullet-}$ gives hydrogen peroxide and oxygen [32]. Radical chemistry of $\text{HOO}^\bullet/\text{O}_2^{\bullet-}$ has been implicated as mediators in a wide variety of processes, such as metal catalyzed oxidation [33,34], environmental chemistry [35,36], and oxidative damage in biological system [37]. $\text{O}_2^{\bullet-}$ was once considered as the main ROS responsible for biological oxidative stress, before it was discovered that $\text{O}_2^{\bullet-}$ very poorly interacts with PUFAs and proteins [38,39]. Later, hydroxyl radical ($^\bullet\text{OH}$) originated from ($\text{O}_2^{\bullet-}$) were suspected as the oxidant, due to its high reactivity [28]. However, $^\bullet\text{OH}$ was found be able to react with organic molecules indistinctly, and at nearly diffusion-controlled rate. The short lifetime of $^\bullet\text{OH}$ radicals ($\sim 10^{-9}$ sec) prevents it from reaching the inner layer of lipid membrane to attack the unsaturated double bonds [40]. However, the protonated form of superoxide anion, hydroperoxyl radical (HOO^\bullet), which predominate at lower pH ($pK_a = 4.7$) [41], is always present in the cell with superoxide anion due to the equilibrium $\text{O}_2^{\bullet-} + \text{H}_2\text{O} \rightleftharpoons \text{HOO}^\bullet + \text{OH}^-$. HOO^\bullet radical behaves like other peroxy radicals, which could abstract hydrogen from lipids; for example, it reacts with linoleic acid to generate pentadienyl type radical [42]. Although the low pK_a of HOO^\bullet holds off its abundance in the cytoplasm (pH 7.4), and it was also reported less than 1% of $[\text{O}_2^{\bullet-}]$ is present in protonated form, HOO^\bullet is hydrophobic and more reactive than $\text{O}_2^{\bullet-}$ [43]. In fact, the important role of HOO^\bullet on membrane lipid

peroxidation was not realized until some researchers reported that the pH values around the charged membranes may be several units lower than in the bulk cytoplasm. It should be also kept in mind that HOO^\bullet has no charge, so it can easily pass into or cross the lipid membrane, providing it action as lipid peroxidation initiator, by abstracting hydrogen atoms like alkylperoxyl radicals do, in contrast with $\text{O}_2^{\bullet-}$, which undergoes no hydrogen abstraction reaction [44]. However, the H-OO \bullet BDE of hydroperoxyl radical has an extremely low value (45 kcal mol⁻¹), which allows it to behave as a potential H-atom donating agent. Recently, some of us showed that HOO^\bullet could reduce phenoxyl radical to their parent phenol because of the extremely low Bond Dissociation Enthalpy (BDE) [45], which is lower than the O-H BDE of phenolic antioxidants (typically 77 to 82 kcal/mol) [41]. And its interesting role in autoxidation inhibition system will be discussed in this chapter.

2.3.1 Highlights on the generation of $\text{HOO}^\bullet / \text{O}_2^{\bullet-}$

Superoxide radicals exist widely in aerobic systems and are produced in enzymatic and non-enzymatic oxidation processes in biological systems, such as Mitochondrial

Table 2.2. The main $\text{O}_2^{\bullet-}$ formation paths in biological processes

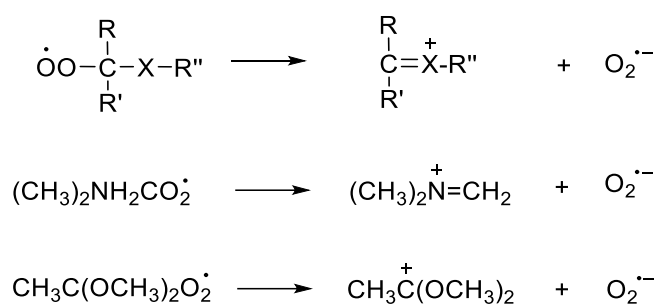
Process	reference
Mitochondrial respiratory chain	[46]
Microsomal oxygenation	[47]
Photosynthetic oxygen reduction	[48]
Enzyme: xanthine oxidase	[49]
NADPH-dependent oxygen reduction by granulocytes and Macrophages	[50]

respiratory chain, NADPH-dependent oxygen reduction, etc. (Table 2.2).

A comprehensive review about superoxide generation in biological system is available in the literature [51], here highlight is made on small compounds which are capable to undergo redox reactions with molecular oxygen to generate superoxide ($\text{O}_2^{\bullet-}$).

Peroxy radicals with heteroatom substitutes to α -carbon

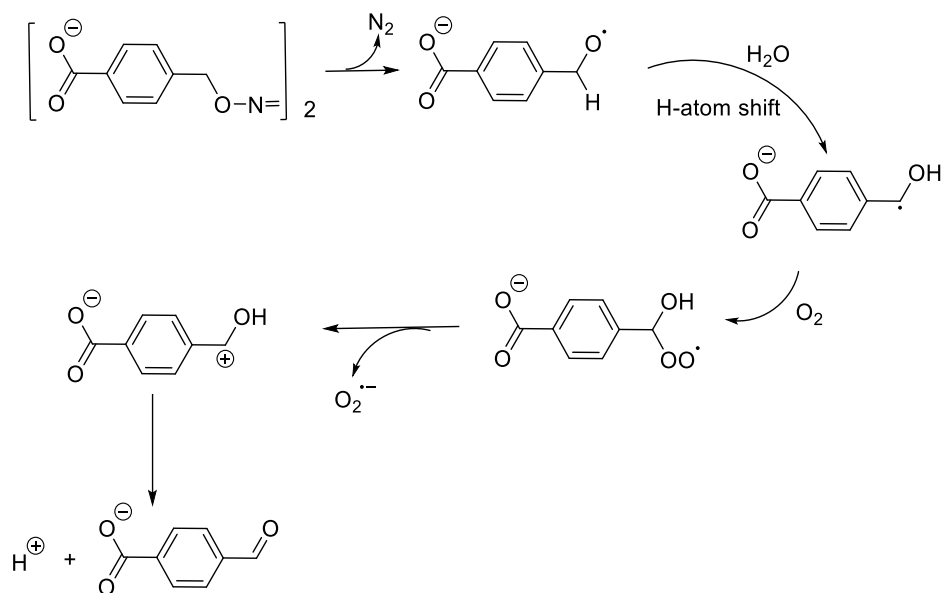
Some peroxy radicals able to eliminate $O_2^{\cdot-}$, due to the stabilization of the formed carbocations by heteroatom substituent X (scheme 2.1), such as 4-morpholinepropanesulfonic acid (MOPS), 4-(2-hydroxyethyl)piperazine-1-ethanesulfonic acid (HEPES) [52] and trimethylamine [53]. Also acetaldehyde dimethyl acetal in dilute aqueous solution was oxidized by HO^{\cdot} radicals in the presence of oxygen, to form a similar peroxy radicals, with oxygen atom substitutes to α -carbon, releasing $O_2^{\cdot-}$, rapidly at a rate of $6.5 \times 10^4 s^{-1}$, according to Schuchmann et al. [54].



Scheme 2.1. Elimination of $O_2^{\cdot-}$ by peroxy radicals.

Azo compounds

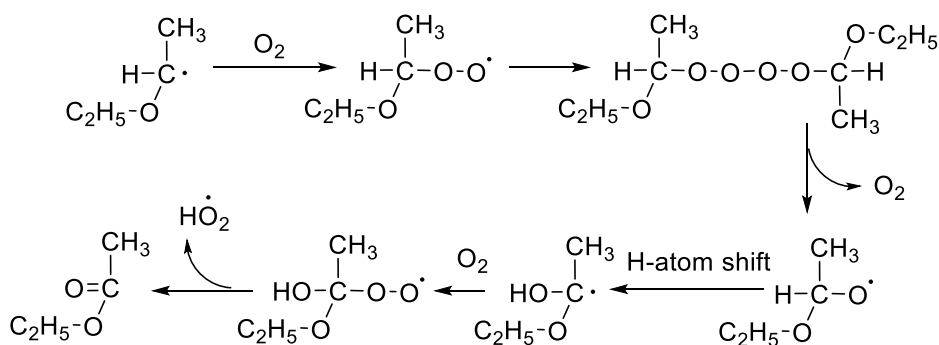
Electron-rich carbon-centered radicals could react with dioxygen to yield the respective carbocations and $O_2^{\cdot-}$. To have an $O_2^{\cdot-}$ supplier which could generate it continuously to satisfy experimental settings to mimic $O_2^{\cdot-}$ *in vivo*, Ingold invented a suitable precursor di-(4-carboxybenzyl)hyponitrite, an azo-compound, which could thermally decompose, and generate $O_2^{\cdot-}$ at a well-defined rate, where the 1,2-H-atom shift was the critical step in the overall reaction to eliminate $O_2^{\cdot-}$ (Scheme 2.2) [55,56].



Scheme 2.2. Thermal decomposition of di-(4-carboxybenzyl) hyponitrite to generate $\text{O}_2^{\bullet -}$

Bimolecular decay of some peroxy radicals

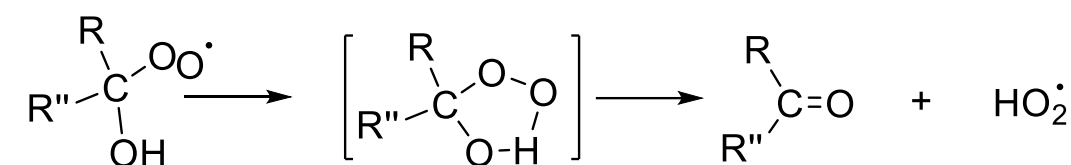
The key intermediate step in such a process was the bimolecular decay of peroxy radicals, which was proposed also involved into the HOO^\bullet elimination mechanism of diethyl ether (scheme 2.3), besides, the 1,2-H shift reaction mentioned above was also important here. Basically, two 1-ethoxyethylperoxy radical, derived from diethyl ether, were found to combine following with the oxygen release and forming a respective oxyl radicals. The oxyl radical subsequently formed a corresponding peroxy radical by adding oxygen. This peroxy radical after a 1,2-H shift reaction, could eliminate HOO^\bullet quickly and spontaneously, yielding ethyl acetate [57].



Scheme 2.3. HOO^\bullet elimination mechanism of diethyl ether.

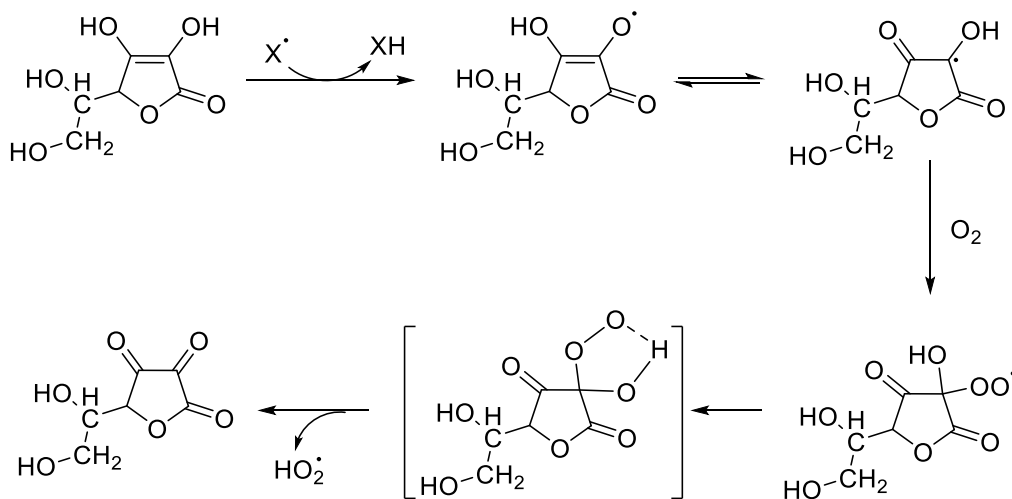
α -hydroxy alkylperoxyl radicals

In addition, α -hydroxy alkylperoxyl radicals resulting from the oxidation of aliphatic compounds in aqueous solution could eliminate $\text{HOO}\cdot$ spontaneously (scheme 2.4), which could also be accelerated by a base. It was proposed that a five-membered transition state is involved in this process. And elimination rate constant increases with increasing methyl substitution in α -position, for example: $k(\text{CH}_2(\text{OH})\text{O}_2\cdot) < 10 \text{ s}^{-1}$; $k(\text{CH}_3\text{CH}(\text{OH})\text{O}_2\cdot) = 52 \text{ s}^{-1}$; $k((\text{CH}_3)_2\text{C}(\text{OH})\text{O}_2\cdot) = 665 \text{ s}^{-1}$. The differences of the elimination rates might be due to the stability of newly formed carbonyl ($>\text{C}=\text{O}$), which is influenced by the interaction with the substituent alkyl groups. [58,59].



Scheme 2.4. $\text{HOO}\cdot$ elimination from α -hydroxy alkylperoxyl radicals.

This reaction involving a five-membered transition might also include the formation of $\text{O}_2\cdot^-$ from vitamin C. Ascorbyl radical formed by extraction of hydrogen atoms from ascorbic acid by free metal or peroxyl radicals could react with oxygen. The oxi-adduct (peroxyl radical) formed could eliminate $\text{HOO}\cdot$, yielding the respective stable dehydroascorbic acid (scheme 2.5) [60-62].

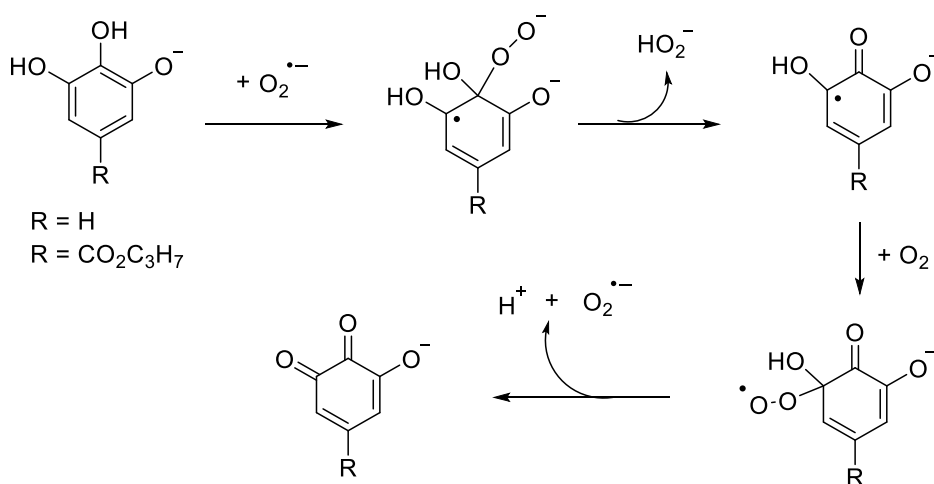


Scheme 2.5. $\text{HOO}\cdot$ generation during the oxidation of vitamin C.

Phenolic antioxidants

Phenolic antioxidants such as pyrogallol are well known to autoxidize rapidly in alkaline solution [63-64], and pyrogallol was used as a $O_2^{\bullet-}$ source to study the activity of enzyme dismutase [65]. It was reported that $O_2^{\bullet-}$ could add to pyrogallol and to the propyl ester of gallic acid relatively rapidly with a rate constant of $k = 3.4 \times 10^5$ and $2.6 \times 10^5 \text{ M}^{-1}\text{S}^{-1}$, respectively, in aqueous alkaline solution [66]. The adduct radical could eliminate HO_2^- following the oxidation to an α -hydroxy peroxy radical, which then eliminates $O_2^{\bullet-}$ and H^+ (HOO^{\bullet}), to propagate the oxidation of pyrogallol by forming a quinone product (scheme 2.6). However, phenolic compounds with two OH groups, such as catechol, react at quite lower rate with $O_2^{\bullet-}$ ($8 \times 10^{-4} \text{ M}^{-1}\text{s}^{-1}$) than pyrogallol through a similar mechanism [66].

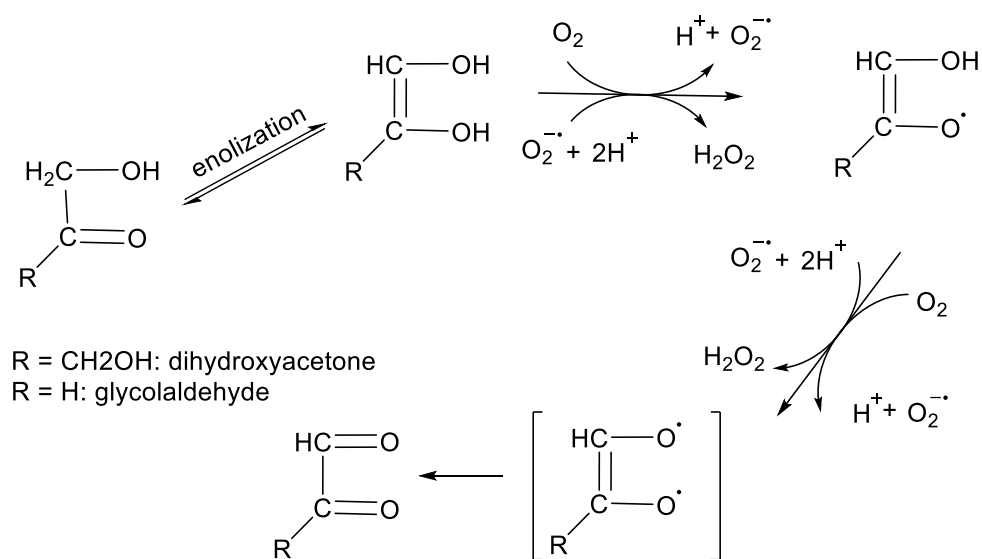
In addition, Mióle et al. proposed that HO^{\bullet} radicals, generated by pulse radiolysis, could add to the simplest phenol rapidly, at a rate of $1.4 \times 10^{10} \text{ M}^{-1}\text{s}^{-1}$ in neutral aqueous solution (pH 7.2 to 6.8), forming a related-radical which then adducts with oxygen to form peroxyhydroxy cyclohexadienyl $^{\bullet}O_2C_6H_5O-H(OH)$ radicals. Radicals $^{\bullet}O_2C_6H_5O-H(OH)$ decompose at a rate constant of $(8.0 \pm 1.0) \times 10^3 \text{ s}^{-1}$ to form $HOO^{\bullet}/O_2^{\bullet-}$ [67].



Scheme 2.6. $O_2^{\bullet-} / HOO^{\bullet}$ propagated oxidation of pyrogallol or the propyl ester of gallic acid.

Carbohydrates, such as simple sugars like D-glucose

Mashino et al. [68] studied the oxidation of dihydroxyacetone initiated by $O_2^{\bullet -}$ provided from the xanthine oxidase reaction in aqueous solution (pH 7.8). It was proposed that simple sugars which are able to tautomerize to enediols might be oxidized by $O_2^{\bullet -}$, involved both in the initiation and in the propagation steps. The mechanism was depicted as in scheme 2.7. The similar oxidation of α , β -dicarbonyl compounds, such as glycolaldehyde was also studied by Okado-Matsumoto and Fridovich. [69]



Scheme 2.7. Oxidation of simple sugar.

D-glucose, the most abundant monosaccharide, was also reported to be able to generate $O_2^{\bullet -}$ due to metal-mediated oxidation in cells [70]. The free radical induced oxidation of D-glucose, in neutral aqueous solution was also studied by Von Sonntag's group. [71,72]. Six peroxy radicals (figure 2.2) derived from D-glucose subjected to flash photolysis in oxygenated aqueous solutions of H_2O_2 (pH 5.5), were able to eliminate HOO^{\bullet} at different rates, where the fastest one was C1-peroxy radical ($k > 7000s^{-1}$, in agreement with the HOO^{\bullet} elimination rate of ethers), and the slowest one was the C5-peroxy radical.

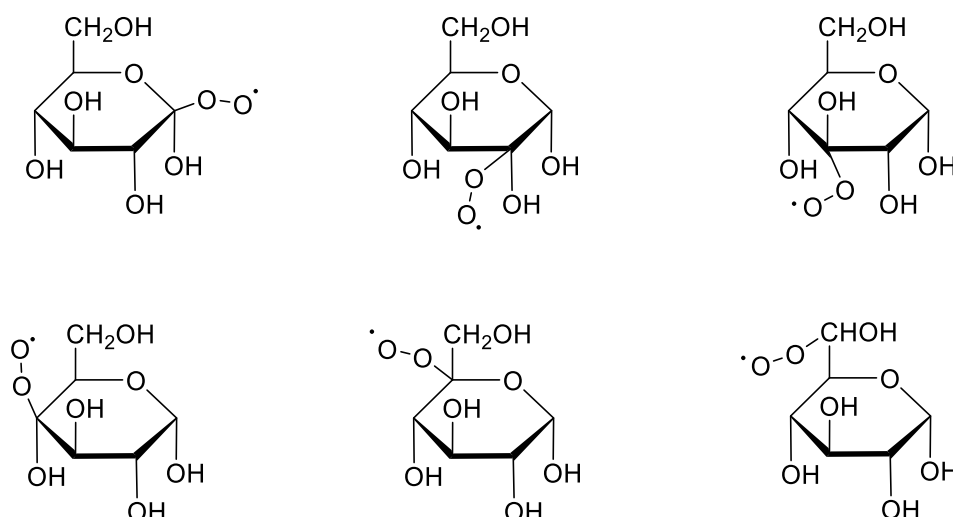
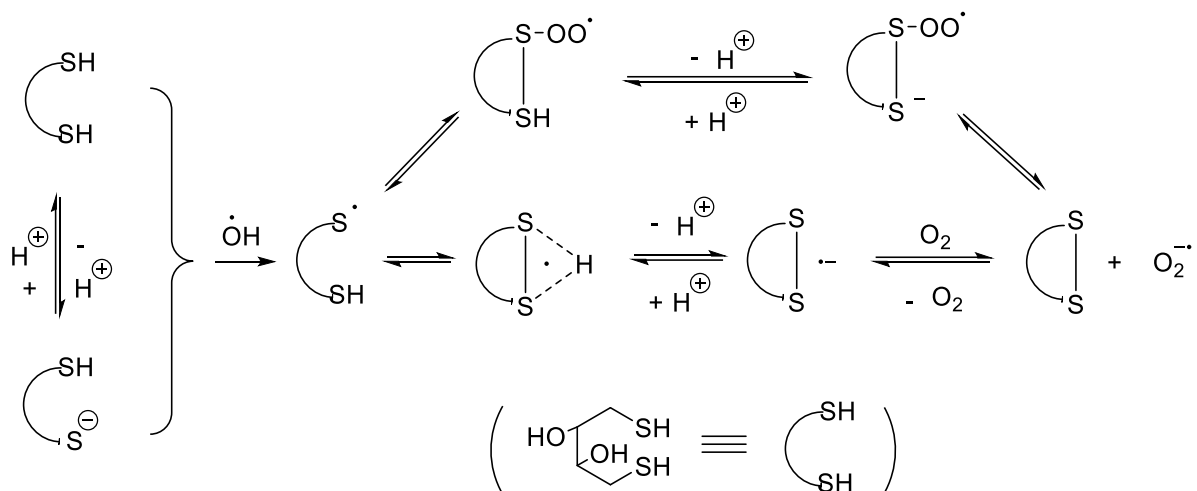


Figure 2.2. Peroxyl radicals of D-glucose.

Some biomolecules such as glycine [73], glycine anhydride, alanine anhydride [74-77] and pteridines [78] were reported to be able to eliminate $O_2^{\bullet-}$ by forming a C=N double bond during their oxidation.

Thiolate ions

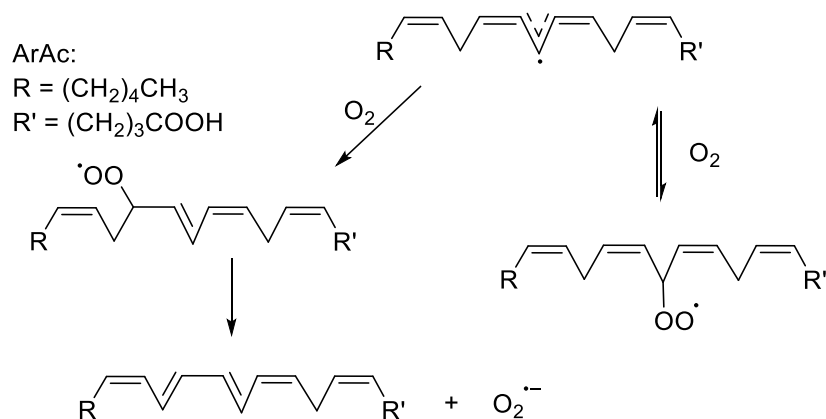
Nan Zhang proposed that the reaction of oxidation of thiolate ions RS^- to disulfide and water was a chain reaction propagated by $O_2^{\bullet-}$, and studied it by the example of compound 1,4-dithiothreitol (DTT) [79]. Basically, in aqueous solutions under pH 8.7, HO^\bullet radical, generated by the radiolysis, abstracts hydrogen from DTT forming DTT-H radical, which further forms a disulfide radical anion by cyclizing and deprotonating. This disulfide radical anion reacts with O_2 rapidly, ($k = 7.1 \times 10^8 \text{ M}^{-1}\text{s}^{-1}$), generating disulfide and $O_2^{\bullet-}$, which in turn could add to the thiolate ions RS^- , forming a radical complex based on the typical three-electron bond of sulfur radicals, which was proposed as the initial step of radical chain reaction. The radical complex then protonates rapidly, giving a sulfinyl radical by decomposition. This sulfinyl radical reacts with thiolate ions RS^- , forming a DTT-H radical, and then occurrence of a chain reaction forms new $O_2^{\bullet-}$ (Scheme 2.8).



Scheme 2.8. Proposed mechanism of the chain oxidation of 1,4-dithiothreitol propagated by $\text{O}_2^{\bullet-}$.

Lipids

As discussed in chapter 1, polyunsaturated fatty acids (PUFA) and esters are easily attacked by radicals forming the corresponding C-centered radicals, which could react with oxygen rapidly and then progress to radical-chain autoxidation. It was found that during the oxidation of arachidonic acid (ArAc) and linoleic acid (LnAc), C-centered radicals formed include 80% nonconjugated R_n^{\bullet} and ~20% conjugated bis-allylic R_{ba}^{\bullet} radicals. Moreover, the R_n^{\bullet} radicals of ArAc could transfer to bis-allylic R_{ba}^{\bullet} radicals rapidly with a rate constant of $7.5 \times 10^4 \text{ s}^{-1}$ via intramolecular H-atom transfer. The ArAc peroxy radicals formed from the conjugated bis-allylic R_{ba}^{\bullet} radicals with oxygen could eliminate superoxide radical anions spontaneously with a rate constant of $3.4 \times 10^4 \text{ M}^{-1}\text{s}^{-1}$ [80].

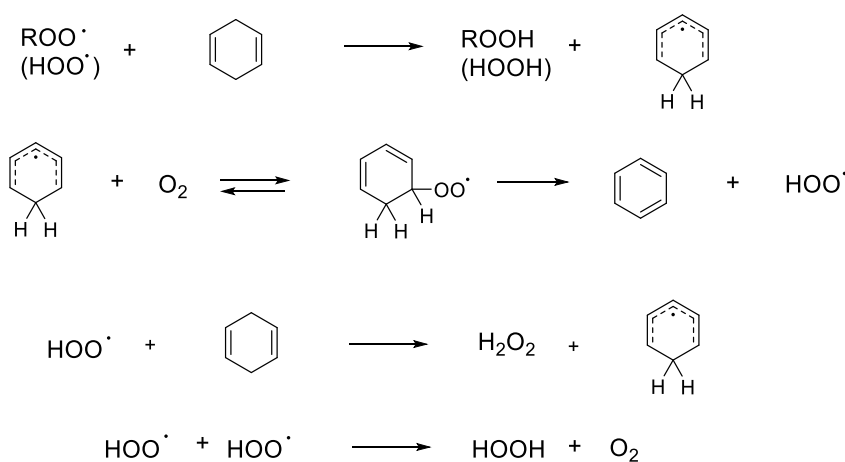


Scheme 2.9. Proposed mechanism for the formation of peroxy radicals and $\text{O}_2^{\bullet-}$ from beta-hydroxyalkyl and bis-allylic radicals produced by the one-electron oxidation of ArAc, respectively.

During our research, squalene, a molecule that possesses three terpene units, was found able to eliminate HOO^\bullet in organic solvents, the mechanism might be the similar $\text{R}_{\text{ba}}^\bullet$ radicals formed during the oxidation of PUFA. Besides, the short chain of alkenes such as ethylene and 1-3-butadienes were also proposed to generate HOO^\bullet during their oxidation [81].

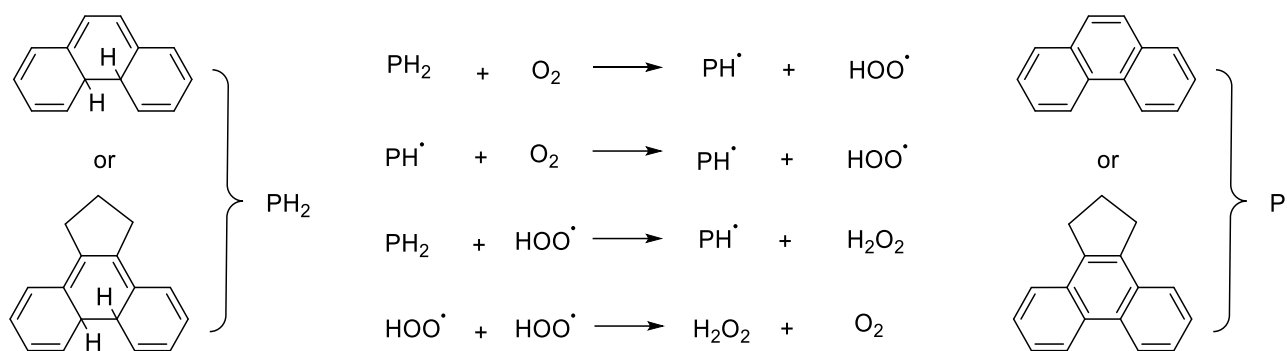
Oxidation of cycloalkenes to aromatic compounds

The formation of HOO^\bullet from cyclohexadienyl peroxy radicals is well known [82,28] and cyclohexadiene (CHD) was used as HOO^\bullet source in the subsequent research in this chapter. The autoxidation scheme of cyclohexadiene is summarized below (scheme 2.10): it is shown that the five-membered transition state previously mentioned might also be involved in the formation of HOO^\bullet from cyclohexadienyl peroxy radicals, but the driving force in this case is the conjugation energy of the aromatic products.



Scheme 2.10. Mechanism of HOO^\bullet generation from cyclohexadiene (CHD).

A similar occurrence was also found in the oxidation of 4a,4b-dihydrophenanthrenes and its derivatives like 9,10-cyclopentano-4a,4b-dihydrophenanthrene; the mechanism shown in Scheme 2.11 was proposed by K. A. Muszkat's group [83,84].

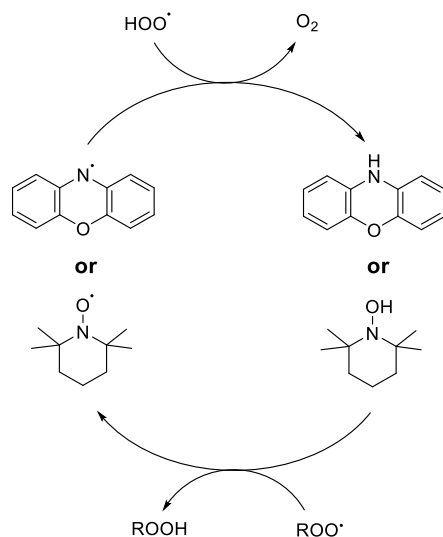


Scheme 2.11. Oxidation mechanism of 4a,4b-dihydrophenanthrenes or its derivatives like 9,10-cyclopentano-4a,4b-dihydrophenanthrene.

2.3.2 Specificity and properties of $\text{HOO}^\cdot / \text{O}_2^{\cdot-}$ pair

Generally, superoxide is considered the primary reactive oxygen species (ROS) and precursor of many other ROS, thus it is certainly regarded as an oxidant species, also due to its high generation during a large number of enzymatic and nonenzymatic oxidations. However, superoxide can also act as a reducing agent since the redox potential $E_0(\text{O}_2/\text{O}_2^{\cdot-})$, the standard potential of the reaction $\text{O}_2 + e^- \rightarrow \text{O}_2^{\cdot-}$ relative to the standard hydrogen electrode (SHE), is -0.33V [85], meaning that $\text{O}_2^{\cdot-}$ tends to release electrons. Besides, its protonated form HOO^\cdot was reported by our group as being both oxidant and reductant, due to the low BDE value of its H-OO^\cdot bond. For instance, nitroxides were found to become extremely effective (and catalytic) radical-trapping antioxidants during the oxidation of styrene in organic solvent when HOO^\cdot sources were present (e.g. cyclohexadienes, triethylamine, 1,4-hydroquinones or benzyl alcohol), and the inhibition mechanism was proposed as due to the involvement of the HOO^\cdot radicals formed during the autoxidation – i.e. formed on co-oxidizing cyclohexadienes, trimethylamine, etc with the substrate – where HOO^\cdot radicals operate the reduction of the nitroxide to the parent hydroxylamine (reaction at diffusion controlled rate, $k = 1.1 \times 10^9 \text{ M}^{-1}\text{s}^{-1}$), thus forming a catalytic antioxidant cycle (Scheme 2.12) [86]. This reaction and the H-donating property of HOO^\cdot are particularly interesting. Recently, Pratt's group also studied the regeneration of the diarylamine phenoxazine from their corresponding aminyl radicals by HOO^\cdot in liposomes model

(Scheme 2.12), and the mechanism was proposed as an H-atom transfer directly from $\text{HOO}\cdot$, or an electron transfer from $\text{O}_2^{\cdot-}$ followed by (or concerted with) a protonation [87], thereby paralleling the mechanism we identified for nitroxides.



Scheme 2.12. Mechanisms of co-antioxidant activity of TEMPO or diarylamine phenoxazine with $\text{HOO}\cdot$.

The reductive properties of $\text{HOO}\cdot$ are quite interesting, since its deprotonated form is abundantly produced in biological system, and it is usually quenched by SOD (Superoxide Dismutase) *in vivo*, and $\text{HOO}\cdot$ was considered as membrane lipid oxidation inducer. Thus, research on its comprehensive role in biological system should be conducted as soon as possible.

2.4 Research objectives

Taking the $\text{HOO}\cdot$ specificity in mind, the research objectives of this chapter were the exploration of the possible synergism of $\text{HOO}\cdot$ with phenols, polyphenols and related phenol-based melanin-like polymers. Phenols and polyphenols are prototypical chain-breaking antioxidants and are used for the preservation of most man-made materials incusing processed food products. On the other hand, they are also naturally contained in so-called healthy foods and dietary intake is considered and important part of physiological antioxidant defenses. Phenols and polyphenols also undergo spontaneous

or enzyme (*e.g.* tyrosinase) catalyzed oxidation to quinoid structures followed by oligomerization or polymerization to afford a variety of tannins and melanin-like polymers, which occurs in fruits and vegetables as well as in animal tissues, and, in all cases, they have been reported to have protective functions, including protection from ROS. Nonetheless, it remains largely unclear why oxidized products arising from polyphenols should have antioxidant properties or why eating fruits containing flavonoids should remain healthy even after they have been, for most part, oxidized by air on storage. Melanins and allomelanins have recently received major attention from the scientific community for their possible role as antioxidants, among others, and new possible applications are being proposed every day. On the other hand, the mechanistic basis is largely unclear, particularly upon consideration that the polyphenolic monomers undergo polymerization to melanins upon their oxidation, hence a modest reducing ability is left on the polymer.

Our hypothesis was that there might be a unifying mechanism that justifies the purported beneficial and antioxidant properties of oxidized phenols and their derivatives, which involves the intermediation of the $\text{HOO}^\bullet / \text{O}_2^{\bullet-}$ system. In other words, our hypothesis was that HOO^\bullet could have a synergic co-antioxidant role with phenols, polyphenols and melanin-like polymers, and this could be exploited rationally to build new antioxidant strategies, or it could explain the antioxidant properties of melanins. We therefore undertook two investigations, specifically aimed at addressing the occurrence, kinetics and mechanism of such a synergic interplay. Its application in food protection and in helping explain the biological role of melanins will be specifically addressed in the following sections of this chapter.

2.5 Synergic Antioxidant Activity of γ -Terpinene with Phenols and Polyphenols

(published in Food Chemistry 2020 as DOI: 10.1016/j.foodchem.2020.128468)

Plant essential oils have been shown to possess a wealth of biological effects, which have often been associated to a purported antioxidant activity [88]. Hundreds of them are classified as Generally Recognized as Safe (GRAS) by the US Food and Drug

Administration and are also studied as potential alternatives to synthetic antioxidants in the food industry [89]. Their antioxidant activities clearly depend on their composition, particularly on the concentration of phenolic components, which have chain-breaking antioxidant activity [18]. On the other hand, recent work from our group has demonstrated that also some non-phenolic components of essential oils can have antioxidant behavior, albeit with different mechanisms, which we helped clarify. [90]

Among such non-phenolic components, γ -terpinene, a pre-aromatic terpene, is widely present in essential oils of many medicinal and aromatic plants, like citrus [91], savory, thyme [92], juniperus, oregano [93], and others. It has been reported to possess not only anti-inflammatory but also antioxidant activity [94]. The antioxidant mechanism of γ -terpinene was first clarified by Foti and Ingold [95]. However, little is known on the possible interplay of the antioxidant activity of γ -terpinene with that of phenolic antioxidants, be them found in the same plant or added to food products to aid their preservation.

Phenolic compounds, including many flavonoids, are abundant in plants [96]. They possess ideal structure as antioxidants and are well-known to inhibit or stop the autoxidation of lipids [97]. Although phenolic antioxidants at a low concentration can provide an effective protection to lipids, they do not work perfectly for long-term protection [98]. Interestingly, research in food preservation has shown that essential oils can extend the shelf life of polyphenols-rich food like berries and that they reduce the decay on storage of naturally contained flavonoids [99]. This apparently suggests a cooperative effect among phenolic antioxidants and essential oils components, although the mechanism is not clarified in its molecular basis. Synergism among antioxidants is certainly one of the most prominent strategies in modern antioxidant research [100-102], besides being the primary strategy set up by nature [103].

With those thoughts in mind, our hypothesis was that there might be synergic antioxidant effect between γ -terpinene and phenolic antioxidants. The present investigation aims to provide an insight into the occurrence and mechanism of such a

synergic effect, and its potential application in food chemistry. α -Tocopherol is perhaps the most important lipid-soluble phenolic antioxidant in nature [103], hence we chose its close mimic PMHC (2,2,5,7,8-pentamethyl-6-chromanol), **1H**, as a model monophenolic antioxidant in our investigation, since it has identical core structure and reactivity compared to the natural counterpart (it differs only by truncation of the lipophilic tail, Fig. 2.3) and can be obtained in high purity [104]. Caffeic acid is ubiquitous in plants [105] and it is a very effective catechol-type antioxidant [106,107], which was chosen as the model structure for polyphenols. Its lipophilic phenetyl ester CAPE (**2H₂**) was selected in our experiments to study the antioxidant interaction of polyphenols with γ -terpinene (Fig. 2.3).

In the present work, we studied the behaviour of monophenolic **1H** and polyphenolic **2H₂** combined with γ -terpinene in the inhibition of the autoxidation of sunflower oil and squalene by differential oximetry. This is a direct method for monitoring the kinetics of oxygen consumption during the inhibited autoxidation of a reference substrate, which we have duly discussed in Chapter 1 and that was demonstrated to be the golden standard in antioxidant testing [108,109,18]. The choice of sunflower oil and squalene as model oxidizable substrates was based on their importance as dietary lipids and on their structural differences (see Fig. 2.3), so to comprise the variability encountered in food products. Sunflower oil is a prototypical natural oxidizable dietary lipid, due to its modest price, high availability in the food industry and facile oxidation [110,111]. Squalene, a triterpenic polyunsaturated hydrocarbon which has attracted a lot of research interest because of its benefit to human health, was chosen as another natural lipidic oxidizable substrate in this study. It is ubiquitous in plants and abundant in vegetable oils [104], it is present also in all animals and in humans, being the precursor of sterols including cholesterol. Moreover, it is used as a diet supplement due to its numerous beneficial properties [112].

The choice was also based on the necessity to use substrates/systems whose autoxidation kinetics is well behaved and accurately calibrated, so to allow quantitative measurements and achieve (hopefully) clear mechanistic insights [104]. We have

previously calibrated the autoxidation kinetics (see Chapter 1), so they appeared as the ideal oxidizable substrates. To prove that results are of general relevance and are not dependent on the substrate, we extended the investigation to styrene, since it is the best-known reference oxidizable substrate in antioxidant testing [100,109]. In order to rationalize the mechanism of antioxidant interaction between γ -terpinene and polyphenolic antioxidants we also performed experiments with well-established 3,5-di-*tert*-butylcatechol (DTBC, **3H₂**) and its oxidized product 3,5-di-*tert*-butyl-*o*-benzoquinone (DTBQ, **3**) as a model catechol/quinone redox couple [113]. Finally, to assess the relevance of our results in real food products we investigated the autoxidation of sunflower oil inhibited by natural vitamin E (*d*- α -tocopherol) and hydroxytyrosol from olive in the presence and absence of γ -terpinene.

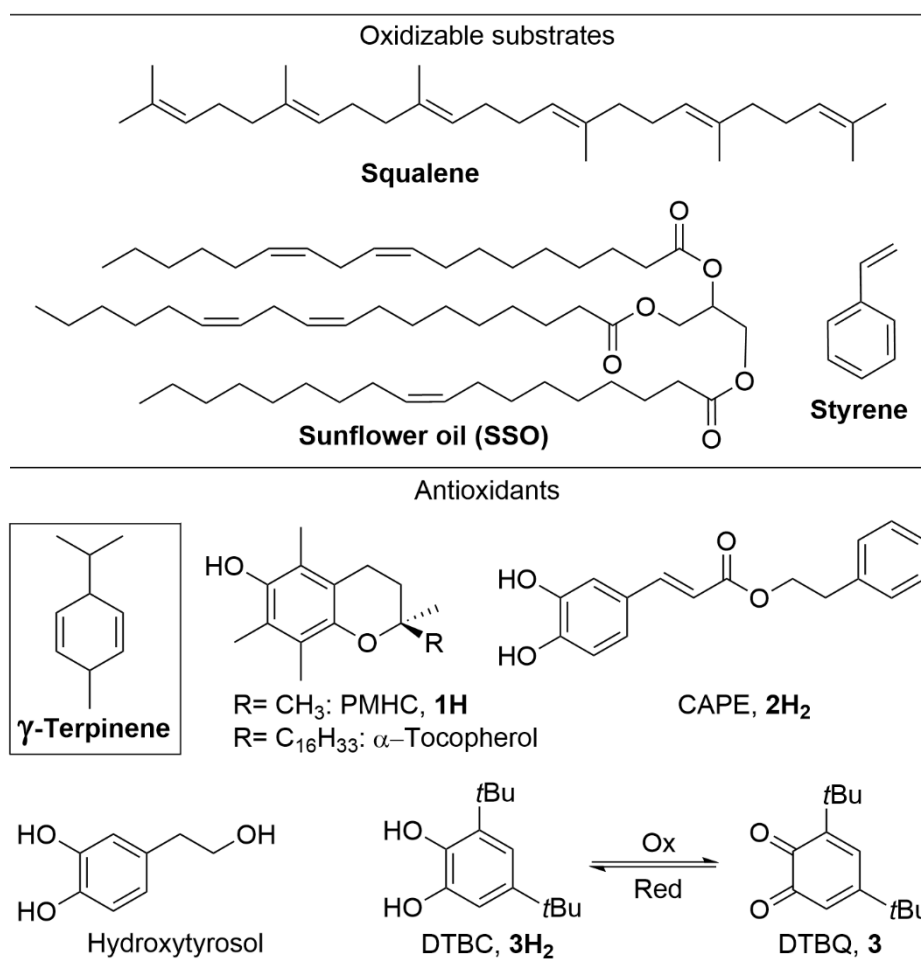


Figure 2. 3. Oxidizable substrates and antioxidants investigated in this study

2.5.1 Inhibition of the autoxidation of natural lipids by phenolic antioxidants with γ -terpinene

Stripped sunflower oil (SSO) was obtained from food-grade commercial sunflower oil by removing natural phenolic components and carotenoids that would impair its oxidation, as described in Chapter 1.

Squalene, from olive oil unsaponifiable fraction, was used after percolation on activated alumina and on silica to remove traces of hydroperoxides, which would affect its rate of peroxidation, as also described in Chapter 1.

The antioxidant behavior of γ -terpinene was investigated in the controlled autoxidation of both SSO and squalene. The analogue of α -tocopherol PMHC (**1H**), and the lipid-soluble phenethyl ester derivative of caffeic acid (CAPE, **2H₂**) were also used as antioxidants in matched experiments with the same lipid substrates. Results summarized in Fig. 2.4 showed that γ -terpinene alone, in the millimolar range, could only slow down the lipid autoxidation by a modest margin, while, as expected, the mono- and poly-phenolic antioxidants (**1H** and **2H₂**) showed neat inhibition of the autoxidation already at micromolar concentrations. Most interesting, when γ -terpinene and each of the phenolic antioxidants were used together in the protection of either SSO or squalene, the antioxidant activity toward both lipids was greatly enhanced as compared to the use of **1H** or **2H₂** alone, being clearly higher than the sum of the contributions of each phenolic antioxidant and γ -terpinene, *i.e.* the combination showed clear synergic antioxidant effect.

In oxygen-uptake kinetics during autoxidation, when a clear inhibited period is observed as in Fig. 2.4 (A,C,D), the slope on the inhibited period is inversely related to the rate constant for peroxy radical trapping by the antioxidant (see equation 20 in experimental section), while its duration (τ) depends on the concentration of the antioxidant and the stoichiometric factor n , *i.e.* the number of radicals trapped by each molecule of antioxidant according to equation 21 in experimental section. An inspection of Fig. 2.4 shows that while γ -terpinene produced no neat inhibition period, and both **1H** or **2H₂** did so, the combination of either **1H** or **2H₂** with γ -terpinene did

not significantly change the slope of the inhibited period as compared to that produced by each of the phenols alone, but it extended its duration in a dose-dependent fashion (see inserts in Figure 2.4 A-D). This kinetic behavior would indicate, that γ -terpinene acts as the co-antioxidant which regenerates the main antioxidant, **1H** or **2H₂**, as it is consumed during the autoxidation, similarly to the behaviour previously observed and discussed for other co-antioxidant couples [114, 102].

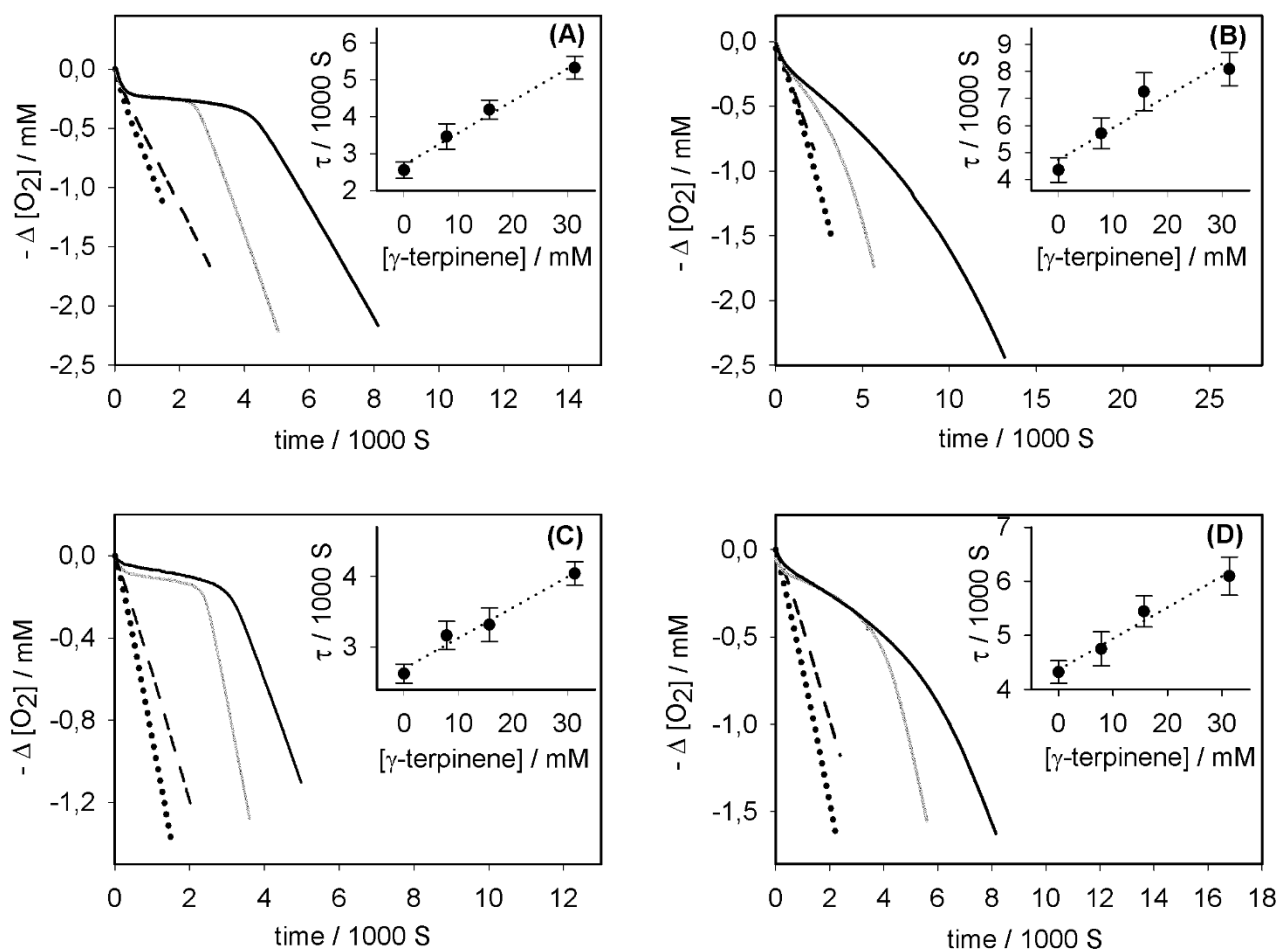


Figure 2. 4. Oxygen consumption during the autoxidation of SSO (A-B), and squalene (C-D). Each panel displays the curves recorded for the autoxidation of the substrates without inhibitors (dotted lines), and in the presence of 15.65 mM γ -terpinene (dashed lines). In panels A and C grey plots represent the inhibition by PMHC **1H** (2.5 μM) alone, while black curves represent inhibition by the mixture of **1H** (2.5 μM) with γ -terpinene (15.65 mM). In panels B and D grey plots represent inhibition by CAPE **2H₂** (2.5 μM) alone, and black curves inhibition by the mixture of **2H₂** (2.5 μM) with γ -terpinene (15.65 mM). Inserts: plots of the experimental inhibition periods τ vs the concentration γ -terpinene for different mixtures **1H** or **2H₂** (2.5 μM) / γ -terpinene.

Such a synergic antioxidant behavior was observed both with SSO and squalene as the oxidizable substrates, despite the structural differences, indicating that the

synergy between γ -terpinene and phenols might be a general property, not related to the oxidizing substrate. To confirm this hypothesis, we further investigated the synergy in the autoxidation of styrene initiated by AIBN. Indeed, styrene is by far the best-known reference oxidizable substrate to test antioxidants [100,109,18] and its clearly defined rate constants for chain propagation ($k_p = 41 \text{ M}^{-1}\text{s}^{-1}$ at 30°C) and chain termination ($2k_t = 4.2 \times 10^7 \text{ M}^{-1}\text{s}^{-1}$ at 30°C) allow quantitative evaluation of synergy, as well as representing a robust model to achieve mechanistic understanding [115].

Results were qualitatively superimposable to those obtained with SSO and squalene as the oxidizable substrates (Fig. 2.5). From the oxygen-uptake plots, the apparent n value of the mixtures was calculated according to equation 21 in experimental section, where R_i is the rate of radical initiation produced by AIBN.0

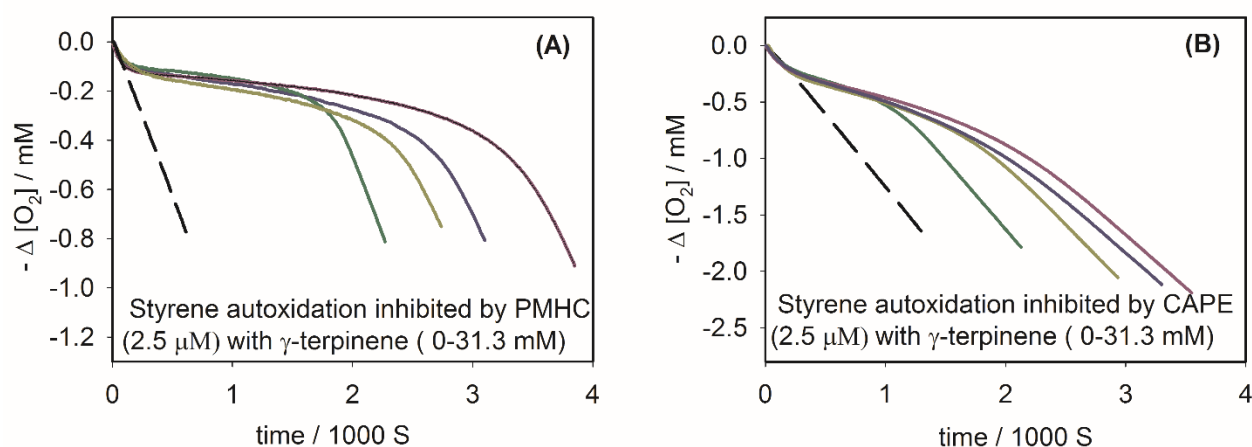


Figure 2.5. Oxygen consumption measured during the autoxidation of styrene initiated by 0.025 M AIBN at 30°C in the absence of antioxidant (dashed line in both panels), and inhibited by (A) PMHC **1H** ($2.5\mu\text{M}$) in the absence of γ -terpinene (green line), in the presence of γ -terpinene (7.83mM -yellow line; 15.7mM -blue line; 31.3mM -purple line), or by (B) CAPE **2H₂** ($2.5\mu\text{M}$) alone (green line) or in the presence of growing amounts of γ -terpinene (the same color coding as in panel A is used).

According to the well-known chain-breaking antioxidant mechanism, each molecule of phenol or catechol inactivates two ROO^\bullet (see reaction 18, 19 in experimental section). Hence, the stoichiometric factors of both **1H** and **2H₂**, have the theoretical value $n = 2$. The apparent n value obtained for the phenolic antioxidants when mixed with different amounts of γ -terpinene, shown in table 2.3, were always larger than 2, and increased with the concentration of γ -terpinene. Moreover, there was no major

difference between the rate of oxygen consumption recorded in the presence or absence of γ -terpinene, hence both for **1H** and **2H₂** the apparent rate constants for inhibition k_{inh} (calculated from equation 20 in experimental section) was not significantly different in the presence/absence of γ -terpinene (see table 2.3), which supports the role γ -terpinene only as the co-antioxidant, able to afford regeneration of the main phenolic antioxidants, similarly to what was observed using SSO or squalene as the oxidizable substrates. It is worth noting that the rate constant k_{inh} measured here for **1H** is in excellent agreement with previous literature [102], while that determined for **2H₂** is reported for the first time but is in line with that of other catechol-type antioxidants [113], which stands for the reliability of our current kinetic measurements.

Table 2.3. Apparent stoichiometric factors (n) and inhibition rate constant (k_{inh}) of PMHC (**1H**) and CAPE (**2H₂**) when mixed with different amounts of γ -terpinene during the autoxidation of styrene initiated by AIBN at 30°.

Synergic combination	[antiox] (μ M)	[γ -terpinene] (mM)	τ (s)	n^a	$-(d[O_2]/dt)_{inh}^1$ ($M s^{-1}$)	app. k_{inh}^a ($10^5 M^{-1} s^{-1}$)
PMHC/ γ -terpinene	2.5	0	1836	2.0 \pm 0.1	3.1 \times 10 ⁻⁸	31.3 \pm 3.5
		7.83	2372	2.6 \pm 0.2	3.5 \times 10 ⁻⁸	28.1 \pm 4.1
		15.65	2751	3.0 \pm 0.2	3.7 \times 10 ⁻⁸	26.2 \pm 5.8
		31.30	3396	3.7 \pm 0.3	3.0 \times 10 ⁻⁸	32.0 \pm 3.9
CAPE/ γ -terpinene	2.5	0	1150	2.0 \pm 0.1	2.0 \times 10 ⁻⁷	4.8 \pm 1.1
		7.83	1650	2.9 \pm 0.2	1.8 \times 10 ⁻⁷	5.5 \pm 0.9
		15.65	1914	3.3 \pm 0.2	1.8 \times 10 ⁻⁷	5.5 \pm 0.7
		23.48	2022	3.6 \pm 0.3	2.1 \times 10 ⁻⁷	4.5 \pm 1.3

All values are average from at least 3 independent measurements. ^a Errors for n and k_{inh} represent \pm SD.

2.5.2. Exploration of the mechanism behind the synergy

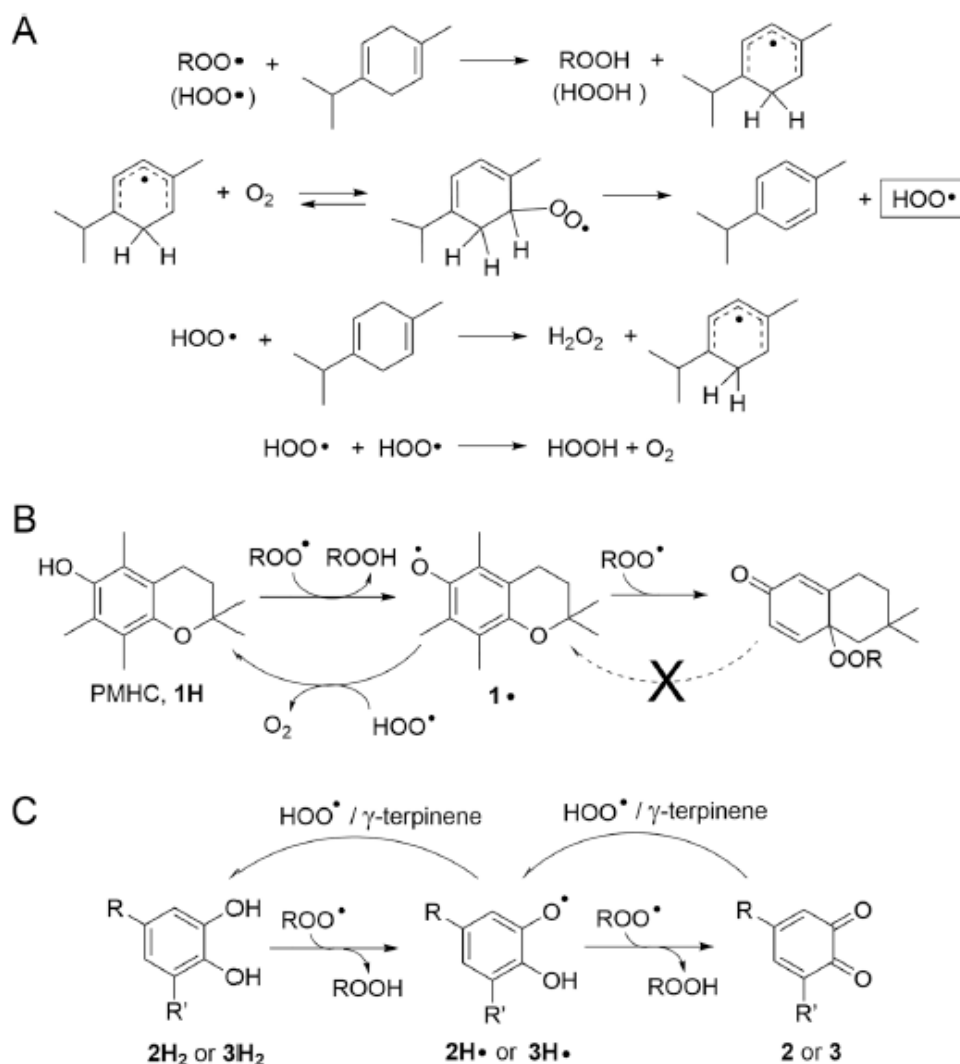
Phenolic antioxidants can retard or block the oxidation of lipids by scavenging chain-carrying peroxy radicals. Both monophenolic antioxidants like α -tocopherol or **1H** and polyphenolic like caffeic acid or **2H₂** have a stoichiometric factor $n = 2$, although they possess different number of active OH groups. The first step of their

antioxidant mechanism is similar: a formal H-atom transfer to a ROO•. The difference is in the second step. For monophenolic antioxidants like **1H**, the phenoxyl radical resulting from the first step will trap a second ROO• by addition to the aromatic ring. Instead, the phenoxyl radical resulting from a catechol is a semiquinone and can donate another hydrogen atom to ROO• to yield the corresponding quinone, as illustrated in scheme 2.13. [113,115].

A synergetic effect between antioxidants based on the regeneration of a more effective antioxidant by a less effective synergist occurs mostly when one antioxidant has a higher reduction potential than the other [114,116,100] or when the radical formed from one antioxidant can be reduced by H-atom transfer from another antioxidant having a weaker X-H bond in the active site [114,115]. A typical example is the long-established synergy between α -tocopherol and ascorbic acid, in which ascorbic acid regenerates α -tocopherol by transferring a hydrogen to α -tocopheroxyl radical [103]. The synergism between α -tocopherol and other co-antioxidants was also investigated [113,114,116,117]. In general, synergism between phenol-type antioxidants was attributed to a similar mechanism in which the fastest antioxidant reacts first with chain-carrying peroxy radicals to yield the corresponding phenoxyl radical that is reduced back by formal H-atom transfer from the co-antioxidant [102].

In this scenario, the synergic contribution of γ -terpinene is less obvious. The antioxidant mechanism of γ -terpinene was disclosed by Foti and Ingold [95] who proposed that the addition of γ -terpinene in the peroxidation of lipids would change the propagation chain-carrier from ROO• to HOO• (hydroperoxyl radical) since γ -terpinene itself is rapidly attacked by ROO• and releases HOO•. Hydroperoxyl radicals, HOO•, can both propagate the oxidation and be quenched by another HOO• or by ROO• (self-termination or cross-termination). Since the self-termination of HOO• and its cross termination with ROO• is much faster than the self-termination of ROO•, the overall termination efficiency would increase in the presence of γ -terpinene, justifying its antioxidant behavior (scheme 2.13 A). This termination-enhancing antioxidant activity

is common to other terpenoids and is expected to bring only limited contribution to the overall antioxidant activity [90].



Scheme 2.13. Mechanism of the antioxidant activity of (A) γ -terpinene alone (after Foti & Ingold, 2003) [95] and of the antioxidant synergy between (B) γ -terpinene and monophenolic antioxidants (using **1H** as model compound) and (C) γ -terpinene and polyphenolic antioxidants (using **2H₂** or **3H₂** as model compound).

The regeneration of the starting phenol from its phenoxyl radical by $\text{HOO}\cdot$ generated from γ -terpinene nicely explains the synergy with monophenols like PMHC **1H** as depicted in scheme 2.13 B; however, in the case of catechols, in principle regeneration could occur both by 1-electron reduction of the semiquinone radical and by (stepwise) 2-electron reduction of the quinone as depicted in scheme 2.13 C. To achieve a better understanding of the regeneration mechanism of phenolic antioxidants by γ -terpinene, matched sets of experiments were conducted by injecting γ -terpinene

into the styrene autoxidation system at the beginning of the experiment and/or after the phenolic antioxidant was consumed, *i.e.* at the time when the substrate starts to oxidize again. PMHC **1H** was again used as the prototype of monophenolic antioxidants, while 2,5-di-*tert*-butyl catechol (DTBC, **3H₂**) was used as model for polyphenols, since it is a better established catechol-type antioxidant [113] and its corresponding quinone (DTBQ, **3**) is also commercially available and stable in solution.

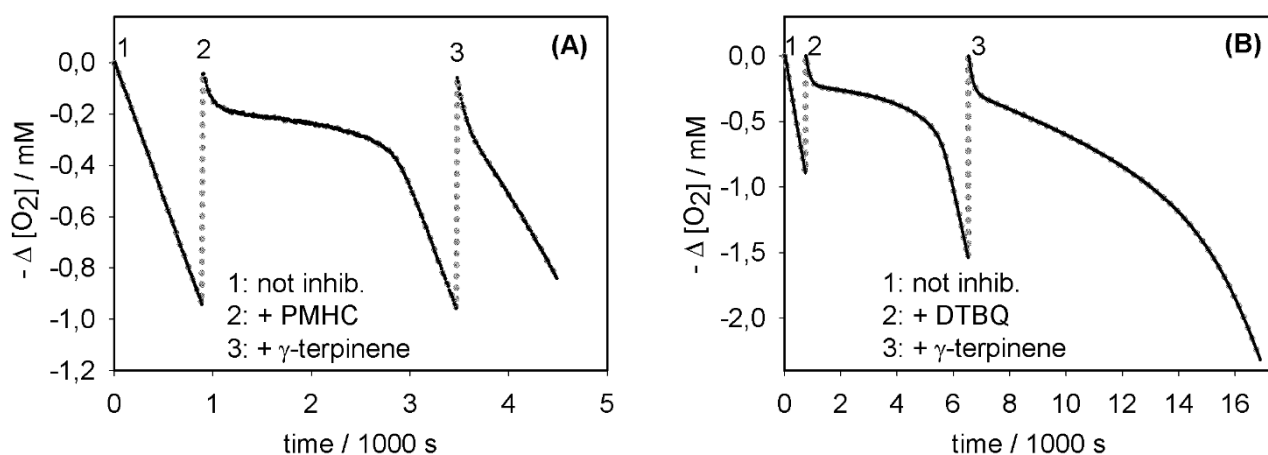


Figure 2.6. Oxygen consumption measured during the autoxidation of styrene initiated by 0.025 M AIBN at 30°C. (A) 1: uninhibited; 2: injection of **1H** (2.5 μM); 3: injection of γ -terpinene (15.7 mM). (B) 1: uninhibited; 2: injection of **3H₂** (7.5 μM); 3: injection of γ -terpinene (15.7 mM).

As shown in Fig. 2.6 A, injecting γ -terpinene into the sample after the inhibition by **1H** had ended, meaning that **1H** had been completely oxidized, could not restart the inhibition; instead if γ -terpinene was injected before **1H**, the subsequent injection of **1H** gave an inhibition period much longer than that observed without prior injection of γ -terpinene (see figure 2.7). This means that the final oxidized products of **1H** could not be regenerated by γ -terpinene, while only the intermediate phenoxyl radical can be efficiently regenerated. This confirms our suggested mechanism depicted in scheme 2.13 B. On the other hand, using the catechol **3H₂** instead of **1H**, injection of γ -terpinene caused the reboot of a new inhibition period when injected after the complete consumption of **3H₂**, *i.e.* when inhibition by **3H₂** had terminated and the autoxidation was running again uninhibited (Fig. 2.6B). This implies that the quinone (**3**) formed as

the final oxidized products of the catechol can be reduced back to the starting antioxidant (see scheme 2.13C).

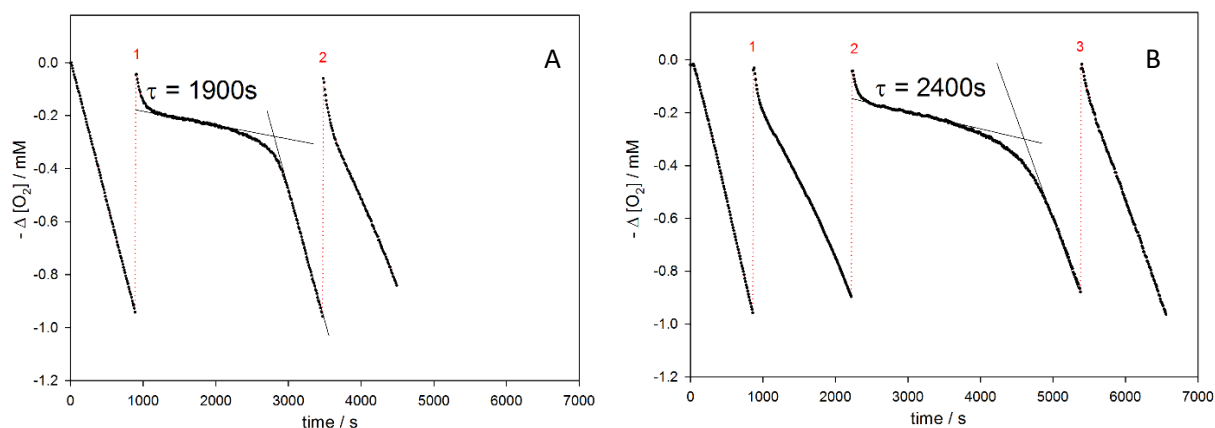


Figure 2.7. Oxygen consumption during the autoxidation of styrene initiated by 0.025 M AIBN at 30° without inhibitors and upon injection of antioxidants at the time points indicated by numbers: (A) 1 = injection of PMHC 1H (2.5 μM), 2 = subsequent injection of γ -terpinene (20 mM); (B) 1 = injection of γ -terpinene (15.7 mM), 2 = subsequent injection of PMHC 1H (2.5 μM), 3 = subsequent injection of γ -terpinene (15.7 mM). Note that inhibition period τ in panel B is larger than in panel A (where it corresponds to $n = 2.1$) despite the identical concentration of injected PMHC.

Quinones are easily formed by the oxidation of related catechols, and they are generally expected to be the main final oxidized product when catechols behave as antioxidants. This was also confirmed in our experimental settings by monitoring the growth of UV absorbance of *ortho*-quinone **3** at 400nm during the autoxidation of styrene inhibited by **3H₂** (Figure 2.8A).

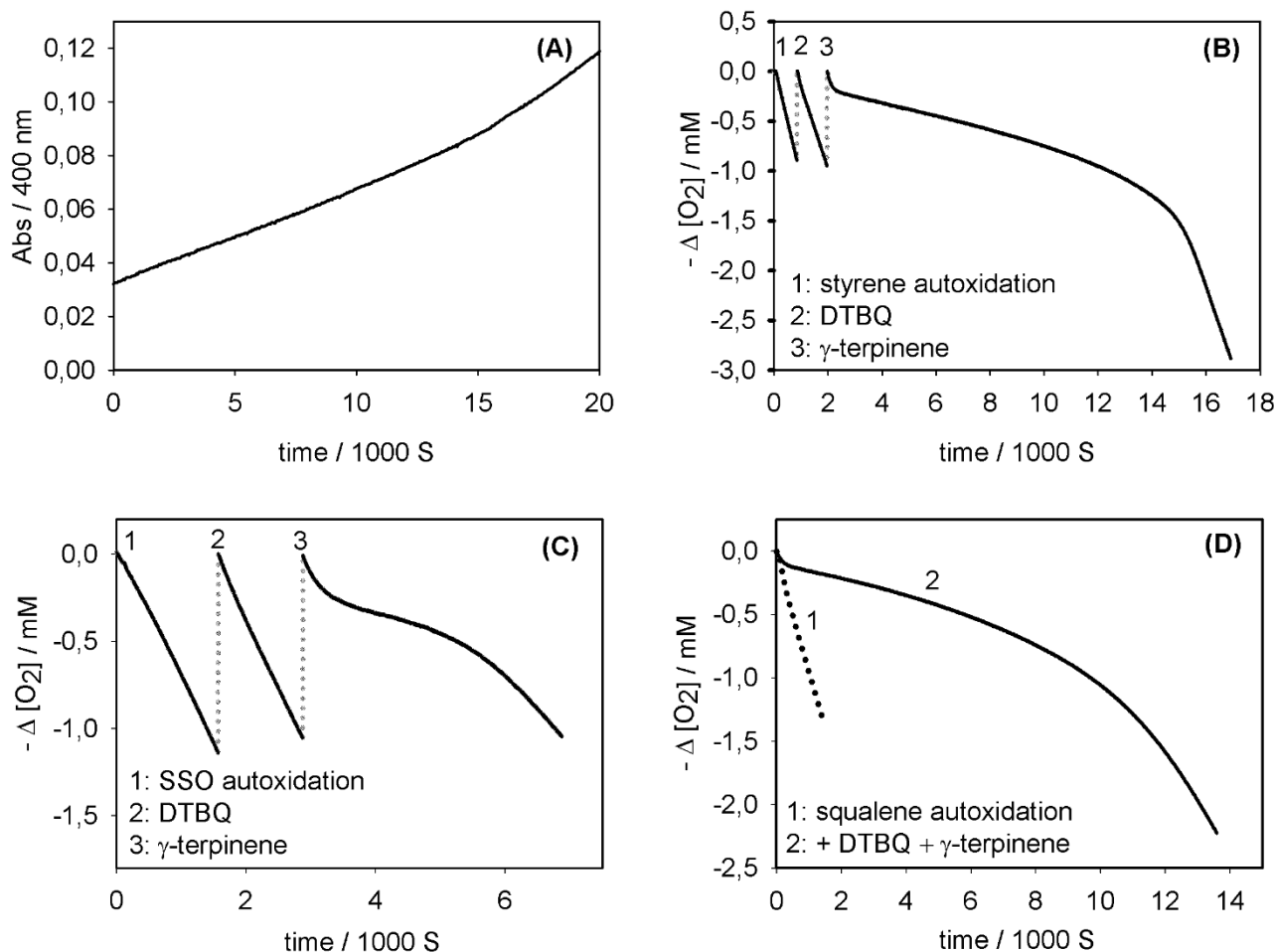


Figure 2.8 (A) Growth of the UV signal at 400 nm due to quinone **3** during the autoxidation of styrene initiated by 0.025 M AIBN at 30°C, inhibited by **3H₂** 67 μM. (B) Oxygen consumption during the autoxidation of styrene initiated by 0.025 M AIBN at 30°C in the absence of antioxidant (1), and upon their addition: 2 = injection of DTBQ **3** (7.5 μM); 3 = injection of γ-terpinene (7.83 mM). (C) Oxygen consumption during the autoxidation of SSO initiated by 0.025 M AIBN at 30°C in the absence of antioxidant (1), and upon their addition: 2 = injection of DTBQ **3** (7.5 μM); 3 = injection of γ-terpinene (7.83 mM). (D) Oxygen consumption during the autoxidation of squalene initiated by 0.025 M AIBN at 30°C in the absence of antioxidant (1), or in the presence of a mixture of DTBQ **3** (7.5 μM) and γ-terpinene (7.83 mM).

To confirm our hypothesis, autoxidation experiments were performed using the oxidized quinone DTBQ **3** as the antioxidant. While the injection of **3** alone in autoxidizing styrene did not produce any inhibition (Fig. 2.8B) subsequent injection of γ-terpinene caused the appearance of a long inhibition period, confirming that the quinone **3** could be regenerated by γ-terpinene to its starting catechol. This was also confirmed by parallel experiments in which the time-course of the concentration of **3** was monitored by UV spectroscopy at 400 nm during autoxidations inhibited by **3** and

γ -terpinene: the UV signal of **3** progressively declined during the autoxidation supporting its reduction to **3H₂** (see Fig. 2.9).

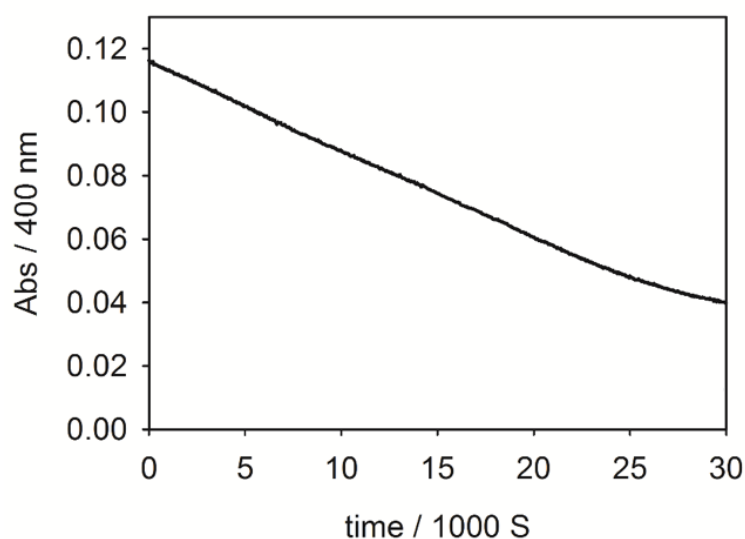


Figure 2.9. Decay of the UV signal at 400 nm due to quinone **3** during the autoxidation of styrene initiated by 0.025 M AIBN at 30°C, inhibited by **3** (67 μ M) and γ -terpinene (15.7 mM).

Additional experiments with co-injection of the the quinone and γ -terpinene in different order confirmed this conclusion (see Fig. 2.10).

We attribute the reduction of **3** (and other quinones) by γ -terpinene during the autoxidation to the release of HOO^\bullet , which would act as the reducing agent. Although this reducing behavior might be counterintuitive for a reputedly oxidizing radical, it is supported by previous solid evidence that it rapidly reduces both phenoxyl radicals [45] and nitroxides [86]. However, to explain the reduction of quinones by γ -terpinene other mechanistic possibilities could also have a role, like those recently disclosed to explain the synthesis of catechols using methylcyclohexadiene as the reducing agent [118].

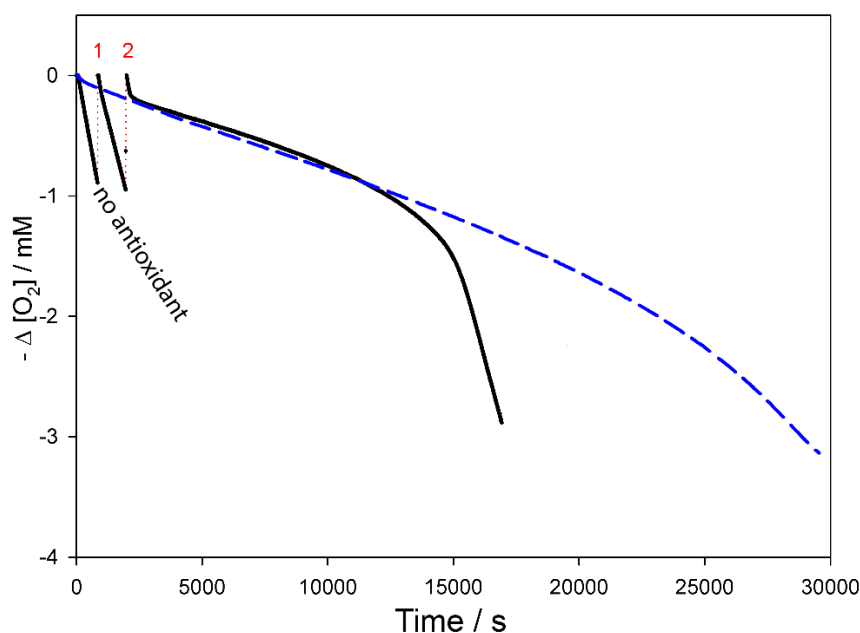


Figure 2.10. Oxygen consumption measured during the autoxidation of SSO initiated by 0.025 M AIBN at 30°C in the absence of antioxidants and (1) upon injection of DTBQ **3** (7.5 μM), (2) upon subsequent injection of γ -terpinene (15.7 mM). The blue dashed line represents the autoxidation under identical settings inhibited by a mixture of DTBQ **3** (7.5 μM) and γ -terpinene (15.7 mM) injected together at the beginning of the autoxidation. Note that despite the identical concentration of the antioxidants their effectiveness is higher if they are added together, possibly meaning that some side reaction is consuming **3** in the absence of γ -terpinene.

2.5.3 Relevance of the interaction between quinones and γ -terpinene in food science and the application of the synergic antioxidant behavior in real food products

The chemistry disclosed in the previous section concerning the possibility for γ -terpinene to enable the antioxidant behavior of quinones by reduction to the parent catechols appears particularly important in the protection of food products, since quinones are often abundant in vegetable tissues, also resulting from air oxidation of the parent polyphenols. This suggests that γ -terpinene could afford unusually effective protection owing to its synergic interplay with such products. On the other hand, it is clear from Fig. 2.6 and 2.8 that the redox cycling of the quinones to the parent catechols, then back to quinones and so on, is not fully efficient and either redox species might be consumed in side reactions, since the inhibition is not infinite or limited only by the consumption of γ -terpinene. Clearly, further studies would be necessary to fully rationalize the reasons for imperfect redox cycling; however, in current investigation

our interest focused on assessing its relevance in food chemistry. Therefore, we switched back to SSO and squalene as relevant dietary lipids and tested the antioxidant protection of quinone **3** in combination with γ -terpinene. With SSO **3** afforded no protection when used alone; however, subsequent addition of γ -terpinene enabled its antioxidant activity (Fig. 2.8C), and co-addition of **3** and γ -terpinene at the beginning of the autoxidation afforded even higher antioxidant protection (see Appendix, Fig. 2.10). Similarly, co-addition of **3** and γ -terpinene afforded full protection of squalene (Fig. 2.8D). Interestingly, with squalene even **3** alone afforded some antioxidant protection (Fig. 2.11) possibly due to the release of HOO^\bullet radical as a side event during the autoxidation of squalene, as previously observed in chapter 1 [104, 118]. This aspect would certainly deserve further investigation. However, its combination with γ -terpinene resulted in much enhanced antioxidant activity (see figure 2.11). Overall, current results demonstrate the effectiveness hence the relevance of the redox interplay between quinones and γ -terpinene in protecting food products, and complete the rationale explaining the synergy between γ -terpinene and both mono- and poly-phenolic antioxidants in this respect.

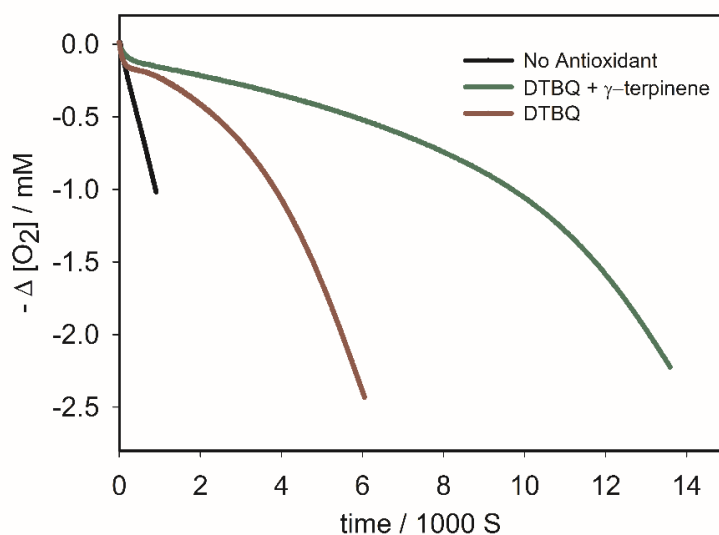


Figure 2.11 Oxygen consumption measured during the autoxidation of squalene initiated by 0.025 M AIBN at 30°C in the absence of antioxidant (black line), inhibited by 2.5 μM DTBQ **3** (red line), or inhibited by 2.5 μM DTBQ **3** and 15.7 mM γ -terpinene (green line).

In our investigation, we used model phenolic antioxidants (**1H**, **2H2** and **3H2**) rather than foodborne examples, since we needed molecules which were perfectly characterized so to achieve clear mechanistic understanding of the synergic antioxidant behavior in combination with γ -terpinene. For the same reason, we chose SSO and squalene, along with styrene, all in chlorobenzene solution, as model oxidizable substrates, since these systems had previously been characterized for quantitative studies. In order to demonstrate that the synergic antioxidant chemistry disclosed here is directly applicable to real food products, we further investigated the autoxidation of neat sunflower oil as a prototypical highly oxidizable food, protected by food born natural vitamin E (*d*- α -tocopherol from vegetable oils, FDA GRAS notice N° 781) and hydroxytyrosol from olive (FDA GRAS notice N° 837) as examples, respectively, of mono- and polyphenolic antioxidants currently approved (and used) in food products. Both models showed clear synergic protection in combination with γ -terpinene, as exemplified in Fig. 2.12, standing for the relevance in food science of the antioxidant chemistry disclosed here.

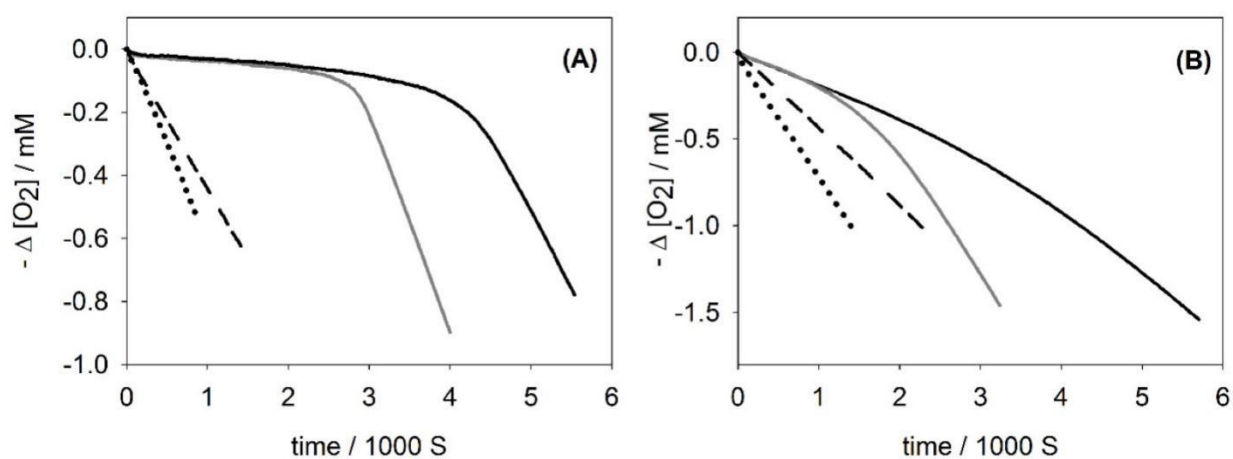


Figure 2.12 Oxygen consumption measured during the autoxidation of sunflower oil initiated by 0.025 M AIBN at 30°C in the absence of antioxidants (dotted lines), inhibited by 15 mM γ -terpinene (dashed lines) or: (A) inhibited by 3 μ M vitamin E (*d*- α -tocopherol, gray line) or by a mixture of 3 μ M vitamin E + 15 mM γ -terpinene (black line); (B) inhibited by 6 μ M hydroxytyrosol (gray line) or by a mixture of 6 μ M hydroxytyrosol + 15 mM γ -terpinene (black line).

Clearly, sunflower oil is a rather simple albeit highly oxidizable food product, in that it represents a homogenous lipid system. This is at variance with many other foods in

which oxidizable lipids are dispersed with aqueous components to form complex heterogeneous environments, which would possibly affect the kinetic behavior of antioxidants due to partitioning issues. This calls for further research to assess the actual contribution of the antioxidant synergic behavior in such heterogeneous systems, which we hope to pursue in future work.

2.5.4 Conclusions on the synergic antioxidant activity of γ -terpinene with phenols in food preservation.

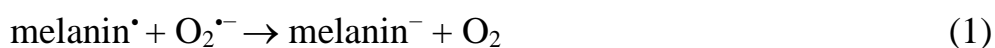
In conclusion, γ -terpinene can enhance the protection of natural lipids or other oxidizable substrates operated by phenolic antioxidants. The synergic mechanism is based on the sacrificial oxidation γ -terpinene with release of HOO^\bullet during the autoxidation. The exact consequence of such chain-transfer process then depends on the structure of the phenolic antioxidants. With monophenolic antioxidants like tocopherol, HOO^\bullet could reduce the phenoxyl radical formed upon trapping chain-carrying radicals (ROO^\bullet) thereby regenerating the starting antioxidant. No synergy is however displayed when the phenol has been fully oxidized to the final oxidation products, meaning that the phenol and γ -terpinene need to be simultaneously present in the system. On the other hand, with polyphenolic catechol antioxidants regeneration to the starting catechol can occur both from the phenoxyl (semiquinone) radicals and from the final oxidized quinone, expanding the usefulness of this synergic antioxidant chemistry. In both cases synergy occurs via establishing a catalytic cycle in which γ -terpinene acts as the sacrificial reductant. Since phenols and polyphenols are normally co-existing with terpinene or structurally related terpenes in vegetable extracts and food products, the synergic activity disclosed here is likely to have major significance and it can be exploited in rational strategies for antioxidant food protection. Additionally, it helps explain the purported beneficial effect of flavonoids even after they have been oxidized due to prolonged storage of food of vegetable products.

Lipids are essential cell membrane constituents [119] and key components in food. Their non-enzymatic oxidation causes deterioration of food flavour, color, texture and

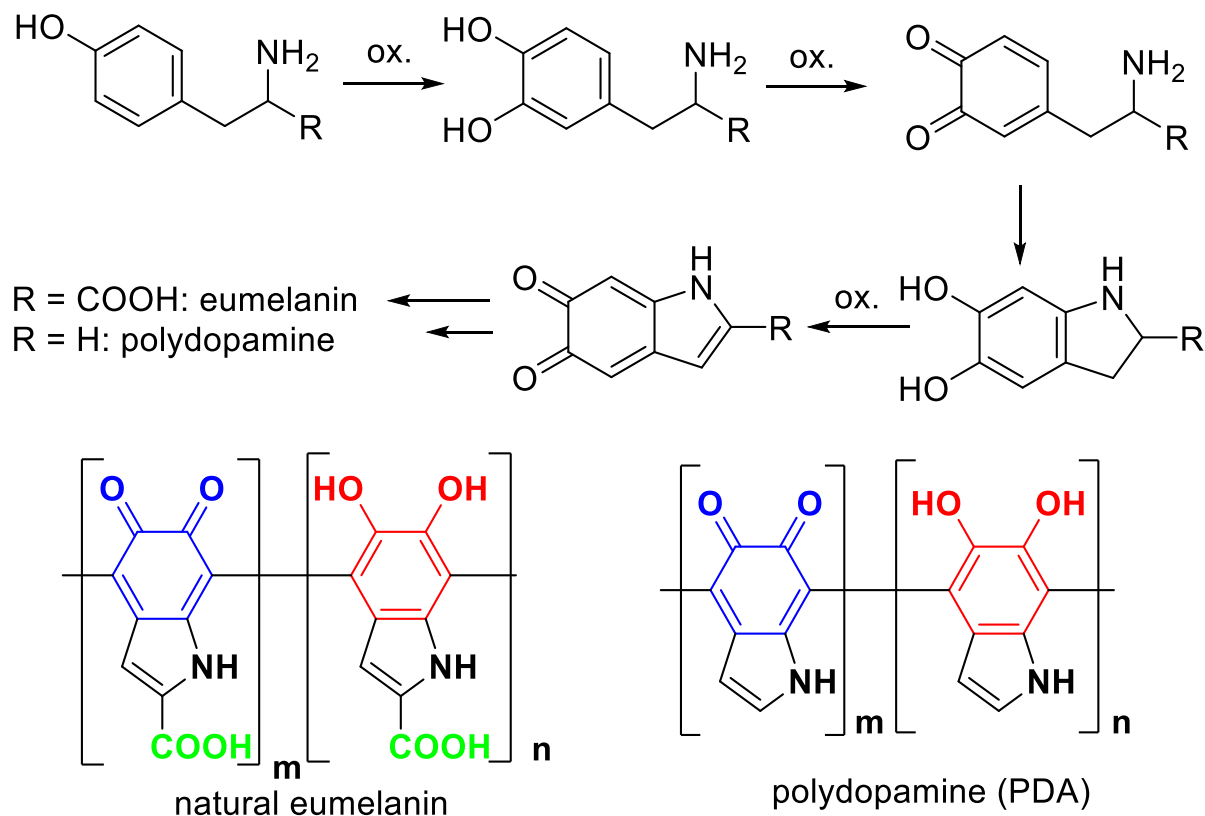
nutritional value [120] beside the formation of toxic off-products like 4-hydroxynonenal and other electrophilic carbonyl compounds [110]. Thus, great research effort in food science has been devoted to protecting lipids from oxidation by antioxidants, especially those obtained from natural sources [120]. We believe that the chemistry disclosed here brings relevant contribution in this respect.

2.6 Hydrogen Atom Transfer from HOO• to *ortho*-Quinones Explains the Antioxidant Activity of Polydopamine (published in *Angewandte Chemie International Edition* 2021 as DOI: 10.1002/ange.202101033)

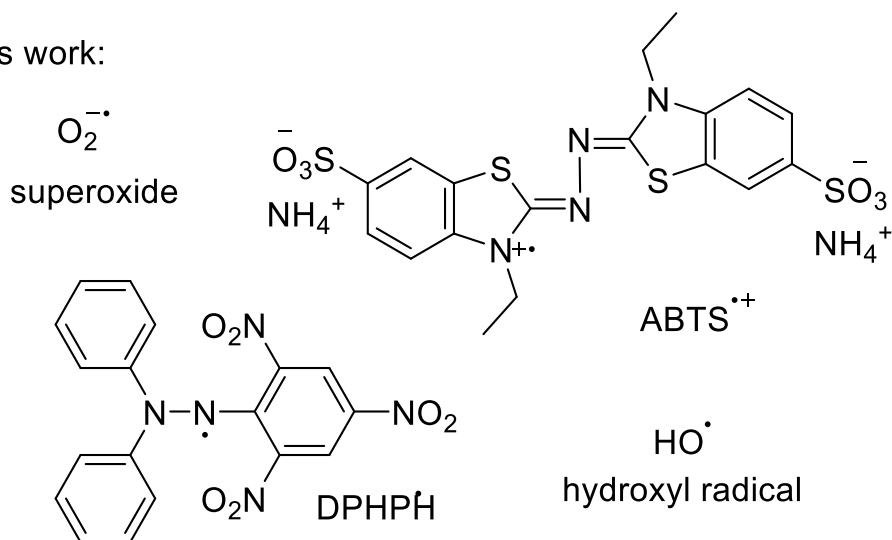
Melanins are a family of intensely colored polymers derived from oxidative polymerization of phenols such as tyrosine, DOPA and dopamine. [121,122] Although the structure of melanins is not fully clarified, there are evidence that it consists of reduced (catechol) or oxidized (*ortho*-quinone) units (see Scheme 2.14). [123,124]. Besides their important role in living organisms [125-128], melanins are currently being investigated for many applications, including energy storage, biocompatible adhesion or coating systems, drug delivery, and skin protection [125,126,129]. Melanins have been proposed to possess a “multi-antioxidative” activity, that has been related, for instance, to their anti-inflammatory [132] wound regeneration [133] and anti-ischemic activity [134]. Natural eumelanin (see Scheme 2.14) has been reported to have the strongest capability to quench radicals, with respect to the melanin from or dopamine polymerization, while negligible activity was reported for those obtained from DHI or DOPA [125]. Polydopamine traps HO• radicals [134] and has superoxide dismutase (SOD)-like activity by the reactions 1 and 2 [134] presumably involving the stable radicals “hosted” inside melanins [129,131,135].



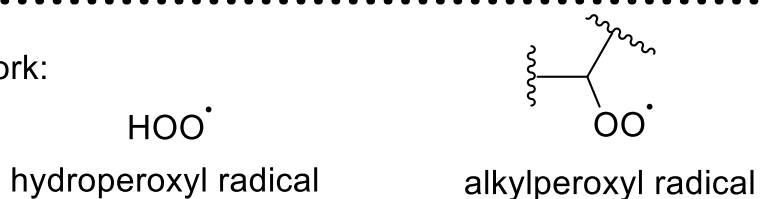
A. Biosynthesis of melanins



B. Previous work:



C. This work:



Scheme 2.14. (A) (Bio)synthetic pathway leading to the formation of melanins; (B, C) radical used to investigate the antioxidant activity of melanins.

The number of papers reporting the antioxidant activity of melanins is steadily increasing, although results are often controversial. The most critical aspects is, however, the fact none of those investigation has been able to provide a clear rationale for the purported antioxidant activity and the mechanism of radical trapping remains unclear. Most mechanistic studies have been performed by using stable persistent radicals such as DPPH• [127,128,130,131] and ABTS^{•+} [127], but these artificial radicals have limited similarity to transient alkylperoxyl radicals (ROO•), the biologically relevant oxygen-centered radicals involved in autoxidation reactions (see Scheme 2.14) [109, 137-138]. The structure of melanins at the molecular level largely depends on the nature of the phenolic monomer [127], on the polymerization conditions (*i.e.* reactants concentration and buffer components) [139,140] and on the post-synthetic functionalization (for example, with amino-terminated polyethylene glycol) [134]. Therefore, results obtained for a particular type of polymer might not be directly applicable to other melanins. A good starting point to face this problem would be having a clear understanding of the radical trapping behavior of the basic structural units that are present in all melanins, namely the 1,2-dihydroxy benzene (catechol) and the 1,2-benzoquinone moieties.

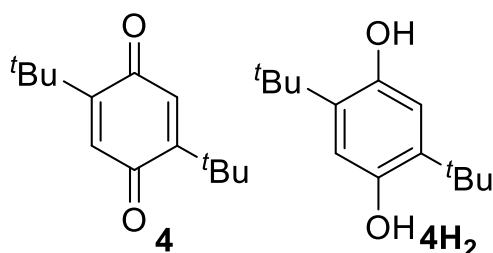
2.6.1 The reaction of *ortho* and *para* quinones with HOO•

Catechol moiety is a well-known reducing agent for peroxyl radicals, [108, 141-142] however, its reactivity may dramatically decrease as effect of intra- or inter-molecular H-bond formation with H-bond accepting groups. [108] The second building block, *ortho*-benzoquinone moiety, does not exhibit a reactivity toward ROO• radicals, [142-146] although the structurally related *para*-benzoquinone (pQ) is able to trap hydroperoxyl (HOO•) radicals via a mechanism triggered by reaction 3[147].



Recently, we and others have employed autoxidation of 1,4-cyclohexadiene (CHD) (scheme 2.10) alone or in mixture with other oxidizable substrates as an expedient to

study the interplay of ROO• and HOO• radicals in determining the activity of antioxidants such as Vitamin E and dialkyl nitroxides (Scheme 2.12). [45,82,86,148]. Herein, we apply this approach to understand the reactivity and the mechanisms of antioxidant action of polydopamine (PDA, Scheme 2.14) and of two model ortho (**3**) (scheme 2.13 C) and para (**4**) quinones (Scheme 2.15). Prompted by Denisov seminal observation that para-benzoquinone behaves as HOO• trap, we demonstrate herein that ortho-benzoquinones are much more effective than the para isomer. Then, we demonstrate that PDA inhibits lipid peroxidation only if its radical chain is carried on by mixed alkylperoxyl (ROO•) and hydroperoxyl (HOO•) radicals. Ortho-quinone moieties appear to be responsible for the antioxidant activity of PDA while the contribution of catechol moieties is proportionally less important.



Scheme 2.15. Model compounds investigated in this study and semiquinones radicals transiently formed during the reactions.

The chain-breaking antioxidant activity of **3** and **4** was evaluated by measuring, at 30 °C and in a low-polarity solvent (chlorobenzene), the rate of O₂ consumption during the azo-bis(isobutyronitrile) (AIBN) initiated oxidation of styrene, a reference organic substrate whose autoxidation at low temperature is propagated by ROO• [149-151]. As expected, [142,143] **3** and **4** had no effect on the peroxidation of styrene (Figure 2.13, traces b-c), in line with what previously observed in section 2.5. When CHD was added to styrene, both quinones efficiently suppressed the peroxidation, as shown by the kinetic traces d and e in Figures 2.13 and 2.14

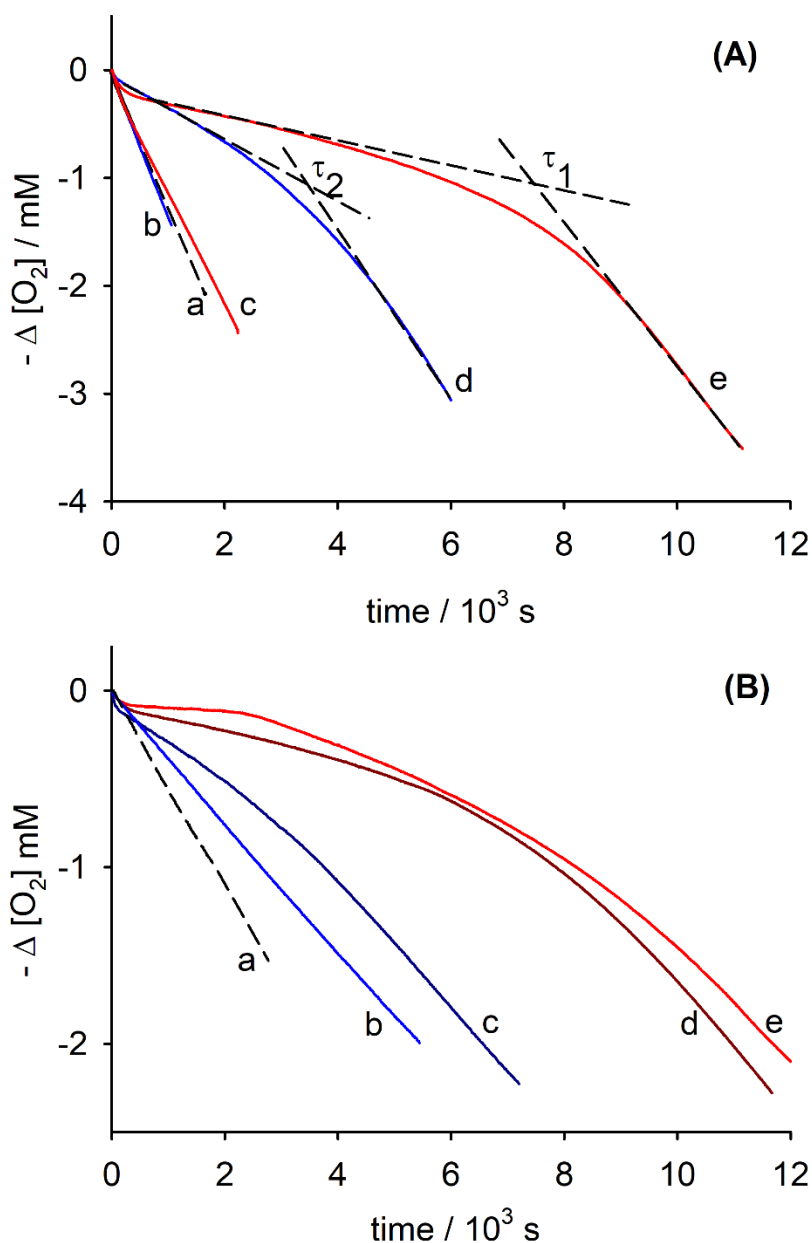


Figure 2.13 O_2 consumption during the autoxidation of styrene in chlorobenzene at 30°C initiated with 25 mM AIBN in the absence of inhibitors (a), and in the presence of quinones: **4** (curve b), **3** (curve c), **4** + 0.023 M CHD (curve d), and **3** + 0.023 M CHD (curve e). The concentration of quinones was $5\ \mu\text{M}$. B) O_2 co-nsumption during the autoxidation of CHD (0.23 M) initiated by 25 mM AIBN at 30°C in chlorobenzene with no antioxidants added (a), with $40\ \mu\text{M}$ of **4** or **4H2** (curves b and c, respectively), and with $5\ \mu\text{M}$ **3H2** or **3** (d and e, respectively).

Control experiments (styrene containing CHD but without quinones) indicated neither inhibition nor retardation, thus the strong inhibition observed for styrene/CHD/quinone can be explained by the reactions reported in Scheme 2.16. Comparing the kinetic traces in Figure 2.13, we should notice that **3** generates longer induction period than **4** used at the same concentration (see τ_1 and τ_2) and, additionally, the rate of O_2 uptake

during the inhibition period is smaller for **3** than for **4**, demonstrating a superior antioxidant activity of the ortho-isomer.

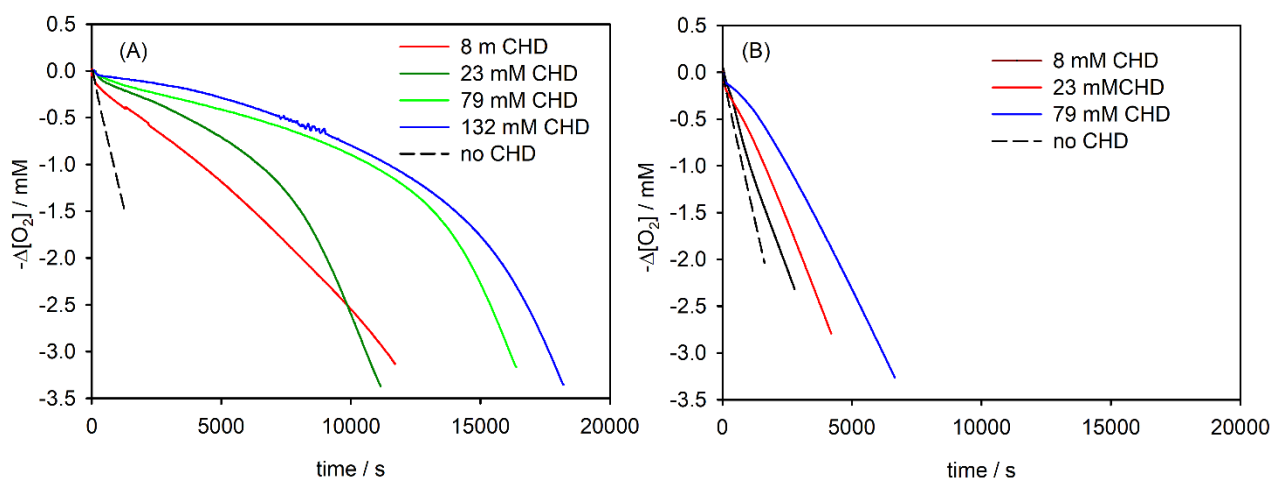
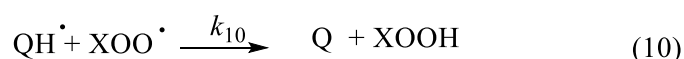
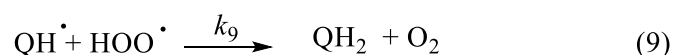
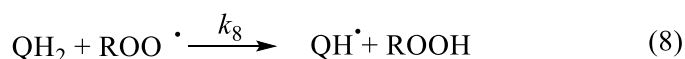
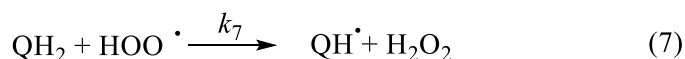
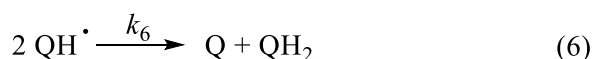
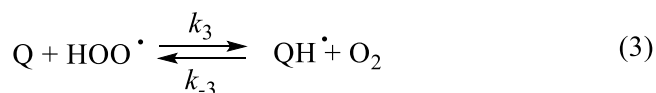


Figure 2.14. O₂ consumption *during* the autoxidation of styrene in chlorobenzene at 30 °C initiated with 25 mM AIBN in the absence of inhibitors in the presence of 5 μM of quinone **3** (A) or **4** (B) and increasing amounts of CHD.



Scheme 2.16 Key reactions explaining the antioxidant activity of ortho and para-quinones, Q, in the presence of 1,4-cyclohexadiene, CHD.

To better clarify the mechanism proposed in Scheme 2.16, we completely replaced styrene with CHD. figure 2.13B presents the kinetic traces recorded for the system,

with the autoxidation propagated exclusively by HOO• radicals. [82] Lines b and e indicate that **3** almost completely stopped the autoxidation of CHD (i.e trapped HOO• with high efficiency), while **4** was less effective even if used at much higher concentration. We also employed **3H₂** and **4H₂** to test their behavior during autoxidation of CHD. Results, reported in figure 2.13B (traces c and d), indicated a smaller and a higher HOO• trapping ability than the corresponding quinones for **3H₂** and **4H₂** respectively [152].

Having clarified the unique behavior of ortho-benzoquinone **3** toward the reaction with HOO•, as previously observed in 2.5 using γ -terpinene as the source of HOO•, and having clarified its superior reactivity compared to the *para* isomer, we set here to quantify its reactivity with HOO•. The rate constants for this reaction was calculated by using equation 12, which relates the rates of the inhibited and non-inhibited autoxidation (R_{inh} and R_0 , respectively) to the rate constant for the reaction of the antioxidant with the chain-carrying radicals and the stoichiometry of radical trapping (n). [151]

$$(R_0/R_{in}) - (R_{in}/R_0) = n k_3 [AH] / (2k_t R_i)^{1/2} \quad (12)$$

The rate of initiation (R_i) was determined experimentally as $3.1 \times 10^{-9} \text{ M s}^{-1}$, while $2k_t$ for CHD in chlorobenzene is $1.2 \times 10^9 \text{ M}^{-1}\text{s}^{-1}$. [82] With the assumptions that the rate of the back reaction k_{-3} is negligible and that $n = 2$, k_3 was obtained as $(1.4 \pm 0.2) \times 10^7 \text{ M}^{-1}\text{s}^{-1}$. Numerical modeling of some representative O₂ consumption traces of CHD and styrene autoxidations was performed by using COPASI, a kinetic simulation software [155-158] as illustrated in figure 2.15A. The values of k_3 and k_7 obtained with this procedure were 1.5×10^7 and $1.5 \times 10^6 \text{ M}^{-1}\text{s}^{-1}$, respectively, while for k_{-3} an upper limit of $65 \text{ M}^{-1}\text{s}^{-1}$ was determined. Results also show that a substantial quantity of catechol **3H₂** is formed from **3** (figure 2.15A). This finding, although in line with previous hypothesis (see section 2.5) is somewhat counterintuitive, as it means that the antioxidant is being reduced, albeit transiently, during the inhibition of CHD autoxidation. Therefore, we attempted to have experimental evidence in support of

numerical modelling. Formation of $3H_2$ was confirmed by ESI-MS analysis performed on the reaction mixture containing **3**, CHD and AIBN (figure 2.15B-C). Quinone **3** was visible only in positive ion mode mainly as $3+Na^+$ peak, while catechol $3H_2$ could be detected in negative ion mode as $3H^-$. The same result was obtained by GC-MS, after derivatization of the sample with trimethylsilyl-*N,N*-dimethylcarbamate (TMSDMC) as silylating agent, so to protect $3H_2$ from decomposition during the analysis (see Appendix, Figure A. 2.3-2.5).

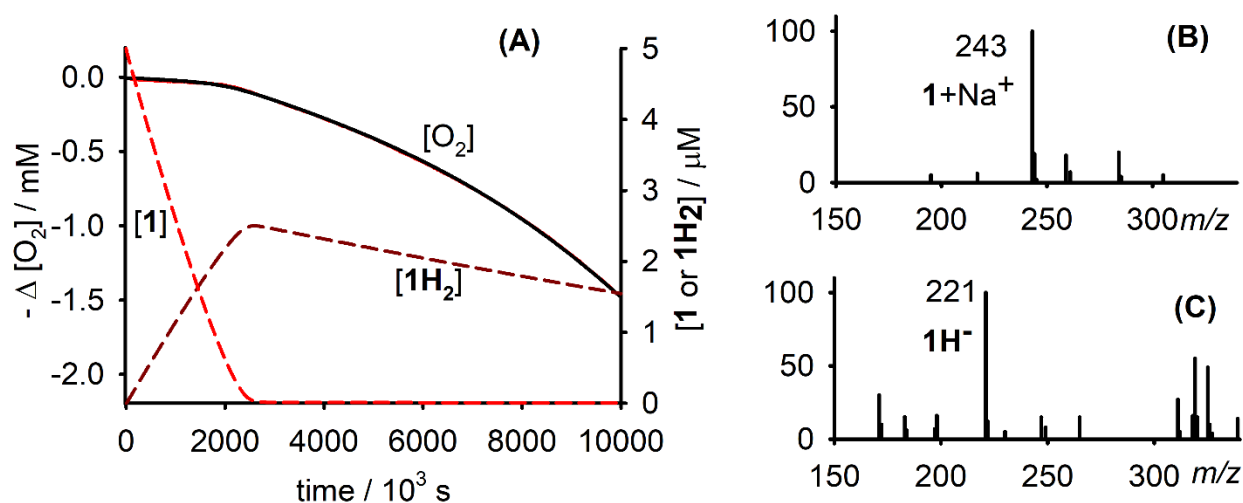


Figure 2.15. (A) Numerical fitting of the O_2 consumption traces during the autoxidation of CHD initiated by AIBN in PhCl at 30 °C inhibited by **3**. Experimental results for oxygen consumption (black, solid line) and the simulated results (red line), perfectly overlapping each other. The transient concentrations of the quinone or hydroquinone species obtained during the simulations are reported. (B-C) ESI-MS spectra showing $3H_2$ formation during the reaction of **3** (0.1 mM) with CHD (0.23 M) and AIBN (50 mM) in MeCN at 30 °C; after 1 hour of reaction in positive (B) and negative (C) ion mode.

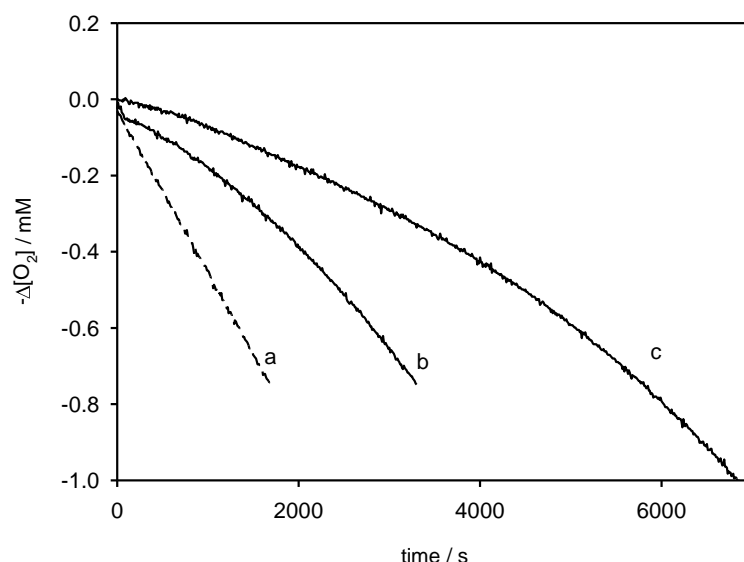
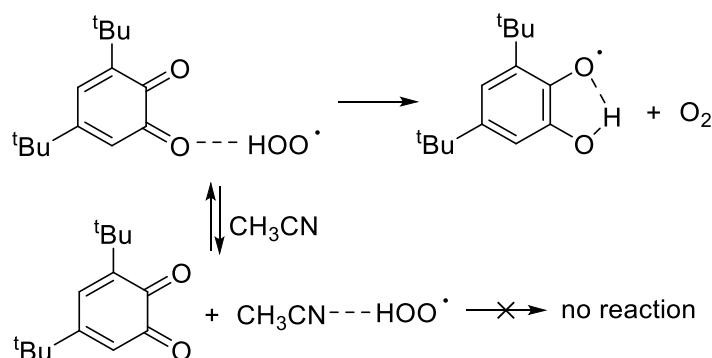


Figure 2.16. O₂ consumption measured during the autoxidation of CHD (0.13 M) in MeCN initiated by AIBN (0.5 mM) at 30 °C in the absence of antioxidants (a) or in the presence of **3** (a) 5 μM, (b) 25 μM.

In acetonitrile, the inhibiting effect of **3** during the autoxidation of CHD was weaker than in PhCl (see figures 2.16). Numerical fitting (see Figure A. 2.6) provided $k_3 = 1.1 \times 10^5 \text{ M}^{-1}\text{s}^{-1}$, that is 180 times smaller than in PhCl. From the observed magnitude of this kinetic solvent effect (KSE) the ability of HOO[•] as H-bond donor (H-bond acidity parameter, α^{H_2}) can be calculated [160,161] as 0.78, in reasonable agreement with previous estimates. [45,162]. KSE is a proof that the reaction of **3** with HOO[•] involves a H-atom transfer and that this process starts with formation of a pre-reaction H-bond complex (see Scheme 2.17), that is competitive with the interaction of HOO[•] radical with a solvent molecule.



Scheme 2.17 Kinetic solvent effect for H-atom donation from HOO[•].

2.6.2 The role of $\text{HOO}\cdot$ in the antioxidant activity of polydopamine (PDA)

Polydopamine (PDA) nanoparticles were synthesized by the oxidative polymerization of dopamine in alkaline water/ethanol solution and were accurately purified by repeated centrifugation cycles (characterization by DLS, TEM and FT-IR is reported in figure 2.17A and B, figure A.2.7-2.9 [163,164]).

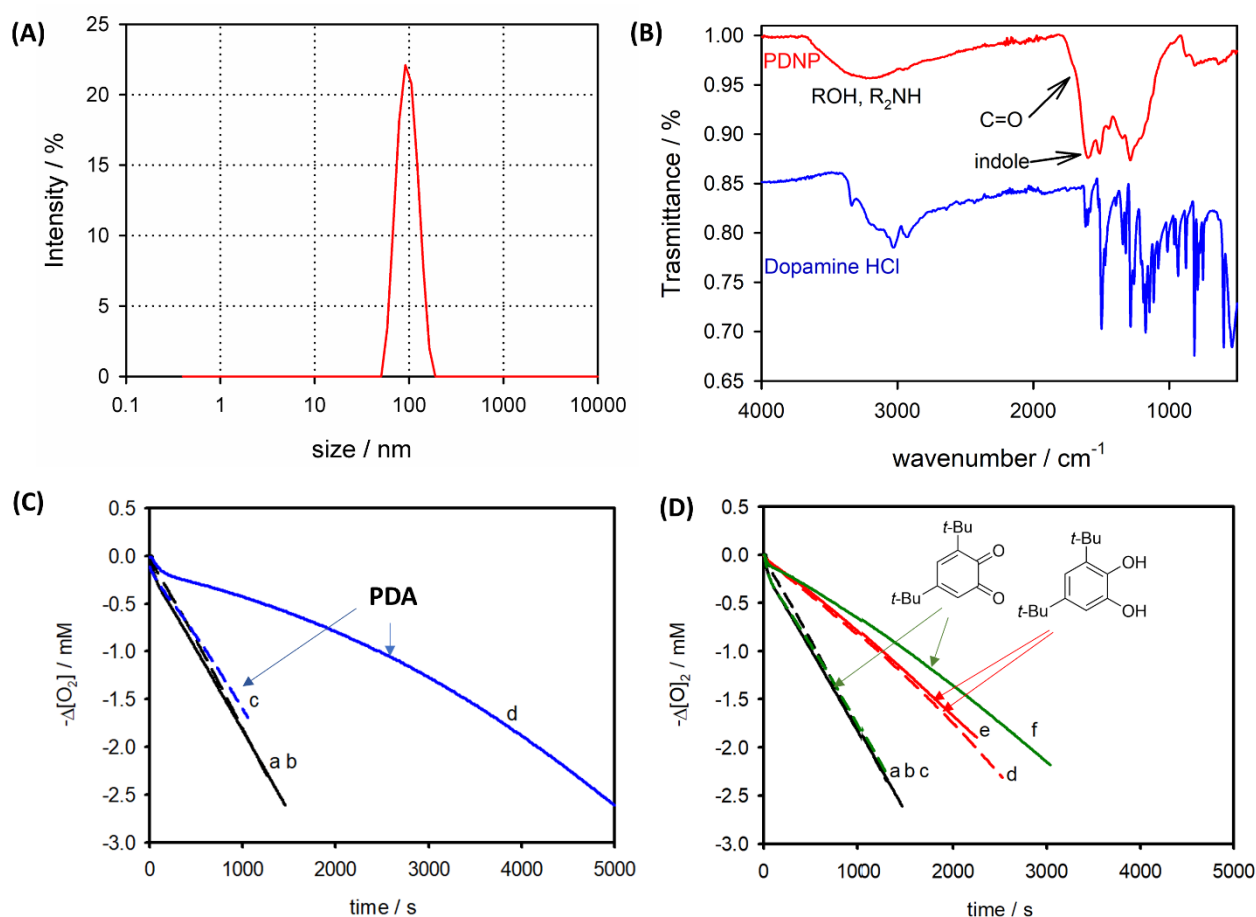
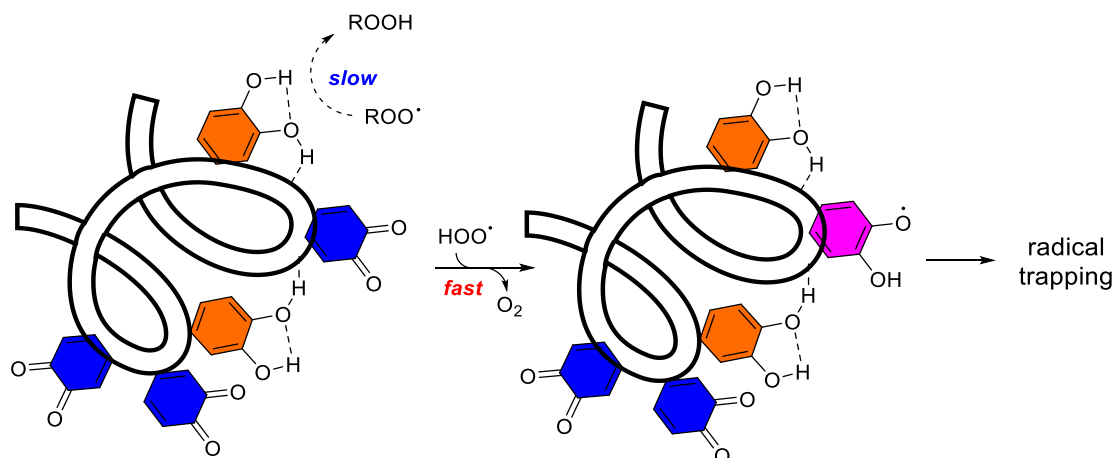


Figure 2.17. (A) dynamic light scattering of PDNPs water solution. (B) ATR-FTIR spectrum of dried PDNP. (C) O_2 consumption recorded during the styrene (2.1 M) autoxidation initiated by AIBN (25 mM) in MeCN without inhibitors (a) and in the presence of: (b) CHD; (c) **PDA** (25 g/mL); (d) **PDA** (25 g/mL) + CHD. (D) Same conditions as C, without inhibitors (a) and in the presence of: (b) CHD; (c) **3** (5 μM); (d) **3H₂** (5 μM); (e) **3H₂** (5 μM) + CHD; (f) **3** (5 μM) + CHD. In all cases, $[\text{CHD}] = 23 \text{ mM}$.

The nanoparticles were concentrated, dispersed in acetonitrile and then used as inhibitor in autoxidation studies. As shown in figure 2.17C, PDA itself had negligible antioxidant activity toward styrene autoxidation (solvent MeCN), presumably due to the low concentration of catechol moieties, or their engagement in strong

intramolecular H-bonds [165]; however after the addition of CHD the antioxidant activity of PDA became much stronger. Under the same conditions, CHD had a negligible effect on $3H_2$ (figure 2.17D traces d and e), while it greatly increased the activity of **3** (traces c and f).



Scheme 2.18. Catechol and quinone units in the polydopamine polymer are non-reactive toward alkylperoxyl radicals ($ROO\bullet$) but upon the reaction with $HOO\bullet$ the quinones are converted to semiquinone radicals with enhanced ability to trap both species, $HOO\bullet$ or $ROO\bullet$.

The negligible reactivity toward $ROO\bullet$ of PDA can be explained by considering that the catechol moieties are strongly bonded to H-bond acceptors, such as carbonyl groups, present into the polymer (scheme 2.18). [166] Not H-bonded catechols, which would be more reactive toward radicals than H-bonded ones, are most probably oxidized during the preparation of PDA. Instead, upon reaction with $HOO\bullet$, *ortho*-quinones can form “exposed” semiquinones and catechol groups able to trap both $HOO\bullet$ and $ROO\bullet$. *Ortho*-semiquinones are interesting radical intermediates because they are stabilized by a strong intramolecular H-bond and are therefore generally unreactive toward O_2 [61]. It can be estimated that the reaction of $HOO\bullet$ with *ortho*-benzoquinone is exothermic by ≈ 16 kcal/mol (while for the para isomer is ≈ 11 kcal/mol) and this explains the high k_3 value measured herein [45,87]. The present results however leave open the question concerning the role of radicals naturally hosted inside melanins to explain the antioxidant activity of these materials. [134,135]. Such radicals have been shown to contribute to the redox properties of melanins and it has

been clarified that they are mainly represented by semiquinone-type radicals. Our current data indicate that they would react at close to diffusion controlled rate with $\text{HOO}\cdot$, hence the intermediacy of $\text{HOO}\cdot$ might also support their important contribution to the overall antioxidant behavior of melanins. Clearly further studies would be needed to fully elucidate this specific point. Current data suggest that the ability of peroxy radical trapping by PDA, in the presence of $\text{HOO}\cdot$ is nicely explained by the chemistry of quinones/ $\text{HOO}\cdot$ system.

2.6.3 Conclusions on the role of $\text{HOO}\cdot$ on the antioxidant behavior of melanins

The simultaneous presence of alkylperoxyl and hydroperoxyl radicals is a common feature in many systems. Alkylperoxyl radicals are responsible for lipid peroxidation of unsaturated membranes [149], while the $\text{HOO}\cdot$ radicals are constantly produced by protonation of superoxide leaking from the mitochondrial respiratory chain [86,87]. Moreover, $\text{HOO}\cdot$ radicals are generated during the autoxidation of alcohols and aliphatic amines [86], such as Lys, Arg, Ser amino acids (leading to the formation of protein carbonyls). The results obtained herein by investigating the reaction of $\text{ROO}\cdot$ and $\text{HOO}\cdot$ radicals with polydopamine and with two reference quinone/hydroquinone couples allows us to propose a mechanism for the antioxidant activity of melanins. *Para*- and *ortho*-benzoquinones **Q** are unable to act as antioxidants by trapping alkylperoxyl radicals ($\text{ROO}\cdot$); however, both turn into radical trapping antioxidants in the presence of hydroperoxyl radicals ($\text{HOO}\cdot$) due to stepwise reduction of **Q** to the semiquinone radical **QH** \cdot and to the parent hydroquinone/catechol **QH**₂. The reduced forms **QH** \cdot and **QH**₂ can trap $\text{ROO}\cdot$ and $\text{HOO}\cdot$ radicals. The redox cycling and overall antioxidant behavior are very efficient for *ortho* quinones because of their reduction via fast H-atom transfer from $\text{HOO}\cdot$ (*i.e.* reaction 3), and because the intramolecularly H-bonded *ortho*-semiquinone radical is not sensitive to the back reaction with O_2 (reaction -3).

Ortho-quinones are good models to rationalize the antioxidant behavior of melanins, as they represent one of the repeating functional units, along with their parent reduced

catechol form. Our measurements demonstrated that, contrary to expectations, polydopamine affords low protection of oxidizable materials when oxidation is mediated only by alkylperoxyl (ROO[•]) radicals. This is explained by i) a low concentration of catechol groups, reasonably because they are oxidized during the synthesis of polydopamine; ii) low reactivity of the catechol units having OH groups blocked by H-bonding to the neighboring quinone or other H-bond acceptors moieties in the polymer chain. We showed herein for the first time that the antioxidant activity of polydopamine develops upon introduction of HOO[•] radicals in the autoxidizing system, due to the reduction of quinone segments to the corresponding semiquinones. The interplay of oxidizing ROO[•] and reducing/oxidizing HOO[•] as chain carrying species is well established in biological systems, thereby making the chemistry disclosed herein an important piece of the puzzle in rationalizing the redox-mediated bioactivity of melanins and of *ortho* and *para*-quinones. The mechanism proposed by us for antioxidant action of polydopamine can be implemented for the rational design of novel antioxidant materials and biomaterials that can be selectively activated by hydroperoxyl radicals.

2.7 Materials and Methods

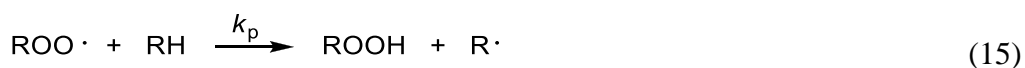
2.7.1. Materials

All chemicals and solvents were commercially available (Aldrich-Fluka-Sigma-Merck, Milan, Italy). 2,2'-Azobis(isobutyronitrile) (AIBN) was recrystallized from methanol. 2,2,5,7,8-Pentamethyl-6-chromanol (PMHC, **1H**) was recrystallized from hexane. Caffeic acid phenethyl ester (CAPE, **2H₂**), 3,5-di-*tert*-butylcatechol (DTBC, **3H₂**) and 3,5-di-*tert*-butyl-*o*-benzoquinone (DTBQ, **3**), 2,5-di-*tert*-butyl-1,4-benzoquinone (**4**), 2,5-di-*tert*-butyl-1,4-hydroquinone **4H₂**, (+)- α -tocopherol type V (1000 IU/g) and 3-hydroxytyrosol were used as received. Squalene ($\geq 98\%$), styrene ($\geq 99\%$), cyclohexadiene (97%) and γ -terpinene (97%) were percolated twice through activated basic alumina and once through silica to remove impurities and traces of

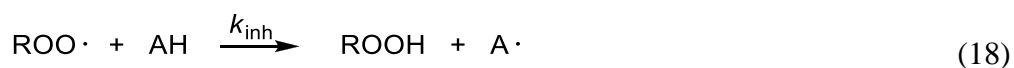
hydroperoxides (see chapter 1). Stripped Sunflower Oil (SSO) was prepared from food-grade sunflower oil (*Helianthus annuus* Seed Oil) purchased from a local market by purification as described in chapter 1. All solvents (PhCl, MeCN, ethanol) were of the highest grade commercially available ($\geq 99.9\%$ HPLC grade) and used as received. Deionized water was Millipore grade.

2.7.2 Measurements of the antioxidant activity

As introduced in chapter 1, hydrocarbon autoxidation is a free-radical chain reaction described by reaction 13-16, and it causes oxygen consumption at a constant rate when it is initiated with a constant rate R_i , under controlled conditions in the absence of inhibitors, as described in equation 17, where k_p and $2k_t$ are, respectively, the rate constant for chain propagation and termination of the oxidizable substrate. Oxygen consumption is instead slowed down or delayed by an inhibition time τ when an antioxidant (AH) is breaking the radical chain, competing with propagation (reaction 18 and 19), depending on the efficacy of the antioxidant [101,109]



$$-\frac{d[\text{O}_2]}{dt} = \frac{k_p [\text{RH}] \sqrt{R_i}}{\sqrt{2k_t}} + R_i \quad (17)$$



Efficacy of antioxidants was studied by measuring the kinetics of oxygen consumption during the autoxidation of a reference substrate, both in the presence and in the absence of antioxidants in a closed system. A two-channel oxygen uptake apparatus developed

in our laboratory, based on a Validyne (Northridge, CA, USA) DP15 differential pressure transducer, was used to record the consumption of the oxygen (see chapter 1). From the plot of oxygen consumption, it was possible to calculate the inhibition rate constant (k_{inh}) and the stoichiometric factor (n) from equation 19 and 20, using the already known rate constants k_p and $2k_t$ of the chosen substrates (see chapter 1).

$$-\frac{d[O_2]}{dt} = \frac{k_p}{rk_{inh}} \frac{[RH]R_i}{[AH]} + R_i \quad (20)$$

$$R_i = n [AH] / \tau \quad (21)$$

The initiation rate R_i was determined in matched preliminary experiments by the inhibitor method, using PMHC as a reference antioxidant and equation 21, where τ is the length of the inhibition time. The length τ could also be used to compare the antioxidant activity directly, the longer the duration, the bigger of the activity [109, 117].

Numerical fitting of the experimental O_2 consumption traces were performed by using the kinetic simulation software COPASI, freely available on the Internet [155]. The reaction scheme used to simulate the experimental data is reported in the table A. 2.1-2.4.

2.7.3 UV-Vis Spectroscopy

Spectra were recorded at 30°C in a Thermo Scientific (Milan, Italy) Biomate 5 coupled with a Heto DBT Hetotherm (Birkerød, Denmark) thermostating water circulator for temperature control. Kinetics of formation and decay of the quinone **3** were monitored at 400 nm in PhCl containing 0.025 M AIBN so to match the rate of radical generation R_i that was set during autoxidation, in presence and absence of γ -terpinene.

2.7.4. Synthesis of polydopamine nanoparticles

Ethanol (3 mL) was mixed with deionized water (7 mL) and dopamine hydrochloride (25 mg) under mild magnetic stirring at 50°C for 30 min [163,164]. The solution of ammonium hydroxide (NH_3 in H_2O 28% w/w, 100 μ L) was cooled and then injected

into the above mixed solution and let react for 24 h. The material was cleaned by five consecutive centrifugation (15000g for 10 min) and washing cycles. The concentration of nanoparticles suspension was 0.5 mg/mL, as determined by weighing the mass after drying. The nanoparticles were characterized by dynamic light scattering (DLS), transmission electron microscopy (TEM) and attenuated total reflection infrared spectroscopy (ATR FT-IR) as described in figure A. 2.7-2.9. The nanoparticles were then concentrated by centrifugation (15000 g), re-dispersed in acetonitrile (final concentration 0.5 mg/mL) before being used as inhibitors of the styrene autoxidation.

2.7.5. ESI-MS Measurements

Mass spectra were obtained by direct infusion with a microsyringe pump (15 μ L/min) into a Micromass ZMD ESIMS spectrometer using the following instrumental settings: positive ions; desolvation gas (N_2), 250 L/h; cone gas (skimmer), 22 L/h; desolvation temperature, 100 $^{\circ}$ C; capillary voltage, 3.0 kV; cone voltage, 10-40 V; hexapole extractor, 3 V; RF lens, 0.3 V.

2.7.6. GC-MS analysis

See Appendix.

2.7.8 Numerical analysis with COPASI software

See Appendix

2.7.9 DLS and TEM analysis of PDA

See appendix

2.7.10 Statistical Analysis

Each inhibition rate constant (k_{inh}) and stoichiometric factor (n) is expressed as an average \pm standard deviation (SD) from at least three independent kinetic measurements.

Appendix to Chapter 2

Kinetic analysis by COPASI software

The numerical modeling of some representative O₂ consumption traces were performed by using a kinetic simulation software (Copasi). [155] This software was used previously in other studies by us and by other research groups to analyze the autoxidation kinetics [156,157]. We used the kinetic equations reported in Scheme 2.16 in addition to those describing the autoxidation of CHD or styrene. The propagation (k_p) and termination ($2k_t$) rate constants in chlorobenzene at 30 °C, are respectively 1400 and $1.2 \times 10^9 \text{ M}^{-1}\text{s}^{-1}$ for CHD.[82] (for CHD, $k_p \equiv k_4$), and 41 and $4.2 \times 10^7 \text{ M}^{-1}\text{s}^{-1}$ for styrene.[149] The rate constant k_6 for disproportionation of 3H^\bullet was assumed to be the same as for the 3,6-di-*tert*-butyl-2-hydroxyphenoxy radical in benzene at room temperature ($8.0 \times 10^5 \text{ M}^{-1}\text{s}^{-1}$)[158]. because of similar steric crowding around the phenoxy oxygen. The rate constants k_9 and k_{10} , *i.e.* for radical-radical cross terminations, were assumed to be $2.0 \times 10^9 \text{ M}^{-1}\text{s}^{-1}$, and the rate constant k_{11} was let free to vary in the range $(1-50) \times 10^8 \text{ M}^{-1}\text{s}^{-1}$.⁴⁴ With these approximations, we could reproduce with good accuracy the experimental O₂ consumption traces as illustrated in figure 2.17. In the case of **3** in CHD, its concentration was adjusted to account for its slightly shorter inhibition period (by about 20%) typically observed, probably due to a side reaction not included into the reaction scheme (see ref. 37 for our attempts aimed at clarifying this point). Different sets of k_3 and k_{-3} values provided a good fitting of the O₂ consumption traces, indicating that these constants cannot be determined independently in a single experiment. However, we noticed that for CHD inhibited by **3**, the rate of O₂ consumption is most sensitive to the **3** + HOO[•] reaction (*i.e.* to k_3), whereas for styrene inhibited by 3H_2 , the *length* of the induction period depends on 3H^\bullet + O₂ reaction (*i.e.* on k_{-3}). Therefore, we adopted the graphical approach shown in figure A. 2.1, with k_3 as a function of k_{-3} for CHD autoxidation inhibited by **3** and for styrene autoxidation inhibited by 3H_2 figure A. 2.1 The crossing point of these plots is the best estimate for the two rate constants. The values of k_3 , k_{-3} and k_7 obtained with

this procedure were $1.5 \times 10^7 \text{ M}^{-1}\text{s}^{-1}$, $65 \text{ M}^{-1}\text{s}^{-1}$ and $1.5 \times 10^6 \text{ M}^{-1}\text{s}^{-1}$, respectively. Interestingly, the k_3 value obtained by numerical fitting is in excellent agreement with that found by using equation 12, the reason being that the k_{-3} value is small enough to make the slope of O_2 consumption during CHD autoxidation sensitive only to the k_3 value. The rate constant for the reaction of 3H_2 with HOO^\bullet ($k_6 = 1.5 \times 10^6 \text{ M}^{-1}\text{s}^{-1}$) is very similar to that previously recorded for the same catechol with ROO^\bullet ($1.1 \times 10^6 \text{ M}^{-1}\text{s}^{-1}$ at 303K in chlorobenzene)²⁴ confirming that HOO^\bullet and ROO^\bullet have similar oxidizing reactivity.

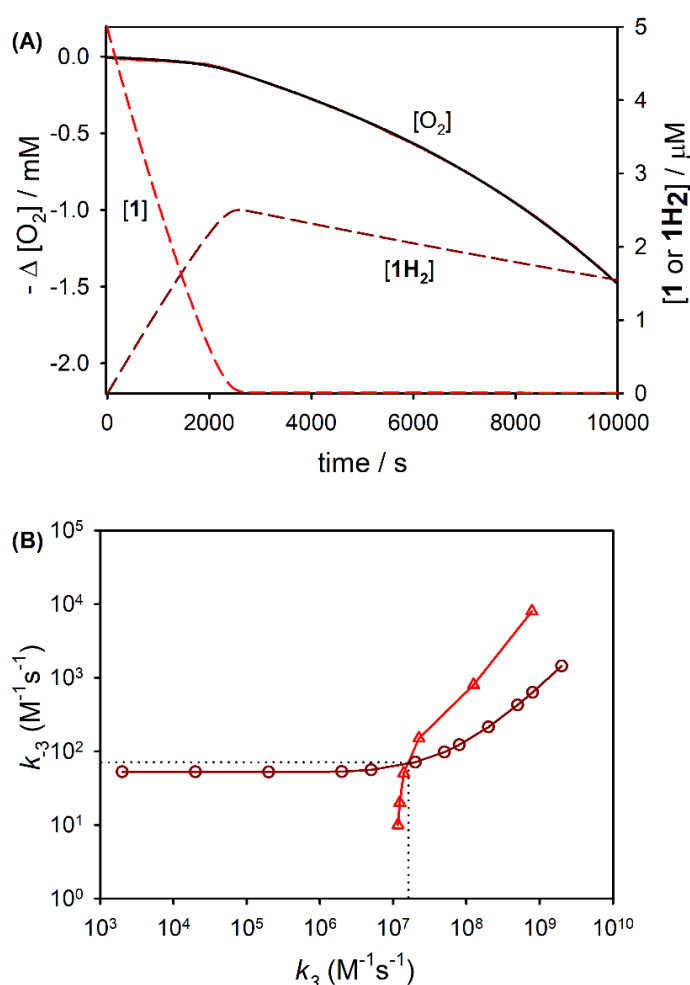


Figure A. 2.1 A) Numerical fitting of the O_2 consumption traces during the autoxidation of CHD initiated by AIBN in PhCl at 30 °C inhibited by **3**. Experimental results for oxygen consumption (black, solid line) and the simulated results (red line) perfectly overlap each other. The transient concentrations of the quinone or hydroquinone species obtained during the simulations are reported. B) Values of k_{-3} as a function of k_3 (logarithmic scale) obtained by numerical fitting of the rates of CHD autoxidations inhibited by **3** (Δ) or of styrene autoxidation inhibited by 3H_2 (\circ).

Table A. 2.1. Species considered in numerical fitting of the autoxidation of 1,4-cyclohexadiene (CHD) initiated by AIBN at 30 °C.

chemical name	symbol used in equations	Initial concentration
I	Initiator	not relevant. Radical initiation is determined directly by R_i .
HOO	$\text{HOO}\bullet$	0
R	cyclohexadienyl alkyl radical	0
O ₂	dissolved O ₂	1.8e-3
O _{2g}	O ₂ in the headspace	1 M ^a
RH	1,4-cyclohexadiene	depending on experiment
HOOH	H ₂ O ₂	0
QH ₂	1,4-di-tert-butyl catechol	depending on experiment
QH	radical from 1,4-di-tert-butyl catechol	0
Q	1,4-di-tert-butyl ortho quinone	depending on experiment
P	non radical product	0

a) The concentration of O₂ in the headspace is set to an arbitrary high value to ensure that the dissolved O₂ concentration remains constant. This approximation holds because during the experiment only a small fraction of O₂ in the system is consumed. In a typical autoxidation experiment, less than 30% of total O₂ is consumed.

Table A. 2.2 Kinetic scheme considered in numerical fitting of the autoxidation of 1,4-cyclohexadiene (CHD) initiated by AIBN at 30 °C in chlorobenzene.

N	Reaction Equations	Rate Constants (M ⁻¹ S ⁻¹) or Fluxes (Ms ⁻¹)	Notes and references
1	I → HOO	$v = 2.5\text{e-}009^a$	Initiation rate (R_i), depends on experiment
2	R + O ₂ → HOO + B	$k = 5\text{e}+009$	B. Maillard, K. U. Ingold, J. C. Scaiano J. Am. Chem. Soc. 1983, 105, 5095-5099
3	HOO + RH → HOOH + R	$k = 1400$	Howard, J. A.; Ingold, K. U. Can. J. Chem. 1965, 43, 2729–2736
4	HOO + HOO → O ₂ + HOOH	$k = 6.3000\text{e}+008$	Howard, J. A.; Ingold, K. U. Can. J. Chem. 1965, 43, 2729–2736
5	QH ₂ + HOO → QH + HOOH	$k = \text{fit}$	initial guess: $k=1\text{e}6$
6	QH + HOO → Q + HOOH	$k = 2\text{e}9$	assumed
7	QH + HOO → QH ₂ + O ₂	$k = 2\text{e}9$	assumed
8	O _{2g} = O ₂	$k_1 = 1.9\text{e}+6$ $k_2 = 1\text{e}+009$	assumed. Equilibrium constant from O ₂ solubility in benzene.
9	QH+QH→Q+QH ₂	$k = 8\text{e}5$	Tumanskii, B. L.; Solodovnikov, S. P.; Prokof'ev, A. I.; Bubnov, N. N.; Kabachnik, M. I.; Izv. Akad. Nauk SSSR Ser. Khim. 1977, 1309 [from Landolt–Börnstein]
10	Q+HOO = QH+O ₂	$k_1 = \text{fit}$ $k_2 = \text{fit}$	
11	QH + HOO → P	$k = \text{fit}$	initial guess: $k=1\text{e}8$ E. T. Denisov, I. V. Khudyakov Chem. Rev. 1987, 87, 1313-1357

a) constant flux.

Table A. 2.3 Species considered in numerical fitting of the autoxidation of styrene initiated by AIBN at 30 °C in chlorobenzene.

chemical name	symbol used in equations	Initial concentration
I	Initiator	not relevant. Radical initiation is determined directly by Ri.
ROO	styryl peroxy radicals	0
R	styryl alkyl radical	0
O2	dissolved O ₂	1.8e-3
O2g	O2 in the headspace	1 M ^a
RH	styrene	depending on experiment
ROOH	styrene polyperoxide or hydroperoxide	0
QH2	1,4-di-tert-butyl catechol	depending on experiment
QH	radical from 1,4-di-tert-butyl catechol	0
Q	1,4-di-tert-butyl ortho quinone	depending on experiment
HOO	HOO•	0
HOOH	H ₂ O ₂	0
P	non radical product	0

a) The concentration of O₂ in the headspace is set to an arbitrary high value to ensure that the dissolved O₂ concentration remains constant. This approximation holds because during the experiment only a small fraction of O₂ in the system is consumed. In a typical autoxidation experiment, less than 30% of total O₂ is consumed.

Table A. 2.4. Kinetic scheme of the autoxidation of styrene initiated by AIBN at 30 °C in chlorobenzene.

N	Reaction Equations	Rate Constants (M ⁻¹ s ⁻¹) or Fluxes (Ms ⁻¹)	Notes and references
1	I → R	v = 5e-009	Initiation rate (Ri), depends on experiment
2	R + O ₂ → ROO	k = 5e+009	B. Maillard, K. U. Ingold, J. C. Scaiano J. Am. Chem. Soc. 1983, 105, 5095-5099
3	ROO + RH → R + ROOH	k = 41	Howard, J. A.; Ingold, K. U. Can. J. Chem. 1965, 43, 2729
4	ROO + ROO → P	k = 2.1e7	Howard, J. A.; Ingold, K. U. Can. J. Chem. 1965, 43, 2729
5	O2g = O2	k1 = 1.9e+6 k2 = 1e+009	assumed. Equilibrium constant from O2 solubility in benzene.
6	ROO → HOO	k = fit	^a
7	QH2 + ROO → QH + HOOH	fit	
8	QH + ROO → Q + ROOH	k = 2e+009	assumed
9	QH+QH→Q+QH2	k = 8e5	Tumanskii, B. L.; Solodovnikov, S. P.; Prokof'ev, A. I.; Bubnov, N. N.; Kabachnik, M. I.; Izv. Akad. Nauk SSSR Ser. Khim. 1977, 1309 [from Landolt-Börnstein]
10	Q+HOO=QH+O2	k1 = fit k2 = fit	
11	HOO + RH → R + HOOH	k = 41	assumed equal to the reaction of ROO•
12	ROO + HOO → O2 + ROOH	k = 6.3000e+008	assumed equal to the reaction HOO• + HOO•

13	$\text{HOO} + \text{HOO} \rightarrow \text{O}_2 + \text{HOOH}$	$k = 6.3000\text{e}+008$	Howard, J. A.; Ingold, K. U. Can. J. Chem. 1965, 43, 2729–2736
14	$\text{QH}_2 + \text{HOO} \rightarrow \text{QH} + \text{HOOH}$	$k = 1\text{e}6$	assumed equal to the reaction $\text{ROO}^* + \text{QH}_2$
15	$\text{QH} + \text{HOO} \rightarrow \text{Q} + \text{HOOH}$	$k = 2\text{e}9$	assumed
16	$\text{QH} + \text{HOO} \rightarrow \text{QH}_2 + \text{O}_2$	$k = 2\text{e}9$	assumed
17	$\text{QH} + \text{HOO} \rightarrow \text{P}$	$k = 1\text{e}8$	E. T. Denisov, I. V. Khudyakov Chem. Rev. 1987, 87, 1313-1357

a) the formation of HOO^* radicals during styrene autoxidation has been recently demonstrated by Pratt and coworkers (reference 33). This reaction explains the slight retardation of styrene autoxidation by ortho-quinones.

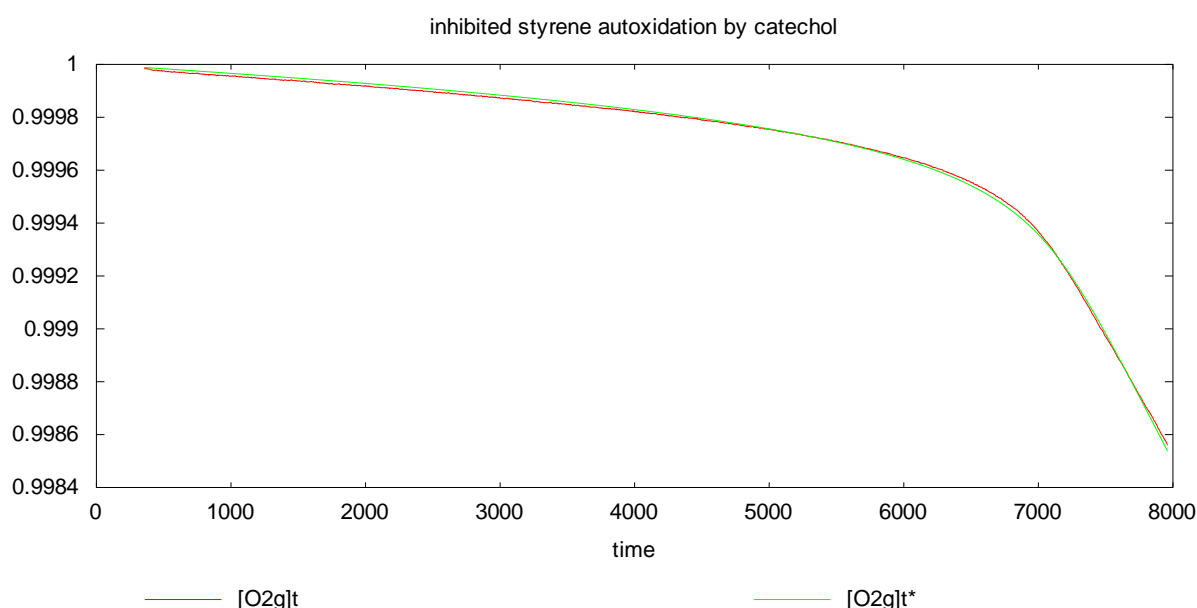


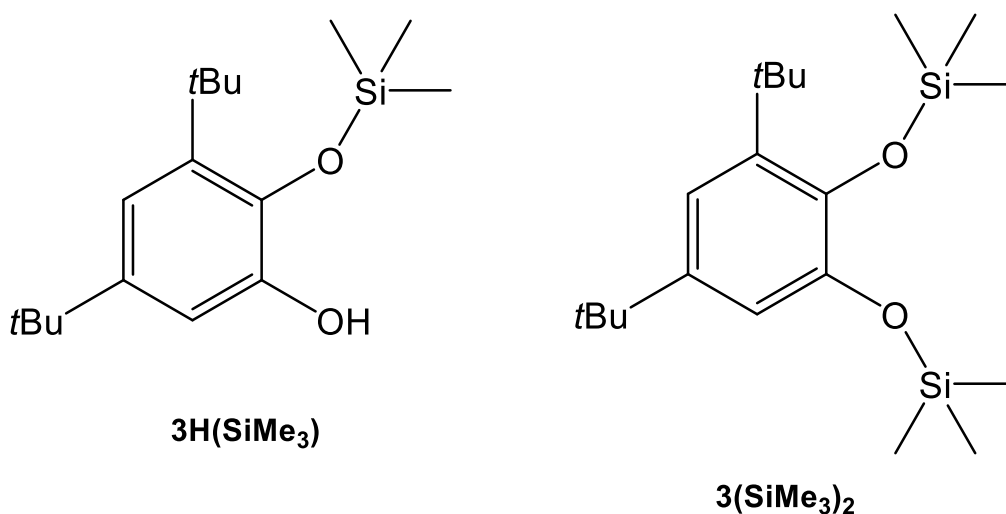
Figure A 2.2 Example of fitting of the autoxidation of styrene inhibited by 3H_2 .

Product analysis of CHD autoxidation initiated by AIBN analyzed by GC-MS.

Materials: Trimethylsilyl-N,N-dimethylcarbamate (TMSDMC, 98%) was purchased from SantaCruzBiotechnology (Dallas, TX, USA)

Derivatization: 3H_2 produced from **3** via autoxidation of CHD in acetonitrile (MeCN) was derivatized by silylating agent, trimethylsilyl-N,N-dimethylcarbamate (TMSDMC). Derivatization reaction of 3H_2 was carried out under standard conditions

for 2 hours and TMSDMC was added in large excess to assure 100% conversion of **3H₂** formed to its silylated derivatives.



Structures of the silylated derivatives **3H₂**,

GC-MS analysis: GC-MS analysis was performed with HP5 capillary column (0.32 mm diameter, 30 m length, 0.25 μ m thickness, Hewlett-Packard) with GC-17A Ver.3 Shimadzu and GCMS-QP5050A Shimadzu mass detector. Mass spectrum was obtained by electron impact ionization mode, scanning from 40 m/z to 650 m/z. Inlet temperature was 280C and oven temperature program was as follows: an initial step starts at 60°C; raising at a rate of 10°C/min to 260°C; then holding at 260°C for 5 min.

GC-FID analysis: GC-FID analysis was performed with HP5 capillary column (0.32 mm diameter, 30 m length, 0.25 μ m thickness, Hewlett-Packard) with Agilent Technologies 7820A GC System. Inlet temperature and oven temperature program were the same as in the case of GC-MS analysis.

Results: One microliter of the reaction mixture was injected through the inlet of GC-MS or GC-FID with split ratio of 2:1. Two significant molecules, **3HSiMe₃** (Mw = 294 Da) and **3(SiMe₃)₂** (Mw = 366 Da) were found. Retention time (RT) of the molecules were 10.75 min and 12.25 min respectively (figure. 2.15). Both molecules were well separated and believed, basing on structural characteristics and mass profiles (figure.

2.17a and 2.17b), to be re-structured products during TMS derivatization originated from hydrogen atom of hydroxyl groups of 3H_2

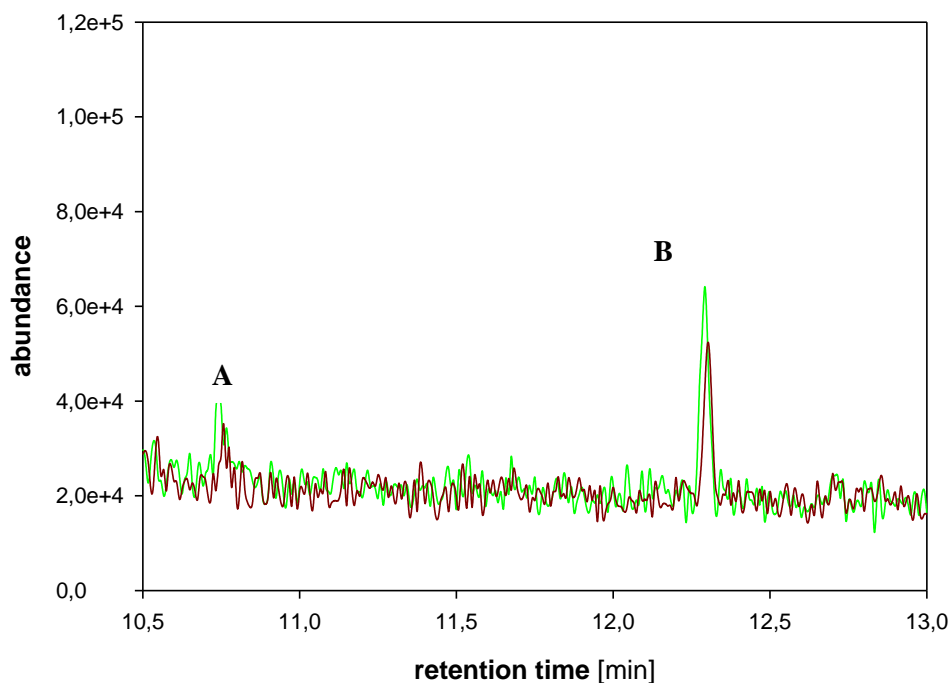


Figure A. 2. 3 Total ion chromatograms (TIC) of derivatization products (A - 3HSiMe_3 ; B - $3(\text{SiMe}_3)_2$) of 3H_2 formed during autoxidation of CHD (0.13 M) initiated by AIBN (0.05 M) in the presence of 3 (6×10^{-5} M) in MeCN at 30°C (brown line) and reference 3H_2 (2×10^{-5} M) in MeCN (green line).

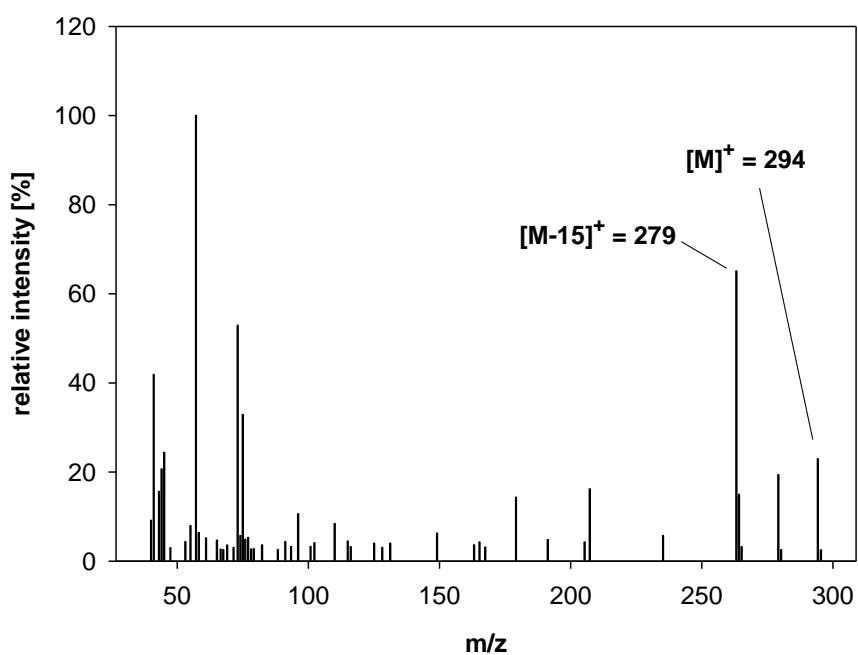


Figure A. 2. 4 Mass pattern of compound **3HSiMe₃** (Mw = 294 Da).

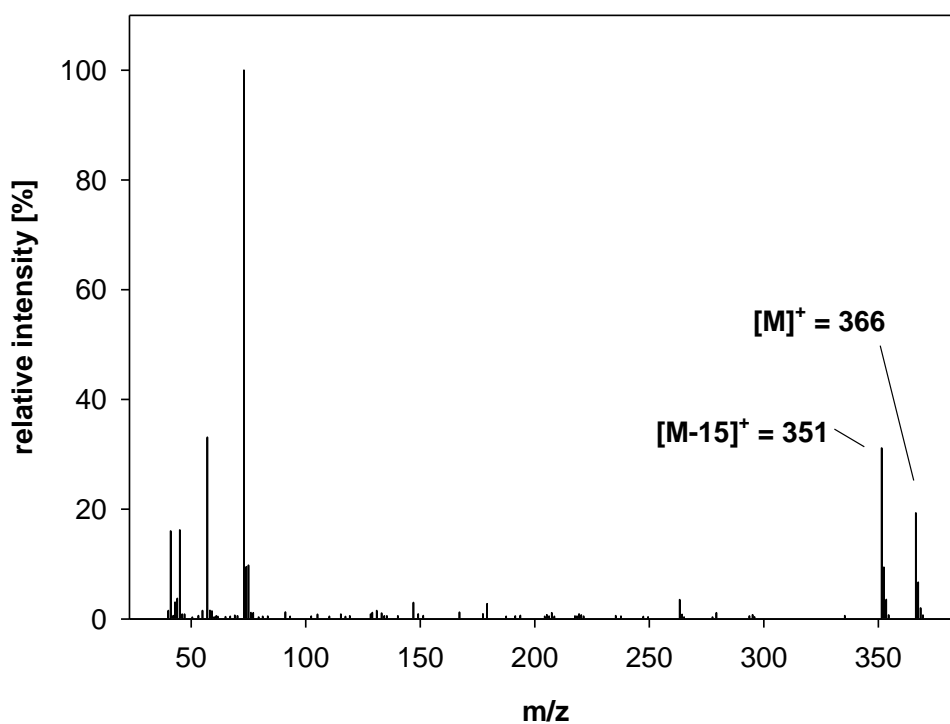


Figure A. 2.5 Mass pattern of compound **3(SiMe₃)₂** (Mw = 366 Da).

GC-FID analysis indicated that during the autoxidation of CHD (0.13 M) in MeCN at 30°C initiated by AIBN (0.05 M) and inhibited by **3** (6×10^{-5} M), the conversion of compound **3** to **3H₂** reached the values of 56%, 77% and 80% after 4, 6 and 17 hours, respectively.

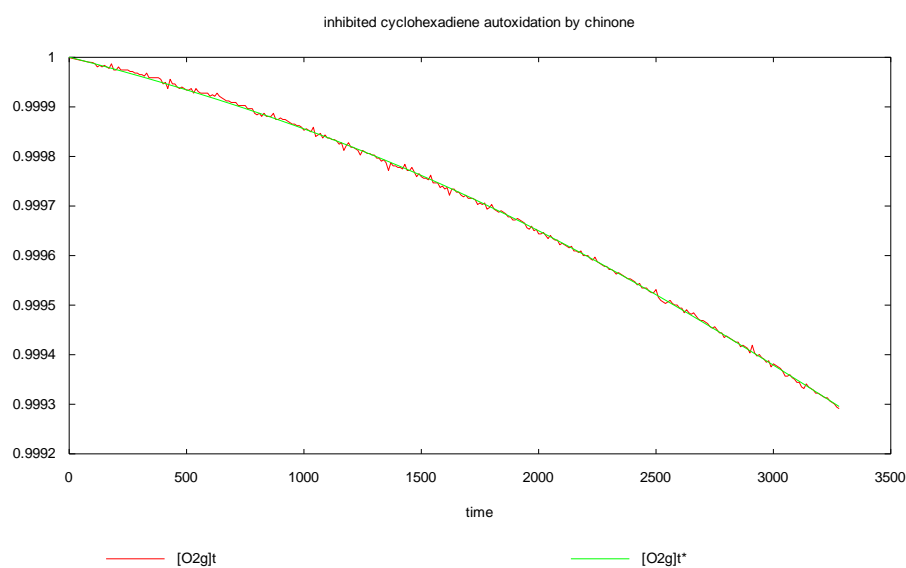


Figure A. 2.6 Example of numerical fitting by Copasi of the O₂ consumption trace (b) reported in figure 2.16.

Dynamic Light Scattering (DLS) analysis of PDA nanoparticles

The determination of the nanoparticles hydrodynamic diameter distributions was carried out through Dynamic Light Scattering measurements employing a Malvern Nano ZS instrument with a 633 nm laser diode. Samples were housed in disposable polystyrene cuvettes of 1 cm optical path length, using water as solvent. The width of DLS hydrodynamic diameter distribution is indicated by PDI (Polydispersion Index). In case of a mono-modal distribution (gaussian) calculated by means of cumulant analysis, $PdI = (\sigma/Z_{avg})^2$, where σ is the width of the distribution and Z_{avg} is average diameter of the particle's population respectively.

	Size (d.nm):	% Intensity:	St Dev (d.nm):
Z-Average (d.nm): 93,37	Peak 1: 98,46	100,0	23,69
Pdl: 0,037	Peak 2: 0,000	0,0	0,000
Intercept: 0,933	Peak 3: 0,000	0,0	0,000

Result quality : Good

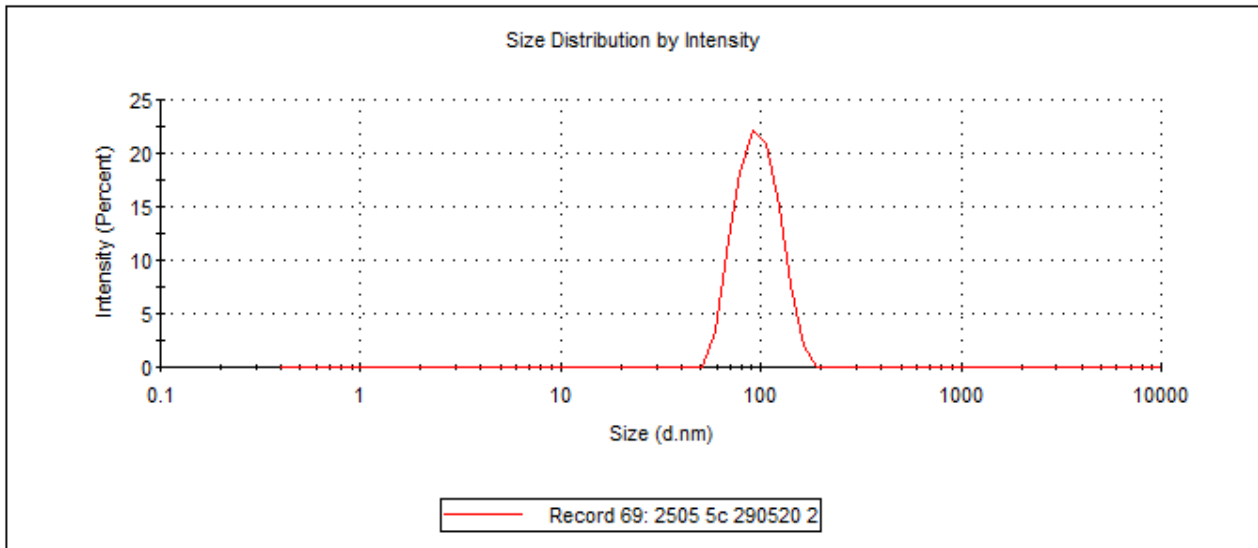


Figure A. 2.7 Dynamic Light Scattering measurement of PDA nanoparticles; size distribution by intensity.

Transmission Electronic Microscopy (TEM) of PDA nanoparticles

A Philips CM 100 transmission electron microscope operating at 80 kV was used. For TEM investigations a Formvar foil supported on conventional copper microgrids (400 mesh) was dried up under vacuum after deposition of a drop of nanoparticles solution diluted with water (1:10).

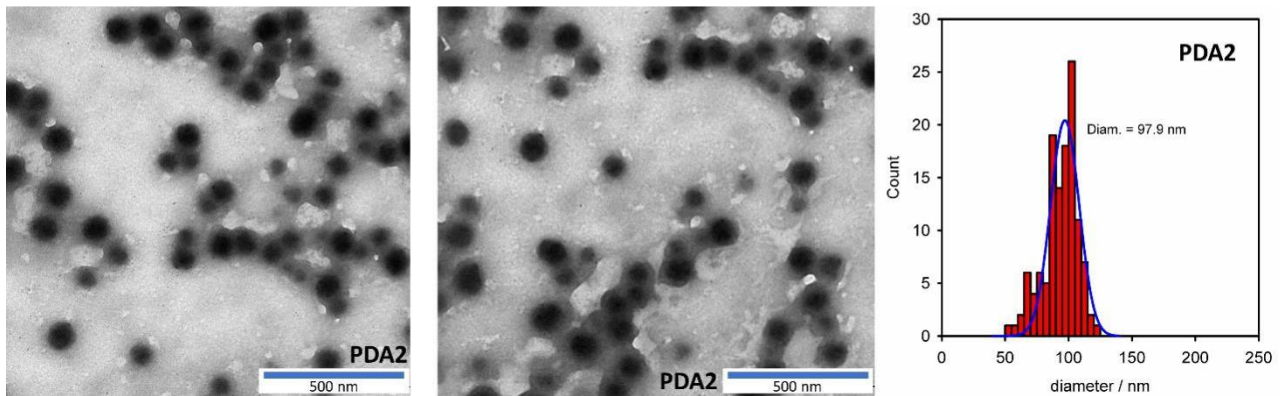
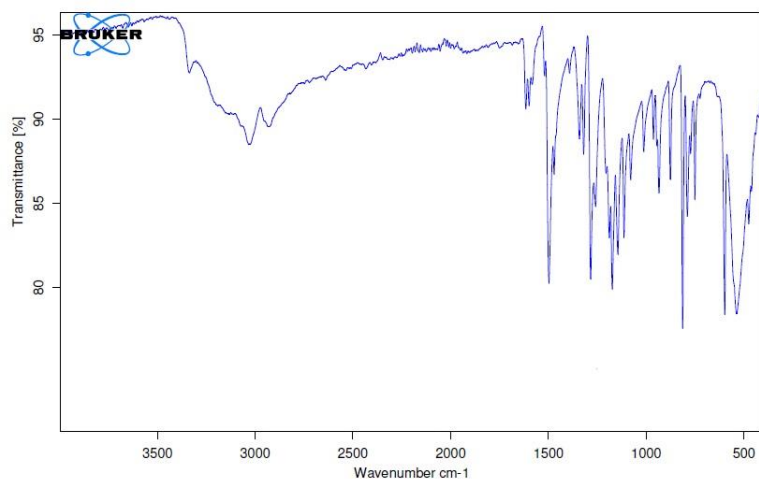
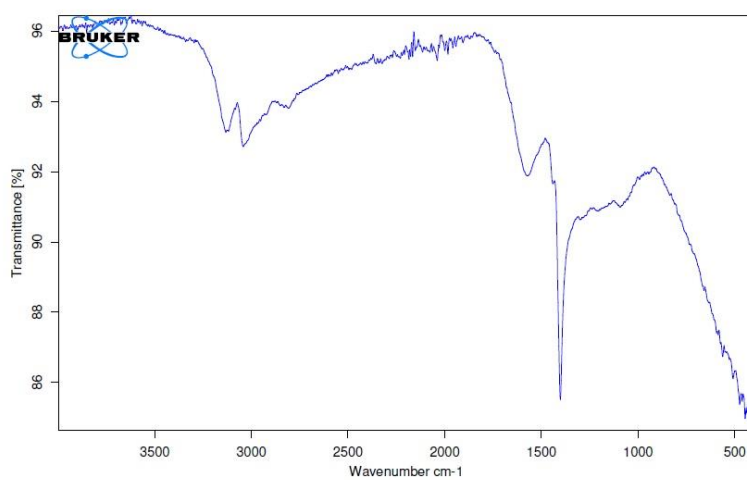


Figure A. 2.8 TEM images of PDA nanoparticles.

A



B



C

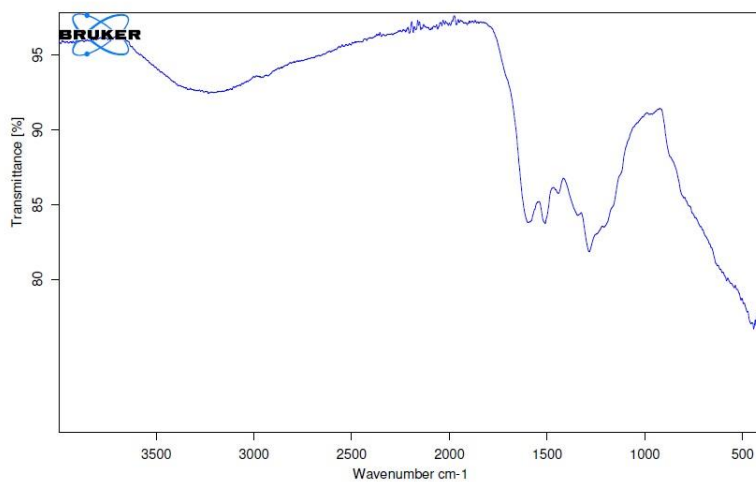


Figure A. 2.9 ATR-FT-IR spectra of: (A) Dopamine HCl (solid); (B) non-purified polydopamine nanoparticles; (C) Purified polydopamine nanoparticles.

References

- [1] Y. Hatefi. The mitochondrial electron transport and oxidative phosphorylation system. *Annual Review of Biochemistry*. 1985, 54, 1015-1069.
- [2] A. E. Senior. ATP synthesis by oxidative phosphorylation. *Physiological Reviews*. 1988, 68(1), 177-231.
- [3] A. J. Kowaltowski, R. F. Castilho, A. E. Vercesi. Mitochondrial permeability transition and oxidative stress. *FEBS Letters*. 2001, 495(1-2), 12-15.
- [4] D. B. Zorov, M. Juhaszova, S. J. Sollott. Mitochondrial reactive oxygen species (ROS) and ROS-induced ROS release. *Physiological Reviews*. 2014, 94(3), 909-950.
- [5] A. A. Dayem, M. K. Hossain, S. B. Lee, K. Kim, S. K. Saha, G. M. Yang, H. Y. Choi, S. G. Cho. The Role of reactive oxygen species (ROS) in the biological activities of metallic nanoparticles. *International journal of molecular sciences. Int. J. Mol. Sci.* 2017, 18(1), 120.
- [6] P. Schröder, J. Krutmann. Environmental oxidative stress – Environmental sources of ROS. In: Grune T. (eds) *Reactions, Processes. The handbook of environmental chemistry*. Springer, Berlin, Heidelberg. 2005, 20, 19-31.
- [7] G. J. Burton, E. Jauniaux. Oxidative stress. *Best Practice & Research Clinical Obstetrics and Gynaecology*. 2011, 25, 287–299.
- [8] B. Halliwell. Reactive Species and Antioxidants. Redox Biology Is a Fundamental Theme of Aerobic Life. *Plant Physiology*. 2006, 141, 312–322.
- [9] J. M. McCord. The evolution of free radicals and oxidative stress. *the american journal of medicine*. 2000, 108, 652-659.
- [10] P. S. Rao, S. Kalva, A. Yerramilli, S. Mamidi. Free radicals and tissue damage: role of antioxidants. *Free Rad. Antiox.* 2011, 11(4), 2-7.
- [11] C. M. Bergamini, S. Gambetti, A. Dondi, C. Cervellati. Oxygen, reactive oxygen species and tissue damage. *Current Pharmaceutical Design*. 2004, 10(14), 1611-1626.
- [12] Z. Liu, Z. Ren, J. Zhang, C. C. Chuang, E. Kandaswamy, T. Zhou, L. Zuo. Role of ROS and nutritional antioxidants in human diseases. *Front. Physiol.* 2018, 9(477), 1-14.
- [13] P. Davalli, T. Mitic, A. Caporali, A. Lauriola, and D. D'Arca. ROS, cell senescence, and novel molecular mechanisms in aging and age-related diseases. *Hindawi Publishing Corporation Oxidative Medicine and Cellular Longevity*. 2016, ID: 3565127.
- [14] M. Fransen, M. Nordgren, B. Wang, O. Apanasets. Role of peroxisomes in ROS/RNS-metabolism: Implications for human disease. *Biochimica et Biophysica Acta (BBA) - Molecular Basis of Disease*. 2012, 1822(9), 1363-1373.
- [15] P. Cejas, E. Casado, C. B. Iniesta, J. D. Castro, E. Espinosa, A. Redondo, M. Sereno, M. Á. García-Cabezas, J. A. F. Vara, A. Domínguez-Cáceres, R. Perona, M. González-Barón. Implications of oxidative stress and cell membrane lipid peroxidation in human cancer. *Cancer Causes Control*, 2004, 15, 707–719.
- [16] T. A. Dix, J. Aikens. Mechanisms and biological relevance of lipid peroxidation initiation. *Chem. Res. Toxicol.* 1993, 6, 2-18.

- [17] R. Amorati, G. F. Pedulli, D. A. Pratt, L. Valgimigli. TEMPO reacts with oxygen-centered radicals under acidic conditions. *Chem. Commun.* 2010, **46**,5139-5141.
- [18] R. Amorati, L. Valgimigli. Methods to measure the antioxidant activity of phytochemicals and plant extracts. *J. Agric. Food Chem.* 2018, **66**(13),3324–3329.
- [19] E.R. Stadtman . Oxidation of free amino acids and amino acid residues in proteins by radiolysis and by metal-catalyzed reactions. *Annual Review of Biochemistry*, 1993, **62**,797-821.
- [20] E. R Stadtman. Free radical mediated oxidation of proteins. In: Ozben T, ed. *Free Radicals, Oxidative Stress, and Antioxidants. Pathological and Physiological Significance*. NATO ASI Series, Series A: Life Sciences, New York: Plenum Press, 1997, 296, 51-65.
- [21] W.M. Garrison. Reaction mechanisms in the radiolysis of peptides, polypeptides, and proteins. *Chern Rev.*, 1987, **87**, 381-98.
- [22] E. R. Stadtman, R. L. Levine. Free radical-mediated oxidation of free amino acids and amino acid residues in proteins. *Amino Acids*, 2003, **25**, 207–218.
- [23] B. S. Berlett, E. R. Stadtman. Protein oxidation in aging, disease, and oxidative stress. *the journal of biological chemistry*. 1997, **272**(33), 20313–20316.
- [24] E. R. Stadtman. Protein oxidation and aging. *Free radical Research*. 2006, **40**(12),1250-1258.
- [25] J. Cadet, T. Delatour, T. Douki, D. Gasparutto, J. P. Pouget, J. L. Ravanat, S. Sauvaigo. Hydroxyl radicals and DNA base damage. *Mutation Research/Fundamental and Molecular Mechanisms of Mutagenesis*. 1999, **424**(1-2), 9-21.
- [26] A. Sapone, B. Gustavino, M. Monfrinotti, D. Canistro, M. Broccoli, L. Pozzetti, A. Affatato, L. Valgimigli, G. CantelliForti, G. F. Pedulli, G. L. Biagi, S. Z. Abdel-Rahman, M. Paolini. Perturbation of cytochrome P450, generation of oxidative stress and induction of DNA damage in *Cyprinus carpio* exposed *in situ* to potable surface water. *Mutation Research/Genetic Toxicology and Environmental Mutagenesis*. 2007, **626**(1-2), 143-154.
- [27] J. Cadet, S. Loft, R. Olinski, M. D. Evans, K. Bialkowski, J. R. Wagner, P. C. Dedon, P. Møller, M. M. Greenberg, M. S. Cooke . Biologically relevant oxidants and terminology, classification and nomenclature of oxidatively generated damage to nucleobases and 2-deoxyribose in nucleic acids. *Free radical Research*. 2012, **46**(4), 367-381.
- [28] D. T. Sawyer, J. S. Valentine. How super is superoxide? *Acc. Chem. Res.* 1981, **14**, 393-400.
- [29] Y. A. Iian, D. Meisel, G. Czapski. The redox potential of the $O_2-O_2^{\cdot -}$ system in aqueous media. *Israel J. Chem.* 1974, **12**(4),891-895.
- [30] B. H. J. Bielski. Reevaluation of the spectral and kinetic properties of HOO^{\cdot} and $O_2^{\cdot -}$ free radicals. *Photochem. Photobiol.* 1978, **28**(4-5), 645-649.
- [31] D. Behar, G. Czapski, J. Rabani, L. M. Dorfman, H. A. Schwartz. The acid dissociation constant and decay kinetics of the perhydroxyl radical1. *J. Phys. Chem.* 1970, **74**(17), 3209-3213.

- [32] B. H. J. Bielski, A. O. Allen. Mechanism of the disproportionation of superoxide radicals. *The Journal of Physical Chemistry*, 1977, 81(11),1048-1050.
- [33] Y. Zheng, Y. Jiao, M. Jaroniec, S. Z. Qiao. Advancing the electrochemistry of the hydrogen - evolution reaction through combining experiment and theory. *Angew. Chem. Int. Ed.* 2015, 54(1), 52–65.
- [34] C. R. Chang, X. F. Yang, B. Long, J. Li. Water-promoted mechanism of alcohol oxidation on an Au(111) surface: understanding the catalytic behavior of bulk gold. *ACS Catal.* 2013, 3(8), 1693–1699.
- [35] M. Kumar, J. S. Francisco. Red - light - induced decomposition of an organic peroxy radical: a new source of the HOO· Radical. *Angew. Chem.* 2015, 127(52), 15937–15940.
- [36] M. Anglada, M. Martins-Costa, J. S. Francisco, M. F. Ruiz-Ljpez. Interconnection of reactive oxygen species chemistry across the interfaces of atmospheric, environmental, and biological processes. *Acc. Chem. Res.* 2015, 48(3), 575–583.
- [37] P. Campomanes, U. Rothlisberger, M. Alfonso-Prieto, C. Rovira. The molecular mechanism of the catalase-like activity in horseradish peroxidase. *J. Am. Chem. Soc.* 2015, 137(34), 11170–11178.
- [38] J. M. McCord, I. Fridovich. Superoxide dismutase an enzymic function for erythrocuprein (hemocuprein). *The Journal of Biological Chemistry*. 1969, 244, 6049-6055.
- [39] R. A. Weisiger, I. Fridovich. Mitochondrial superoxide dismutase site of synthesis and intramitochondrial localization. *the journal of biological chemistry*. 248, 1973, 4793-4796.
- [40] G. Czapski. Reaction of ·OH. *Methods in Enzymology*. 1984, 105(984), 209-215.
- [41] J. J. Warren, T. A. Tronic, J. M. Mayer. Thermochemistry of proton-coupled electron transfer reagents and its implications. *Chem. Rev.* 2010, 110(12), 6961–7001.
- [42] B. H. Bielski, R. L. Arudi, M. W. Sutherland. A study of the reactivity of HO₂/O₂⁻ with unsaturated fatty acids. *The Journal of Biological Chemistry*, 1983, 258, 4759-4761.
- [43] B. Min, D. U. Ahn. Mechanism of lipid peroxidation in meat and meat products - a review. *Food Sci. Biotechnol.* 2005, 14(1), 152-163.
- [44] W. BOB, M. Saran, G. Czapski. biological and clinical aspects of superoxide and superoxide dismutase. (Bannister, W. H., and Bannister, J. V., eds) Elsevier. North-Holland, New York, 1980,1-3.
- [45] J. Cedrowski, G. Litwinienko, A. Baschieri, R. Amorati. Hydroperoxyl radicals (HOO•): vitamin e regeneration and h-bond effects on the hydrogen atom transfer. *Chemistry-A European Journal*, 22(46), 2016,16441-16445.
- [46] A. Boveris. Mitochondrial production of superoxide radical and hydrogen peroxide. Tissue hypoxia and ischemia Part of the Advances in Experimental Medicine and Biology book series, Springer, Boston, MA. 1977,78, 67-82.
- [47] K. M. Mohazzab, M. S. Wolin. Properties of a superoxide anion-generating microsomal NADH oxidoreductase, a potential pulmonary artery PO₂ sensor.

American Journal of Physiology-Lung Cellular and Molecular Physiology. 1994, 267(6), L823-L831.

[48] M. Haumann, P. Liebisch, C. Müller, M. Barra, M. Grabolle, H. Dau. Photosynthetic O₂ formation tracked by time-resolved X-ray experiments. *Science*. 2005, 310(5750), 1019-1021.

[49] R. Hille, T. Nishino. Xanthine oxidase and xanthine dehydrogenase. *The FASEB Journal*. 1995, 9(11), 995-1003.

[50] Y. Bromberg, E. Pick. Activation of NADPH-dependent superoxide production in a cell-free system by sodium dodecyl sulfate. *The Journal of Biological Chemistry*. 1985, 260 (25), 13539-13545.

[51] M. D. Brand, C. Affourtit, T. C. Esteves, K. Green, A. J. Lambert, S. Miwa, J. L. Pakay, N. Parker. Mitochondrial superoxide: production, biological effects, and activation of uncoupling proteins. *Free Radical Biology and Medicine*. 2004, 37(6), 755-767.

[52] G.R. Hodges, K.U. Ingold. Superoxide, amine buffers and tetranitromethane: A novel free radical chain reaction. *Free Radical Research*. 2000, 33(5), 547-550.

[53] S. Das, M. N. Schuchmann, H. P. Schuchmann, C. V. Sonntag. The production of the superoxide radical anion by the OH radical - induced oxidation of trimethylamine in oxygenated aqueous solution. The kinetics of the hydrolysis of (hydroxymethyl)dimethylamine. *Chemische Berichte*. 1987, 120(3), 319-323.

[54] M. N. Schuchmann, H. P. Schuchmann, C. V. Sonntag. Hydroxyl radical induced oxidation of acetaldehyde dimethyl acetal in oxygenated aqueous solution. Rapid O₂⁻ release from the CH₃C(OCH₃)₂O₂• Radical. *J. Am. Chem. Soc.* 1990, 112, 403-407.

[55] K. U. Ingold, T. Paul, M. J. Young, L. Doiron. Invention of the first azo compound to serve as a superoxide thermal source under physiological conditions: concept, synthesis, and chemical properties. *J. Am. Chem. Soc.* 1997, 119(50), 12364–12365.

[56] K. G. Konya, T. Paul, S. Lin, J. Lusztyk, K. U. Ingold. Laser flash photolysis studies on the first superoxide thermal source. First direct measurements of the rates of solvent-assisted 1,2-hydrogen atom shifts and a proposed new mechanism for this unusual rearrangement. *J. Am. Chem. Soc.* 2000, 122(31), 7518–7527.

[57] M. N. Schuchmann, C.V. Sonntag. hydroxyl radical induced oxidation of diethyl ether in oxygenated aqueous solution. a product and pulse radiolysis study. *J. Phys. Chem.* 1982, 86, 1995-2000.

[58] E. Bothe, M. N. Schuchmann, D. Schulte-Frohlinde, C.V. Sonntag. HOO• elimination from α-hydroxyalkylperoxyl radicals in aqueous solution. *Photochemistry and Photobiology*, 1978, 28(4-5), 639-643.

[59] E. Bothe, G. Behrens, D. Schulte-Frohlinde. Mechanism of the first order decay of 2-hydroxy-propyl-2-peroxyl radicals and of O₂⁻ formation in aqueous solution. *Zeitschrift für Naturforschung B*. 2014, 32(8), 886-889.

[60] R. J. Wilson, A. E. Beezer, J. C. Mitchell. A kinetic study of the oxidation of L-ascorbic acid (vitamin C) in solution using an isothermal microcalorimeter. *Thermochimica Acta*. 1995, 264(15), 27-40.

- [61] O. Miyawaki, T. Sugiyama, E. Inoue. Kinetic analysis of the oxidation of ascorbic acid in an open reactor with gas bubbling. *Japan Journal of Food Engineering*. 17(2), 2016, 51 – 55.
- [62] M. Scarpa, R. Stevanato, P. Viglino, A. Rigo. Superoxide ion as active intermediate in the autoxidation of ascorbate by molecular oxygen. *The Journal of Biological Chemistry*. 1983, 258(11), 6695-6697.
- [63] C. J. Doona, K. Kustin. Kinetics and Mechanism of Pyrogallol Autoxidation: Calibration of the Dynamic Response of an Oxygen Electrode. *International journal of chemical kinetics* 1993, 25(4),239-247.
- [64] S. Marklund and G. Marklund. involvement of the superoxide anion radical in the autoxidation of pyrogallol and a convenient assay for superoxide dismutase. *Eur. J. Biochem.* 1974, 47, 469-474.
- [65] R. Gao, Z. Yuan, Z. Zhao, X. Gao. Mechanism of pyrogallol autoxidation and determination of superoxide dismutase enzyme activity. *Bioelectrochemistry and Bioenergetics*. 1998, 45(1), 41-45.
- [66] D. J. Deeble, B. J. Parsons, G. O. Phillips, H. P. Schuchmann, C. V. Sonntag. Superoxide radical reactions in aqueous solutions of pyrogallol and n-propyl gallate : the involvement of phenoxyl radicals. A pulse radiolysis study. *Int. J. Radiat. Biol.* 1988, 54(2), 179-193.
- [67] O. I. Mióle, M. T. Nenadovic. Pulse radiolytic investigations of some peroxyhydroxycyclohexadienyl radicals. *The Journal of Physical Chemistry*, 1976, 80(9), 940-944.
- [68] T. Mashino, I. Fridovich. Superoxide radical initiates the autoxidation of dihydroxyacetone. *Archives of Biochemistry and Biophysics*. 1987, 254(2),547-551.
- [69] A. Okado-Matsumoto, I. Fridovich. The Role of α , β -dicarbonyl compounds in the toxicity of short chain sugars-glycolaldehyde. *The Journal of Biological Chemistry*. 2000, 275, 34853-34857.
- [70] W. F. Graier, S. Simecek, W. R. Kukovetz, G. M. Kostner. High D-glucose-induced changes in endothelial Ca^{2+} /EDRF signaling are due to generation of superoxide anions. *Diabetes*. 1996, 45(10), 1386-1395.
- [71] E. Bothe, D. Schulte-Frohlinde, C. V. Sonntag. Radiation chemistry of carbohydrates. Part 16. Kinetics of HOO elimination from peroxy radicals derived from glucose and polyhydric alcohols. *J. Chem. Soc., Perkin Trans.* 1978, 2(5), 416-420.
- [72] M. N. Schuchmann, C. V. Sonntag. Reactions of ozone with D-glucose in oxygenated aqueous solution-direct action and hydroxyl radical pathway), *Aqua (London)*. 1989, 38(5), 311-317.
- [73] S. Abramovitch, J. Rabani. Pulse radiolytic investigations of peroxy radicals in aqueous solutions of acetate and glycine. *J. Phys. Chem.* 1976, 80(14), 1562- 1565.
- [74] C. V. Sonntag, H. P. Schuchmann. The elucidation of peroxy radical reactions in aqueous solution with the help of radiation-chemical methods. *Ange.Chem. Int.* 1991, 30(10),1229-1253.

- [75] J. Mieden, M. N. Schuchmann, C. V. Sonntag. Acid-base properties of peptide peroxy radicals in aqueous solution. *Free Radical Res. Commun.* 1989, 6(2-3), 127-128.
- [76] E. Hayon, M. Simic. Pulse radiolysis study of cyclic peptides in aqueous solution. absorption spectrum of the peptide radical -NHCHCO-. *J. Am. Chem. Soc.* 1971, 93(25),6781-6786.
- [77] H. Y. Chen, S. Jang, T. R. Jinn, J.Y.Chang, H. F. Lu, F.Y. Li. Oxygen radical-mediated oxidation reactions of an alanine peptide motif - density functional theory and transition state theory study. *Chemistry Central Journal.* 2012, 6, 33.
- [78] M. Kirsch, H. G. Korth, V. Stenert, R. Sustmann, H. D. Groot. The autoxidation of tetrahydrobiopterin revisited/Proof of superoxide formation from reaction of tetrahydrobiopterin with molecular oxygen. *The Journal of Biological Chemistry.* 2003, 278(27), 24481–24490.
- [79] N, Zhang, H. P. Schuchmann, C. V. Sonntag. The reaction of superoxide radical anion with dithiothreitol: a chain process. *J. Phys. Chem.* 1991, 95, 4718-4722.
- [80] C. Crean, N. E. Geacintov, V. Shafirovich. Pathways of arachidonic acid peroxy radical reactions and product formation with guanine radicals. *Chem. Res. Toxicol.* 21(2), 2008, 358–373.
- [81] E. M. Pliss, V. A. Machtin, A. M. Grobov, R. E. Pliss, A. V. Sirick. Kinetics and Mechanism of Radical - Chain Oxidation of 1,2 - Substituted Ethylene and 1,4 - Substituted Butadiene - 1,3. *Int. J. Chem. Kinet.* 2017, 49(3), 173–181.
- [82] J. A. Howard, K. U. Ingold. Absolute rate constants for hydrocarbon autoxidation. VI. Alkyl aromatic and olefinic hydrocarbons. *Can. J. Chem.* 1967, 45, 785–792.
- [83] A. Bromberg, K. A. Muszkat. Oxidation of 4a,4b-dihydrophenanthrenes. I. Kinetics of the thermal reaction of 9,10-cyclopentano-4a,4b-dihydrophenanthrene with oxygen. *Journal of the American Chemical Society.* 1969, 91(11),2860-2866.
- [84] K. A. Muszkat, Ernst Fischer. Structure, Spectra, Photochemistry, and Thermal Reactions of the 4a,4b-Dihydrophenanthrenes. *J. Chem. Soc. B*, 1967, 0, 662-678.
- [85] P. M. Wood. The redox potential of the system oxygen-superoxide. *FEBS letters.* 1974, 44(1), 22-24.
- [86] A. Baschieri, L. Valgimigli, S. Gabbanini, G. A. DiLabio, E. Romero-Montalvo, R. Amorati. Extremely fast hydrogen atom transfer between nitroxides and HOO· radicals and implication for catalytic coantioxidant systems. *J. Am. Chem. Soc.* 2018, 140(32), 10354–10362.
- [87] J. F. Poon, O. Zilka, D. A. Pratt. Potent ferroptosis inhibitors can catalyze the cross-dismutation of phospholipid-derived peroxy radicals and hydroperoxy radicals. *J. Am. Chem. Soc.* 2020, 142(33), 14331–14342.
- [88] F. Bakkali, S. Averbeck, D. Averbeck, M. Idaomar. Biological effects of essential oils – A review. *Food and Chemical Toxicology*, 2008, 46 (2), 446–475.
- [89] M. Pateiro, F. J. Barba, R. Dominguez, A. S. Sant'Ana, A. M. Khaneghah, M. Gavahian, B. Gómez, J. M. Lorenzo. Essential oils as natural additives to prevent oxidation reactions in meat and meat products: A review. *Food Research International*, 2018, 113, 156-166.

- [90] A. Baschieri, M. D. Ajvazi, J. L. F. Tonfack, L. Valgimigli, R. Amorati. Explaining the antioxidant activity of some common non-phenolic components of essential oils. *Food Chemistry*, 2017, 232, 656-663.
- [91] T. Barboni, F. Luro, N. Chiaramonti, J.-N. Desjobert, A. Muselli, J. Costa. Volatile composition of hybrids Citrus juices by headspace solid-phase micro extraction/gas chromatography/mass spectrometry. *Food Chemistry*, 2009, 116, 382–390
- [92] A. De Lisi, L. Tedone, V. Montesano, G. Sarli, D. Negro. Chemical characterisation of thymus populations belonging from Southern Italy. *Food Chemistry*, 2011, 125, 1284–1286.
- [93] M. Bendahou, A. Muselli, M. Grignon-Dubois, M. Benyoucef, J.-M. Desjobert, A.-F. Bernardini, J. Costa. Antimicrobial activity and chemical composition of *Origanum glandulosum* Desf. essential oil and extract obtained by microwave extraction: Comparison with hydrodistillation. *Food Chemistry*, 2008, 106, 132–139.
- [94] T. R. Ramalho, M. T. Oliveira, A. L. Lima, C. R. Bezerra-Santos, M. R. Piuvezam. Gamma-terpinene modulates acute inflammatory response in mice. *Planta Medica*, 2015, 81(14), 1248-1254.
- [95] M. C. Foti, K. U. Ingold. Mechanism of inhibition of lipid peroxidation by γ -terpinene, an unusual and potentially useful hydrocarbon antioxidant. *Journal of Agricultural and Food Chemistry*, 2003, 51, 2758–2765.
- [96] B. Dimitrios, Sources of natural phenolic antioxidants. *Trends in Food Science & Technology*, 2006, 17(9), 505-512.
- [97] S. Maqsood, S. Benjakul, A. Abushelaibi, A. Alam. Phenolic compounds and plant phenolic extracts as natural antioxidants in prevention of lipid oxidation in seafood: A detailed review. *Comprehensive Reviews in Food Science and Food Safety*, 2014, 13(6), 1125-1140.
- [98] E. Choe, D. B. Min. Mechanisms of Antioxidants in the Oxidation of Foods. *Comprehensive Reviews in Food Science and Food Safety*, 2009, 8, 345-358.
- [99] P. Jin, X. Wu, F. Xu, X. Wang, J. Wang, Y. Zheng. Enhancing Antioxidant Capacity and Reducing Decay of Chinese Bayberries by Essential Oils. *J. Agric. Food Chem.* 2012, 60, 3769–3775.
- [100] H. Johansson, D. Shanks, L. Engman, R. Amorati, G. F. Pedulli, L. Valgimigli. Long-lasting antioxidant protection: a regenerable bha analogue. *J. Org. Chem.*, 2010, 75(22), 7535-7541.
- [101] R. Amorati, G. F. Pedulli, L. Valgimigli, Kinetic and thermodynamic aspects of the chain-breaking antioxidant activity of ascorbic acid derivatives in non-aqueous media. *Organic & Biomolecular Chemistry*, 2011, 9(10), 3792-3800.
- [102] L. Valgimigli, D. Bartolomei, R. Amorati, E. Haidasz, J. J. Hanthorn, S. J. Nara, J. Brinkhorst, D. A. Pratt. (2013). 3-Pyridinols and 5-pyrimidinols: Tailor-made for use in synergistic radical-trapping co-antioxidant systems. *Beilstein J. Org. Chem.* 2013, 9, 2781–2792.
- [103] E. Niki, T. Saito, A. Kawakami, Y. Kamiya. Inhibition of oxidation of methyl linoleate in solution by vitamin E and vitamin C. *J. Biol. Chem.*, 1984, 259, 4177–4182.

- [104] A. Baschieri, R. Pizzol, Y. Guo, R. Amorati, L. Valgimigli. Calibration of squalene, p-cymene, and sunflower oil as standard oxidizable substrates for quantitative antioxidant testing. *Journal of Agricultural and Food Chemistry*, 2019, 67(24), 6902-6910.
- [105] A. D. Meinhart, F. M. Damin, L. Caldeirão, M. de Jesus Filho, L. C. da Silva, L. da Silva Constant, J. T. Filho, R. Wagner, H. T. Godoy. Chlorogenic and caffeic acids in 64 fruits consumed in Brazil. *Food Chemistry*, 2019, 286, 51–63.
- [106] J. H. Chen, C. T. Ho. Antioxidant Activities of Caffeic Acid and Its Related Hydroxycinnamic Acid Compounds. *J. Agric. Food Chem.*, 1997, 45, 2374–2378.
- [107] S. Markovic', J. Tošovic. Comparative study of the antioxidative activities of caffeoylquinic and caffeic acids. *Food Chemistry*, 2016, 210, 585–592.
- [108] R. Amorati, A. Baschieri, G. Morroni, R. Gambino, L. Valgimigli. Peroxyl Radical Reactions in Water Solution: A Gym for Proton-Coupled Electron-Transfer Theories. *Chemistry-A European Journal*, 2016, 22, 7924-7934.
- [109] R. Amorati, L. Valgimigli. Advantages and limitations of common testing methods for antioxidants. *Free Radic Res*, 2015, 49(5), 633-649.
- [110] M. D. Guillen, E. Goicoechea. Formation of oxygenated α,β -unsaturated aldehydes and other toxic compounds in sunflower oil oxidation at room temperature in closed receptacles. *Food Chemistry*, 2008, 111(1), 157-164.
- [111] S. A. Smith, R. E. King, D. B. Min. Oxidative and thermal stabilities of genetically modified high oleic sunflower oil. *Food Chemistry*, 2007, 102(4), 1208-1213.
- [112] L. H. Reddy, P. Couvreur. Squalene: A natural triterpene for use in disease management and therapy. *Adv. Drug Delivery Rev.* 2009, 61, 1412–1426.
- [113] R. Amorati, L. Valgimigli, P. Dinér, K. Bakhtiari, M. Saeedi, Engman, L. Multi-faceted Reactivity of Alkyltellurophenols Towards Peroxyl Radicals: Catalytic Antioxidant Versus Thiol-Depletion Effect. *Chemistry-A European Journal*, 2013, 19, 7510-7522.
- [114] R. Amorati, F. Ferroni, M. Lucarini, G. F. Pedulli, L. Valgimigli. A Quantitative Approach to the Recycling of α -Tocopherol by Coantioxidants. *J. Org. Chem.* 2002, 67(26), 9295-9303.
- [115] R. Matera, S. Gabbanini, S. Berretti, R. Amorati, G. R. De Nicola, R. Iori, L. Valgimigli. Acylated anthocyanins from sprouts of *Raphanus sativus* cv. Sango: Isolation, structure elucidation and antioxidant activity. *Food Chemistry*, 2015, 166, 397-406.
- [116] P. Pedrielli, L. H. Skibsted. Antioxidant synergy and regeneration effect of quercetin, (–)-epicatechin, and (+)-catechin on α -tocopherol in homogeneous solutions of peroxidating methyl linoleate. *Journal of Agriculture and Food Chemistry*, 2002, 50, 7138–7144.
- [117] U. Thiyam, H. Stöckmann, K. Schwarz. Antioxidant activity of rapeseed phenolics and their interactions with tocopherols during lipid oxidation. *Journal of the American Oil Chemists' Society*, 2006, 83, 523–528.

- [118] A. Baschieri, R. Amorati, L. Valgimigli, L. Sambri. 1-Methyl-1,4-cyclohexadiene as a Traceless Reducing Agent for the Synthesis of Catechols and Hydroquinones. *J. Org. Chem.* 2019, *84*, 13655-13664.
- [119] D. Lingwood, K. Simons. Lipid rafts as a membrane-organizing principle. *Science*, 2010, *327*(5961), 46-50.
- [120] A. B. Falowo, P. O. Fayemi, V. Muchenje. Natural antioxidants against lipid-protein oxidative deterioration in meat and meat products: A review. *Food Research International*, 2014, *64*, 171-181.
- [121] J. H. Ryu, P. B. Messersmith, H. Lee. Polydopamine Surface Chemistry: A Decade of Discovery. *ACS Appl. Mater. Interfaces*. 2018, *10*, 7523–7540.
- [122] Y. Liu, K. Ai, L. Lu. Polydopamine and its derivative materials: synthesis and promising applications in energy, environmental, and biomedical fields. *Chem. Rev.* 2014, *114*, 5057-5115.
- [123] J. Liebscher, R. Mrówczyński, H. A. Scheidt, C. Filip, N. D. Hādade, R. Turcu, A. Bende, S. Beck. Structure of polydopamine: a never-ending story? *Langmuir* 2013, *29*, 10539-10548.
- [124] P. Manini, V. Lino, P. Franchi, G. Gentile, T. Sibillano, C. Giannini, E. Picardi, A. Napolitano. L. Valgimigli, C. Chiappe, M. D'Ischia. A Robust Fungal Allomelanin Mimic: An Antioxidant and Potent π - Electron Donor with Free - Radical Properties that can be Tuned by Ionic Liquids. *Chem. Plus. Chem.* 2019, *84*, 1331-1337.
- [125] L. Panzella, G. Gentile, G. D'Errico, N. F. D. Vecchia, M. E. Errico, A. Napolitano, C. Carfagna, M. D'Ischia. A typical Structural and π - Electron Features of a Melanin Polymer That Lead to Superior Free - Radical - Scavenging Properties. *Angew. Chem. Int. Ed.* 2013, *52*, 12684 –12687.
- [126] I. Carballo-Carbajal, A. Laguna, J. Romero-Giménez, T. Cuadros, J. Bové, M. Martínez-Vicente, A. Parent, M. Gonzalez-Sepulveda, N. Peñuelas, A. Torra, B. Rodríguez-Galván, A. Ballabio, T. Hasegawa, A. Bortolozzi, E. Gelpi, M. Vila. Brain tyrosinase overexpression implicates age-dependent neuromelanin production in Parkinson's disease pathogenesis. *Nat. Commun.* 2019, *10*, 1-19.
- [127] E. Monzani, S. Nicolis, S. Dell'Acqua, A. Capucciati, C. Bacchella, F. A. Zucca, E. V. Mosharov, D. Sulzer, L. Zecca, L. Casella. Dopamine, Oxidative Stress and Protein–Quinone Modifications in Parkinson's and Other Neurodegenerative Diseases. *Angew. Chem. Int. Ed.* 2019, *58*, 6512-6527.
- [128] P. Tang, L. Han, P. Li, Z. Jia, K. Wang, H. Zhang, H. Tan, T. Guo, X. Lu. Mussel-Inspired Electroactive and Antioxidative Scaffolds with Incorporation of Polydopamine-Reduced Graphene Oxide for Enhancing Skin Wound Healing. *ACS Appl. Mater. Interfaces*. 2019, *11*, 7703–7714.
- [129] X. Bao, J. Zhao, J. Sun, M. Hu, X. Yang. Polydopamine Nanoparticles as Efficient Scavengers for Reactive Oxygen Species in Periodontal Disease. *ACS Nano*. 2018, *12*, 8882-8892.
- [130] K.-Y. Ju, Y. Lee, S. Lee, S. B. Park, J.-K. Lee. Bioinspired Polymerization of Dopamine to Generate Melanin-Like Nanoparticles Having an Excellent Free-Radical-Scavenging Property. *Biomacromol.* 2011, *12*, 625–632.

- [131] P. Yang, Z. Gu, F. Zhu, Y. Li. Structural and Functional Tailoring of Melanin-Like Polydopamine Radical Scavengers. *CCS Chem.* 2020, 2, 128–138.
- [132] H. Zhao, Z. Zeng, L. Liu, J. Chen, H. Zhou, L. Huang, J. Huang, H. Xu, Y. Xu, Z. Chen, Y. Wu, W. Guo, J. H. Wang, J. Wang, Z. Liu. Polydopamine nanoparticles for the treatment of acute inflammation-induced injury. *Nanoscale.* 2018, 10, 6981-6991.
- [133] Y. Liang, X. Zhao, T. Hu, Y. Han, B. Guo. Mussel-inspired, antibacterial, conductive, antioxidant, injectable composite hydrogel wound dressing to promote the regeneration of infected skin. *J. Colloid Interf. Sci.* 2019, 556, 514-528.
- [134] Y. Liu, K. Ai, X. Ji, D. Askhatova, R. Du, L. Lu, J. Shi. Comprehensive Insights into the Multi-Antioxidative Mechanisms of Melanin Nanoparticles and Their Application To Protect Brain from Injury in Ischemic Stroke. *J. Am. Chem. Soc.* 2017, 139, 856-862.
- [135] M. Ambrico, P. Manini, P. F. Ambrico, T. Ligonzo, G. Casamassima, P. Franchi, L. Valgimigli, A. Mezzetta, C. Chiappe, M. d’Ischia. Nanoscale PDA disassembly in ionic liquids: structure–property relationships underpinning redox tuning. *Phys. Chem. Chem. Phys.* 2019, 21, 12380-12388.
- [136] M. C. Foti. Use and Abuse of the DPPH• Radical. *J. Agric. Food Chem.* 2015, 63, 8765-8776.
- [137] G. Litwinienko, K. U. Ingold. Solvent Effects on the Rates and Mechanisms of Reaction of Phenols with Free Radicals. *Acc. Chem. Res.* 2007, 40, 222-230.
- [138] R. Amorati, S. Menichetti, C. Viglianisi, M C. Foti, Proton–electron transfer pathways in the reactions of peroxy and dpph radicals with hydrogen-bonded phenols. *Chem. Commun.* 2012, 48, 11904-11906.
- [139] N. F. Della Vecchia, A. Luchini, A. Napolitano, G. D’Errico, G. Vitiello, N. Szekely, M. d’Ischia, L. Paduano, Tris buffer modulates polydopamine growth, aggregation, and paramagnetic properties. *angmuir* 2014, 30, 9811–9818.
- [140] M. L. Alfieri, L. Panzella, S. L. Oscurato, M. Salvatore, R. Avolio, M. E. Errico, P. Maddalena, A. Napolitano, M. d’Ischia, The chemistry of polydopamine film formation: the amine-quinone interplay. *Biomimetics* 2018, 3, 26.
- [141] K. Jodko-Piórecka, G. Litwinienko. Antioxidant activity of dopamine and L-DOPA in lipid micelles and their cooperation with an analogue of α -tocopherol. *Free Radic Biol. Med.* 2015, 83, 1-11.
- [142] R. Amorati, L. Valgimigli, L. Panzella, A. Napolitano, M. D’Ischia, 5-S-Lipoylhydroxytyrosol, a Multidense Antioxidant Featuring a Solvent-Tunable Peroxyl Radical-Scavenging 3-Thio-1,2-dihydroxybenzene Motif. *J. Org. Chem.* 2013, 78, 9857–9864.
- [143] K. Miyauchi, T. Urakami, H. Abeta, H. Shi, N. Noguchi, E. Niki, Action of pyrroloquinolinequinol as an antioxidant against lipid peroxidation in solution. *Antioxid. Redox Signaling.* 1999, 1, 547-554.
- [144] L. R. C. Barclay, M. R. Vinqvist, K. Mukai, S. Itoh, H. Morimoto. Chain-Breaking Phenolic Antioxidants: Steric and Electronic Effects in Polyalkylchromanols, Tocopherol Analogs, Hydroquinones, and Superior Antioxidants of the

Polyalkylbenzochromanol and Naphthofuran Class. *J. Org. Chem.* 1993, 58, 7416-7420.

[145] A. Citterio, A. Arnoldi, F. Minisci. Nucleophilic character of alkyl radicals. 18. Absolute rate constants for the addition of primary alkyl radicals to conjugated olefins and 1, 4-benzoquinone. *J. Org. Chem.* 1979, 44, 2674-2682.

[146] B. Maillard, K. U. Ingold, J. C. Scaiano, Rate constants for the reactions of free radicals with oxygen in solution. *J. Am. Chem. Soc.* 1983, 105, 5095-5099.

[147] E. T. Denisov. Cyclic mechanisms of chain termination in the oxidation of organic compounds. *Russ. Chem. Rev.* 1996, 65, 505-520.

[148] K. A. Harrison, E. A. Haidasz, M. Griesser, D. A. Pratt, Inhibition of hydrocarbon autoxidation by nitroxide-catalyzed cross-dismutation of hydroperoxyl and alkylperoxyl radicals. *Chem. Sci.* 2018, 9, 6068–6079.

[149] G. W. Burton, K. U. Ingold. Autoxidation of biological molecules. 1. Antioxidant activity of vitamin E and related chain-breaking phenolic antioxidants in vitro. *J. Am. Chem. Soc.* 1981, 103, 472-6477.

[150] R.; Amorati, G. F. Pedulli, L. Valgimigli. Kinetic and thermodynamic aspects of the chain-breaking antioxidant activity of ascorbic acid derivatives in non-aqueous media. *Org. Biomol. Chem.* 2011, 9, 3792–3800.

[151] R. Amorati, A. Baschieri, L. Valgimigli. Measuring antioxidant activity in bioorganic samples by the differential oxygen uptake apparatus: recent advances. *J. Chem.* 2017, 2017, 1-12.

[152] H-atom abstraction from CHD by the semiquinone radicals of the investigated compounds (i.e. $\text{QH}\cdot + \text{CHD} \rightarrow \text{QH}_2 + \text{CHD-H}\cdot$) was ruled out because when performing inhibited autoxidation studies at different CHD concentrations, the same O_2 consumption profile was obtained. Also, the direct reaction of 1 with CHD was found to be marginal because of the low [CHD] used. See: A. Baschieri, R. Amorati, L. Valgimigli, L. Sambri. 1-Methyl-1, 4-cyclohexadiene as a Traceless Reducing Agent for the Synthesis of Catechols and Hydroquinones. *J. Org. Chem.* 2019, 84, 21, 13655-13664.

[153] S. Valcic, J. A. Burr, B. N. Timmermann, D. C. Liebler. Antioxidant Chemistry of Green Tea Catechins. New Oxidation Products of (–)-Epigallocatechin Gallate and (–)-Epigallocatechin from Their Reactions with Peroxyl Radicals. *Chem. Res. Toxicol.* 2000, 13, 801-810.

[154] L. Valgimigli, R. Amorati, M. G. Fumo, G. A. DiLabio, G. F. Pedulli, K. U. Ingold, D. A. Pratt. The Unusual Reaction of Semiquinone Radicals with Molecular Oxygen. *J. Org. Chem.* 2008, 73, 1830-1841.

[155] S. Hoops, S. Sahle, R. Gauges, C. Lee, J. Pahle, N. Simus, M. Singhal, L. Xu, P. Mendes, U. Kummer. COPASI—a COMplex PATHway SIMulator. *Bioinformatics* 2006, 22, 3067–3074.

[156] M. Griesser, R. Shah, A. T. V. Kessel, O. Zilka, E. A. Haidasz, D. A. Pratt. The Catalytic Reaction of Nitroxides with Peroxyl Radicals and Its Relevance to Their Cytoprotective Properties. *J. Am. Chem. Soc.* 2018, 140, 3798–3808.

- [157] R. Amorati, P. T. Lynett, L. Valgimigli, D. A. Pratt. The Reaction of Sulfenic Acids with Peroxyl Radicals: Insights into the Radical - Trapping Antioxidant Activity of Plant - Derived Thiosulfonates. *Chem.--Eur. J.* 2012, 18, 6370 – 6379.
- [158] B. L. Tumanskii, S. P. Solodovnikov, A. I. Prokof'ev, N. N. Bubnov, M. I. Kabachnik. Affect of the solvent on the disproportionation of 3,6-di-tert-butyl-2-hydroxyphenoxy radicals. *Russ Chem Bull.* 1977, 26, 1206–1210.
- [159] E. T. Denisov, I. V. Khudyakov. Mechanisms of action and reactivities of the free radicals of inhibitors. *Chem. Rev.* 1987, 87, 1313-1357.
- [160] M. Jha, D. A. Pratt. Kinetic solvent effects on peroxyl radical reactions. *Chem. Commun.* 2008, 1252-1254.
- [161] D. W. Snelgrove, J. Luszyk, J. T. Banks, P. Mulder, K. U. Ingold. Kinetic Solvent Effects on Hydrogen-Atom Abstractions: Reliable, Quantitative Predictions via a Single Empirical Equation. *J. Am. Chem. Soc.* 2001, 123, 469-477.
- [162] M. C. Foti, S. Sortino, K. U. Ingold. New Insight into Solvent Effects on the Formal HOO. + HOO. Reaction. *Chem.--Eur. J.* 2005, 11, 1942-1948.
- [163] Y. Huang, Y. Li, Z. Hu, X. Yue, M. T. Proetto, Y. Jones, N. C. Gianneschi. Mimicking Melanosomes: Polydopamine Nanoparticles as Artificial Microparasols. *ACS Cent. Sci.* 2017, 3, 564–5699.
- [164] X. Jiang, Y. Wang, M. Li. Selecting water-alcohol mixed solvent for synthesis of polydopamine nano-spheres using solubility parameter. *Sci. Rep.* 2014, 4, 6070.
- [165] M. C. Foti, L. R. C. Barclay, K. U. Ingold. The Role of Hydrogen Bonding on the H-Atom-Donating Abilities of Catechols and Naphthalene Diols and on a Previously Overlooked Aspect of Their Infrared Spectra. *J. Am. Chem. Soc.* 2002, 124, 12881-12888.
- [166] G. Litwinienko, G. A. DiLabio, P. Mulder, H. G. Korth, K. U. Ingold. Intramolecular and Intermolecular Hydrogen Bond Formation by Some Ortho-Substituted Phenols: Some Surprising Results from an Experimental and Theoretical Investigation. *J. Phys. Chem. A* 2009, 113, 6275–6288.
- [167] Al. Fattahi, S. R. Kass, J. F. Liebman, M. A. R. Matos, M. S. Miranda, V. M. F. Morais. The Enthalpies of Formation of o-, m-, and p-Benzoquinone: Gas-Phase Ion Energetics, Combustion Calorimetry, and Quantum Chemical Computations Combined. *J. Am. Chem. Soc.* 2005, 127, 6116-6122.

Chapter 3

Kinetic study by combined UV-Vis spectroscopy and oximetry on monophenolase / diphenolase activities of tyrosinase inhibited by glabridin.

Summary

In this chapter, tyrosinase inhibition by glabridin from *Glycyrrhiza glabra* was studied by both UV–Vis spectroscopy and oximetry kinetic analysis. Tyrosinase is the key enzyme involved in the biosynthesis of melanin in species ranging from bacteria and fungi to humans. Hence its role is broadly important in living organisms and its control, including its inhibition, is of great importance, with several relevant applications ranging from food preservation on storage to control of human skin pigmentation. As tyrosinase activity is essentially an oxidation process we surmised it would be possible to investigate it with great accuracy by oxygen consumption kinetics, which is the core expertise of our research group.

UV–Vis spectroscopy is routinely used in enzyme activity tests and remains as the most versatile method. However, the instability of the oxidation products L-dopa and dopaquinone forces to monitor tyrosinase kinetics only by monitoring the accumulation of late product dopachrome. Thus we set to improve the reliability of spectrophotometric measurements by parallel oximetry studies, to measure the kinetics of oxygen consumption during reaction progress, since the uptake of oxygen is stoichiometrically related to the generation of dopachrome. The two kinetic methods were matched to afford a robust combined investigation approach. They afforded the competitive dissociation constants K_I of glabridin as 13.95 nM and 61.22 nM, for monophenolase and diphenolase activities, respectively, supporting glabridin as one of the most effective, reference natural inhibitors. We believe that our improved investigation method would prove very valuable in future studies.

3.1 Pigmentation and tyrosinase

3.1.1 Pigmentation

Melanin is a group of dark pigments widely distributed in different kingdoms such as bacteria, fungi, plants, and animals including humans [1]. Besides the antioxidant potential mentioned in second chapter, it also became the focus of material science in different fields (photo bioelectronics, nanomedicine and mussel-inspired surface coating) due to its versatile properties for biomedical and technological applications [2,3]. Colors in skin, hair bulbs and eyes of mammals including humans are due to the synthesis and distribution of melanin, which is produced in pigment cells (melanocytes) located in melanosomes [4,5], specialized cytoplasmic organelles at the basal layer of epidermis, and a series of chemical reactions is involved, which is collectively called melanogenesis (fig. 3.1) [6,7].

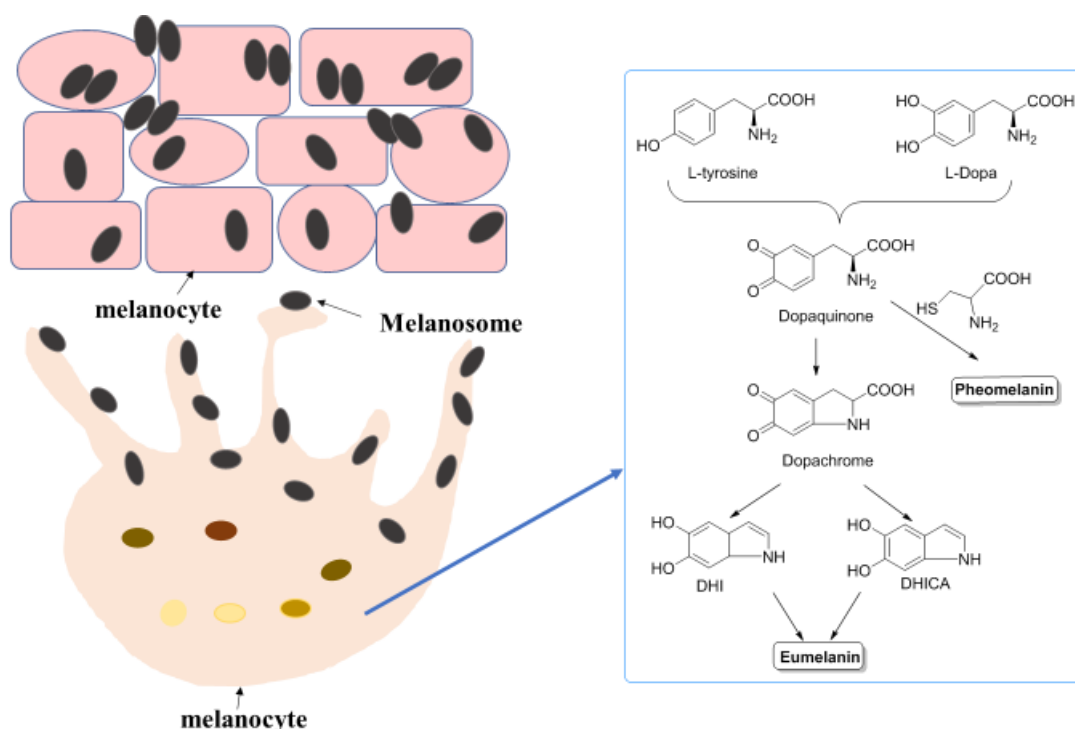
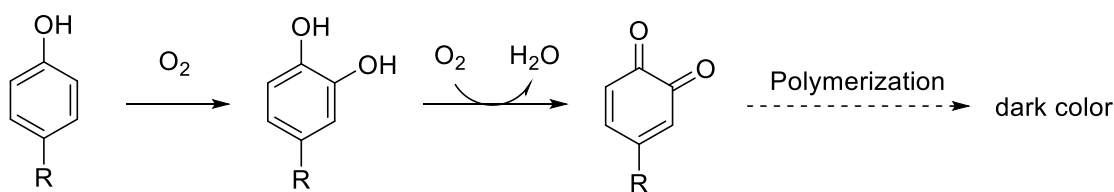


Figure 3.1. Schematic representation of melanogenesis pathway (in the blue frame on the right) inside melanocytes, and melanosome transfer.

Melanin in fact is a complex of several component molecules with different properties and proportion, and melanin formed during melanogenesis in skin basically include eumelanin and pheomelanin (Figure 3.1) [8], where the most common one is

eumelanin responsible for the black or brown color, while pheomelanin is responsible to the color of red hair [9]. Besides skin pigments, neuromelanin found in the brain is believed to protect neurons [10,11]. It is well known that melanogenesis in the human skin can be triggered and accelerated by exposure to UV light, and the resulting melanin is able to absorb UV radiation, so to protect skin cells from subsequent UV exposure [12]. Any interference with melanin biosynthesis processes can lead to pigmentation disorders, including both increase and decrease of melanin [13]. Besides the biological importance of melanin, however, human skin hyperpigmentation is an undesirable consequence of melanin's role [14,15]. Therefore, control of skin pigmentations has been a long-term goal of cosmetic and pharmaceutical applications, as a result of dramatic social attention in specific cultures. Production of melanin in food gives rise to a dark color (enzymatic browning), accompanied by other deterioration processes such as changes of flavor, unpleasant odor and loss of nutritional value, especially during postharvest processing and storage of vegetables and fruits [16]. Therefore, food preservation should not be limited to inhibiting lipid autoxidation by phenolic or non-phenolic antioxidants, but needs also to inhibit browning which depends on melanin synthesis. Both the synthesis of melanin in skin and in food is mainly catalyzed by tyrosinase. In the presence of oxygen, tyrosinase catalyzes the oxidation of monohydroxy phenols (phenol, L-tyrosine, *o-p*-cresol) by insertion of another OH group on the benzene ring to convert them into *ortho*-dihydroxy phenols (catechol, L-dopamine, adrenalin), followed by catalyzing the dehydrogenation from dihydroxy phenols to *o*-quinones, which then undergo polymerization to form dark colors (Scheme 3.1)[17].



Scheme 3.1 key oxidation steps of phenols to melanin.

3.1.2 Tyrosinase

Tyrosinase is the key enzyme in melanin synthesis, which initiates and catalyzes a series of reactions to convert amino acid L-tyrosine into melanin biopolymer [18]. They have been separated and studied from various sources, such as fungal, plant, animal [19]. The commence of all tyrosinases is the type III copper center within the active sites, although tyrosinase structures occurring across all species are diverse [20,21]. The two copper atoms coordinated by surrounding histidine residues serve as the active sites due to the highly reactive intermediates formed by their interacting with dioxygen. Generally, tyrosinase exists in three states: deoxy-tyrosinase, met-tyrosinase and oxy-tyrosinase (fig 3.2) [22,23].

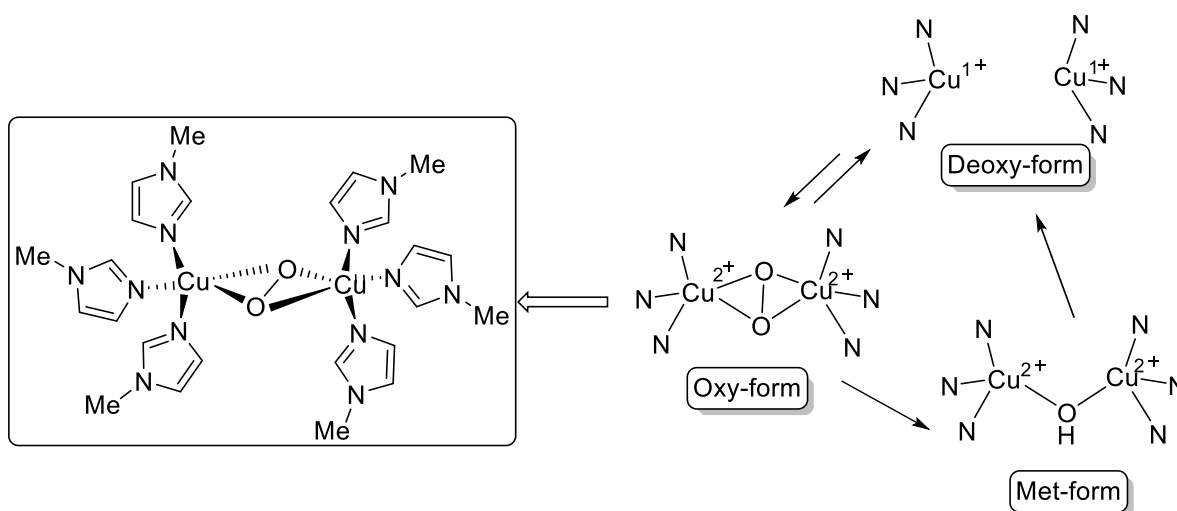


Figure 3.2. Tyrosinase active site and its three forms.

Tyrosinase is involved in two different oxidative catalytic cycles: the *ortho*-hydroxylation of monophenols by oxygen to *o*-diphenols (monophenolase reaction) and the oxidation of *o*-diphenols by oxygen to *o*-quinones (diphenolase activity), as shown in Figure 3.3 [24]. Tyrosinases' monophenolase forms *ortho*-diphenols from L-tyrosine, which can react only with the *oxy*-tyrosinase. However, the diphenolase reaction cycle involves both the *oxy* and *met* forms of tyrosinase, and *o*-quinones formed are subsequently polymerized to melanin.

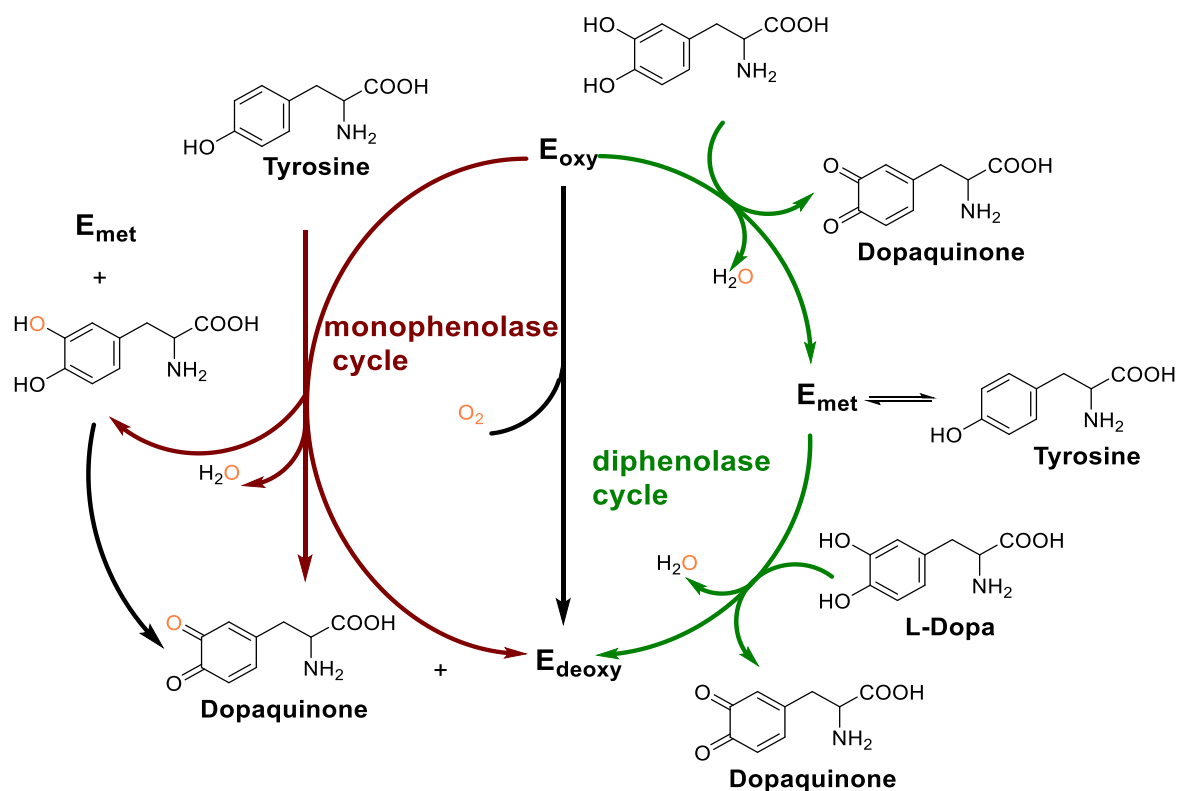


Figure 3.3. Monophenolase and diphenolase catalytic activities of tyrosinase enzyme.

As shown above, melanin synthesis is ultimately regulated by tyrosinase, thus the most effective approaches to control skin pigmentation or food browning are the inhibition of tyrosinase [25]. With special focus on skin pigmentation, to date, a large number of compounds with a tyrosinase inhibition activity of synthetic, semi-synthetic or natural origin have been introduced into the market [26], and among them, the most commonly used are arbutin [27], tretinoin (trans-retinoic acid) [28], alpha-hydroxy acids (lactic, glycolic, citric, malic, pyruvic and tartaric acid) [29], kojic acid [30], azelaic acid [31] and various forms of vitamin C [32]. However, many skin-whitening agents on the market have been subject to some proven adverse effects on human health [33].

In recent years, the use of products of natural origin has grown increasingly in the medical, food and cosmetic fields [34]. As far as cosmetics are concerned, many companies have focused their research on alternative sources, such as natural active ingredients to be used in cosmetic products to offer safer alternatives to synthetic ones, responding to changing market demands without losing effectiveness. In addition,

natural products are preferred thanks to their wider consumer appreciation and better biodegradability [35]. Numerous studies aimed at finding bleaching agents of natural origin, capable of replacing those of synthetic derivation. Most molecules identified as tyrosinase inhibitors are characterized by the presence of one or more phenolic groups [36]. The discovery that some polyphenols have a depigmentation effect given by their analogy with the natural substrates of tyrosinase has stimulated scientific research on these substances as potential agents useful to counteract melanin accumulation. These compounds are widely distributed in leaves, barks, roots, seeds and flowers [37]. Many polyphenol derivatives have been studied in depth (in particular flavonols, isoflavonoids, and coumarin) and it has been shown that the components that share a catecholic and/or resorcinol residue and the substitution in position 4 of resorcinol manifest a greater anti-tyrosinase activity [38]. Flavonoids also have antioxidant and anti-inflammatory properties and are able to inhibit the production of ROS [39]. Since they do not alter cellular proliferation, the suppression of melanogenesis have a little invasive and safe action. A valuable review on those natural and bioinspired phenolic inhibitors was presented by Panzella et al. [40]. In the past few decades, the inhibition of tyrosinase in the treatment of hyperpigmentation has collected relevant scientific efforts, and it is still a very interesting research topic, not only in the discovery of new and effective tyrosinase enzyme inhibitors, but also the important insights into their inhibitory mechanism.

3.2 The Fundamentals of Enzyme Inhibition Mechanism

Enzyme inhibition means the enzyme active sites are influenced by the so-called inhibitors, which usually are small molecular compounds, causing a decrease or loss of catalytic activity of the enzyme. Generally, enzyme inhibition is divided into two mainly types: reversible and irreversible inhibition based on the mode of inhibitor's interaction with enzyme active site [41]. The irreversible inhibitors usually bind covalently thus modify the enzyme, which might destroy the functional groups of active sites [42]. Irreversible inhibitors often contain reactive electrophilic groups, such

as phenyl sulfonates, haloalkanes or nitrogen mustards, which react with enzyme residues such as cysteine or L-tyrosine by forming covalent adducts, that can not be reversed. However, the reversible inhibitors usually interact with residues in the active sites by multiple non-covalent bond forces, such as hydrogen bonds, hydrophobic interactions and ionic bonds, thus no irreversible chemical reactions happen [43]. Before looking into the mechanism details of different reversible inhibition types, it is convenient to briefly address the concept of enzyme complex and Michaelis-Menten kinetics, which are the fundamentals of enzyme inhibition research.

3.2.1- Michaelis-Menten kinetics and Lineweaver–Burk plot

Generally, a steady-state means that the concentrations of intermediates are constant or not changing perceptibly during the ongoing chemical reaction which will change the intermediates' concentration [44]. And It is very important in enzymatic analysis, where the concentrations of the enzyme or of the enzyme-substrate complex are small compared to the substrate and considered constant, as described in Figure 3.4.

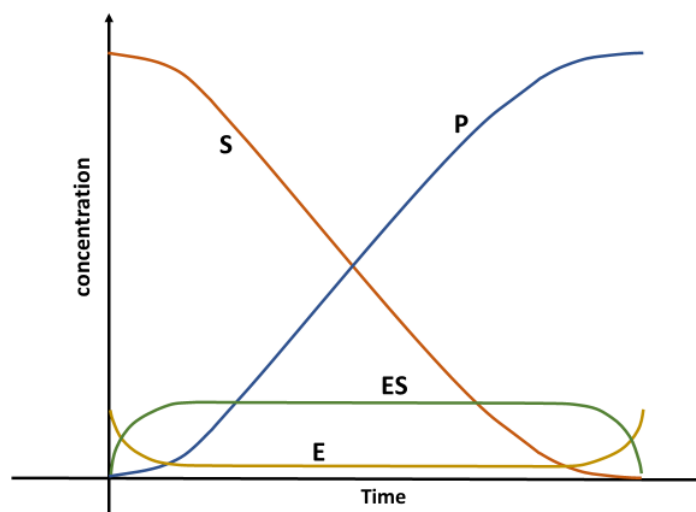
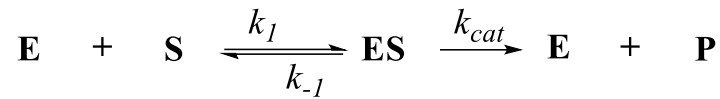


Figure 3.4. Change on the concentration of enzyme(E), substrate(S), enzyme-substrate complex(ES) and product (P) during the time course of reaction.

The idea of enzyme-substrate complex was introduced and discussed by Brown and Henri at the beginning of the 20th century [45,46]. Later on, Leonor Michaelis and Maud Menten proposed a mathematical model of the enzyme catalytic reaction, the Michaelis-Menten kinetics, based on the concept of enzyme-substrate complex and

steady-state [47]. Until now, Michaelis-Menten kinetics is still one of the best-known models of enzyme kinetics and is broadly applied in enzyme kinetic research. Usually an enzymatic reaction involving one substrate is assumed to follow Michaelis–Menten kinetics which is presented schematically in Scheme 3.2:



Scheme 3.2. basic one substrate enzyme kinetic model.

where E, S, ES and P represent enzyme, substrate, enzyme-substrate complex, and product, respectively. The double arrows between S and ES represents the reversible mode of enzyme-substrate binding, and the rate constants k_1 and k_{-1} represent the forward and reverse rate constant, respectively. The product formation step is represented by a single forward arrow with catalytic rate constant, k_{cat} .

The Michaelis-Menten equation, where the initial reaction rate V_0 (usually expressed as the product formation rate $d[\text{P}]/dt$) is related to the concentration of substrate [S] and derived on the basis of the steady-state assumption, is shown below in Eq. 3.1. Details on its derivation are reported in appendix.

$$v = \frac{d[\text{P}]}{dt} = V_{\max} \frac{[\text{S}]}{K_M + [\text{S}]} \quad (\text{Eq 3.1})$$

In Michaelis-Menten (M-M) equation V_{\max} represents the maximum reaction rate when the substrate concentration is saturating, K_m is the Michaelis-Menten constant, which is equal to the substrate concentration where the reaction rate is half of V_{\max} .

Enzyme kinetics are studied by measuring and plotting the initial velocity (V_0) as a function of the substrate concentration [S]: the resulting hyperbolic plot (Figure 3.5) could be used to compute V_{\max} and K_m .

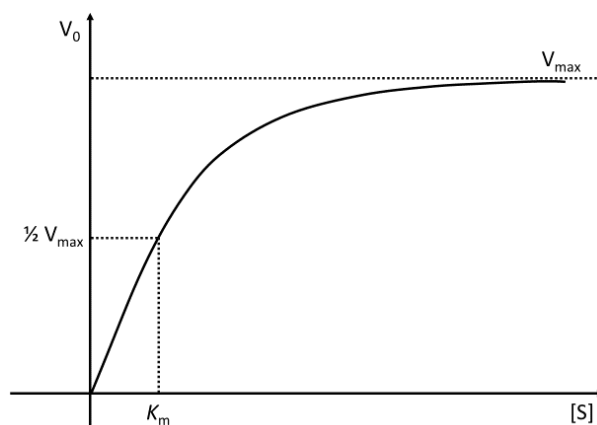


Figure 3.5. Hyperbolic plot of Michaelis-Menten kinetic model.

From the Michaelis-Menten hyperbolic plot we can see that at low substrate concentration $[S]$, the initial velocity (V_0) increases almost linearly with increasing $[S]$, however, further increase of $[S]$ induces less than proportional increase of (V_0). In the end, V_0 will arrive its maximal value (V_{\max}) and will not change with increase of substrate anymore.

Based on Michaelis-Menten equation, Lineweaver–Burk plot, described by Hans Lineweaver and Dean Burk [48] was widely used to determine terms in enzyme kinetics before the wide availability of nonlinear regression software. Further, Lineweaver–Burk plot could provide a quick and intuitive judgement of different enzyme inhibition types (details will be given in the following). Basically, it consists in the double reciprocal plot generated by plotting the reciprocals of V_0 on the y-axis and $1/[S]$ on the x-axis. The equation (Eq. 3.2) and resulting linear plot (Figure 3.6) are shown below.

$$\frac{1}{V} = \frac{K_m + [S]}{V_{\max} [S]} = \frac{K_m}{V_{\max}} \frac{1}{[S]} + \frac{1}{V_{\max}} \quad (\text{Eq. 3.2})$$

It is obvious from the plot that the x-intercept equals to $-1/K_m$, and the y-intercept is $1/V_{max}$. Other methods of linearization of M-M equation are Hanes-Woolf and Eadie-Hofstee plots, which similarly can afford the enzyme kinetic parameters.

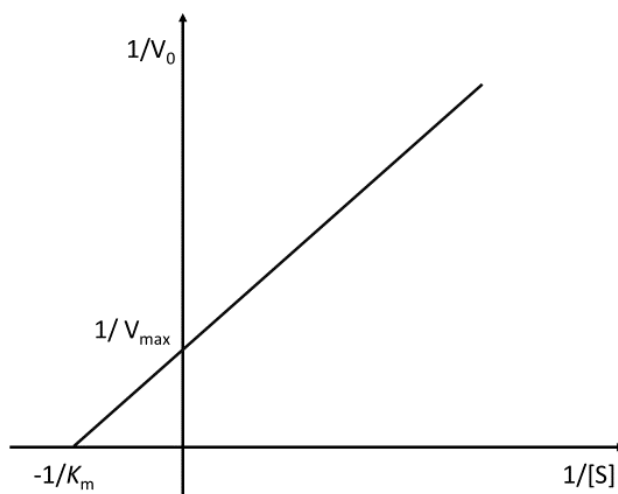


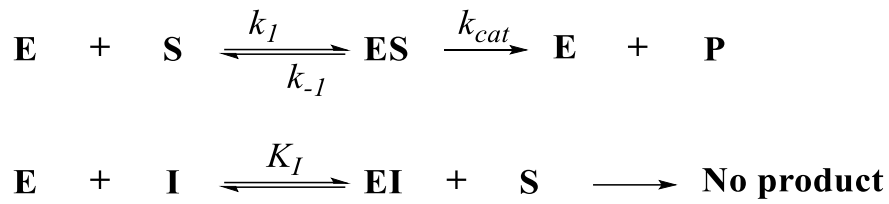
Figure 3.6. Double reciprocal linear plot of Lineweaver-Burk kinetic model.

3.2.2 Types of reversible inhibition (plots interpretation)

As discussed above, enzyme inhibition, in fact, is the enzyme interaction with an inhibitor. According to the Michaelis-Menten kinetic model, there are at least two kinds of enzyme states, thus the enzyme inhibition might happen in different manners, depending on where the inhibitors interact, or on which enzyme kinetic parameters they affect. Here we only discuss the reversible inhibition. The most common modes of reversible inhibition include competitive reversible inhibition, uncompetitive reversible inhibition, non-competitive inhibition and mixed reversible inhibition [4-51].

Competitive Inhibition

In competitive inhibition (Scheme 3.3), the inhibitors compete with the substrate for binding to the free enzyme: this kind inhibitor generally possess affinity to the active site of the enzyme like the substrate does, and competitive inhibitors are thought to have similarity in structure with the substrate.



Scheme 3.3. Schematical kinetic model of competitive inhibition

The competitive inhibition effects are shown in the Figure 3.7: V_{max} doesn't change with the increase of the inhibitor; however, K_m will increase accordingly, meaning more substrate is needed to reach the $\frac{1}{2} V_{max}$. Usually, this kind of inhibition can be overcome by increasing the substrate concentration.

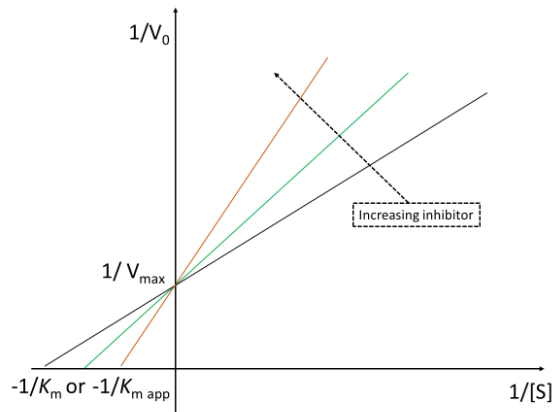
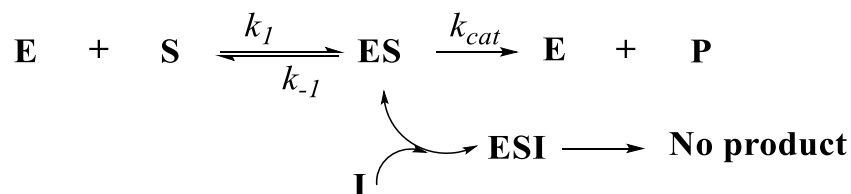


Figure 3.7. The theoretical effect of a competitive inhibitor on the LB plots of substrate-initial rate relationship.

Uncompetitive Inhibition

In uncompetitive inhibition, inhibitor binds only to the substrate-enzyme complex reversibly (Scheme 3.4), meaning that binding sites for the inhibitors are created after the substrate binding.



Scheme 3.4. Schematically kinetic model of uncompetitive inhibition

The inhibition effects are shown in the Figure 3.8: both V_{\max} (because of inhibitor combining to the substrate-enzyme complex to form a nonproductive complex) and K_m will decrease (looking like a better binding efficiency of substrate) with the increase of inhibitors.

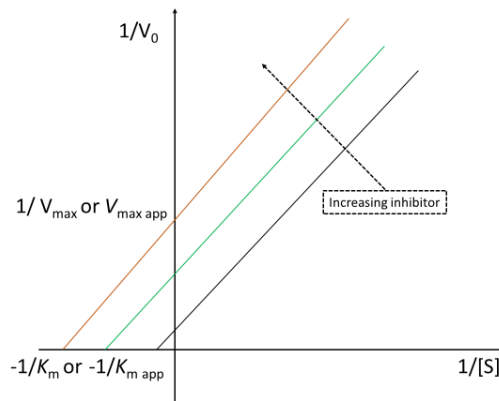
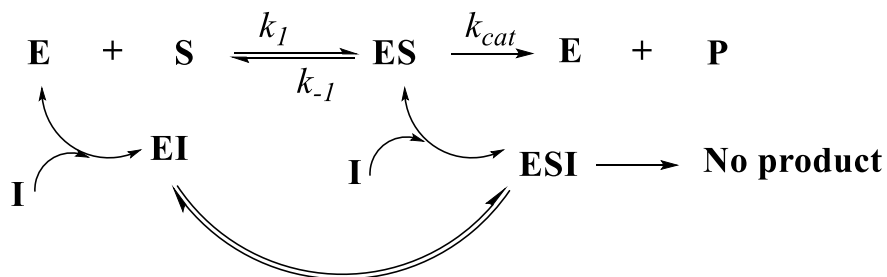


Figure 3.8. The theoretical effect of uncompetitive inhibitor on the LB plots of substrate-initial rate relationship.

Pure Noncompetitive Inhibition

In pure noncompetitive inhibition, inhibitor could bind to both the free enzyme and the substrate-enzyme complex, simultaneously, and substrate binding and inhibitor binding do not affect each other (Scheme 3.5), resulting in unchanged K_m with different concentrations of the inhibitors (Figure 3.9).



Scheme 3.5. Schematically kinetic model of pure non-competitive inhibition

The ternary complex (ESI) is not productive, thus the inhibition effect looks like removing some enzyme from the system, which in the end will decrease the V_{\max} with increase of inhibitor.

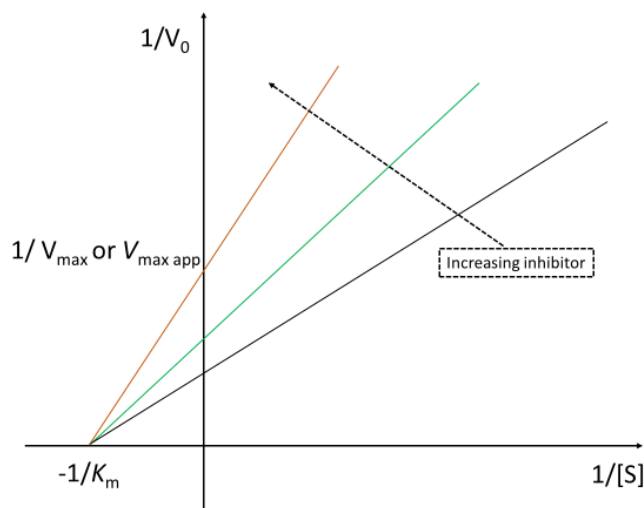
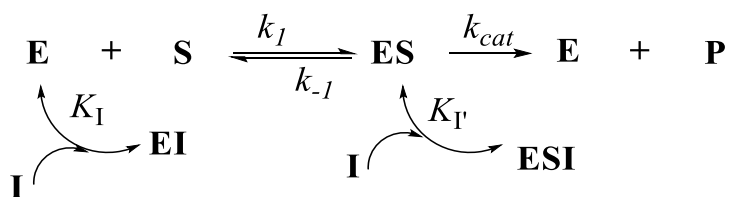


Figure 3.9. The theoretical effect of pure non-competitive inhibitor on the LB plots of substrate-initial rate relationship.

Mixed Inhibition

The last one is mixed inhibition, where inhibitor can bind both to the enzyme and the substrate-enzyme complex, but unlike the non-competitive inhibition, substrate binding and inhibitor binding do affect each other, resulting in both apparent change of V_{\max} and K_m (Scheme 3.6). That's why non-competitive inhibition is also named as pure non-competitive inhibition, which in fact is found mainly in textbooks and theory. The plots details were not shown here, since the slopes and intercepts might be around all over the places of the cartesian graph.



Scheme 3.6. Schematic kinetic model of mixed inhibition.

3.2.3 Quantitative description of different reversible inhibitions

All the plots mentioned in the previous sections, including Michaelis-Menten non-linear plot, and Lineweaver–Burk, Hanes-Woolf and Eadie–Hofstee linear plots, can be used to both diagnose the inhibition type and estimate the apparent values of the

kinetic parameters, especially the inhibition constants. The relationship between the apparent V_{\max} and K_m and inhibition constants are shown in table 3.1 [52].

Table 3.1. Relationships between apparent K_m , V_{\max} and the inhibition constant for different reversible inhibition types.

Type of inhibition	V^{app}	V^{app}/K_m^{app}	K_m^{app}
Competitive	V	$\frac{V/K_m}{1 + [I]/K_I'}$	$K_m(1 + [I]/K_I')$
Mixed	$\frac{V}{1 + [I]/K_I}$	$\frac{V/K_m}{1 + [I]/K_I'}$	$\frac{K_m(1 + [I]/K_I')}{1 + [I]/K_I}$
Non-competitive ^a	$\frac{V}{1 + [I]/K_I}$	$\frac{V/K_m}{1 + [I]/K_I'}$	K_m
Uncompetitive	$\frac{V}{1 + [I]/K_I}$	V/K_m	$\frac{K_m}{1 + [I]/K_I}$

a) For pure non-competitive inhibition, $K_I = K_I'$

3.4 Research objects

As introduced above, physiological production of the melanin pigment, known as melanogenesis, plays an important role in the protection from UV exposure by absorbing the ultraviolet sunlight and removing reactive oxygen species (ROS), contributing to the prevention of sun-induced skin injury [52]. However, accumulation of excessive epidermal pigmentation can cause various hyperpigmentation disorders such as melasma, lentigines, age spots, and sites of actinic damage [53,54]. Regulation of such disorders has been a long-standing objective for cosmetic and pharmaceutical preparations, tackling different pathogenetic processes [55], wherein, regulation of melanin synthesis through inhibition of tyrosinase is being intensely studied for the prevention of hyperpigmentation and tyrosinase inhibitors could eventually act as skin whitening agents in cosmetics [56,57]. There is overlapping of application of antioxidants and compounds for pigmentation control in cosmetics and several compounds with known antioxidant activity are used also as skin whitening agents.

Stepping from this overlapping our goal was to investigate tyrosinase inhibition along with the antioxidant behavior.

UV–Vis spectroscopy is routinely used in enzyme activity tests and remains the most widely used method, where analysis of product accumulation is preferred due to its higher sensitivity than monitoring the depletion of substrate [58]. Typically the measured absorption is that of dopachrome (475nm), spontaneously formed from the *o*-dopaquinone [59], and as shown in Figure 3.10, one half of *o*-dopaquinone is going to dopachrome, while the other half is going back to L-dopa [60]. However, since tyrosinase activity is essentially an oxidation process operated by oxygen, where oxygen is directly involved into the accumulation of late product dopachrome, we set to improve the reliability of spectrophotometric measurements by parallel oximetry studies, to measure the kinetics of oxygen consumption during reaction progress.

This technique is the main distinctive expertise of our research group and we aimed at exploiting it to strengthen current investigation approaches. It was reported that the uptake of oxygen is stoichiometrically related to the generation of dopachrome [12], where only half of *o*-dopaquinone proceeds to spontaneous cyclization to form dopachrome, implying $\frac{1}{2}$ O₂ consumption; however, the half *o*-dopaquinone regenerating L-dopa undergoes another oxidation cycle to consume $\frac{1}{2}$ O₂ again, thus in total, the stoichiometric number of O₂ to dopa is 1 (Figure 3.10) [61].

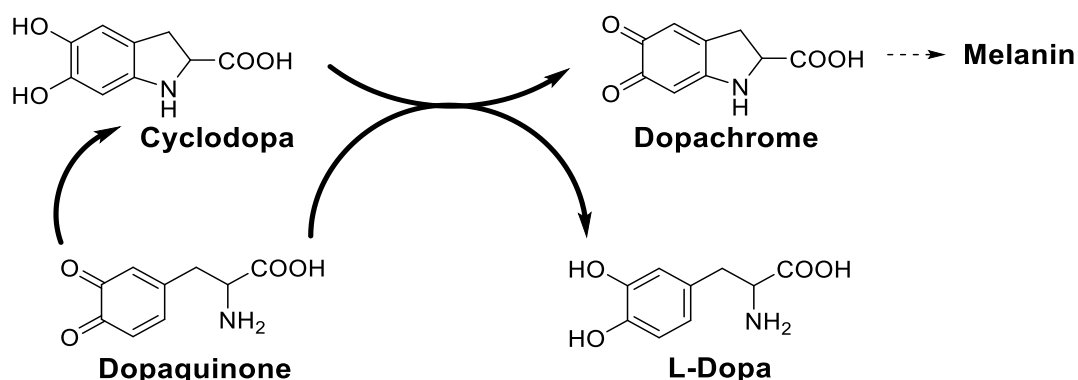


Figure 3.10. Non-enzymatic cyclization of dopaquinone to form dopachrome regenerating L-dopa.

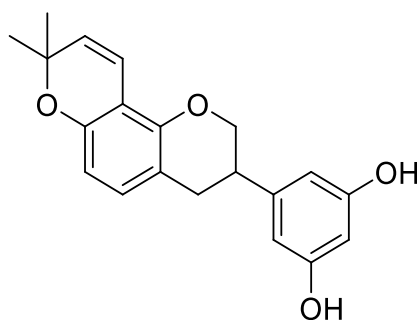
We therefore set and optimized a matched approach to monitor tyrosinase kinetics both

by conventional UV-Vis spectroscopy and by oximetry and we applied this approach to the investigation of mushroom tyrosinase inhibition.

Many tyrosinase inhibitors from natural and synthetic sources have been recently reviewed though many of them suffer from limitations, such as low activity and high cytotoxicity, poor skin penetration, and low stability [34,62]. Many flavonols were identified as tyrosinase inhibitors [63], usually behaving as competitive inhibitor for the monophenolase activity due to the 3-hydroxy-4-keto moiety which provides copper chelating properties [64]. Polyphenols from green tea [65], *Heterotheca inuloides* [66], *Artocarpus incisus* [67], *Morus alba* [68] showed moderate to good inhibitory activity of tyrosinase. The extracts from roots of licorice (*Glycyrrhiza glabra* L.) have gained special interest as anti-melanogenetic agents, mainly for the presence of the prenylated isoflavonoid glabridin. Nerya and coworkers [69] demonstrated strong tyrosinase inhibitory activity for both glabridin (Figure 3.11) and the isoflavan glabrene from the roots of the *G. glabra*: glabridin was the first confirmed inhibitor with 15-fold the activity of kojic acid and exhibited higher depigmenting activity than arbutin [70], whereas glabrene was found to be 100-fold less active than glabridin. Other natural components isolated from the roots of *Glycyrrhiza* species (*i. e.* licochalcone A) [71] were found effective inhibitors of tyrosinase activity. Kim and coworkers [72] isolated glyasperin C from *G. uralensis* and showed it to be twice as active as glabridin against mushroom tyrosinase. However, glabridin had the best melanogenesis inhibitory activity in human cell culture, among tested compounds, and was judged the most interesting candidate as skin-whitening agent. Although glabridin is one of the most effective natural inhibitors, there is major uncertainty on its actual activity on quantitative grounds, despite its central role as reference compound [73].

Indeed, IC₅₀ values in the inhibition of monophenolase activity of mushroom tyrosinase (the typical reference in current literature) as different as 2.93 μM [73], 0.77 μM [69] and 0.09 μM [74] have been reported, spanning over almost two orders of magnitude. Similar spreading affects results on diphenolase activity. Only one kinetic investigation

addressing the mechanism of inhibition is available in the literature, which indicates noncompetitive inhibition both for monophenolase and diphenolase activity with respective values of inhibition constant K_I of 0.38 mM and 0.81 mM. These surprisingly high values are at odds with the much lower K_I values available for reportedly less effective inhibitors like kojic acid (K_I in the range 18-23 μM for monophenolase activity) [75], 6,7,4'-trihydroxyisoflavone ($K_I = 1.9 \mu\text{M}$) [76], or oxyresveratrol (K_I in the range 0.3-0.4 μM) [77], it should be recalled that lower K_I values mean higher inhibiting activity. Since glabridin is often chosen as reference tyrosinase inhibitor to test other molecules, on using it, it occurred to us that both its mechanism and inhibition constants may require revision. Given its importance, we started this new area of research for our group with a detailed kinetic study on the inhibition of both monophenolase and diphenolase activities by glabridin, as a test-bench for our new oxygen uptake approach.



Glabridin

Figure 3.11. Structure of glabridin (from *Glycyrrhiza glabra* L.)

3.5 Results and Discussion

In order to study monophenolase and diphenolase activities of tyrosinase, L-tyrosine or L-dopa were used as substrate, respectively, following the *o*-hydroxylation of L-tyrosine to L-dopa and its further oxidation to *o*-dopaquinone, or just the second step, respectively. The inhibitory activity of glabridin was preliminarily evaluated by a UV-Vis spectrophotometer monitoring product formation (dopachrome) at λ_{max} of

absorption (475 nm), in parallel, the oxygen consumption under identical settings was also studied in matched kinetic experiments by the oximetry method set-up in our lab (Figure 3.12).

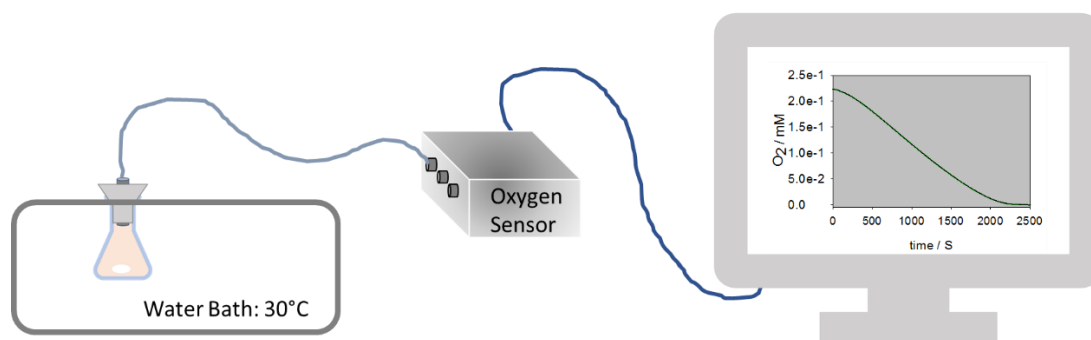


Figure 3.12. Schematic set-up of the oxygen sensor

3.5.1 Correlation of oxygen consumption to dopachrome generation

The stoichiometric ratios of oxygen consumption to dopachrome accumulation for both substrate L-tyrosine and L-dopa were determined, respectively, by García-Cánovas et al. [78] and by Riley et al. [79], by correlating the total oxygen consumption and product formation in the end of the reaction process. In our experiments, the correlation of the initial velocity, both of oxygen consumption and dopachrome formation, was instead studied, either in the presence or absence of enzyme inhibitors, since the initial velocity is the parameter universally used to analyze the M-M kinetics. Besides, the further spontaneous polymerization of dopachrome (to melanin) will also influence the apparent dopachrome absorbance at the later stages of enzyme reaction; therefore, we felt that using initial rates of dopachrome formation and oxygen consumption would bring to less biased kinetic data. As shown in Figure 3.13, for both substrates L-dopa and L-tyrosine correlation between initial velocities is more accurate than the one between the final amount of product generation and substrate consumption, since the UV absorbance is still growing when the oxygen consumption is complete.

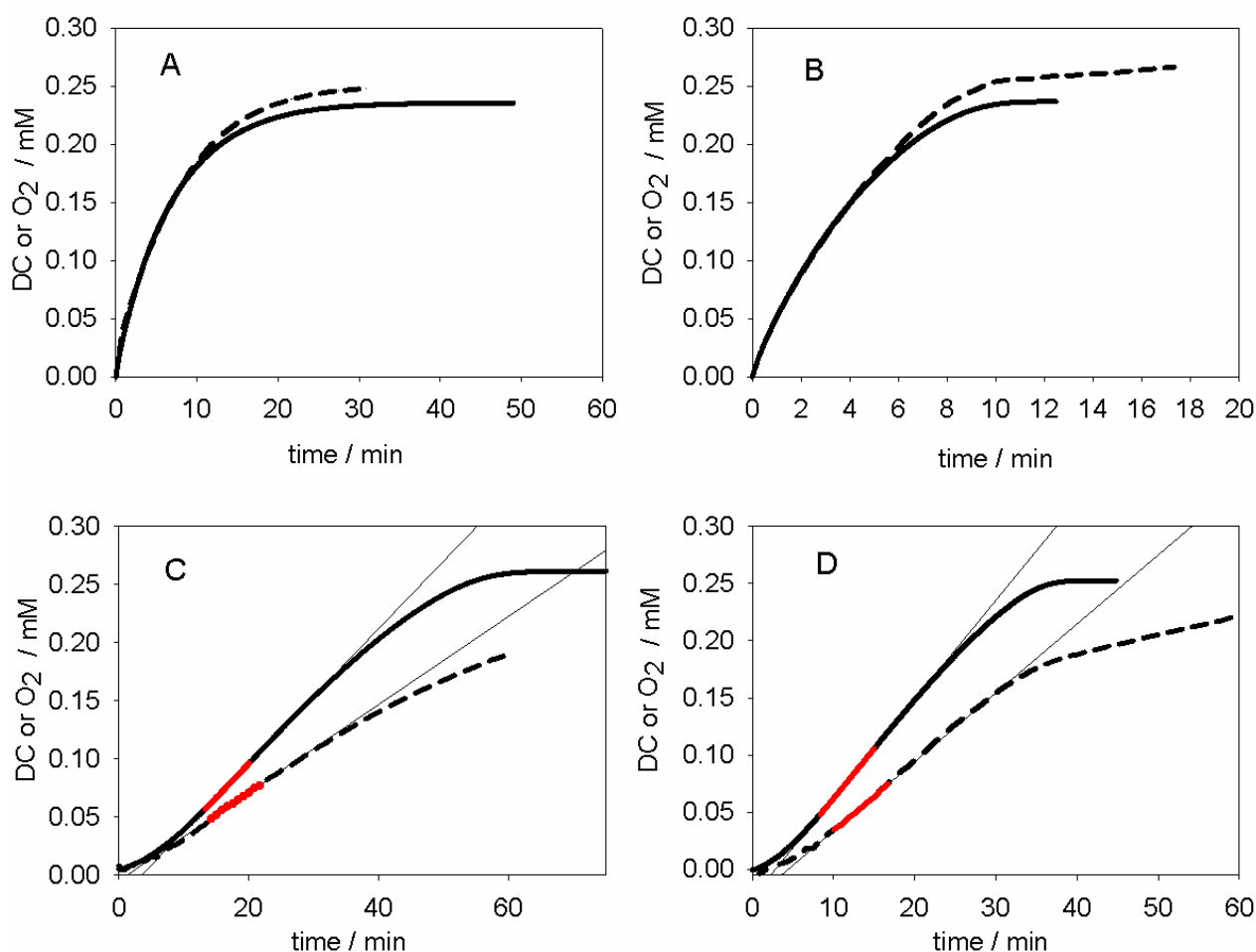


Figure 3.13. Representative time traces of O₂ consumption (solid lines) and dopachrome formation (dashed lines) during the oxidation of L-dopa 1.6 mM (A: tyrosinase 3.85 U/ml; B: tyrosinase 5.78 U/ml) and L-tyrosine 1.6 mM (C: tyrosinase 7.70 U/ml; D: 11.55 U/ml) at 30°C, pH 6.8. The regression lines in plots C and D were drawn using the indicated (red) time range for the initial rate, and ratios (average 1.5 ± 0.1) of their slopes was used to determine the stoichiometric ratio between oxygen consumption and dopachrome production for substrate L-tyrosine.

Moreover, not every single experiment was conducted until reaction completion, thus it would not have been possible to guarantee that every oximetry experiment was conducted with identical time-duration as the UV experiment, at the same condition. Therefore, the stoichiometric ratios of the initial rates of oxygen consumption and dopachrome accumulation for both substrates L-tyrosine and L-dopa were determined from the ratios of initial rates of reaction.

The initial rates correlation experiments were conducted by measuring the initial reaction velocity of the oxidation of both L-dopa and L-tyrosine by different sets of

enzyme or substrate concentration, as shown in Figure 3.14, and the stoichiometry ratio of oxygen consumption / dopachrome formation were calibrated as 1.0 ± 0.1 and 1.5 ± 0.2 (oxygen to dopachrome) for substrate L-dopa and L-tyrosine, respectively.

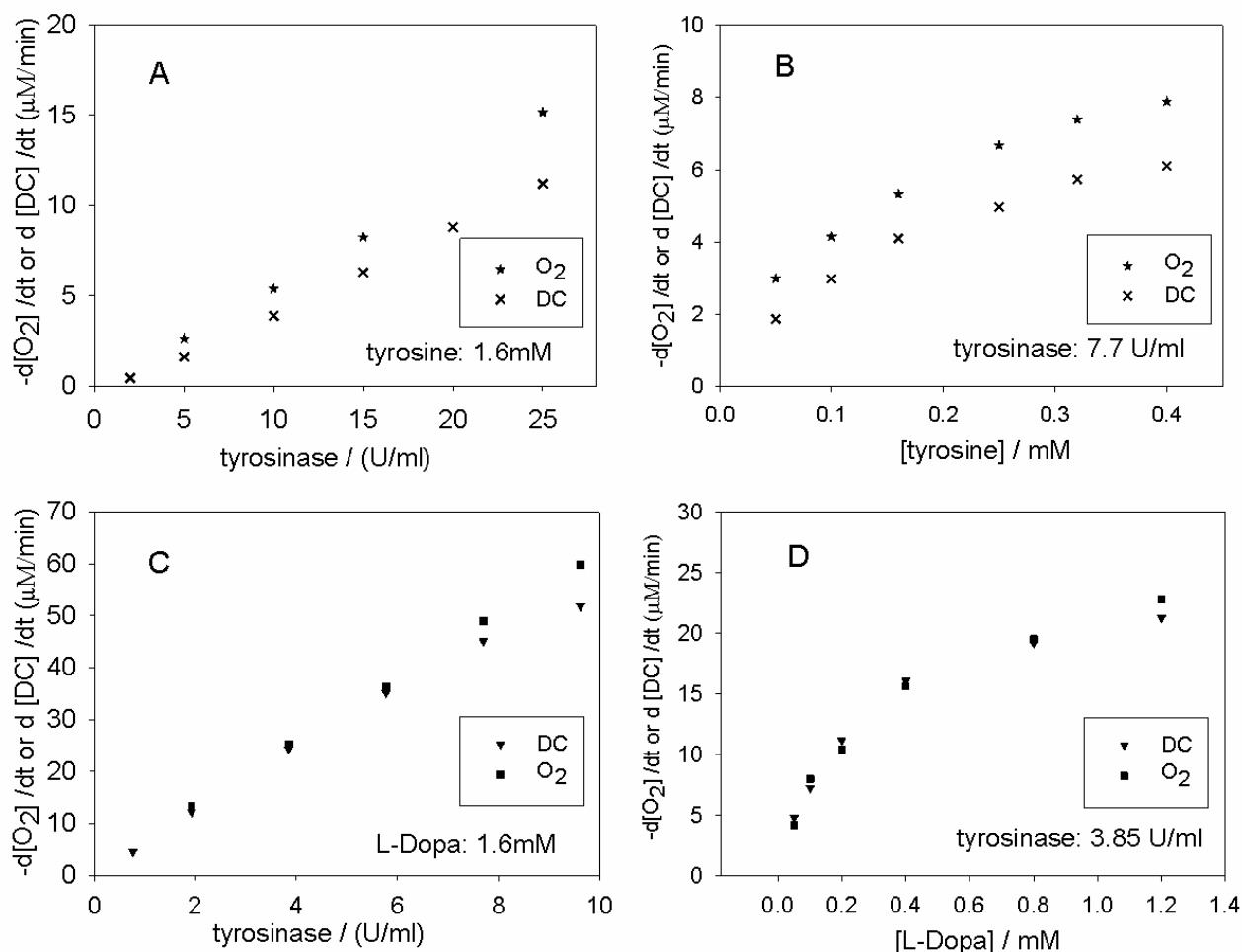


Figure 3.14. Correlation of the stoichiometry of oxygen (O_2) consumption to dopachrome (DC) production during oxidation of both L-tyrosine (A and B) and L-dopa (C and D), correlating initial rates of DC production and O_2 consumption as a function of tyrosinase concentration at fixed concentration of substrate (A and C), and initial velocity of DC production and O_2 consumption as a function of tyrosinase concentration at fixed concentration of tyrosinase (B and D).

3.5.2 kinetic study on both monophenolase and diphenolase activities of tyrosinase inhibited by glabridin: UV-Vis spectroscopy and oximetric methods.

Preliminarily, the kinetic behaviour of mushroom tyrosinase in the oxidation of L-tyrosine and L-dopa have been studied by both UV and Oximetry without inhibitors. As shown in Figure 3.15. the production rate of dopachrome and the rate of oxygen consumption affords excellent matching.

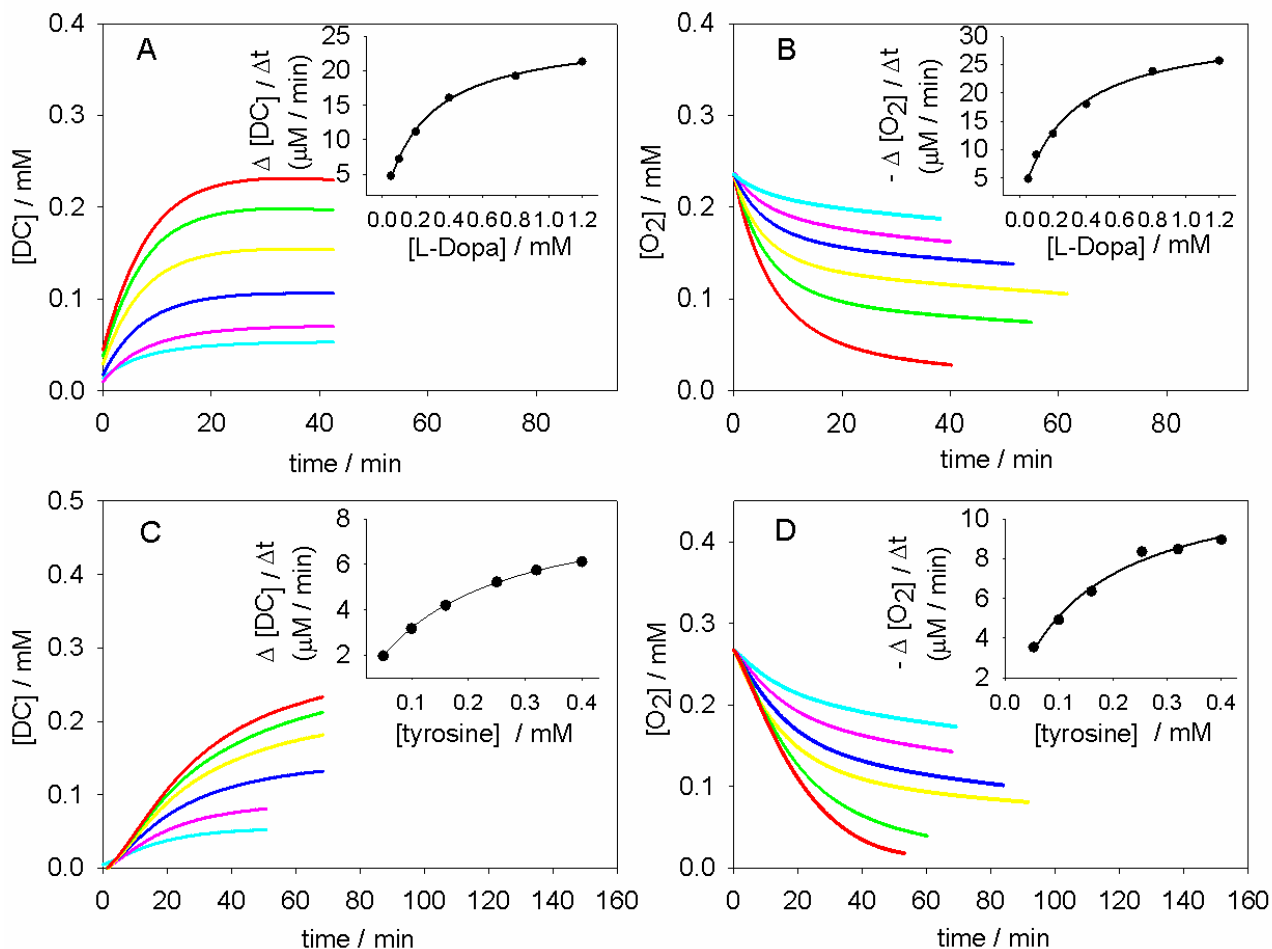


Figure 3.15. Time-course of DC production and O_2 consumption during the oxidation of L-dopa (A, B) and L-tyrosine (C, D) catalyzed by tyrosinase (3.85 U/ml for L-dopa and 7.70 U/ml for L-tyrosine). The inserts are the initial rates of oxygen consumption (B, D) and dopachrome formation (A, C) during oxidation of both L-dopa (A and B) and L-tyrosine (A and B) with the corresponding non-linear fitting of Michaelis-Menten kinetics (solid lines).

The initial rates collected from the reaction progress satisfy the Michaelis-Menten kinetics. The K_m and V_{max} values for the monophenolase activity and the diphenolase activity of tyrosinase were analysed by non-linear regressions, and results are listed in Table 3.2. The reaction mechanism and the kinetic parameters of the tyrosinase enzyme have been studied by Fenoll et al. [80] using a more sophisticated and accurate spectrophotometric method than the simple evaluation of the dopachrome product. Their Michaelis-Menten constants ($K_m = 0.25$ mM and 0.28 mM for L-tyrosine and L-dopa respectively) are in reasonable agreement with our kinetic data. In addition, our data also match with Espín's data [60], where the V_{max} for L-tyrosine and L-dopa are 1.8 μ M/min and 24.5 μ M/min respectively.

Table 3.2. Michaelis-Menten kinetics parameters measured both by UV-Vis spectrophotometry and by oximetry.

activity	substrate	dopachrome formation		oxygen consumption	
		K_m (mM)	V_{max} ($\mu\text{M}/\text{min}$)	K_m (mM)	V_{max} ($\mu\text{M}/\text{min}$)
monophenolase	L-tyrosine	0.18±0.01	9±0.12	0.17±0.02	8.4±0.06
diphenolase	L-DOPA	0.26 ±0.02	25.8±0.53	0.21±0.02	24.18±0.96

Given the higher rate of the diphenolase reaction, the V_{max} of this process was calculated at the beginning of the process (between $t=0$ and $t=3$ min) and monophenolase activity was evaluated between 5 and 20 min.

3.5.3 Inhibition kinetics by glabridin

Glabridin (Figure 3.11) is one of the most effective natural inhibitors of tyrosinase, but there is major uncertainty on its actual activity on quantitative grounds, in spite of its central role as reference compound, as previously discussed. Given its importance, we investigated its kinetic of inhibition in detail, addressing both monophenolase and diphenolase activities, by both methods (spectrophotometry and oxygen uptake) in matched studies. Results are summarized in Figure 3.16, and the method to get the raw initial rates is described in the experimental section).

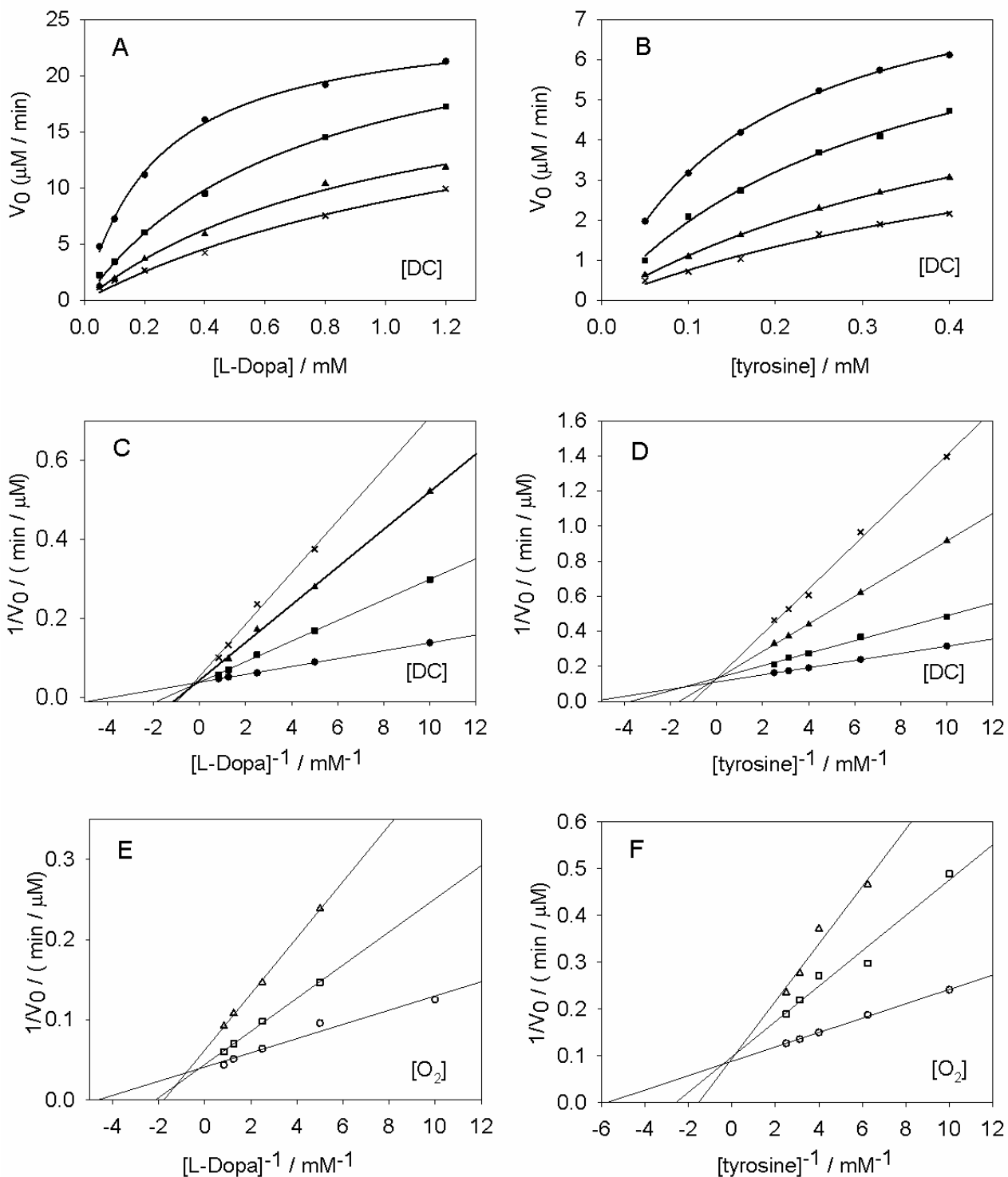


Figure 3.16. Plots A and B are the non-linear fittings based on Michaelis-Menten kinetics of glabridin inhibition of monophenolase and diphenolase tyrosinase activity. Data were obtained by UV-Vis spectrophotometry: (A) diphenolase activity on L-Dopa, glabridin concentrations: ●-0 nM, ■- 90 nM, ▲-180 nM, x-300 nM; (B) monophenolase activity on L-tyrosine, glabridin concentrations: x- 0nM, ▲- 15 nM, ■-37 nM, ●-50nM. (C) and (D) are the Lineweaver-Burk plots corresponding to A and B. (E) and (F) are the Lineweaver-Burk plots of glabridin inhibition on monophenolase and diphenolase activity studied by oximetry method: (E) diphenolase activity on L-Dopa, glabridin concentrations: ○-0nM, □-80nM, Δ-200nM; (F) monophenolase activity on L-tyrosine, glabridin concentrations: ○-0nM, □-20nM, Δ-40nM. Enzyme concentration for substrate L-dopa and L-

tyrosine were 3.85 U/ml and 7.7U/ml respectively, all experiments were conducted at pH 6.5 and 30°C. Due to the higher rate of the diphenolase reaction, the V_{\max} of this process was evaluated at the beginning of the process (between t=0 and t=2 min), the V_{\max} of monophenolase activity was instead evaluated between 5 and 30 min.

Data in the literature on the activity profile of this molecule indicate a non-competitive inhibitory activity, which implies that glabridin is a compound capable of binding with the same affinity both the free enzyme and the complex substrate- enzyme. However, both the UV and oximetry analysis of our study did not show pure non-competitive but preferring competitive inhibition as shown in Figure 3.16, where the V_{\max} (intercept on Y-axis in Lineweaver-Burk plots) keeps constant, while the values of K_m (intercept of X-axis) increase with the inhibitor's concentration.

For an inhibitor, the determination of K_I is important to define inhibition efficiency as the lower (numerically) is the value of the constant, the more the balance is shifted towards the formation of the EI complex, therefore the catalyzed reaction will be more inhibited. Herein, in order to assess more closely the type of inhibition, to a first judgment it was considered as a mixed inhibition, since the value of V_{\max} in Figure 3.16 is not exactly constant, particularly in oxygen uptake plots (Figure 3.16 E-F).

Mixed inhibitors interfere with both the free enzyme and enzyme-substrate complex, so there are two dissociation constants K_I and K_I' that need to be considered (Scheme 3.6), the first relating to the inhibitor bonded to the enzyme and the other indicating the inhibitor bonded to the ES complex. We can define K_I and K_I' as described as below [80].

$$K_I = \frac{[E][I]}{[EI]} \quad (\text{Eq. 3.3})$$

$$K_I' = \frac{[ES][I]}{[ESI]} \quad (\text{Eq. 3.4})$$

As described in Table 3.3, in order to determine K_I and K_I' for a mixed inhibition from M-M kinetic treatment, it is necessary to introduce the parameters α and an α' , which are given as follows:

$$\alpha = \frac{K_m^{app}}{K_m} \alpha' \quad (\text{Eq. 3.5})$$

$$\alpha' = \frac{V_{max}}{V_{max}^{app}} \quad (\text{Eq. 3.6})$$

Where K_m and K_m^{app} are respectively is the Michaelis-Menten constant, (substrate concentration giving half-maximum rate) in the absence and in the presence of the inhibitor, and V_{max} and V_{max}^{app} are respectively the maximum rate measured in the absence and in the presence of the inhibitor. K_I and K_I' values can then be obtained from the following equations at each given concentration of the inhibitor [I].

$$\alpha = 1 + \left(\frac{[I]}{K_I}\right) \quad (\text{Eq. 3.7})$$

$$\alpha' = 1 + \left(\frac{[I]}{K_I'}\right) \quad (\text{Eq. 3.8})$$

The apparent M-M kinetics parameters K_m and K_m^{app} and α and an α' from data in Figure 3.16, are listed in Table 3.3 and Table 3.4, for substrate L-tyrosine and L-dopa respectively. The calculation of inhibition constants K_I and K_I' for various concentration of glabridin as the inhibitor are also collected in Table 3.3 and Table 3.4, for substrate L-tyrosine and L-dopa respectively.

Table 3.3. Kinetic parameters of tyrosinase diphenolase activity inhibition by glabridin. Kinetics data were obtained both by non-linear and linear regression fit (see experimental section) at different glabridin concentrations.

[Glabridin] (nM)	Dopachrome (DC) formation				Oxygen (O2) consumption			average
	0	90	180	300	0	80	200	
V_{max} or V_{max}^{app} ($\mu\text{M}/\text{min}$)	25.8±0.53	25.74±1.14	22.74±2.52	18.54±4.32	24.18±0.96	22.5 ± 1.32	16.02±1.26	
K_m or K_m^{app} (mM)	0.26 ±0.02	0.67±0.06	1.08±0.02	1.21±0.46	0.21±0.02	0.47±0.08	0.56±0.05	
$\alpha = (K_m^{app} \times \alpha') / K_m$		2.17	4.79	6.58		2.34	3.95	
$\alpha' = V_{max} / V_{max}^{app}$		1.00	1.14	1.39		1.075	1.51	
$K_I = [I] / (\alpha - 1)$		77.24	47.54	53.75		59.86	67.71	61.22 ±10.43

$K_I = [I]/(\alpha'-1)$	39130.4	1337.7	766.13	1071.4	392.65	8539.7 ±15298.6
-------------------------	---------	--------	--------	--------	--------	--------------------

V_{\max} or V_{\max}^{app} refer to not inhibited and inhibited assays, respectively, and K_m or K_m^{app} refer to not inhibited and inhibited assays, respectively. Data were obtained both by UV-Vis spectrophotometry and oximetry method.

Table 3.4. Kinetic parameters of tyrosinase monophenolase activity inhibition by glabridin. Kinetics data were obtained by non-linear and linear regression fit at different glabridin concentrations.

[Glabridin] (nM)	Dopachrome (DC) formation				Oxygen (O ₂) consumption ^a			average
	0	15	37	50	0	20	40	
V_{\max} or V_{\max}^{app} ($\mu\text{M}/\text{min}$)	9.00±0.12	7.50 ±0.6	7.80 ±0.24	7.56±1.20	8.40±0.06	7.62±1.20	7.92±1.38	13.95± 3.46 284.13± 93.68
K_m or K_m^{app} (mM)	0.18±0.01	0.27±0.04	0.61±0.03	0.97±0.20	0.17±0.02	0.39±0.06	0.65±0.08	
$\alpha = (K_m^{\text{app}} \times \alpha')/K_m$		1.74	3.86	6.25		2.46	3.99	
$\alpha' = V_{\max} / V_{\max}^{\text{app}}$		1.20	1.15	1.19		1.10	1.06	
$K_I = [I]/(\alpha-1)$		20.21	12.95	9.53		13.70	13.37	
$K_I = [I]/(\alpha'-1)$		74.38	239.81	267.42		190.77	648.30	

^a V_{\max} or V_{\max}^{app} were calibrated by using the stoichiometry ratio of 1.5 for O₂/DC (see 3.5.1).

As it can be seen, glabridin shows very potent activity in inhibiting both monophenolase and diphenolase activities of tyrosinase. Notably, spectrophotometry and oximetry afford results in very good agreement, despite the major difference between the techniques, validating our new oxygen-uptake kinetic approach for the study of tyrosinase inhibition. Concerning the mechanism of inhibition, it is interesting to note that K_I quantifying the inhibition based on interaction of glabridin (I) with the ES complex is over two orders of magnitude larger than K_I describing the competitive inhibition (interaction of I with E), for diphenolase activity, and over 10-folds larger for inhibition of monophenolase activity. This means that less than 1% the inhibition of diphenolase activity and less than 10% the inhibition of monophenolase activity by glabridin is due to binding to ES *i.e.* to uncompetitive behavior. For most of its activity glabridin competes with substrate (L-tyrosine or L-dopa) for the enzyme's active site

in a classical competitive mode with K_I values of 13.95 nM and 61.22 nM, respectively. This is at variance with the previously reported mechanism and the absolute magnitude of K_I values measured here for glabridin fully justify its reputation as one of the most potent natural tyrosinase inhibitors, and explain its much higher activity compared to Kojic acid, at variance with previous literature.

3.5.4 Determination of IC_{50} (half-maximal inhibitory concentration)

In biochemistry, inhibitors are usually described in terms of inhibition type and inhibition constant, as we have done above. This is obviously the appropriate method since it has a clear connection with the inhibitory mechanism and offers full understanding of the inhibition on kinetic bases. However, enzyme inhibition is of crucial importance also in pharmacology, where pharmacologists are more interested in the consequences of inhibition than in inhibition mechanism. That's why it is common to see the inhibition performance being reported as IC_{50} values in the enzyme inhibition literature. The value of IC_{50} , a quantitative parameter, indicates the concentration of an inhibitor that is able to produce a rate of enzyme reaction which is half that observed in the absence of the inhibitor under the same conditions, and IC_{50} value is usually expressed as molar concentration. Usually a dose-response diagram is used to track the effect of inhibitors on the initial rate of enzymatic reaction at a fixed concentration of substrate [81], and there is also an equation (Eq. 3.9), Langmuir isotherm equation [82], describing the effect of inhibitor concentration on reaction.

$$\frac{V_I}{V_0} = \frac{1}{1 + \frac{[I]}{IC_{50}}} \quad (\text{Eq. 3.9})$$

The IC_{50} of glabridin inhibition of tyrosinase for substrates L-tyrosine and L-dopa at different substrate concentration were calculated and shown in Table 3.5. It is clearly possible to see the positive correlation between the IC_{50} value and the concentration of substrates. This demonstrates that IC_{50} values depend on the exact experimental settings and somewhat limits their usefulness in quantifying inhibitors' performance.

Thus, IC₅₀ data were listed here to give a reference to compare with current literature, showing that the IC₅₀ for both substrates (L-tyrosine and L-dopa) are significantly smaller, down to 4 orders of magnitude, compared to literature data, which already contradict each-other and span over 2 orders of magnitude (*e.g.* 2.93 μM [73] to 0.09 μM [74] for monophenolase activity).

Table 3.5. IC₅₀ values calculated according to Eq. 3.9 for tyrosinase inhibition by glabridin at different concentrations of L-tyrosine and L-dopa substrates.

[L-dopa] (mM)	0.05	0.10	0.16	0.25	0.32	0.40
IC ₅₀ (nM)	80.89	81.57	96.37	114.03	229.67	292.63
[L-tyrosine] (mM)	0.05	0.10	0.16	0.25	0.32	0.40
IC ₅₀ (nM)	16.50	21.02	22.78	29.32	31.6	38.4

The IC₅₀ were calculated from the data of Figure 3.16 using UV-Vis experiments.

3.5.5 Is Glabridin a substrate for tyrosinase?

Several molecules with reported inhibiting activity of tyrosinase have also been found to be able to act as alternative substrates for tyrosinase. This means that, beside slowing down the production of “normal” intermediates in the biosynthesis of melanin, they can, nonetheless, be transformed by the enzyme. This is because mushroom tyrosinase is a polyphenol oxidase (PPO) enzyme, which have no strict specificity of only one substrate. Particularly inhibitors with a relevant ability to access the enzyme’s active site (*e.g.* competitive inhibitors) with a non-hindered phenolic or polyphenolic structure might act as alternative substrate. For instance, this is the case for catechins [83], caffeic acid [84], ferulic acid [85], neohesperidin and other phenolic compounds [85]. Since glabridin is a phenolic compound it cannot be excluded that it also acts as alterantive substrate. To the best of our wknowledge this has never been assessed before. Although I have not investigated this point personally, it was investigated in a parallel study in our research group, and I am shortly mentioning the results, since this behavior might potentially interfere with the spectrophotometric assay and bring to misleading results [85]. Incubation of mushroom tyrosinase under identical contitions

used in the assay with glabridin 200 nM or 1 mM in the absence of other substrates, i.e. without tyrosine or L-DOPA, showed no reaction in 60 min either when monitored spectrophotometrically or by oxygen sensing. Since the two concentrations of glabridin tested correspond, respectively, to the highest level it was employed as inhibitors and one of the highest concentration used for the natural substrate tyrosine, the absence of any detectable reaction allow excluding that glabridin acts as alternative substrate under our testing conditions.

3.6 Conclusions and perspective

Accurate quantitative analysis in this study indicated that the inhibition kinetics of tyrosinase by glabridin is of mixed type, where glabridin is able to interfere both with the E and the ES binding forms with two distinct dissociation constants K_I and K_I' . Results allowed to solve a long-standing controversy on glabridin inhibiting mechanism both for monophenolase and diphenolase activities, showing its prevailing competition with the respective substrates (L-tyrosine or L-dopa). Our results afforded for first time competitive dissociation constants K_I as 13.95 nM and 61.22 nM, for monophenolase and diphenolase activities, respectively, supporting its role as one of the most effective, reference natural inhibitors. Our new oximetry method showed to be practical and reliable to investigate tyrosinase inhibition and nicely complements and supports conventional spectrophotometric measurements. Further studies will certainly benefit for this achievement.

Given the possibility of application of the oximetry approach in the tyrosinase inhibition analysis, which was confirmed in this study, we also have a positive attitude towards the application of this method in the analysis of other oxidative enzyme inhibition, where oxygen is consumed during reaction process. Besides, since the oxygen sensor monitors the oxygen concentration every second, this might provide more possibility and accuracy to analyze the kinetic data, for example, by fitting the whole reaction progress with Copasi software mentioned in chapter two (or with other software), instead of limiting to the initial rate, which brings higher error.

As for the tyrosinase inhibitors, there are plenty research focusing on the revealing of new molecules, both synthetic and natural, where the Michaelis-Menten kinetics are often reduced only to reporting IC_{50} values. As we discussed in this chapter, IC_{50} seems not a good parameter to show the potential of the inhibitors, given its dependence on the chosen substrate concentration. Instead, the inhibition constants are comparatively better parameters. Among investigations reporting a full kinetic analysis, often kojic acid or arbutin are used as a reference inhibitor, although they possess moderate inhibition activity. Thus, compounds with high inhibition efficacy like glabridin might provide more meaningful references, which will be enabled by the solid kinetic data provided in this chapter.

According to the whole process of tyrosinase-catalyzed melanin formation (Figure 3.3), tyrosinase inhibition kinetics should be treated as a two-substrates enzyme inhibition kinetic, where oxygen is another substrate beside L-tyrosine or L-dopa. However, tyrosinase, and even other oxidase, are normally considered as one substrate enzyme kinetics due to the complexity of the mathematical analysis and the difficulty to monitor the oxygen concentration as a substrate. In other word, the concentration of oxygen is taken as constant during the initial period of the reaction. The chemistry discussed in this chapter brings another inspiration, suggesting the study of tyrosinase with a simple dual-substrate enzyme segmentation method, which can become more easily accessible, given the possibility of real-time oxygen concentration monitoring, allowed by our current oxygen uptake method.

3.7 Experimental section

3.7.1 Materials

Glabridin ($\geq 98\%$), L-tyrosine ($\geq 98\%$), L-dopa ($\geq 98\%$), water, acetonitrile, methanol (HPLC grade) were purchased from Sigma-Aldrich (St. Louis, MO, USA). Commercial mushroom tyrosinase (EC 1.14.18.1, activity = 3130 units/mg) was purchased from Sigma-Aldrich and used without further purification. It was diluted in potassium phosphate buffer solution (50 mM, pH 6.8) and stored in small aliquots at -20°C . All other reagents were of analytical grade from Sigma-Aldrich-Fluka.

3.7.2 kinetics evaluation by UV-Vis spectrophotometer

Kinetic evaluation of monophenolase and diphenolase inhibition of tyrosinase with or without glabridin was carried out using UV-Vis spectrophotometry at 30°C in a Thermo Scientific (Milan, Italy) Biomate 5 coupled with a Heto DBT Hethotherm (Birkerød, Denmark) thermostating water circulator for temperature control. The samples were analyzed in polystyrene micro cuvettes (≥ 1.5 mL, $l = 1$ cm, $12.5 \times 12.5 \times 45$ mm). Absorbance of dopachrome was measured at 475 nm from 20 min to 60 min (1 scan / 55s) reading the solution against a reference cuvette containing all reaction components except the substrate, which was replaced with potassium phosphate buffer (50 mM, pH 6.8). Absorbance variation *vs* time at different substrate concentration allowed to obtain initial velocity ($V = \Delta A / \Delta \text{min}$) which was converted in $\mu\text{M}/\text{min}$ according Lambert-Beer law as follows¹: $V (\mu\text{M}/\text{min}) = V (\Delta A / \Delta \text{min}) \times 10^6 / \epsilon_{\lambda_{\text{max}}} \times l$. The molar extinction coefficient (ϵ) for dopachrome at $\lambda_{\text{max}} = 475$ nm is $3700 \text{ M}^{-1} \text{ cm}^{-1}$ and UV path (l) was 1 cm. Michaelis-Menten parameters (K_m e V_{max}) were obtained processing initial velocity *vs* substrate concentration data by nonlinear regression using Sigmaplot software.

The effect of inhibition of monophenolase activity was evaluated at fixed tyrosinase units (3.85 U/mL for L-dopa, 7.70 U/ml for L-tyrosine) at varying substrate concentrations (6 levels of L-dopa and L-tyrosine, from 0 to 1.2 mM and 0 to 0.4 mM respectively) testing reactions without and with glabridin (varied from 0 to 300 nM for L-dopa and 0 to 50 nM for L-tyrosine).

Given the difficulty to maintain the activity of enzyme, the tyrosinase activity was analysed at the beginning of every integral week during the experimental period according to supplier indications, in order to adjust to fixed tyrosinases units for different substrates. Briefly, Sigma unit corresponds to the amount that will cause an increase in absorbance at 280 nm of 0.001 per minute at pH 6.8 in a 3 mL reaction mixture containing L-tyrosine. Sigma units were used thoroughly in this study.

3.7.3 kinetics evaluation by oximetry

Kinetic evaluation of tyrosinase monophenolase and diphenolase kinetics or inhibition by glabridin was carried out using oximetry at 30°C by the oxygen sensor (Pyrosience Bremen, Germany) immersed in a water bath controlled by Heto DBT Hetotherm (Birkerød, Denmark). The consumption of oxygen in only one single sample could be studied at one time, which costs considerably more time than UV-Vis spectrophotometry. The samples were contained in 1 ml glass flask had-made by a local scientific glass blower. The oxygen consumption was recorded every second, and all reaction components, except the inhibitor concentration, were maintained identical to those set for UV-Vis spectrophotometry.

The raw data collect directly from the oxygen sensor is a percentage, of the saturation oxygen concentration in the flask, corresponding to 0.236 mM at 30°C which reflects in the computer reading as 20%. Thus, the oxygen concentration during the time course of the enzymatic oxidation of L-dopa or L-tyrosine were converted into $\mu\text{M}/\text{min}$ by the following equation: $V (\mu\text{M}/\text{min}) = V (\Delta P / \Delta s) \times 0.236 \times 10^6 \times 60 / P_0$ The initial rate of the oxygen consumption (reported in Figure 3.16) was obtained by SigmaPlot regression of the initial data range of oxygen consumption *vs* time, as illustrated in the

following representative Figure 3.17, and the initial rates are collected in Table 3.6, which were used to further analyze data according to Michaelis-Menton kinetic.

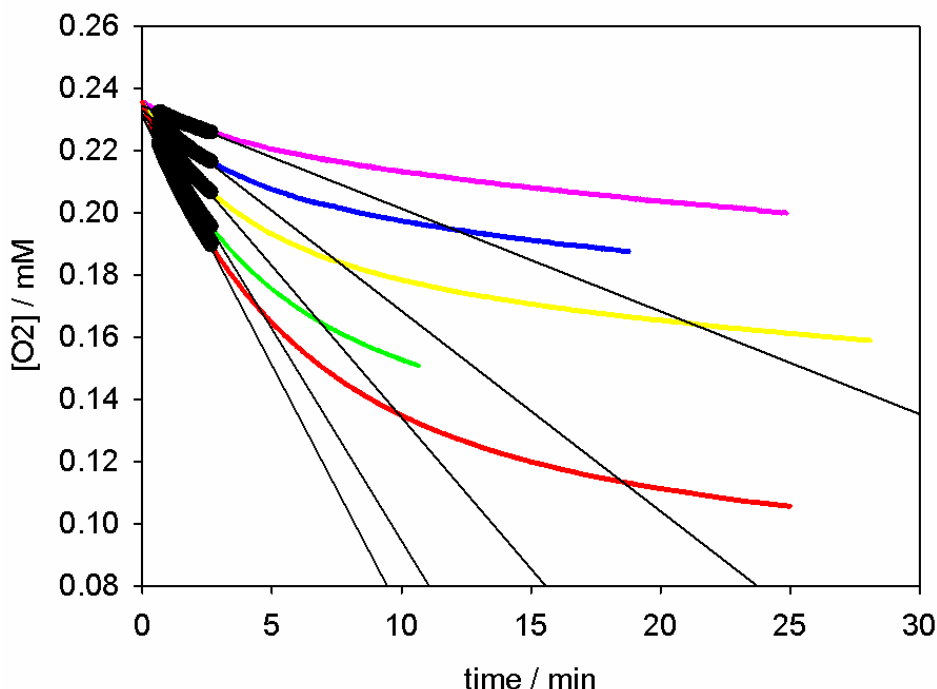


Figure 3.17. The time progresses of O₂ consumption during the oxidation of L-dopa at different initial concentration from 0.1 mM (purple line) to 1.2 mM (red line), inhibited by glabridin (80 nM). The black lines are the linear regression (V_0) for every L-dopa concentration, taken in the highlighted time range (40s to 160s).

Table 3.6. Raw data of initial rates obtained from the linear fitting by Sigamplot software of initial rates of oxygen consumption for different L-dopa concentrations.

[L-dopa] (mM)	0.1	0.2	0.4	0.8	1.2
$V_0 = \text{slope of O}_2$ uptake (mM/s)	5.71×10^{-8}	1.14×10^{-7}	1.70×10^{-7}	2.37×10^{-7}	2.63×10^{-7}

The non-linear analysis was conducted by non-linear fitting of initial velocity V_0 as a function of L-dopa concentration with the hyperbolic equation $y = \frac{a x}{b + x}$ using sigmaplot software, where y, x, a and b represent V_0 , [S], V_{\max} and K_m respectively. The results of fitting are shown in Figure 3.18.

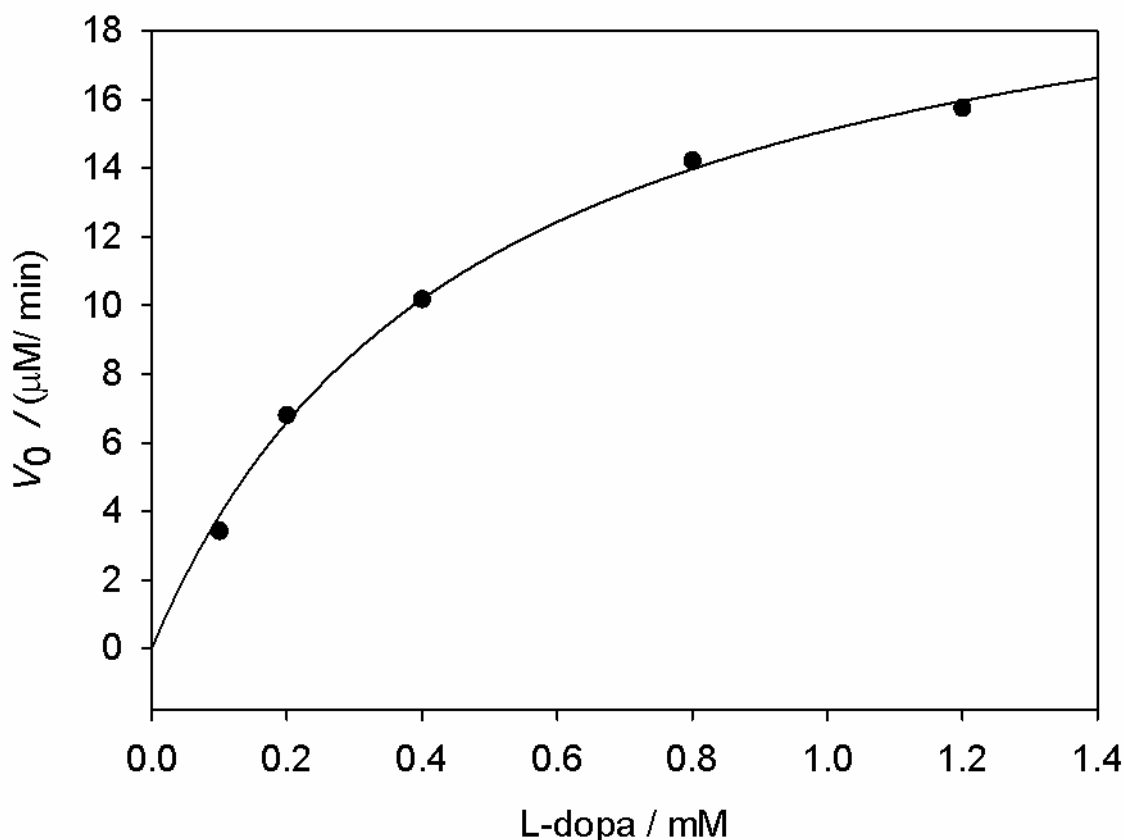


Figure 3.18. Initial rates of oxygen consumption during tyrosinase catalyzed oxidation of L-dopa and the corresponding non-linear fitting to Michaelis-Menten kinetics.

The results from the non-linear fitting by Sigmaplot is shown in table 3.7

Table 3.7. Non-linear fitting report by Sigmaplot of figure 3.18

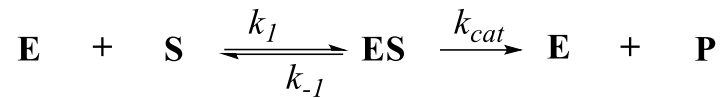
Parameter	Value	Standard Error
a	22.29	0.9109
b	0.4759	0.4586

Where the value of a and b represent V_{\max}^{app} and K_m^{app} , respectively.

Identical kinetic data collection and treatment was applied when using L-tyrosine as the substrate and either in the absence of inhibitor or for each concentration of glabridin.

Appendix

Derivation of M-M kinetic equations



basic one substrate enzyme kinetic model.

Applying the law of mass action, the rate of a reaction is proportional to the product of the concentrations of the reactants, which gives a system of four non-linear ordinary differential equations that define the rate of change of reactants with time

$$\frac{d[\mathbf{E}]}{dt} = -k_1[\mathbf{E}][\mathbf{S}] + k_{-1}[\mathbf{ES}] + k_{cat}[\mathbf{ES}]$$

$$\frac{d[\mathbf{S}]}{dt} = -k_1[\mathbf{E}][\mathbf{S}] + k_{-1}[\mathbf{ES}]$$

$$\frac{d[\mathbf{ES}]}{dt} = k_1[\mathbf{E}][\mathbf{S}] - k_{-1}[\mathbf{ES}] - k_{cat}[\mathbf{ES}]$$

$$\frac{d[\mathbf{ES}]}{dt} = k_1[\mathbf{E}][\mathbf{S}] - k_{-1}[\mathbf{ES}] - k_{cat}[\mathbf{ES}]$$

$$\frac{d[\mathbf{P}]}{dt} = k_{cat}[\mathbf{ES}]$$

In this mechanism, the enzyme E is a catalyst, which only facilitates the reaction, so that its total concentration free plus combined is given by $[\mathbf{E}] + [\mathbf{ES}] = [\mathbf{E}]_0$. This conservation law can also be observed by adding the first and third equations above. In their original analysis, Michaelis and Menten assumed that the substrate is in instantaneous chemical equilibrium with the complex, which implies:

$$k_1[\mathbf{E}][\mathbf{S}] = k_{-1}[\mathbf{ES}].$$

$$[\mathbf{E}] = [\mathbf{E}]_0 - [\mathbf{ES}]$$

$$k_1([\mathbf{E}]_0 - [\mathbf{ES}])[\mathbf{S}] = k_{-1}[\mathbf{ES}]$$

$$k_1[\mathbf{E}]_0[\mathbf{S}] - k_{-1}[\mathbf{ES}][\mathbf{S}] = k_{-1}[\mathbf{ES}]$$

$$k_{-1}[\text{ES}] + k_1[\text{ES}][\text{S}] = k_1[\text{E}]_0[\text{S}]$$

$$[\text{ES}](k_{-1} + k_1[\text{S}]) = k_1[\text{E}]_0[\text{S}]$$

$$[\text{ES}] = \frac{k_1[\text{E}]_0[\text{S}]}{k_{-1} + k_1[\text{S}]}$$

$$[\text{ES}] = \frac{k_1[\text{E}]_0[\text{S}]}{k_1\left(\frac{k_{-1}}{k_1} + [\text{S}]\right)}$$

Upon simplification, we get

$$[\text{ES}] = \frac{[\text{E}]_0[\text{S}]}{K_m + [\text{S}]}$$

Where K_m is the dissociation constant for the enzyme-substrate complex. Hence the velocity of the reaction – the rate at which P is formed - is

$$v = \frac{d[\text{P}]}{dt} = V_{\max} \frac{[\text{S}]}{K_m + [\text{S}]}$$

where V_{\max} is the maximum reaction velocity.

References:

- [1] P. A. Riley. Melanin. *The International Journal of Biochemistry & Cell Biology*. 1997, 29(11), 1235-1239
- [2] M. d'Ischia, A. Napolitano, A. Pezzella, P. Meredith, M. Buehler. Melanin Biopolymers: Tailoring Chemical Complexity for Materials Design. *Angewandte international edition chemie*. 2020, 59 (28), 11196-11205.
- [3] M. d' Ischia, K. Wakamatsu, F. Cicoira, E. Di Mauro, J.-C. Garcia-Borron, S. Commo, I. Galvan, G. Ghanem, K. Kenzo, P. Meredith, et al. Melanins and melanogenesis: from pigment cells to human health and technological applications. *Pigm. Cell Melanoma Res*. 2015, 28, 520– 544.
- [4] M. Seiberg. Keratinocyte–Melanocyte Interactions During Melanosome Transfer. *Pigment Cell Research*. 2001, 14(4),236-242.
- [5] J. Vachtenheim. J. Borovanský. “Transcription physiology” of pigment formation in melanocytes: central role of MITF. *Experimental dermatology*. 2010, 19(7), 617-627.
- [6] P. A. Riley. Melanogenesis and Melanoma. *Pigment Cell Research*. 2003, 16(5), 548-552.
- [7] S. Ito. A Chemist's View of Melanogenesis. *Pigment Cell Research*. 2003, 16(3), 230-236.
- [8] S. Ito, K. Wakamatsu. Quantitative Analysis of Eumelanin and Pheomelanin in Humans, Mice, and Other Animals: a Comparative Review. *Pigment Cell Research*. 2003, 16(5), 523-531.
- [9] H. Ozeki, S. Ito. K. Wakamatsu, A. J. Thody. Spectrophotometric Characterization of Eumelanin and Pheomelanin in Hair. *Pigment Cell Research*. 1996, 9 (5), 265-270.
- [10] C. D. Marsden. Neuromelanin and Parkinson's disease. *Journal of Neural transmission. Supplementum*, 1983, 19, 121-141.
- [11] D. G. Graham. On the origin and significance of neuromelanin. *Archives of Pathology & Laboratory Medicine*, 1979, 103(7), 359-362.
- [12] M. Brenner, V. J. Hearing. The Protective Role of Melanin Against UV Damage in Human Skin. *Photochemistry and Photobiology*. 2008, 84(3), 539-549.
- [13] E. Nicolaidou, A. D. Katsambas. Pigmentation disorders: hyperpigmentation and hypopigmentation. *Clinics in Dermatology*. 2014, 32(1), 66-72.
- [14] A. G. Pandya, I. L. Guevara. Disorders of hyperpigmentation. *Dermatologic Clinics*. 2000, 18(1), 91-98.
- [15] J. P. Ortonne, D. L. Bissett. Latest Insights into Skin Hyperpigmentation. *Journal of Investigative Dermatology Symposium Proceedings*. 2008, 13(1), 10-14.
- [16] J. R. Whitaker, C. Y. Lee. Recent Advances in Chemistry of Enzymatic Browning. *Enzymatic Browning and Its Prevention*. 1995,1,2-7.
- [17] K. M. Moon, E. B. Kwon, B. Lee, C. Y. Kim. Recent Trends in Controlling the Enzymatic Browning of Fruit and Vegetable Products. *Molecules*. 2020, 25(12), 2754.
- [18] V. del Marmol, F. Beermann. Tyrosinase and related proteins in mammalian pigmentation. *FEBS letters*. 1996, 381 (3), 165-168.

- [19] A. Nawaz, T. Shafi, A. Khaliq, H. Mukhtar, I. ul Haq. Tyrosinase: Sources, Structure and Applications. *Int J biotech & bioeng.* 2017, 5(3),142-148.
- [20] K. Lerch. Tyrosinase: Molecular and Active-Site Structure. *Enzymatic Browning and Its Prevention.* 1995,5,64-80.
- [21] C. Olivares, F. Solano. New insights into the active site structure and catalytic mechanism of tyrosinase and its related proteins. *Pigment cell & melanoma research.* 2009, 22(6), 750-760.
- [22] A. Sánchez-Ferrer, J. N. Rodríguez- López, F. García-Cánovas, F. García-Carmona. Tyrosinase: a comprehensive review of its mechanism. *Biochimica et Biophysica Acta (BBA) - Protein Structure and Molecular Enzymology.* 1995, 1247(1),1-11.
- [23] C. A. Ramsden, P. A. Riley. Tyrosinase: The four oxidation states of the active site and their relevance to enzymatic activation, oxidation and inactivation. *Bioorg. Med. Chem.* 2014, 22, 2388–95
- [24] S. Mondal, A. Thampi, M. Puranik. Kinetics of Melanin Polymerization during Enzymatic and Nonenzymatic Oxidation. *J. Phys. Chem. B* 2018, 122, 7, 2047–2063.
- [25] H. Ando, H. Kondoh, M. Ichihashi, V. J. Hearing. Approaches to Identify Inhibitors of Melanin Biosynthesis via the Quality Control of Tyrosinase. *Journal of Investigative Dermatology* 2007, 127(4), 751-761.
- [26] S. Zolghadri, A. Bahrami, M. Tareq, H. Khan, J. Munoz-Munoz, F. Garcia-Molina, F. Garcia-Canovas. A. A. Saboury. A comprehensive review on tyrosinase inhibitors. *Journal of Enzyme Inhibition and Medicinal Chemistry.* 2019, 34(1),279-309.
- [27] P. Rudeekulthamrong, J. Kaulpiboon. Optimization of amyloamylase for the synthesis of α -arbutin derivatives as tyrosinase inhibitors. *Carbohydrate Research.* 2020, 494, 108078.
- [28] K. Yoshimura, K. Tsukamoto, M. Okazaki, V. M. Virador, T.-C. Lei. Y. Suzuki, Y. Kitano, KiyonoriHarii. Effects of all-*trans* retinoic acid on melanogenesis in pigmented skin equivalents and monolayer culture of melanocytes. *Journal of Dermatological Science.* 2002, 27(1), 68-75.
- [29] A. Usuki, A. Ohashi, H. Sato, Y. Ochiai, M. Ichihashi, Y. Funasaka. The inhibitory effect of glycolic acid and lactic acid on melanin synthesis in melanoma cells. *Experimental Dermatology.* 2003, 12(2), 43-50.
- [30] R. Saruno, F. Kato, T. Ikeno. Kojic Acid, a Tyrosinase Inhibitor from *Aspergillus albus*. *Agric. Biol. Chem.* 1979, 43(6), 1337-.1338.
- [31] K. U. Schallreuter, J. W. Wood. A possible mechanism of action for azelaic acid in the human epidermis. *Arch Dermatol Res* 1990, 282, 168-171.
- [32] W. Yi. X. Wu, R. Cao, H. Song, L. Ma. Biological evaluations of novel vitamin C esters as mushroom tyrosinase inhibitors and antioxidants. *Food Chemistry,* 2009,117(3), 381-386.
- [33] C. Vanessa, R. L. K. Azevedo, P.-L. A. Franco, B. M. Luis, A. M. A. Zezzi, B. S. Bittencourt, G. Marcelo. Effects of bleaching agents containing fluoride and calcium on human enamel. *Quintessence International.* 2010, 41(8), 157-165.

- [34] Y.J. Kim, H. Uyama. Tyrosinase inhibitors from natural and synthetic sources: structure, inhibition mechanism and perspective for the future. *CMLS, Cell. Mol. Life Sci.* 2005, 62, 1707–1723.
- [35] K. U. Zaidi, S. A. Ali, A. Ali, I. Naaz. Natural Tyrosinase Inhibitors: Role of Herbals in the Treatment of Hyperpigmentary Disorders. *Mini Reviews in Medicinal Chemistry*, 2019, 19(10), 796-808.
- [36] S. Parvez, M. Kang, H.-S. Chung, H. Bae. Naturally occurring tyrosinase inhibitors: mechanism and applications in skin health, cosmetics and agriculture industries. *Phytherapy Research*. 2007, 21(9), 805-816.
- [37] I. Chiochio, M. Mandrone, C. Sanna, A. Maxia, M. Tacchini. F. Poli. Screening of a hundred plant extracts as tyrosinase and elastase inhibitors, two enzymatic targets of cosmetic interest. *Industrial Crops and Products*. 2018, 122(15),498-505.
- [38] E. O. Ilkay, T. H. K. Mahmud. Flavonoid Derivatives as Potent Tyrosinase Inhibitors – A Survey of Recent Findings Between 2008-2013. *Current Topics in Medicinal Chemistry*, 2014, 14, 1486-1493.
- [39] K. Sakuma, M. Ogawa, K. Sugibayashi, K.-I. Yamada, K. Yamamoto. Relationship between tyrosinase inhibitory action and oxidation-reduction potential of cosmetic whitening ingredients and phenol derivatives. *Archives of Pharmacal Research*. 1999, 22, 335–339.
- [40] L. Panzella, A. Napolitano. Natural and Bioinspired Phenolic Compounds as Tyrosinase Inhibitors for the Treatment of Skin Hyperpigmentation: Recent Advances. *Cosmetics*, 2019, 6(4), 57.
- [41] R. Angela, S. Whisnant, D. Gilman. Studies of reversible inhibition, irreversible inhibition, and activation of alkaline phosphatase by capillary electrophoresis. *Analytical Biochemistry*. 2002, 307(2), 226-234.
- [42] D. S. Johnson, E. Weerapana, B. F. Cravatt. Strategies for discovering and derisking covalent, irreversible enzyme inhibitors. *Future Med. Chem.* 2010, 2(6), 949–964.
- [43] B. Ring, S.A. Wrighton, M. Mohutsky. Reversible Mechanisms of Enzyme Inhibition and Resulting Clinical Significance. *Enzyme Kinetics in Drug Metabolism*, 2014, 1113, 37-56.
- [44] L. A. Segel. On the validity of the steady state: Assumption of enzyme kinetics. *Bulletin of Mathematical Biology*. 1988, 50(6), 579-593.
- [45] A. J. Brown. XXXVI.—Enzyme action. *Chem. Soc., Trans.*, 1902, 81,373-388.
- [46] V. Henri, Lois générales de l'action des diastases, *Journal of American Chemical society*. 1903, 780-782.
- [47] L. Michaelis, M. M. L. Menten. The kinetics of invertin action
Translated by T.R.C. Boyde Submitted 4 February 1913. *FEBS letters*. 2013, 587(17), 2712-2720.
- [48] H. Lineweaver, D. Burk. The Determination of Enzyme Dissociation Constants, *Journal of the American Chemical Society*. 1934, 56(3), 658–666.
- [49] R. S. Ochs. Understanding Enzyme Inhibition. *J. Chem. Educ.* 2000, 77(11), 1453.

- [50] R. Sharma. Enzyme Inhibition: Mechanisms and Scope, Enzyme Inhibition and Bioapplications. Journal of Chemical Education. 2012.
- [51] T. Robin, S. Reuveni, M. Urbakh. Single-molecule theory of enzymatic inhibition. *Nat Commun.* 2018, 9, 779
- [52] A. Cornish-Bowden. Fundamentals of enzyme kinetics (4thed) Portland Press Ltd, London, 2000.
- [53] K. A. Cayce, A. J. McMichael, S. R. Feldman. Hyperpigmentation: An overview of the common afflictions. *dermatology nursing*, Pitman. 2004, 16(5), 401-6, 413-6.
- [54] S. K. Fistarol, P. H. Itin. Disorders of pigmentation. *Journal of the German Society of Dermatology.* 2010, 8(3), 187-202.
- [55] S. Schalka. New data on hyperpigmentation disorders. *Journal of the European Academy of Dermatology and Venereology.* 2017, 31(S5), 18-21.
- [56] T.-S. Chang. Natural Melanogenesis Inhibitors Acting Through the Down regulation of Tyrosinase Activity. *Materials.* 2012, 5, 1661-1685.
- [57] J. M. Gillbro, M. J. Olsson. The melanogenesis and mechanisms of skin-lightening agents-existing and new approaches. *Int J Cosmet Sci.* 2011, 33, 210-221.
- [58] P. Ruzza, P. A. Serra, D. Fabbri, M. A. Dettori, G. Rocchitta, G. Delogu. Hydroxylated biphenyls as tyrosinase inhibitor: A spectrophotometric and electrochemical study. *European Journal of Medicinal Chemistry.* 2017, 126, 1034-1038.
- [59] A. F. Murray, H. Satooka, K. Shimizu, W. Chavasiri, I. Kubo. Polygonum odoratum essential oil inhibits the activity of mushroom derived tyrosinase. *Heliyon.* 2019, 5(11), e02817.
- [60] J. C. Espín, R. Varón, L. G. Fenoll, M. A. Gilabert, P. A. García-Ruíz. Kinetic characterization of the substrate specificity and mechanism of mushroom tyrosinase. *European Journal of Biochemistry.* 2000, 267(5), 1210-1279.
- [61] M. J. Peñalver, A. N. P. Hiner, J. N. Rodríguez-López, F. García-Canovas, J. Tudela. Mechanistic implications of variable stoichiometries of oxygen consumption during tyrosinase catalyzed oxidation of monophenols and o-diphenols. *J. Biochim. Biophys. Acta.* 1597, 2002, 140-148.
- [62] S.Y. Lee, N. Baek, T. G. Nam. Natural, semisynthetic and synthetic tyrosinase inhibitors. *J Enzyme Inhib Med Chem.* 2015, 16, 1-13.
- [63] T.-S. Chang. An Updated Review of Tyrosinase Inhibitors. *Int. J. Mol. Sci.* 2009, 10, 2440-2475.
- [64] I. Kubo, I. Kinst-Hori. Flavonols from saffron flower: tyrosinase inhibitory activity and inhibition mechanism. *J. Agric. Food Chem.* 1999, 47, 4121-4125.
- [65] J. K. No, D. Y. Soung, Y. J. Kim, K. H. Shim, Y. S. Jun, S. H. Rhee, T. Yokozawa, H. Y. Chung. Inhibition of tyrosinase by green tea components. *Life Sci.* 1999, 65, PL241-246.
- [66] I. Kubo, I. Kinst-Hori, S. K. Chaudhuri, Y. Kubo, Y. Sánchez, T. Ogura. Flavonols from Heterothecainuloides: tyrosinase inhibitory activity and structural criteria. *Bioorg Med Chem.* 2000, 8, 1749-1755.

- [67] K. Shimizu, R. Kondo, K. Sakai. Inhibition of tyrosinase by flavonoids, stilbenes and related 4-substituted resorcinols: structure-activity investigations. *Planta Med.* 2000, 66, 11-15.
- [68] S.H. Lee, S.Y. Choi, H. Kim, J.S., Hwang, B.G. Lee, J.J. Gao, S.Y. Kim, Mulberroside F isolated from the leaves of *Morus alba* inhibits melanin biosynthesis. *Biol. Pharm. Bull.* 2002, 25, 1045-1048
- [69] O. Nerya, J. Vaya, R. Musa, S. Izrael, R. Ben-Arie, S. Tamir. Glabrene and isoliquiritigenin as tyrosinase inhibitors from licorice roots. *J Agric Food Chem.* 2003 26(51), 1201-1207.
- [70] T. Yokota, H. Nishio, Y. Kubota, M. Mizoguchi. The inhibitory effect of glabridin from licorice extracts on melanogenesis and inflammation. *Pigment Cell Res.* 1998, 11, 355-361.
- [71] B. Fu, Li, H., Wang, X., Lee, F.S., Cui, S. Isolation and identification of flavonoids in licorice and a study of their inhibitory effects on tyrosinase. *J. Agric. Food Chem.* 2005, 53, 7408-7414.
- [72] H. J. Kim, S. H. Seo, B. G. Lee, Y. S. Lee. Identification of tyrosinase inhibitors from *Glycyrrhiza uralensis*. *Planta Med.* 2005, 71, 785-787.
- [73] K. Yamauchi, T. Mitsunaga, I. Batubara. Isolation, identification and tyrosinase inhibitory activities of the extractives from *Allamanda cathartica*. *Nat. Resources*, 2011, 2, 167-172.
- [74] L. G. Fenoll, J. N. Rodríguez-Lopez, F. García-Molina, F. García-Canovas and J. Tudela. Unification for the Expression of the Monophenolase and Diphenolase Activities of Tyrosinase. *IUBMB Life*, 2002, 54, 137–141.
- [75] Y. M. Kim, J. Yun, C.-K. Lee, H. Lee. K. R. Min, Y. Kim. Oxyresveratrol and Hydroxystilbene Compounds. Inhibitory effects on tyrosinase and mechanism of action. *J. Biol. Chem.* 2002, 277, 16340–16344.
- [76] T.-S. Chang, H.-Y. Ding, S. S.-K. Tai, C.-Y. Wu. Mushroom tyrosinase inhibitory effects of isoflavones isolated from soygerm koji fermented with *Aspergillus oryzae* BCRC 32288. *Food Chem.* 2007, 105, 1430-1438.
- [77] J. Sharad. Glycolic acid peel therapy - a current review. *Clin Cosmet Invest Dermatol.* 2013, 6, 281-288.
- [78] J. N. Rodríguez-López, J. R. Ros-Martínez, R. Varón, F. García-Cánovas. Calibration of a Clark-type oxygen electrode by tyrosinase-catalyzed oxidation of 4-tert-butylcatechol. *Analytical Biochemistry*, 1992, 202(2), 356-360.
- [79] S Naish-Byfield, P. A. Riley. Oxidation of monohydric phenol substrates by tyrosinase. An oximetric study. *Biochem J.* 1992, 288 (1), 63–67.
- [80] L.G. Fenoll, J. N. Rodríguez-López, F. García-Sevilla, P. A. García-Ruiz, R. Varón, F. García-Cánovas, J. Tudela. Analysis and interpretation of the action mechanism of mushroom tyrosinase on monophenols and diphenols generating highly unstable o-quinones. *BBA-Protein Struct. M.* 2001, 1548(1), 1-22.
- [81] M. J. Stewart, I. D. Watson. "Standard units for expressing drug concentrations in biological fluids". *British Journal of Clinical Pharmacology.* 1983, 16 (1), 3–7.

- [82] R. A. Copeland. *Enzymes: A Practical Introduction to Structure, Mechanism, and Data Analysis*, 2nd Edition. Wiley-VCH, New York. 2000.
- [83] Seo, S.-Y.; Sharma, V. K.; Sharma, N. Mushroom Tyrosinase: Recent Prospects *J. Agric. Food Chem.* 2003, 51 (10), 2837–2853.
- [84] Gheibi, N.; Taherkhani, N.; Ahmadi, A.; Haghbeen, K.; Ilghari, D. Characterization of inhibitory effects of the potential therapeutic inhibitors, benzoic acid and pyridine derivatives, on the monophenolase and diphenolase activities of tyrosinase *Iran. J. Basic Med. Sci.* 2015, 18 (2), 122–129.
- [85] F. Mayr, S. Sturm, M. Ganzera, B. Waltenberger, S. Martens, S. Schwaiger, D. Schuster, H. Stuppner. Mushroom Tyrosinase-Based Enzyme Inhibition Assays Are Not Suitable for Bioactivity-Guided Fractionation of Extracts. *J. Nat. Prod.* 2019, 82, 136–147. DOI: 10.1021/acs.jnatprod.8b00847.